The Proceedings of 2nd International Conference on Rheology

14 & 15 December 2021
Tehran, Iran

In the Name of God

The Proceedings of

2nd International Conference on Rheology

14 & 15 December, 2021, Tehran, Iran

icor-isr.ir

The Proceedings of 2nd International Conference on Rheology
Tehran, 2021

Conference Office: Department of Polymer Engineering, Amirkabir University of Technology, Tehran, Iran
Tel: 0930 230 7582, Telfax: +9821 4478 7060
E-mail: info@icor-isr.ir, Website: icor-isr.ir

Editor: Salwa Farhangzadeh
Technical Editor: Sarvenaz Alikhani
Typesetting and Layout: Ashraf Tatlari

Iranian Society of Rheology
Office: Department of Polymer Engineering, Amirkabir University of Technology, Tehran, Iran
Tel: 0930 230 7582, Telfax: +9821 6454 2437
E-mail: info@ir-sor.com, Website: ir-sor.com

Welcome Message

Established in 2016, Iranian Society of Rheology (ISR) aims to expand the knowledge of rheology and enhance scientific collaboration between rheologists from industry and academia. As a member of the International Committee on Rheology (ICR), ISOR serves as a national focal point and center of excellence to achieve this goal in cooperation with higher education institutes and industry.

As ISR and ICOR president, it gives me great pleasure to address all rheologists, students, and interested in this field, 2nd International Conference on Rheology (ICOR 2021) organized by Iranian Society of Rheology on 14, 15 December 2021, Tehran, Iran.

Our past experiences of organizing ICOR 2019 and three national conferences in Iran have demonstrated its capability of providing a highly knowledge-sharing opportunity and meeting point for scholars and industry experts in the region and throughout the world.

ICOR 2021 is open to all interested in rheology, from newcomers to established experts.

We are looking forward to your valuable participation in ICOR 2021.

Goharpey

Fatemeh Goharpey
ISR and ICOR 2021 President

Dear All,

The Second International Conference on Rheology, organized by the Iranian Society of Rheology was held at the Amirkabir University of Technology in Tehran.
In this event, there were two plenary lectures starting in two successive days. The conference also brought together 22 international and 8 national keynote speakers. In our program we also included 22 oral presentations. In addition, there was a poster exhibition where 45 posters were presented. In the conference program three short courses were also presented two days before starting the conference.
All in all, the Second International Conference on Rheology in Tehran was extremely productive. The internationally known plenary speakers and keynote lecturers together with oral presenters successfully covered different topics of the conference. We extend our profound gratitude to the plenary speakers. We are also deeply grateful to the keynote lecturers and oral presenters. Finally, we are especially thankful to the panelists and all the conference participants for the willingness and courage to openly share their ideas and experiences.
Thank you all for fully participating and contributing to this conference which made it our collective success and achievement.

Hossein Nazockdast
Scientific Committee Chair

Ismail Ghasemi
Executive Committee Secretary

Contents

Scientific Committee

Name	Organization
Nazockdast H.	Amirkabir University of Technology, nazdast@aut.ac.ir
Ramazani Saadat-Abadi A.	Sharif University of Technologhy, ramazani@sharif.edu
Abbassi F.	Sahand University of Technology, f.abbasi@sut.ac.ir
Abbassi Sourki F.	Iran Polymer and Petrochemical Institute, f.abbasi@ippi.ac.ir
Ahmadi Sh.	Iran Polymer and Petrochemical Institute, sh.ahmadi@ippi.ac.ir
Alaei J.	Research of Institute of Petroleum Industry, aalaiej@gmail.com
Alavi S.M.Z.	University of Tehran, zia.alavi@ut.ac.ir
Dabir B.	Amirkabir University of Technology, drbdabir@aut.ac.ir
Famili M.H.N.	Tarbiat Modares University, nfamili@modares.ac.ir
Foudazi R.	University of Oklahoma, rfoudazi@nmsu.edu
Gharanjig K.	Institute for Color Science & Technology, gharanjig@icrc.ac.ir
Ghasemi I.	Iran Polymer and Petrochemical Institute, i.ghasemi@ippi.ac.ir
Golshan Ebrahimi N.	Tarbiat Modares University, ebrahimn@modares.ac.ir
Goharpey F.	Amirkabir University of Technology, goharpey@aut.ac.ir
Haghtalab A.	Tarbiat Modares University, haghtala@modares.ac.ir
Haririan I.	University of Tehran, haririan@tums.ac.ir
Hashemabadi S.H.	Iran University of Science and Technology, hashemabadi@iust.ac.ir
Kaffashi B.	University of Tehran, kaffashi@ut.ac.ir
Katbab A.A.	Amirkabir University of Technology, katbab@aut.ac.ir
Khademzadeh Yeganeh J.	Qom University of Technology, jkh.yeganeh@gmail.com
Khosrokhavar R.	Iranian Association of Polymer and Chemical Engineers, ramin@khosrokhavar.com
Mehranpour M.	Islamic Azad University, m.mehranpour@srbiau.ac.ir
Mirzadeh H.	Amirkabir University of Technology, mirzadeh@aut.ac.ir
Moghimi E.	University of Crete, Greece, esmaeel@iesl.forth.gr
Moini Jazani O.	Isfahan University of Technology, o.moini@eng.ui.ac.ir
Mohammadigoushki H.	Florida State University, hmohammadigoushki@eng.famu.fsu.edu
Mohammadi N.	Amirkabir University of Technology, mohamadi@aut.ac.ir
Nazockdast E.	University of North Carolina, ehssan@email.unc.edu
Nekoomanesh Haghighi M.	Iran Polymer and Petrochemical Institute, m.nekoomanesh@ippi.ac.ir
Norouzi M.	Polymer Shahrood University of Technology, mnorouzi@shahroodut.ac.ir
Pircheraghi G.	Sharif University of Technologhy, pircheraghi@sharif.ir
Pishvaei M.	Institute of Color Science and Technology, pishvaei@icrc.ac.ir
Rafizadeh M.	Amirkabir University of Technology, mehdi@aut.ac.ir
Ranjbar Z.	Institute for Color Science & Technology, ranjbar@icrc.ac.ir
Rashedi R.	Jam Petrochemical Company, r_rashedi@jpcomplex.com
Rastegar S.	Amirkabir University of Technology, s.rastegar@aut.ac.ir
Razavi M.A.	Ferdowsi University of Mashhad, s.razavi@um.ac.ir
Razavi Aghjeh M.K.	Amirkabir University of Technology, karimrazavi@sut.ac.ir
Razzaghi Kashani M.	Tarbiat Modares University, mehdi.razzaghi@modares.ac.ir

Scientific Committee

Name	Organization
Sadeghy K.	University of Tehran, sadeghy@ut.ac.ir
Salami-Hosseini M.	Sahand University of Technology, salami@sut.ac.ir
Salehi Barmi M.	Research of Institute of Petroleum Industry, msalehibarmi@gmail.com
Shams Eshaghi K.	Isfahan University of Technology, k_shams@cc.iut.ac.ir
Sharif F.	Amirkabir University of Technology, sharif@aut.ac.ir

Executive Committee

Name	Organization
Goharpey F.	Amirkabir University of Technology, goharpey@aut.ac.ir
Ghasemi I.	Iran Polymer and Petrochemical Institute, i.ghasemi@ippi.ac.ir
Alikhani S.	Iranian Society of Rheology, s.alikh71@gmail.com
Farhangzadeh S.	Iran Polymer and Petrochemical Institute, s.farhangzadeh@ippi.ac.ir
Garmabi H.	Amirkabir University of Technology, garmabi@aut.ac.ir
Khosrokhavar R.	Iranian Association of Polymer and Chemical Engineers, ramin@khosrokhavar.com
Mehranpour M.	Islamic Azad University, m.meranpour@srbiau.ac.ir
Mirghasemi A.	Iranian Society of Rheology, mirghasemi.a@gmail.com
Mohammadzad H.	Iranian Society of Rheology, mohammadzad.h2020@gmail.com
Nazockdast H.	Amirkabir University of Technology, nazdast@aut.ac.ir
Nekoomanesh M.	Iran Polymer and Petrochemical Institute, m.nekoomanesh@ippi.ac.ir
Parian S.	Varesh Shimi Co, parian@vareshchimie.ir
Rashedi R.	Jam Petrochemical Company, r_rashedi@jpcomplex.com
Zabeti V.	Amirkabir University of Technology, vista_zabeti@aut.ac.ir

Plenary Presenters

- Gerald G. Fuller, Stanford Univeristy, USA
- Dimitris Vlassopoulos, Forth - University of Crete, Greece

Keynote Speakers

Name	Name
Shervin Ahmadi	Esmaeel Moghimi
Mohammad Zia Alavi	Hadi Mohammadigoushki
Mahdi Davoodi	Ehssan Nazockdast
Peter Fischer	Mohammad Reza Nofar
Reza Foudazi	George Petekidis
Ian Frigaard	Malihe Pishvaei
Ismaeil Haririan	Ahmad Ramazani Saadat-Abadi
Savvas G. Hatzikiriakos	Mehdi Razzaghi-Kashani
Sarah Hormozi	Amir Rezvani
Ahmad Jabbarzadeh	Kayvan Sadeghi
Safa Jamali	Mehdi Salami-Hosseini
Fardin Khabaz	Patrick Spicer
Alex G. Kuchumov	S. Mohamad Taghavi
Ronald G. Larson	Sachin Velankar
Joao Maia	

Organizer

- Iranian Society of Rheology (ISR)

Co-organizers

- Polymer Engineering and Color Technology, Amirkabir University of Technology (AUT)
- Iran Polymer Science and Technology Society (IPSTS)
- Iran Polymer and Petrochemical Institute (IPPI)

Sponsors

- Jam Petrochemical Company
- Varesh Shimi Bahar
- Farnam Baspar
- Dana Polymer Fanavar
- Dana Polymer Holding
- Puya Polymer
- Rangdaneh Sirjan
- Laleh Petrochemical Company
- Pipe and Fitting of PE Association
- Pasargad Oil Company

Short Courses Program

No.	Title	Presenter	Date
1	Rheology of Emulsions	Reza Foudazi	12 December
2	Colloidal Suspension Rheology	Safa Jamali	13 December
3	Course I: MCR 702e Multidrive-Advanced Methods in Rheology and DMA for Extended Material Characterization	Matthias Walluch	13 December
	Course II: SmartPave 102e (Asphalt Application)-ASTM/AASHTO Methods	Mrinali Rochlan	
	Course III: Powder Rheology	Helena Weingrill	

Abstracts of

Plenary & Keynote Lectures

The Interfacial Mechanics of Ocular Cell Layers: Friction, Adhesion and Delamination

Gerald G. Fuller

Stanford University, Stanford, USA
ggf@stanford.edu

Abstract: The ocular surface is comprised of stratified layers of cells: corneal epithelial cells and conjunctival cells. These layers are subject to sliding friction during the course of a blink cycle and are protected by the tear film. This aqueous liquid film is enriched with endogenously expressed mucins, which are known to contribute to its lubricious character. Maintaining the stability of this film is essential to ocular health since it helps to eliminate foreign matter and regulates optical acuity. Maintenance of a stable tear film requires a delicate balance of its constituents and when this does not occur, the film can break, leading to conditions referred to as dry eye disease (DED). This presentation describes two experimental platforms designed to interro gate the interaction of layers of ocular cells with one another, as in the case of the sliding friction of corneal epithelial cells across conjunctival cells, and the direct interaction of ocular cell layers with air. The first set of experiments investigates the problem of mucin deficiency where reduced biosynthesis or loss of functional mucins has been reported in some DED patients. Here we developed a mucin-deficient dry eye mimetic cell model to investigate the contributions of mucins and mucin-like glycoproteins to the interfacial, rheological, and adhesive properties of ocular epithelial surfaces. Cell-to-cell adhesion and sliding friction were directly measured using a newly developed Live Cell Rheometer (LCR). It is demonstrated that membrane-tethered mucins are essential for biolubrication. Supplementation with recombinant human lubricin, a mucin-like glycoprotein, restored the lubrication function induced by the lack of cell surface mucins in a dose-dependent manner. The second set of experiments examined the direct interaction of air bubbles against stratified ocular cell layers. Here, small bubbles were released below cell layers that were oriented face-down. Tilting of the surface layer introduced a simple gravitati onal force onto the bubble, causing it to tug on the cell layer with fore-and-aft advancing and receding contact angles. Remarkably, the cell layers, which were adherent to the bubbles, delaminated from the substrates onto which they were attached (collagen-coated glass). This simple experiment allows one to directly measure the surface energies of the cell layers, the tensile strength of the layers, and the force of adhesion of the layers onto various substrates.

The Unusual Rheology of Ring Polymers and their Blends with Linear Chains

Dimitris Vlassopoulos

FORTH, Institute of Electronic Structure & Laser and University of Crete,
Department of Materials Science & Technology, Heraklion, Greece
dvlasso@iesl.forth.gr

Abstract: Unlike polymers with free ends, unconcatenated ring polymers exhibit unexpected flow properties with implications in the understanding of biological function. It is now established that entangled rings relax stress via power-law, sharply departing from their linear counterparts which exhibit a rubbery plateau. Concomitantly, their nonlinear shear rheology is very distinct, exhibiting a power-law thinning exponent of about -0.6, much weaker than that of linear chains (-0.9). Likewise, extensional thickening is reported at low rates during elongation. In the presentation we summarize this knowledge and use it to promote rheology modification by means of loopy structures. We present new data on nonlinear shear viscosity and normal stresses over a wide range of molar masses and Weissenberg numbers. We also present linear and nonlinear extensional properties of blends including ring and linear polymers of varying composition and focus on the ability of small amounts of rings to alter the rheology of linear polymers and in particular to enhance their viscoelastic response by means of threading-unthreading transition. This presentation reflects collaboration with D. Parisi, K. Peponaki (Crete), G. Sakellariou (Athens), T. Chang (Pohang), Q. Huang and O. Hassager (DTU), T. O'Connor (CMU), G. Grest (Sandia), and M. Rubinstein (Duke).

References:

M. Kapnistos et al., *Nature Materials*, **7**, 997-1002 (2008).
Q. Huang et al., *Phys. Rev. Lett.*, **122**, 208001 (2019).
D. Parisi et al., *Macromolecules*, **53**, 1685-1693 (2020).
A. Borger et al., *ACS Macro Lett.*, **9**(10), 1452-1457 (2020).
D. Parisi et al., *Macromolecules*, **54**, 2811-2827 (2021).
D. Parisi et al., *J. Rheol.*, **65**, 695-711 (2021).

Multi-Scale Modeling of Surfactants, Colloids, and Polymers, and Their Applications

Ronald G. Larson

Department of Chemical Engineering, University of Michigan, USA
rlarson@umich.edu

Abstract: Continuum-level thermodynamic and transport properties relevant to industrial applications can now be computed from molecular-scale interactions using multi-scale molecular dynamics (MD) simulations and Brownian dynamics (BD) simulations, along with biasing methods, such as umbrella sampling, and forward flux sampling. We demonstrate the power of these methods by computing the dynamics and rheology of surfactant solutions, polymers, and colloid-polymer mixtures used in consumer and industrial products, such as shampoos, and paints. The complex structures and rheology of these fluids require multi-scale modeling that can include atomistic and coarse-grained molecular simulations, as well as colloidal scale simulations, and model-reduction schemes to connect commercially important rheological properties to chemical composition. We also compare the predicted results to experimental data, and extract information, that is unavailable, or not easily available, from experiments.

Tuning Colloidal Gels by Shear: New Routes to Manipulate Mechanical Properties

George Petekidis

IESL-FORTH & Materials Science & Technology Department, University of Crete, Heraklion, Greece
georgp@iesl.forth.gr

Abstract: Attractive colloids form out-of-equilibrium states such as colloidal gels and attractive glasses, which often exhibit strong thixotropy. Their mechanical properties are affected by pre-shear history and show a time evolution after nonlinear steady or oscillatory shear tests due to shear induced structural changes and subsequent restructuring and stress relaxation after shear cessation. Both in model and industrial systems such preshear protocols can be used to enable fine-tuning of the structure and mechanical properties. In fact such systems may be driven in different metastable states, possibly, not accessible via a thermodynamic route, i.e. changing interactions or volume fraction.

Here we present a variety of experiments (combining rheometry and confocal microscopy) and computer simulations on colloidal gels with different attraction strengths and volume fractions both for spherical or rodlike particles as building blocks. We follow microstructural changes at the single particle and the cluster level during yielding induced either by steady or by oscillatory shear. In the latter we distinguish between reversible and irreversible rearrangements of single particles (spheres or rods) or clusters as a function of strain amplitude and frequency, and relate them with the rheological response and final mechanical properties of the gel. We thus demonstrate how steady or oscillatory shear is able to tune the gel structure (both local density and orientational order) and how this is linked with the mechanical properties of the sample.

Keywords: Colloidal gels, shear induced tuning, thixotropy

The Design and In-Vivo Validation of Satiety Controlling Food-Controlling Human Fat Digestion with Help from Rheology

Pascal Bertsch, Jotam Bergfreund, Nathalie Scheuble, and Peter Fischer

Institute of Food, Nutrition and Health, ETH Zürich, Switzerland
peter@fischerphoto.ch

Abstract: Malnutrition, which includes overeating as well as nutrient deficiencies is one of the most pressing problems towards a healthy population and personal well-being. From a variety of approaches the stimulated release of satiety hormones offers a soft control on food intake [1]. In a conceptual study we present the design of food systems and its fate during human gastric and intestine digestion including its physiological resonance. A feedback loop between bulk and interfacial rheology [2-4], in-vivo gastric magnetic resonance imaging, and physiology in humans and rats does not only establishing the in-vitro/in-vivo correlation of fat digestion but also provides pathways to limit or stimulate food uptake (Figure 1). Besides controlling nutritional uptake, the mechanical performance of food after consumption is also a key factor affecting hydrophobic drug release [5]. In summary, the designed food systems as well as the analysis of their physicochemical changes during digestion provide in-vivo based guidelines for functional food formulations.

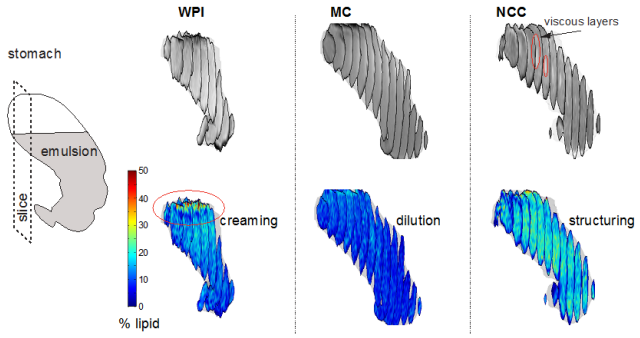

Figure 1. Intragastric emulsion structure formation in a healthy subject. On the left, the schematic illustrates the MR image slice orientation relative to the stomach shape. The columns separate and visualize the reconstructed and segmented multi-slice image data at 60 min after emulsion ingestion in 3D for the three emulsion systems stabilized with why protein isolate (WPI), methylated cellulose (MC), and nanocrystalline cellulose (NCC).

[1] Golding M, Wooster TJ: The influence of emulsion structure and stability on lipid digestion, Current Opinion in Colloid and Interface Science 15 (2010) 90.
[2] Bertsch P, Fischer P: Adsorption and interfacial structure of nanocelluloses at fluid interfaces, Advances in Colloid and Interface Science 276 (2020) 102089.
[3] Bergfreund J, Bertsch P, Fischer P: Effect of the hydrophobic phase on interfacial phenomena of surfactants, proteins, and particles at fluid interfaces, Current Opinion in Colloid and Interface Science (2021).
[4] Bertsch P, Bergfreund J, Windhab EJ, Fischer P: Physiological fluid interfaces: Functional microenvironments, drug delivery targets, and first line of defense, Acta Biomaterialia 130 (2021) 32.
[5] Scheuble N, Schaffner J, Schumacher M, Windhab EJ, Liu D, Parker H, Steingoetter A, Fischer P: Tailoring emulsions for controlled lipid release: Establishing in vitro-in vivo correlation for digestion of lipids, ACS Applied Materials and

Interpenetrating and Interconnected Grafted Nano Cylinders from Amphiphilic Star Block Copolymers

Esmaeel Moghimi, I. Chubak, L. Cipelletti, K. Mortensen, C.N. Likos, D. Vlassopoulos

Forth-University of Crete, Greece
esmaeel.moghimi@gmail.com

Abstract: A powerful combination of rheological, small angle X-ray and dynamic light scattering experiments along with computer simulations are utilized to examine the self-organization of a new class of tunable soft patchy colloidal particles of the star family, whose arms are diblock copolymers. These stars were synthesized by K. Ntetsikas and N. Hadjichristidis (KAUST). By tuning the solvent quality and block sequence a variety of intriguing opportunities to control the structure and dynamics of such soft colloids emerges, the most notable being the transition from high temperature disordered liquid to a low-temperature solid crystalline structure. The proposed state diagram with the re-entrant transition where an ordered/solid state can be formed both on heating and cooling shows the richness of the structural and rheological (linear and nonlinear) behavior of this kind of patchy particles. The main difference from respective ordered micelles when the solvophobic block is the inner one, is the organization into bridged grafted cylinders and interpenetrated grafted cylinders, respectively.

Dynamics of Self-Assembled Micellar Solutions in Uniaxial Extensional Flows

Hadi Mohammadigoushki

Department of Chemical and Biomedical Engineering, Florida State University, USA
hmohammadigoushki@eng.famu.fsu.edu

Abstract: Micelles represent an important class of self-assembled structures formed by amphiphilic molecules in aqueous solutions. These structures can exist in different forms including spherical, cylindrical, or vesicle type in dilute and semi-dilute regimes. Surfactant micelles provide a model fluid system due to their appealing rheological and thermodynamic properties. These systems are easy to prepare and are not susceptible to mechanical shear-degradation. This makes them promising candidates in plethora of applications, including, in household products, oil-gas fields, in biomedicine, cleaning processes, nano-templating, and catalysis. In this talk, I will address recent findings of my lab that involve flow and dynamics of viscoelastic micellar solutions in predominantly extensional flows. First, I will show the presence of a curious extensional flow-induced structure formation in dilute micellar solutions that give rise to extremely high transient extensional viscosities. Moreover, I will show that wormlike micelles may undergo extensional flow-induced micellar breakage in the semi-dilute regime. Finally, if time allows, I will show that extensional flow can be used as a microstructural probing technique that is capable of distinguishing various micellar structure (i.e., linear and branched) from each other.

Rheology of Lyotropic Liquid Crystals from Self-assembly of Amphiphilic Block Copolymers, Water and Oil

Reza Foudazi

School of Chemical, Biological and Materials Engineering, University of Oklahoma, USA
rfoudazi@ou.edu

Abstract: Self-assembly of amphiphilic block copolymers in the presence of immiscible solvents (oil/water) leads to the formation of lyotropic liquid crystals (LLCs) with the length scale in the range of 2-50 nm. Usually, LLC structures are polycrystalline and contain defects. If monomers are present in the LLC formulation, they can be polymerized to produce polyLLCs with periodic nanostructure for different application such as ultrafiltration and ion-gel membranes. The rheological properties of LLCs should be studied for designing processing protocols. In this talk, therefore, we present a model to predict the elastic modulus and yielding of LLCs from their characteristic length and intermicellar interactions. We show that the shear modulus of LLCs depends on the inverse of intermicellar distance with a power-law model. The experimental results suggest that at relatively low frequencies, defects control the rheological behavior of LLCs, while at high frequencies the contributions in micellar scale are dominant. We also show that strains in nonlinear regime can lead to alignment of grains.

Gel Structure of PVC Plastisol Used as Automotive Underbody Coatings

Malihe Pishvaei and Behrouz Eftekhari

Department of Resin and Additives, Faculty of Surface coating and Novel Technologies,
Institute of Color Science and Technology, Tehran, Iran
Pishvaei@icrc.ac.ir

Abstract: The PVC plastisol is a dispersion of fine particles of resin in a liquid plasticizer in which the particle interactions lead to the formation of microstructures. Depending on how such structures respond to the shear stress, one observes different types of flow behavior. Given the change of flocculation structure and shear-thinning behavior during the shear period, the Herschel-Bulkley model is more suitable for calculating the static yield stress of these materials. In this study, static yield stress changes along with the thixotropy (hysteresis area) are investigated for various industrial PVC plastisol used as automotive underbody coatings (UBC). The results show that with increasing the thixotropic behavior in different samples the yield stress increases. On the other hand, the gel like behavior is observed for all samples at room temperature as the storage modulus are higher than loss modulus over the entire experimentally accessible frequency range, and both are nearly constant.

Keywords: Plastisol, Static Yield Stress, Viscosity, Thixotropy, Hysteresis Area

Introduction

The PVC plastisol is a dispersion of fine particles in a liquid plasticizer to produce a fluid like mixture that can be spread on a substrate. The coated substrates (Fig.1) are then heated in an oven to gel and fuse the plastisol in to the final rubbery products [1].

The aging characteristics or the change in viscosity of a plastisol with time during the storage are very important. The mechanisms involved in plastisol aging include particle deagglomeration, particle swelling, particle dissolution, particle solvation, and plastisol structure development [2]. In this work, static yield stress changes along with the thixotropic properties (hysteresis area) were investigated for various industrial plastisols, both of freshly prepared samples and aged plastisols as well. Furthermore, the viscoelastic properties of samples were studied at the room temperature.

Experimental

Different commercial plastisols were examined as presented in Table 1. Anton-Paar MCR 300 rheometer with cone and plate geometry was used to measure the rheological properties. The viscosity of the samples were measured from shear velocities of 0.001 to 1000 1/s with a rest time of 300 (s) at 1000 1/s and return velocity in the same range at 25°C. The frequency sweep tests were performed in the linear viscoelastic area of samples.

Table 1. Commercial PVC Plastisol Samples.

Sample	Application	Company
1	UBC	Henkel
2	UBC	Daghigh Shimi
3	Sealer (S.)	Henkel
4	Sealer	Daghigh Shimi
5	UBC (aged sample 1)	Henkel
6	UBC (aged sample 2)	Gama Thinner
7	S. (aged sample 3)	Henkel
8	UBC	Daghigh Shimi
9	UBC	Gama Thinner
10	Sealer	Gama Thinner
11	UBC (aged sample 8)	Daghigh Shimi
12	UBC (aged sample 9)	Gama Thinner
13	S. (aged sample 10)	Gama Thinner

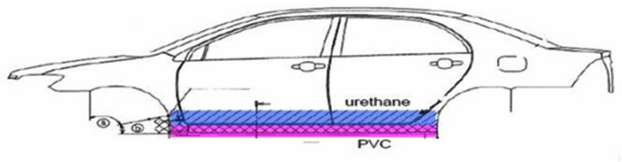

Figure 1. Automotive underbody coatings (UBC).

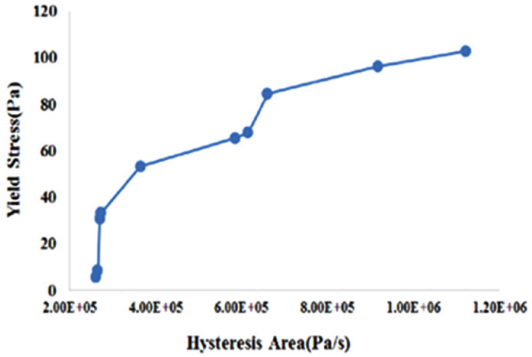

Figure 2. Experimental values of yield stress and thixotropy for 10 different PVC plastisols.

Results and Discussion

Flow tests were performed for various industrial PVC plastisol samples. Thixotropy can be defined as a (reversible) decrease of viscosity of the material in time when the material is made to flow. Yield stress is an important term to describe the flowability of paste materials. The static yield stress was calculated based on the experimental data and using the Herschel-Bulkley equation from the shear rate - shear stress diagram for each sample.

Generally, the yield stress appears when the particle repulsions are strong enough to induce a regular arrangement of particles or a sort of "macrocrystallization". The hysteresis area (Pa/s) was also obtained from the shear rate - shear stress diagram. The area within the hysteresis loop represents the energy consumed in structure breakdown. Figure 2 shows the changes in the hysteresis area in terms

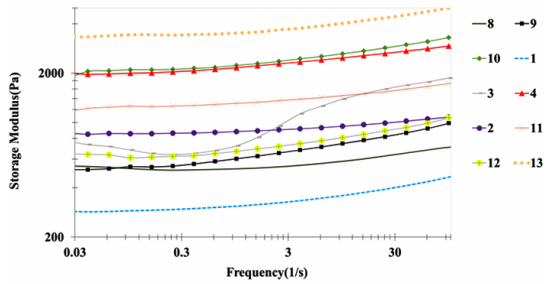

Figures 3. Storage modulus versus frequency for 10 different PVC plastisols.

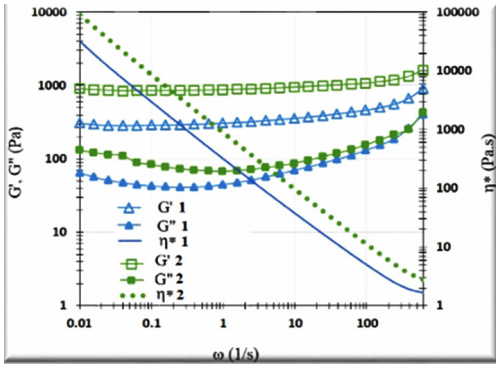

Figure 4. Viscoelastic properties of 2 plastisols: G' solid points, G'' open points and complex viscosity: solid line and dashed line.

of static yield stress. Samples with a larger hysteresis area show greater yield stress and vice versa. The results confirm that the yield stress and the thixotropy in PVC plastisols are caused by the same fundamental physics and this may be related to the microstructure-strength [3].

Beyond the gel point, the materials behave like viscoelastic Hookean solids at low frequencies or large scales[4].; However, the rubbery plateau as an evidence for gel like behaviour were observed for all samples in this study for PVC plastisols at room temperature (Figs. 3,4).

Conclusion

1- PVC plastisols behave like an elastic solid i.e. with G'>G" over the entire experimentally accessible frequency range, and where both of modulii are nearly constant (i.e. independent of frequency). 2- The results confirm that the yield stress and the thixotropy in PVC plastisols are caused by the same fundamental physics and this is related to the microstructure-strength.

References

1- Rasteiro, M. G., Toma´s, A., Ferreira L., Figueiredo S., *J Appl Polym Sci*, **112**, 2809-2821, 2009.
2- Hoffmann D. J., Garcia L. G., *J Macromol Sci Phys,* **20**, 335-348, 1981.
3- S, Jarni, et al., Rheological behavior of cement pastes from MRI velocimetry, Cement and concrete *research* 35.10 (2005) 1873-1881.
4- Pishvaei, M.; Graillat, C.; McKenna, T.F.; Cassagnau, P.; *Polymer* **46** (2005), 1235-1244.

Methane Emissions and Yield Stress Fluids

Ian Frigaard

University of British Columbia, Canada
frigaard@mail.ubc.ca

Abstract: Natural resource industries are significant contributors to greenhouse gas emissions globally, with sources ranging from gas flaring and well leakage to waste storage and methanogenesis. Yield stress fluids play an interesting role in this plot, as both hero and villain! Often yield stress fluids are those used to seal potential flow paths or prevent bubble migration. On the other hand, yield stress fluids are difficult to remove from small spaces, can themselves lead to preferential pathways for gas flow and allow trapping of gas, that represents a later release risk. This talk outlines some of the interesting fluid mechanics that is present in such processes.

Molecular Dynamics and Its Application in Molecular Rheology and Tribology

Ahmad Jabbarzadeh

School of Aerospace, Mechanical and Mechatronic Engineering, University of Sydney, Australia
ahmad.jabbarzadeh@sydney.edu.au

Abstract: In the past few decades, molecular dynamics (MD) simulations and their coarse grain variants have become indispensable tools for rheologists and tribologists to study complex problems in their field. The advent of modern areas of science such as nanotechnology and the need to understand physical phenomena, including rheology and tribology at the molecular scale, has helped the growth of research both experimentally and computationally at nanoscales. The application of molecular dynamics to rheology has helped to understand the behaviour of polymers qualitatively; also, significant progress has been made in predicting quantitative rheological properties such as the viscosity of simpler liquids (such as alkanes). In particular, the application of MD to the behaviour of confined fluids and lubricants at nano-scales has revealed some important properties and explained the underlying physics of observed phenomena that include enhanced viscosity and relaxation times. MD has also been a valuable tool in studying the relationship between molecular structure and rheological properties, shear-induced crystallization, phase transition, wetting and fluid-structure interactions. [1-12]

[1]. Jun Han Park, Bo Sung Shin, and Ahmad Jabbarzadeh, Anisotropic Wettability on One-Dimensional Nanopatterned Surfaces: The Effects of Intrinsic Surface Wettability and Morphology, Langmuir 37 (48), 14186-14194 (2021). DOI: 10.1021/acs.langmuir.1c02634.

[2]. Jabbarzadeh, A. The Origins of Enhanced and Retarded Crystallization in Nanocomposite Polymers. Nanomaterials, 9, 1472 (2019).

[3]. Jabbarzadeh, A., & Halfina, B. Unravelling the effects of size, volume fraction and shape of nanoparticle additives on crystallization of nanocomposite polymers. Nanoscale Advances, 1, 4704-4721 (2019).

[4]. Jabbarzadeh, Ahmad, and Xin Chen. "Surface Induced Crystallization of Polymeric Nano-particles: Effect of Surface Roughness." Faraday Discussions, 204, 307-321 (2017).

[5]. Jabbarzadeh, A. "Friction anisotropy and asymmetry in self assembled monolayers". *Tribology International*, 102, 600-607 (2016).

[6]. Moshfegh, A., A. Jabbarzadeh, "Fully explicit dissipative particle dynamics simulation of electroosmotic flow in nanochannels", *Microfluidics and Nanofluidics*, 20, 1-17 (2016).

[7]. A. Jabbarzadeh, "Friction Anisotropy in Confined Alkanes: Linear and Branched Molecules" *Tribology International*, 97,108–115 (2016).

[8]. A. Moshfegh, A. Jabbarzadeh, "Dissipative Particle Dynamics: Effects of Parameterisation and Thermostating Schemes on Rheology", *Soft Materials*, 13, 106-117 (2015).

[9]. A. Jabbarzadeh, P. Harrowell, R. I. Tanner, "Crystal bridges, tetratic order, and elusive equilibria: The role of structure in lubrication films", *Journal of Physical Chemistry B*, 111, 11354-11365 (2007).

[10].A. Jabbarzadeh, J. D. Atkinson and R. I. Tanner," The effect of molecular shape on rheological properties in molecular dynamics simulation of star, H, comb and linear shape polymer melts" *Macromolecules*, 36, 5020-5031 (2003).

[11].A. Jabbarzadeh and R.I. Tanner, "Flow Induced Crystallization: Unravelling the Effects of Shear Rate and Strain", *Macromolecules*, 43, 8136–8142 (2010).

[12].A. Jabbarzadeh and R. I. Tanner, "Crystallization of Alkanes under Quiescent and Shearing Conditions" *Journal of Non-Newtonian Fluid Mechanics*, 160, 11-21 (2009).

Settling Behavior of Elliptic Particles in Viscoplastic Fluids

Kayvan Sadeghy

University of Tehran, Tehran, Iran
sadeghy@ut.ac.ir

Abstract: Settling of heavy particles in a flowing or stationary liquid is encountered in many industrial applications; for example settling tanks, slurry pipelines, and the drilling of oil wells. The particles are often realized to be irregular in shape, and such particles are experimentally observed to exhibit a settling behavior that is dramatically different from spherical ones. Numerical results reported in the literature for elliptic particles settling in Newtonian fluids could closely capture some of these settling modes. In our recent work, we have shown that for viscoplastic fluids new modes of settling might emerge for elliptic particles. It has also been shown that the settling behavior of such particles is very sensitive to their initial inclination angle and also the initial off-center positioning. Work is currently ongoing in our research group to extend these results to porous particles. Preliminary results suggest that porosity can be used as an influential parameter for controlling the settling behavior of elliptic particles.

Application of Numerical Methods in Studying the Rheological Properties of Multiphase Fluids

Mahdi Salami Hosseini and Mehdi Mostafaiyan

Sahand University of Technology, Tabriz, Iran
salami@sut.ac.ir

Abstract: The prediction of rheological behavior of multiphase fluid is very crucial in many applications. So, the exact estimation of the material function of such systems is very demanding. There are some challenges in estimating the material function which mostly encountered in case of using numerical and analytical methods. In most of the cases, we cannot employ the analytical methods, since the problem will be very complex and sometimes there in solution. Numerical methods suffer from the errors arising from the solution method. One of the main issues will appear when we are dealing with low velocities and/or frequency, such as low frequency behaviors in Small Amplitude Oscillatory Shear (SAOS) tests where numerical methods lead to provide spurious currents which is not physical. To overcome such difficulties, we proposed a newly developed Finite Element Analysis (FEA) scheme where it eliminate such fictional about 5 orders where its effect can be neglected. Some case of rheological test such as SAOS are simulated and the results are discussed. It is promising that the results show good agreement and the method can be used to study the various multiphase systems.

Cellular Fluid Dynamics

Ehssan Nazockdast

Department of Applied Physical Sciences, University of North Carolina at Chapel Hill, USA
ehssan@email.unc.edu

Abstract: Recent advancements in optical and electron microscopy provide us with the most detailed picture of the interior structure of the biological cell. These images show the cell interior as a very heterogenous and crowded environment filled with dynamic biopolymers, membranes, droplets, and vesicles that span from nano- to micron-scale. These structures are immersed in the fluidic cytoplasm, which mediates the transport of forces/stresses within and across the cell through hydrodynamic interactions. I will discuss two problems, where cellular fluid dynamics is at the heart of understanding the biological phenomenon: (1) poroelasticity to model cell mechanics and mechanotransduction, and (2) dynamics of filaments moving through the cell membrane.

Buoyant Injection of Viscoplastic Fluids

Seyed Mohammad Taghavi and Soheil Akbari

Department of Chemical Engineering, Université Laval, Québec, Canada
seyed-mohammad.taghavi@gch.ulaval.ca

Abstract: When an oil or gas well reaches the end of its lifetime, the plug and abandonment (P&A) process is performed, which includes placing a cement plug in the wellbore to isolate the reservoir and avoid the contamination of fresh water resources, soil, and atmosphere. From a fluid mechanics perspective, the placement process involves the injection of a heavy cement slurry (viscoplastic) into a light wellbore fluid (typically Newtonian). Inspired by the P&A process, we consider the fundamental problem of the injection of a heavy viscoplastic fluid (with a significant yield stress) into a light Newtonian fluid. We analyze the flow problem through experiments and modeling techniques, considering a buoyant miscible injection flow, with a small density difference between the two fluids. In our experiments, we consider the injection flow of a Carbopol solution (yield stress fluid) into salt water (Newtonian fluid). Accordingly, we also develop a mathematical model for the continuous downward injection of a viscoplastic fluid (following the Herschel-Bulkley constitutive equation) into another Newtonian fluid, inside a vertical closed-end pipe. The developed model describes the competition between the yield stress, the buoyancy, and the interfacial shear stress. Using the model and experiments, we successfully classify the different flow regimes that describe the flow dynamics, versus the governing dimensionless numbers. In particular, we observe and quantify three distinct flow regimes: a break-up regime, a coiling regime, and a buckling regime.

Keywords: Fluid injection, Viscoplastic fluids, Break-up, Coiling, Buckling

Nanocrystalline Cellulose (CNC) Suspension Rheology

Marziyeh Danesh and Savvas G. Hatzikiriakos

Department of Chemical & Biological Engineering, University of British Columbia, Vancouver, Canada
savvas.hatzi@ubc.ca

Abstract: The rheological properties and microstructure of nanocrystalline cellulose (CNC) aqueous suspensions at different concentrations have been investigated. The suspension is isotropic up to 3 wt.%, and phase separates to liquid crystalline and isotropic domains at higher concentrations where the samples exhibit a fingerprint texture and the viscosity profile shows a three-region behavior, typical of liquid crystals. The suspension behaves as rheological gel at even higher concentrations where the viscosity profile shows a single shear thinning behavior over the whole range of shear rates investigated. The effects of ultrasound energy and temperature on the rheological properties and structure of these suspensions were studied using polarized optical microscopy and rheometry. Our results indicate that the amount of applied ultrasound energy affects the microstructure of the suspensions, and the pitch of the chiral nematic domains. The flow behavior of Nanocrystalline Cellulose (CNC) hydrogels in the presence of a monovalent electrolyte (NaCl) as a function of CNC and salt concentration was also explored using a variety of linear and nonlinear rheological tests. We have first observed an apparent “slip yield stress” at small wall shear stress values that is mainly due to the onset of solid-like slippage of the hydrogels before their true yielding and deformation. This flow regime and the “slip yield stress” can be eliminated using sandpaper of optimum grit size. At higher wall shear stress values, two yielding points for CNC/salt network are seen in strain sweep tests due to network disruption and cluster deformation that depend on the concentration of both CNC (1-5wt%) and electrolyte (0-100mM). The first yield stress is due to yielding and flow of clusters, while the second one is due to breakage of clusters to small flocs and individual fibers. These yielding stresses were obtained by a variety of tests including strain amplitude sweep, creep and steady shear and their values are compared confirming their existence. Rheo-SALS (Small Angle Light Scattering) measurements confirmed structural changes as the scattering patterns change from isotropic to highly anisotropic with increase of deformation and rate of deformation. Moreover, Confocal Laser Scanning Microscopy (CLSM) and Polarized Microscopy (POM) images confirm the gradual breakup of clusters to smaller ones and eventually to nearly individual fibers with increase of the applied shear strain and rate.

Keywords: Nanocrystalline Cellule (NCC), Rheology, Suspension, Sonication, Chiral Nematic, Liquid Crystal

Evaluating the Effectiveness of Rice Bran Oil for Rejuvenating Rheological Properties of Aged Asphalt Binders in Recycled Asphalt Pavements

Mohammad Zia Alavi

University of Tehran, Tehran, Iran
zia.alavi@ut.ac.ir

Abstract: Due to the recent dramatic increase of asphalt binder cost as well as consideration of environmental concerns toward sustain development, the use of recycled asphalt pavement materials (RAP) has been increased over the years. One of the main issues for using RAP, especially at high percentages, in new asphalt mixes is the detection of the amount and properties of available aged asphalt binders in RAP. In mixes with high RAP content, usually, some chemical agents can be used to mobilize, soften, and rejuvenate the aged binders in RAP. This study focused on evaluating the effectiveness of rice bran oil for use as an additive for asphalt binder rejuvenation. For this purpose, the rheological properties of aged unmodified and polymer modified asphalt binders, after adding different amounts of rice bran oil, were evaluated. The rheological properties were measured using the dynamic shear rheometer (DSR), for binder resistance to permanent deformation and fatigue cracking, and the bending beam rheometer (BBR), for binder resistance to low-temperature cracking. The results showed that rice bran oil especially at higher doses was effective in regaining desired properties of aged binder against fatigue and low-temperature cracking. In addition, the asphalt binder softening due to the addition of rice bran oil was not too much to jeopardize the properties of the asphalt binder to combat permanent deformation at high temperatures.

Keywords: Asphalt binder, Rejuvenator, Rheology, Cracking, Recycled asphalt pavement

Application of Rheology in Controlling Competitive Reactions During Reactive Extrusion

Shervin Ahmadi

Petrochemical Faculty, IPPI. P.O. Box 14965/115, Tehran, Iran
Sh.Ahmadi@ippi.ac.ir

Abstract: During the last decade the polymer industry has experienced enormous rates of growth. due to an increasing demand for high performance polymer materials, the use of extruders as continuous reactors for polymers has attracted considerable attention in polymerization, polymer modification and blending applications. This presentation is an attempt to present a survey of recent application of rheology in controlling competitive reactions during reactive extrusion. Experimental studies for various reactive melt blending systems such as grafting of maleic anhydride on polyethylene, polypropylene degradation process and chain branching of the polyethylene are reviewed and some rheological and design aspects of reactive extrusion systems are addressed.

Keywords: Reactive extrusion, Viscosity, Grafting, Chain branching, degradation

Polymer Tribology and Its Correlation to Polymer Rheology

Mehdi Razzaghi-Kashani

Polymer Engineering Department, Faculty of Chemical Engineering,
Tarbiat Modares University, Tehran, Iran
mehdi.razzaghi@modares.ac.ir

Abstract: Many polymers and polymer composites are used in tribological applications in last few decades. Tribology, as a multidisciplinary topic, covers three main subjects as friction, wear, and lubrication. In macro- and micro-tribology of soft and deformable polymers, rheological characteristics of the polymer, such as viscoelastic properties in both linear and non-linear regimes, are employed to predict and control the coefficient of friction and abradability of these polymers. The role of interfacial effects (interphase and interface) in tribological properties of soft polymer composites are crucial. In nano-tribology scale, the slippage of polymer chains at the interface with filler particles needs to be engineered. In this regard, tribological interactions by introducing long chain silanes on the surface of silica in silicone rubber composites was proposed.

Rheology in Modern Pharmaceutics

Ismaeil Haririan

University of Tehran, Tehran, Iran
haririan@tums.ac.ir

Abstract: Nanotechnologies are based on chemistry of colloids. Colloids are mixtures of a solvent and suspended particles. They possess some optical and kinetic properties such as Brownian motion, Faraday Tyndall Effect, Coagulation, peptization, Dialysis as well as Diffusion, Osmotic pressure, Sedimentation and Viscosity. The viscosity of colloidal dispersion is affected by the shape of particles of the disperse phase. Heterogenous (rough) dispersion are used in Pharmaceutics such as suspension which are heterogeneous fluid containing solid particles that are sufficiently large for sedimentation. Particle size is > 1 μm. Stability of emulsions is important because of Emulsion inversion. Rheology of Flocculated emulsions such as Creaming & Slight Flocculation are dealing with great importance in drug manufacturing. Microfluidics, used for handling of Biomaterials which are used in contact with biological systems or in medical devices, refer to the behavior and control of liquids constructed to volumes near the μL range. Surface tension, Laminar flow and Diffusion in microfluidic systems are properties that differ greatly from macroscopic fluids. Microfluidic devices made by PDMS (Polydimethylsiloxane) which is trans-parent, non-fluorescent, biocompatible and nontoxic biomaterial, often have flows in the high-Peclet number and Low–Reynolds regime. Silicon Biomaterials are used as Wound care, Contact lenses (silicon – hydrogel), Single-use transport system in pharmaceutical manufacturing, and also Diagnostic devices and Tissue Engineering. On the other hands, solution viscosity, surface tension and controlled flow rate are among the parameters of electrospinning process for preparing scaffolds of tissue engineering. Flow control, here, is very important during initial application and during the curing process as well. Systems mentioned above are few examples of application of rheology in everyday designing and controlling the Pharmaceutical preparations and will be discussed in detail.

Capillarity and Wetting in Particulate Suspensions

Sachin Velankar

Department of Chemical Engineering, University of Pittsburgh, USA
velankar@pitt.edu

Abstract: The soft materials community has enormous knowledge about the structure and rheology of suspensions comprising particles dispersed in a liquid. Much less is known about suspensions composed of particles suspended in two immiscible fluids – systems in which capillary forces between particles play a major role. Such two-fluid particle suspensions can show a rich diversity of microstructures: particle networks aggregated by fluid menisci, compact capillary aggregates, Pickering emulsions, and bicontinuous morphologies. These microstructures result from a coupling between interfacial tension between the fluids, particle wettability, and viscous forces during mixing. Mixtures across a wide range of particle sizes and fluids shows similar behavior suggesting that such coupling has some universal features. Our experimental studies have explored this coupling in particles dispersed in two immiscible polymeric liquids. This talk will catalog the transitions between various microstructures, and the corresponding changes in rheology, as composition is changed. We will show how a non-equilibrium state diagram can be constructed for ternary mixtures of particles and two fluids, and how this state diagram can be tuned by factors such as particle shape or fluid viscosities. Clear understanding of such a non-equilibrium state diagram can guide new approaches for materials processing. We will provide examples of macroporous materials or conductive polymer composites, whose development was guided by these insights.

Dispersion Done (much) Better: Harnessing Extensional Flow in Polymer Blending and Compounding

João Maia

Case Western Reserve University, Department of Macromolecular Science and Engineering, Cleveland, OH, USA
joao.maia@case.edu

Abstract: The dispersive mixing capability of twin-screw extruders (TSE) is hindered by the fact that standard kneading elements (KE) impose a shear-dominated flow and, thus, suffer from limited ability to effectively disperse highly viscous disperse phases, be they polymeric or solids, in a polymeric matrix. Extensional flows, on the other hand, suffer from no such limitations and are theoretically capable of providing much improved dispersive mixing. However, attempts to perform extension-dominated mixing in extrusion operations have been few and far in between, with decidedly underwhelming results.
In this presentation, a recently developed type of extensional mixing element (EME) for single-screw extruders (SSE) and intermeshing TSEs will be reviewed and its efficiency in improving dispersive mixing significantly when compared, with nanoparticles of different geometries with standard two-lobed KEs will be demonstrated. In particular, we will show that the EMEs are highly efficient mixers for a number of systems, including immiscible and compatibilized polymer blends and polymer nanocomposites (0D, 1D and 2D). We will also demonstrate that by extending the EME concept to use in SSEs, it is also possible to significantly improve their dispersive mixing capability (a known shortcoming of SSEs), to the point the mixing levels become similar to those of TSEs equipped with standard KEs.

Rheology as a Tool to Control the Jet Ability of Inkjet Inks

Amir Rezvani Moghaddam

Department of Polymer Engineering, Sahand University of Technology, Tabriz, Iran
arezvai@sut.ac.ir

Abstract: In recent years, inkjet technology has been nominated as a promising method to print desired patterns in industrial applications such as display fabrication, control-release drug delivery, anti-counterfeit and 3D printing. Rheology as a tool which is the deformation study of the ink under an applied stress/strain can be useful to determine the behavior of ink in channel, nozzle and on the substrate during the printing process and control the drop ejection properties. The viscosity of inkjet ink is one of the rheological properties responsible to achieve high print quality. Usability of inks, good ink transfer and resolution parameters of the printed patterns can be directly related to the viscosity value of the ink. In this presentation, I will talk about “Rheology” as a tool to control the jet ability of inkjet inks.

Designing Complex Fluid Rheology-Microstructure and Measurements

Jie Song and Patrick Spicer

School of Chemical Engineering, University of New South Wales, Sydney, Australia
p.spicer@unsw.edu.au

Abstract: The formation of colloidal gels is a common technique for creating yield stress fluids at low volume fractions by exploiting attractive interactions between particles to form a sparse elastic network. In formulated products and biological cells, rod-shaped colloids and fibers can reduce material usage versus more compact particles because of their larger frequency of interaction and efficient use of volume. Nanocellulose, prepared by fermentation or degradation of plant fibers, has been studied recently for its unique mechanical, electrical, and biological properties, but the rheology of nano cellulose dispersions, and the application of their unique microstructure, is of increasing interest as well. Here we study the lower volume fraction limits of stable gel formation by the cellulose fibers and introduce a new microrheological approach to characterizing such fragile, yet efficient, networks. We also discuss the rational design of commercial fluid products by combination of multiple fluid properties to achieve benefits in fluid flow, suspension, and long-term stability.

Effect of Matrix Molecular Weight on the Dispersion Behavior of Cellulose Nanocrystal

Mohammadreza Nofar

Metallurgical & Materials Engineering Department, Faculty of Chemical and Metallurgical Engineering, Istanbul Technical University, Maslak, Istanbul, Turkey
nofar@itu.edu.tr

Abstract: In this study, the effect of molecular weight and crystallizability of PLA matrix on the PLA/CNC nanocomposite morphology was systematically investigated using rheological experiments. PLA/CNC nanocomposites containing 1, 3, 5, 7, and 10 wt% of CNC were prepared using solution casting method. The comparison of the effect of PLA molecular weight indicated that CNC could form a percolation network at lower contents when low molecular weight PLA was used as the matrix. This finding attributed to the easier interpenetration of shorter PLA chains and CNC nanoparticles in the solvent. On the other hand, it was observed that the use of PLA with higher crystallizability caused further reduction of the onset of CNC percolation network concentrations. This was because during the solvent evaporation step, which was at around 85oC, the isothermal cold crystallization of PLA around the dispersed CNCs could become more favorable and thereby the heterogeneous crystal nucleation could prevent the driving force of the CNCs towards aggregation.

Keywords: Polylactide, Cellulose Nanocrystals, Nanocomposites, CNC dispersion, rheological properties

Application of 0D and FSI in Patient-Specific Modeling of Blood Flow in Children with Congenital Heart Disease

Alex G. Kuchumov[1], Marat Kamaltdinov[2], and Artem Porodikov[3]

1. Department of Computational Mathematics, Mechanics and Biomechanics, Perm National Research Polytechnic University, Russia
2. Department of Mathematical Simulation of Systems and Processes, Federal Scientific Center for Medical and Preventive Health Risk Management Technologies, Russia
3. S.G. Sukhanov Cardiovascular Federal Center, Russia
kychymov@inbox.ru

Abstract: Children mortality rates due to congenital heart disease are rapidly increasing recently in the World. One of the surgical methods for the congenital heart disease treatment is modified Blalock–Taussig shunt (MBTS) placement. Often, surgeons use their own experience to choose the shunt for the operation that leads to a number of complications. To improve the efficiency of decision-making in surgical practice, it is necessary to develop patient-specific model, which allows to predict outcomes of medical interventions. We proposed a concept scheme of the circulatory system by combination of 0D model (systemic blood flow) + 3D model (aorta and pulmonary artery). A mathematical 0D formulation of the problem of modeling systemic circulation has been developed, which contains 13 differential equations. The model parameters are obtained based on the real patient data. A numerical implementation is carried out to solve the model relations using the 4 order Runge-Kutta method. The simulation results allow to determine the parameters of pressure and blood flow from time to time in any part of the proposed arterial circulation scheme, as well as the blood flow passing through the shunt, depending on its resistance. Moreover FSI simulations of blood flow in aorta and pulmonary artery with were performed. To proceed FSI modelling, it is necessary to know either mechanical properties of aorta and graft or rheological properties of blood. We examined both Newtonian and non-Newtonian (Carreau's model) models for blood flow simulations. Experimental studies of the mechanical properties vascular Gore-Tex® grafts adopted for pediatric modified Blalock-Taussig shunts were carried out. Parameters of two models (5-parameter Mooney-Rivlin model and the 3-parameter Yeoh model) were determined by uni-axial experimental curves fitting. The obtained data were used for patient-specific FSI modeling of local blood flow in the "aorta – MBTS – pulmonary artery" system in three variants of shunt location: central, right and left. The aortic wall is considered to be anisotropic, whereas Gore-Tex® vascular graft is modelled as an isotropic hyperelastic material. As a result of the problem solution, the hemodynamic parameters distributions (velocity, pressure, wall shear stress, time-averaged wall shear stress, oscillatory shear index) were found.

Keywords: blood - 0D model - FSI - shunt

Introduction

Children mortality rates due to congenital heart disease (CHD) are rapidly increasing recently in the World. Russia lags behind China and the US. Nevertheless, the number of children with CHD is quite large. To restore blood circulation during congenital heart disease, modified Blalock–Taussig shunts are used. This is small polymer tubes connecting aorta and pulmonary artery One of the surgical methods for the congenital heart disease treatment is modified

Blalock–Taussig shunt (MBTS) placement [1]. The complications of MBTS installation are mainly related to the thrombosis development when small shunts are used and hypervolemia occurrence when larger diameter shunts. Thus, the choice of optimal shunt diameter and selection the place to install is quite complicated task that have not been solved yet. Often, surgeons use their own experience to choose the shunt for the operation that leads to a number of complications.

The different hemodynamic parameters such oscillatory shear index, wall shear stress and time-averaged wall shear stress are known to be predictors of atherosclerosis and thrombosis. So, patient-specific modelling can be promising tool for evaluation of the treatment efficiency.

The main goal of the overall project is to develop a patient-specific model to assess and predict the effectiveness of MBTS surgery.

Theoretical

We proposed 0D/3D model of blood circulation, where aorta, pulmonary artery and aortic valve were considered as 3D models; the other parts are modelled by 0D elements (Fig. 1).

A mathematical 0D formulation of the problem of modeling systemic circulation has been developed, which contains 13 differential equations and several dozen algebraic relations. The model parameters in the first approximation are obtained based on real survey data and analysis of literature sources. A numerical implementation is carried out to solve the model relations using the Runge-Kutta methods of 4 orders of magnitude. The simulation results allow to determine the parameters of pressure and blood flow from time to time in any part of the design scheme, as well as the blood flow passing through the shunt, depending on its resistance.

2-way FSI analysis was performed to take into account a compliance of aorta and shunt. Ansys CFX (Ansys Inc., USA) was used for numerical computations.

Magnetic resonance imaging (MRI) data sets of 10 patients were acquired for creation of aorta–shunt patient-specific models. The segmentation and 3d model creation was performed by adopting ITK–SNAP software (www.itksnap.org). The information

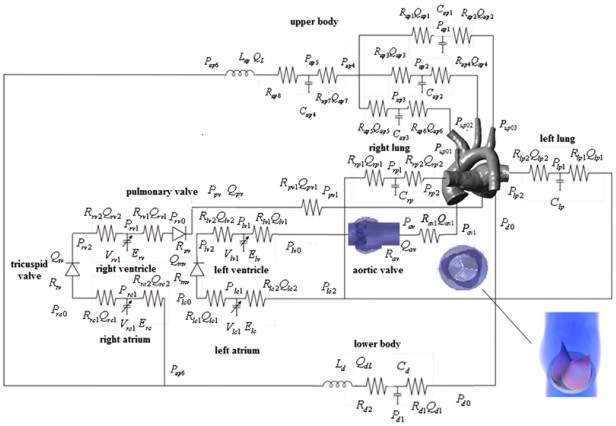

Fig 1. Concept scheme of blood circulation by 0D/3D coupling.

on the MBTS performance in 6 months after shunt installation was also used for hemodynamic parameters comparison. The aorta mechanical properties considered as a hyperelastic material were taken from paper [2]. Mechanical tests of shunts (n=10) by using Zwick (Zwick Roell Group, Germany) testing machine were performed to find their mechanical properties. The ends of solid aorta domain were constrained by specifying zero displacements in all directions and prohibiting the rotation about all axes. Blood was considered as Newtonian and non-Newtonian fluid (Carreau's model) to reveal the differences between these two approaches.

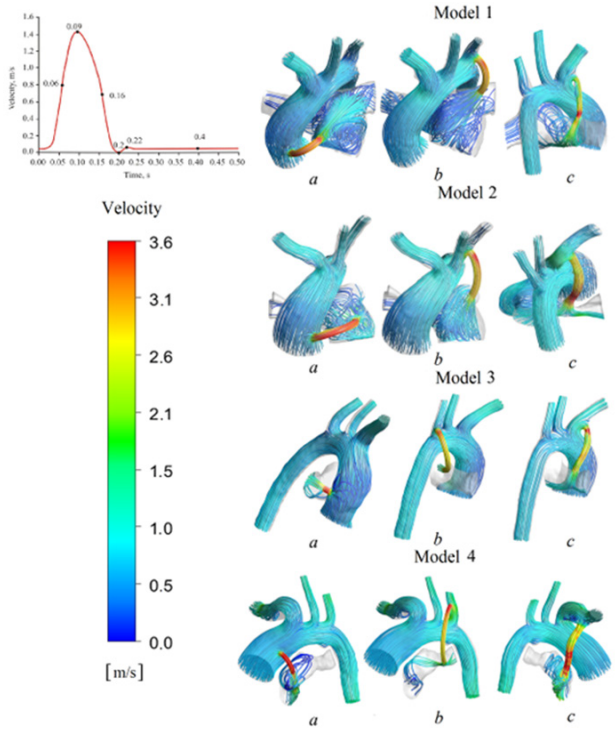

Fig. 2. Veocity distribution: a) central shunt, b) right shunt, c) left shunt.

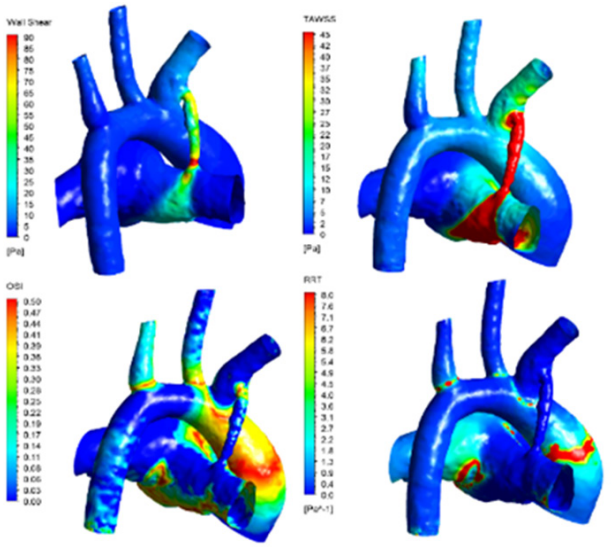

Fig. 3. WSS, TAWSS, OSI, and RRT distributions in the aorta-shunt region in a patient.

Results and Discussion

As a result of the problem solution, the hemodynamic parameters distributions (velocity, pressure, wall shear stress, time-averaged wall shear stress, oscillatory shear index, relative residence time) were found. The most interesting results correspond to the maximum value of the blood flow rate.

Fig. 2 shows the distribution of velocity characteristics of the blood flow. In the aortic region, blood flow has a uniform distribution. As blood move away from the descending part of the aorta, there is an equalization of blood flow velocity. The reverse situation can be observed in the pulmonary artery, where mainly a vortex blood flow with the exception of model 3 due to its geometric features can be seen. At the peak of systole, the maximum values of blood flow are shifted to the shunt region. Local blood velocity increase occurs due to the lumen narrowing and heterogeneity of the shunt shape (right shunt configuration).

Using formulas presented in paper [3], we computed OSI, RRT, WSS, and TAWSS and compared to clinical data to validate a correlation between hemodynamic parameters prediction of thrombosis with real situation. Fig. 3 contains an example of distributions for one patient.

Conclusion

We developed a model of blood circulation as a 0D/3D system. So, now can take into account blood flow in aorta with/without shunt. Some benchmark tests were performed to evaluate patient-specific parameters based on the clinical data.

Acknowledgements

The reported study was funded by RFBR and Perm Territory, project number 20-41-596005.

References

1. Kuchumov A., Selyaninov A., *Adv in Intel Sys and Comp*, **1018**, 576–580, 2020.
2. Jia Y. et al., *Ann Thorac Surg*, **99**, 1399–1407, 2015.
3. Chen Y. et al., *Sci Rep*, **7**, 40724, 2019.

Stabilization of Purely Elastic Instabilities in Cross-Slot Geometries

Mahdi Davoodi

Schlumberger Cambridge Research Center, UK
mdavoodi@slb.com

Abstract: Here, two-phase flows of Newtonian and/or viscoelastic fluids in a 'cross-slot' geometry are investigated both experimentally and numerically in the creeping-flow limit. A series of microfluidic experiments – using Newtonian fluids – have been carried out in different cross-section aspect ratios to support our numerical simulations. The numerical simulations rely on a volume of fluid method and make use of a log-conformation formulation in conjunction with the simplified viscoelastic Phan-Thien and Tanner model. Downstream from the central cross, once the flow has become fully developed, we also estimate analytically the thickness of each fluid layer for both two- and three-dimensional cases. In addition to providing a benchmark test for our numerical solver, these analytical results also provide insight into the role of the viscosity ratio. Injecting two fluids with different elastic properties from each inlet arm is shown to be an effective approach to stabilize the purely elastic instability observed in the cross-slot geometry based on the properties of the fluid with the larger relaxation time. Our results show that interfacial tension can also play an important role in the shape of the interface of the two fluids near the free-stagnation point (i.e. in the central cross). By reducing the interfacial tension force, the interface of the two fluids becomes curved and this can consequently change the curvature of streamlines in this region which, in turn, can modify the purely elastic flow transitions. Thus, increasing interfacial tension is shown to have a stabilizing effect on the associated steady symmetry-breaking purely elastic instability. However, at high values of the viscosity ratio, a new time-dependent purely elastic instability arises most likely due to the change in streamline curvature observed under these conditions. Even when both fluids are Newtonian, outside of the two-dimensional limit, a weak instability arises such that the fluid interface in the depth (neutral) direction no longer remains flat.

Theoretical Modeling and Experimental Study of Rheological Behavior of Bentonite-Based Drilling Fluid Containing Synthetic Polymer

Ahmad Ramazani S.A.

Department of Chemical and Petroleum Engineering, Sharif University of Technology, Tehran, Iran
ramazani@sharif.edu

Abstract: We propose a new model capable of describing the complex bonds dynamic as well as simulating the viscoelastic behavior of a class of associative covalent adaptive networks known as vitrimers. In contrast to conventional thermosets, vitrimers represent a novel class of plastics in which covalent chemical bonds can be efficiently and reliably exchanged between different positions of the polymer network without risking structural damage or permanent loss of material properties. They show creep and stress-cracking resistance at low temperatures and are malleable at high temperatures. In this study, a combination of coarse-grained molecular dynamics (MD) and Monte Carlo (MC) simulations is employed to predict the microstructure, dynamics, and linear rheology of vitrimers. Using the time-temperature superposition (TTS) principle, the moduli of a vitrimer network are compared with that of a permanently crosslinked one over a wide range of frequencies. Results of the temperature dependence of the horizontal shift factors, which are the normalized relaxation of time, of the vitrimer show an Arrhenius temperature dependence at a temperature above the topology freezing temperature, while at lower temperatures, they follow the Williams-Landel-Ferry's (WLF) equation. On the other hand, the shift factors obtained from the rheology of a permanently crosslinked network obey the WLF equation behavior over the selected range of the temperature. Using the same shift factors, the mean squared displacement data of the network segments are collapsed on universal curves. Furthermore, these two sets of dynamical and rheological quantities are linked to each other via the generalized Stokes-Einstein relationship. Results will also be presented for the temperature dependence of the characteristic time of the intermediate scattering function, and the correlation between this characteristic time and the shift factors used in creating the universal rheological and dynamic curves using TTS will be discussed. The results and methodology presented in this study provide a molecular-level understanding of the dynamics of vitrimers and help to quantify the characteristics that lead to the experimental thermophysical properties.

Relationship between Microstructural Relaxation and Macroscopic Properties of Vitrimers

Fardin Khabaz

University of Akron, USA
fkhabaz@uakron.edu

Abstract: We propose a new model capable of describing the complex bonds dynamic as well as simulating the viscoelastic behavior of a class of associative covalent adaptive networks known as vitrimers. In contrast to conventional thermosets, vitrimers represent a novel class of plastics in which covalent chemical bonds can be efficiently and reliably exchanged between different positions of the polymer network without risking structural damage or permanent loss of material properties. They show creep and stress-cracking resistance at low temperatures and are malleable at high temperatures. In this study, a combination of coarse-grained molecular dynamics (MD) and Monte Carlo (MC) simulations is employed to predict the microstructure, dynamics, and linear rheology of vitrimers. Using the time-temperature superposition (TTS) principle, the moduli of a vitrimer network are compared with that of a permanently crosslinked one over a wide range of frequencies. Results of the temperature dependence of the horizontal shift factors, which are the normalized relaxation of time, of the vitrimer show an Arrhenius temperature dependence at a temperature above the topology freezing temperature, while at lower temperatures, they follow the Williams-Landel-Ferry's (WLF) equation. On the other hand, the shift factors obtained from the rheology of a permanently crosslinked network obey the WLF equation behavior over the selected range of the temperature. Using the same shift factors, the mean squared displacement data of the network segments are collapsed on universal curves. Furthermore, these two sets of dynamical and rheological quantities are linked to each other via the generalized Stokes-Einstein relationship. Results will also be presented for the temperature dependence of the characteristic time of the intermediate scattering function, and the correlation between this characteristic time and the shift factors used in creating the universal rheological and dynamic curves using TTS will be discussed. The results and methodology presented in this study provide a molecular-level understanding of the dynamics of vitrimers and help to quantify the characteristics that lead to the experimental thermophysical properties.

Slurries of Complex Fluids

Sarah Hormozi

Cornell University, USA
hormozi@cornell.edu

Abstract: Suspensions of non-Brownian particles in viscous fluids, for which thermal fluctuations are negligible, are relevant in industrial processes (e.g. waste disposal, concrete, drilling muds, metalworking chip transport, and food processing) and in natural phenomena (e.g. flows of slurries, debris, and lava). It is also relevant to mention that some biological and smart materials can be designed from various suspensions, drawing attention to applications in physiology, biolocomotion, shock absorbers, and beyond. This countless number of suspensions has a wide range of nonlinear rheological behaviors, such as shear thinning, shear thickening, shear banding, yield stress, and finite normal stress differences even when inertia is negligible. For applications enumerated above, even small increases in efficiency when processing slurries of complex fluids could make significant positive economic and environmental impacts. Obviously, a thorough understanding of the rheology and fluid mechanics of these materials in natural and industrial settings is essential to improving the efficiency of production. However, this is extremely challenging due to the complex rheology of the suspending fluids, the interaction of fluid and particle phases, and multiple-body and short-range interactions of particles. My presentation will introduce an array of experimental and modeling techniques that my research team uses to investigate the rheological properties and fluid dynamical behavior of complex suspensions. The goal is to establish a continuum framework and refine it through a series of microstructure investigations. I will discuss how our recent results can be used to address and resolve some of the industrial issues. Finally, open questions will be disclosed, which must be answered to build a firm foundation for a long-term contribution to the area of complex suspensions.

Colloidal Gels: Rheology, Thixotropy and Microstructure

Safa Jamali

Department of Mechanical and Industrial Engineering, Northeastern University, Boston, MA, USA
s.jamali@northeastern.edu

Abstract: Colloidal particles have been proposed to be the building blocks for new generation of structured materials with superior properties. The transient and dynamic nature of microstructural changes in colloidal gels results in a thermokinematic memory and a pronounced sensitivity to shear and thermal history of the particulate system. This is commonly referred to as material "Thixotropy". I will discuss the origin of thixotropic effect in these time and rate-dependent materials, through investigation of hysteresis across different length scales: from particle-level local measurements of particle coordination number (microscale), to structural heterogeneities and density fluctuations (mesoscale), to transient shear stress to an imposed deformation (macroscale). Based on these understandings I will discuss structure formation under an applied deformation in general. Aggregation of attractive colloids have been extensively studied not only from a theoretical perspective, but also with respect to fraction of solid particles, and the range, type and strength of attractive or repulsive forces in between particles. Colloidal gels, as disordered assemblies of attractive colloids also have been investigated with regards to percolation, phase separation, and characteristics of the resulting fractal networks. Despite a tremendous progress in our understanding of the gelation process, and different routes for arrest of the dynamics in attractive colloids, the interplay between the transport processes and many-body effects in such systems has limited our ability to drive the system towards a specific configuration. I will talk about gelation of short-ranged attractive colloids, far from equilibrium and will present a Time-Rate-Transformation diagram adapted from understanding of materials processing in much stiffer glassy metallic systems for targeted assembly of attractive colloidal particles.

Conference Articles

(In order of code number)

14-15 December 2021, Tehran, Iran
2nd International Conference on Rheology
ICOR 2021
article A-10-234-12

Effect of Rheometrical Parameters of EPDM in Flexible Elastomeric Foaming

Peyman Ezzati[1*], Arvin Mohammadi[2], Nima Taremi[2], Mohammad Hashemi[2], and Mohammad Reza Alizadehfard[1]
1. Osmotec, P.O. BOX 571, Turramurra NSW 2074 Sydney, Australia
2. Linkran Industrial Group, P.O. Box 90210, Tehran, Iran

*peyman@osmotec.com.au

Abstract
In this study rheometrical behavior of EPDM compound in closed cell flexible elastomeric foam (FEF) was investigated. In manufacturing of EPDM FEF, rheometrical parameter shown that production are based on curing and blowing behavior. Studies of rheometric diagram of EPDM foam with different kind of formulation show curing and blowing occurred. The parameters that showed difference in formulations are such as scorch time, curing rate index (CRI), minimum torque (ML) and maximum torque (MH). Scorch time studies has shown that process must be start with progress of blowing and curing must occur at the second. CRI in highest level helps cells with N_2 gas cur simultaneously with help of ultrafast curing acceleration. MH and ML are the parameters with different volume in diverse of formulation and must be check for each product. MH: 300% modulus, ML: viscosity, MH-ML: Chain Length Duration (CLD).

Keywords: EPDM, rheologic, rheometrie, diagarm, closed cell, FEF

Introduction

Closed-cell elastomeric insulation is one of the most modern insulations in the world, which provides thermal, cooling, and acoustic insulation properties. In this regard, their up-to-date production has special sensitivities. Elastomeric Insulations In addition to being a low-density swollen foam, they are also an elastomeric piece that has elastic properties. This piece of elastic foam has millions of closed-cells containing nitrogen gas, which is made in the production process and performs the main load of insulation. EPDM is commonly used as a base elastomer in the fabrication of closed-cell elastomeric insulation. In this research, an attempt has been made to study and obtain the best form of insulation that has both of this properties such as low density and uniformity and complete closed-cells by examine the torques graph had shown in rheometrical test.

Experimental

Raw Materials and Testing

In this study EPDM from, Keltan Company with 3430 G grade was used. ADC was used as a foaming agent. Sulfur was used as the curing agent and fast curing systems were used as accelerators. DOP oil was used as a softener of mixture. Soot with grade 330 was used.

Results and Discussion

A rheometer is a laboratory measuring instrument that, unlike viscometers, is used to measure some augmentation parameters such as dynamic viscosity, shear velocity and shear stress. The operation mechanism of this device is by examining the power required to rotate a stirrer inside the sample, parameters such as dynamic viscosity are measured by this test. It is a tool for determining the characteristics of rubber and vulcanized (baked) compounds. As you know, the raw materials of rubbers in raw form have low properties that cannot be used in industries, but when combines with additives and bakes create a uniform, stable mixture. The important obstacle is the appropriate time of curing these materials which is not stable, according to the type of material and additives in it and due to the lack of re-deformation after curing rubber, it is necessary to provide appropriate information before injection or molding. Timing is very important in

this mold of rubber forming process or in injecting, since the material shaping does not change after baking, the curing agent must be in the final stage and after adding all the necessary additives should be added. To perform rheometric tests from the MDR rheometer of the GDM Turkey Company. In the temperature of 180 °C in 10 min. The arch-density of the produced foams was measured

Table 1. Formulation of FEF based on EPDM in phr*.

Sample	FEF 1	FEF2	FEF3
EPDM	100	100	100
C.B. 330	10	10	10
DOP	50	50	50
ADC	75	75	75
S	1	3	5
Accelerators	8.5	8.5	8.5
*phr: per hundred resin			

by device made in China. Curing agent must be in the final stage after adding all the necessary additives. The scenario of flexible elastomeric closed-cell Insulation foam production is that the compound which enters the furnace moves from a low temperature from 130 °C to a high temperature as 180 °C inside the furnace. Upon the first entering temperature zone, nitrogen gas is releases slowly from ADC. This gas must be trapped inside the final cells and then it cooks to keep the gas inside with no evacuation. The scorch time should be accurate so compound cooking start at last as all the nitrogen gas releases. After that, the cooking process must be fast enough to cook the cell quickly to makes millions of cells at the same time. In order of making flexible closed cells with such elastic properties so that bursting does not occur in the cell under tensile and compressive stresses. To meet all the expectations, three samples of mixtures with three different amounts of sulfur were produced. In the sample with the highest sulfur, the maximum torque was accord, indicating a modulus value of 300% higher. But the values of the torque were same and it cannot be considered effective in the production of closed cell foam because the mooney viscosity of the compounds had the same values. The cooking speed of all three mixes was almost the same because a kind of static cooking system was used with the same accelerators from the fast family. But to some extent, with the increase of sulfur, the cooking speed almost increased. In the three mixtures produced, the difference between the maximum and minimum torque, which indicates the length of the cross joints, increased. This higher value in sulfur indicates that the C-Sn-C bond length is longer and more elastic in trapping more nitrogen gas. Therefore, the best state of production of closed cell elastomeric insulation was seen in sample number 3, density was 44 kg/m^3. But samples number 2 and 3 were 65 and 95 kg/m^3.

Table 2. Rheometerical parameters of samples.

Sample	FEF 1	FEF2	FEF 3
MH (n.m)	2.57	2.08	1.65
ML (n.m)	0.24	0.23	0.22
S2 (min: s)	5	5	5
S90 (min: s)	1:54	2:05	2:41
CRI	25	20	18
Density (kg/m^3)	95	65	44

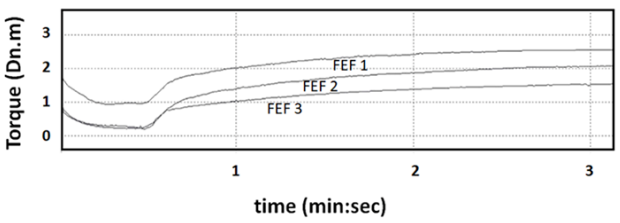

Fig 1. Rheometer diagram based on data from Table 1.

Acknowledgment

We would like to thank the Board of Directors and the Managing Director of Linkran Industrial Group for investing in research on Linkran elastomeric insulation.

References

[1] Kass K., Blumberga A., Blumberga D., Zogla G., Kamenders A., and Kamendere E., Pre-assessment method for historic building stock renovation evaluation, *Energy Proced.*, **113**, 346-353, 2017.

[2] Dylewski R. and Adamczyk J., The environmental impacts of thermal insulation of buildings including the categories of damage: a polish case study, *J. Clean. Prod.*, **137**, 878-887, 2016.

[3] Blumberga A., Timma L., and Blumberga D., System dynamic model for the accumulation of renewable electricity using power-to-gas and power-to-liquid concepts, *Environ. Clim. Technol.*, **16**, 54-68, 2015.

[4] Kamenders A., Vilcane L., Indzere Z., and Blumberga D., Heat demand and energy resources balance change in latvia, *Energy Proced.*, **113**, 411-416, 2017.

[5] Adityaa L., Mahliaa T.M.I., Rismanchic B., Nge H.M., Hasane M.H., Metselaare H.S.C., Oki M., and Aditiyab H.B., A review on insulation materials for energy conservation in buildings, *Renew. Sustain. Energy Rev.*, **73**, 1352-1365, 2017.

[6] Fanga Z., Lia N., Lia B., Luod G., and Huanga Y., The effect of building envelope insulation on cooling energy consumption in summer, *Energy Build.*, **77**, 197-205, 2014.

[7] Schuchardt G.K., Integration of decentralized thermal storages within district heating (DH) networks, *Environ. Clim. Technol.*, **18**, 5-16, 2016.

14-15 December 2021, Tehran, Iran
2nd International Conference on Rheology
ICOR 2021
article A-10-234-13

The Effect of Rheometrical Parameters of EPDM in Flexible Elastomeric Foaming

Peyman Ezzati[1*], Arvin Mohammadi[2], Nima Taremi[2], Mohammad Hashemi[2], and Mohammad Reza Alizadehfard[1]
1. Osmotec, P.O. BOX 571, Turramurra NSW 2074 Sydney, Australia
2. Linkran Industrial Group, P.O. Box 90210, Tehran, Iran

*peyman@osmotec.com.au

Abstract
In this study, rheometrical behavior of EPDM compound in closed-cell flexible elastomeric foam (FEF) was investigated. In the manufacturing of EPDM FEF, rheometrical parameters shown that products are based on curing and blowing behavior. Studies of rheometric diagram of EPDM foam with a different kind of formulation show curing and blowing occurred. The parameters that showed differences in formulations are such as scorch time, curing rate index (CRI), minimum torque (ML), and maximum torque (MH). Scorch time studies have shown that process must start with the progress of blowing and curing must occur at the second. CRI at the highest level helps cells with N_2 gas cur simultaneously with help of ultrafast curing acceleration. MH and ML are the parameters with different volumes in diverse formulations and must be check for each product. MH: 300% modulus, ML: viscosity, MH-ML: Chain Length Duration (CLD).

Keywords: EPDM, rheologic, rheometrie, diagarm, closed cell, FEF

Introduction

Closed-cell elastomeric insulation is one of the most modern insulations in the world, which provides thermal, cooling and acoustic insulation properties. In this regard, their up-to-date production has special sensitivities. Elastomeric Insulations In addition to being a low-density swollen foam, they are also an elastomeric piece that has elastic properties. This piece of elastic foam has millions of closed-cells containing nitrogen gas, which is made in the production process and performs the main load of insulation. EPDM is commonly used as a base elastomer in the fabrication of closed-cell elastomeric insulation. In this research, an attempt has been made to study and obtain the best form of insulation that has both of this properties such as low density and uniformity and complete closed-cells by examine the torques graph had shown in rheometrical test.

Experimental

Raw Materials and Testing

In this study EPDM from, Keltan Company with 3430 G grade was used. ADC was used as a foaming agent. Sulfur was used as the curing agent and fast curing systems were used as accelerators. DOP oil was used as a softener of mixture. Soot with grade 330 was used.

Results and Discussion

A rheometer is a laboratory measuring instrument that, unlike viscometers, is used to measure some augmentation parameters such as dynamic viscosity, shear velocity and shear stress. The operation mechanism of this device is by examining the power required to rotate a stirrer inside the sample, parameters such as dynamic viscosity are measured by this test. It is a tool for determining the characteristics of rubber and vulcanized (baked) compounds. As you know, the raw materials of rubbers in raw form have low properties that cannot be used in industries, but when combines with additives and bakes create a uniform, stable mixture. The important obstacle is the appropriate time of curing these materials which is not stable, according to the type of material and additives in it and due to the lack of re-deformation after curing rubber, it is necessary to provide appropriate information before injection or molding. Timing is very important in this mold of rubber forming process or in injecting, since the material shaping does not change after baking, the curing agent must be in the final stage and after adding all the necessary additives should be added. To perform rheometric tests from the MDR rheometer of the GDM Turkey Company. In the temperature of 180 °C in 10 min. The arch-density of the produced foams was measured by device made in China. Curing agent must be in

Table 1. Formulation of FEF based on EPDM in phr*.

Sample	FEF 1	FEF2	FEF 3
EPDM	100	100	100
C.B. 330	10	10	10
DOP	50	50	50
ADC	75	75	75
S	1	3	5
Accelerators	8.5	8.5	8.5
*phr: per hundred resin			

the final stage after adding all the necessary additives. The scenario of flexible elastomeric closed-cell Insulation foam production is that the compound which enters the furnace moves from a low temperature from 130 °C to a high temperature as 180 °C inside the furnace. Upon the first entering temperature zone, nitrogen gas is releases slowly from ADC. This gas must be trapped inside the final cells and then it cooks to keep the gas inside with no evacuation. The scorch time should be accurate so compound cooking start at last as all the nitrogen gas releases. After that, the cooking process must be fast enough to cook the cell quickly to makes millions of cells at the same time. In order of making flexible closed cells with such elastic properties so that bursting does not occur in the cell under tensile and compressive stresses. To meet all the expectations, three samples of mixtures with three different amounts of sulfur were produced. In the sample with the highest sulfur, the maximum torque was accord, indicating a modulus value of 300% higher. But the values of the torque were same and it cannot be considered effective in the production of closed cell foam because the mooney viscosity of the compounds had the same values. The cooking speed of all three mixes was almost the same because a kind of static cooking system was used with the same accelerators from the fast family. But to some extent, with the increase of sulfur, the cooking speed almost increased. In the three mixtures produced, the difference between the maximum and minimum torque, which indicates the length of the cross joints, increased. This higher value in sulfur indicates that the C-Sn-C bond length is longer and more elastic in trapping more nitrogen gas. Therefore, the best state of production of closed cell elastomeric insulation was seen in sample number 3, density was 44 kg/m^3. But samples numbers 2 and 3 were 65 and 95 kg/m^3.

Acknowledgment

We would like to thank the Board of Directors and the Managing Director of Linkran Industrial Group for investing in research on Linkran elastomeric insulation.

Table 2. Rheometerical parameters of samples.

Sample	FEF 1	FEF 2	FEF 3
MH (n.m)	2.57	2.08	1.65
ML (n.m)	0.24	0.23	0.22
S2 (min: s)	5	5	5
S90 (min: s)	1:54	2:05	2:41
CRI	25	20	18
Density (kg/m^3)	95	65	44

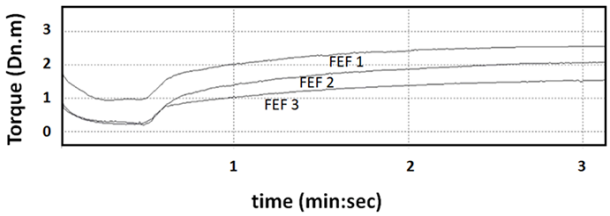

Fig 1. Rheometer diagram based on data from Table 1.

References

[1] Blumberga A., Timma L., and Blumberga D., System dynamic model for the accumulation of renewable electricity using power-to-gas and power-to-liquid concepts, *Environ. Clim. Technol.*, **16**, 54-68, 2015.

[2] Kamenders A., Vilcane L., Indzere Z., and Blumberga D., Heat demand and energy resources balance change in latvia, *Energy Proced.*, **113**, 411-416, 2017.

[3] Miezis M., Zvaigznitis K., Stancioff N., and Soeftestad L., Climate change and buildings energy efficiency–the key role of residents, *Environ. Clim. Technol.*, **17**, 30-43, 2016.

[4] Zamovskis M., Vanaga R., and Blumberga A., Mathematical modelling of performance of new type of climate adaptive building shell, *Energy Proced.*, **113**, 270-276, 2017.

[5] Fortuna S., Mora T.D., Peron F., and Romagnoni P., Environmental performances of a timber-concrete prefabricated composite wall system, *Energy Proced.*, **113**, 90-97, 2017.

[6] Adityaa L., Mahliaa T.M.I., Rismanchic B., Nge H.M., Hasane M.H., Metselaare H.S.C., Oki M., and Aditiyab H.B., A Review on Insulation Materials for Energy Conservation in Buildings, *Renew. Sustain. Energy Rev.*, **73**, 1352-1365, 2017.

[7] Fanga Z., Lia N., Lia B., Luod G., and Huanga Y., The effect of building envelope insulation on cooling energy consumption in summer, *Energy Build.*, **77**, 197-205, 2014.

[8] Schuchardt G.K., Integration of decentralized thermal storages within district heating (DH) Networks, *Environ. Clim. Technol.*, **18**, 5-16, 2016.

[9] Muresan A.A. and Attia S., Energy efficiency in the romanian residential building stock: a literature review, *Renew. Sustain. Energy Rev.*, **74**, 349-363, 2017.

[10] Vilhena A., Silva C., Fonseca P., and Couto S., Exterior walls covering system to improve thermal performance and increas service life of walls in rehabilitation interventions, *Construct. Build. Mater.*, **142**, 354-362, 2017.

14-15 December 2021, Tehran, Iran
2nd International Conference on Rheology
ICOR 2021
article A-10-234-16

Effect of Rheometrical Parameters of NBR in Flexible Elastomeric Foam

Peyman Ezzati[1*], Arvin Mohammadi[2], Nima Taremi[2], Mohammad Hashemi[2], and Mohammad Reza Alizadehfard[1]
1. Osmotec, P.O. BOX 571, Turramurra NSW 2074 Sydney, Australia
2. Linkran Industrial Group, P.O. Box 90210, Tehran, Iran

*peyman@osmotec.com.au

Abstract
In this study rheometrical behavior of NBR compound in closed cell flexible elastomeric foam (FEF) was investigated. In manufacturing of NBR, FEF curing and blowing affected on production which shown in rheometrical parameters. Rheometer diagram studies of different FEF foamed formulation based on NBR showed curing and blowing phenomenon simultaneously. These parameters were such as scorch time, curing rate index (CRI) minimum torque (ML) and maximum torque (MH). Scorch time showed that process must be design in the way that blowing should start at first and after blowing curing must occur. Blown cells whit N_2 gas contains must cure simultaneously so that it needs ultrafast curing acceleration and CRI in highest level. MH and ML parameters, must be check for each and individual product. MH, ML, MH-ML despite 300% modulus, viscosity, chain length duration (CLD) respectively.

Keywords: NBR, rheologic, rheometrie, diagarm, closed cell, FEF

Introduction

Closed-cell elastomeric insulation is one of the most modern insulations in the world, which provides thermal, cooling and acoustic insulation properties. In this regard, their up-to-date production has special sensitivities. Elastomeric insulations in addition to being a low-density swollen foam, they are also an elastomeric piece that has elastic properties. This piece of elastic foam has millions of closed-cells containing nitrogen gas, which is made in the production process and performs the main load of insulation. NBR is commonly used as a base elastomer in the fabrication of closed-cell elastomeric insulation. In this research, an attempt has been made to study and obtain the best form of insulation that has both of this properties such as low density and uniformity and complete closed-cells by examine the torques graph had shown in rheometrical test.

Experimental

Raw Materials and Testing

In this study NBR from, Kumho Company with 3430 G grade was used. ADC was used as a foaming agent. Sulfur was used as the curing agent and fast curing systems were used as accelerators. DOP oil was used as a softener of mixture. Soot with grade 330 was used.

Results and Discussion

A rheometer is a laboratory measuring instrument that, unlike viscometers, is used to measure some augmentation parameters such as dynamic viscosity, shear velocity and shear stress. The operation mechanism of this device is by examining the power required to rotate a stirrer inside the sample, parameters such as dynamic viscosity are measured by this test. It is a tool for determining the characteristics of rubber and vulcanized (baked) compounds. As you know, the raw materials of rubbers in raw form have low properties that cannot be used in industries, but when combines with additives and bakes create a uniform, stable mixture. The important obstacle is the appropriate time of curing these materials which is not stable, according to the type of material and additives in it and due to the lack of re-deformation after curing rubber, it is necessary to provide appropriate information before injection or molding. Timing is very important in this mold of rubber forming process or in injecting, since the material shaping does not change after baking, the curing agent must be in the final stage and after adding all the necessary additives should be added. To perform rheometric tests from the MDR rheometer of the GDM Turkey Company. In the temperature of 180 °C in 10 min. The arch-density of the produced foams was measured by device made in China. Curing agent must be in the final stage after adding all the necessary additives. The scenario of flexible elastomeric closed-cell Insulation foam

Table 1. Formulation of FEF based on EPDM in phr*.

Sample	FEF 1	FEF2	FEF 3
NBR	100	100	100
C.B. 330	10	10	10
DOP	50	50	50
ADC	75	75	75
S	1	3	5
Accelerators	8.5	8.5	8.5
*phr: per hundred resin			

production is that the compound which enters the furnace moves from a low temperature from 130 °C to a high temperature as 180 °C inside the furnace. Upon the first entering temperature zone, nitrogen gas is releases slowly from ADC. This gas must be trapped inside the final cells and then it cooks to keep the gas inside with no evacuation. The scorch time should be accurate so compound cooking start at last as all the nitrogen gas releases. After that, the cooking process must be fast enough to cook the cell quickly to makes millions of cells at the same time. In order of making flexible closed cells with such elastic properties so that bursting does not occur in the cell under tensile and compressive stresses. To meet all the expectations, three samples of mixtures with three different amounts of sulfur were produced. In the sample with the highest sulfur, the maximum torque was accord, indicating a modulus value of 300% higher. But the values of the torque were same and it cannot be considered effective in the production of closed cell foam because the mooney viscosity of the compounds had the same values. The cooking speed of all three mixes was almost the same because a kind of static cooking system was used with the same accelerators from the fast family. But to some extent, with the increase of sulfur, the cooking speed almost increased. In the three mixtures produced, the difference between the maximum and minimum torque, which indicates the length of the cross joints, increased. This higher value in sulfur indicates that the C-Sn-C bond length is longer and more elastic in trapping more nitrogen gas. Therefore, the best state of production of closed cell elastomeric insulation was seen in sample number 3, density was 44 kg/m^3. But samples number 2 and 3 were 65 and 95 kg/m^3.

Acknowledgment

We would like to thank the board of directors and the managing director of linkran industrial group for investing in research on Linkran elastomeric insulation.

Table 2. Rheometerical parameters of samples.

Sample	FEF 1	FEF 2	FEF 3
MH (n.m)	2.57	2.08	1.65
ML (n.m)	0.24	0.23	0.22
S2 (min: s)	5	5	5
S90 (min: s)	1:54	2:05	2:41
CRI	25	20	18
Density (kg/m^3)	95	65	44

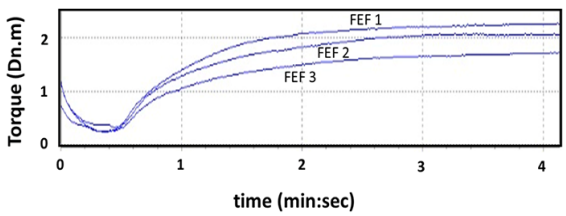

Fig 1. Rheometer diagram based on data from Table 1.

References

[1] Kass K., Blumberga A., Blumberga D., Zogla G., Kamenders A., and Kamendere E., Pre-assessment method for historic building stock renovation evaluation, *Energy Proced.*, **113**, 346-353, 2017.

[2] Dylewski R. and Adamczyk J., The environmental impacts of thermal insulation of buildings including the categories of damage: a polish case study, *J. Clean. Prod.*, **137**, 878-887, 2016.

[3] Blumberga A., Timma L., and Blumberga D., System dynamic model for the accumulation of renewable electricity using power-to-gas and power-to-liquid concepts, *Environ. Clim. Technol.*, **16**, 54-68, 2015.

[4] Kamenders A., Vilcane L., Indzere Z., and Blumberga D., Heat demand and energy resources balance change in latvia, *Energy Proced.*, **113**, 411-416, 2017.

[5] Miezis M., Zvaigznitis K., Stancioff N., and Soeftestad L., Climate change and buildings energy efficiency–the key role of residents, *Environ. Clim. Technol.*, **17**, 30-43, 2016.

[6] Zamovskis M., Vanaga R., and Blumberga A., Mathematical modelling of performance of new type of climate adaptive building shell, *Energy Proced.*, **113**, 270-276, 2017.

[7] Fortuna S., Mora T.D., Peron F., and Romagnoni P., Environmental performances of a timber-concrete prefabricated composite wall system, *Energy Proced.*, **113**, 90-97, 2017.

14-15 December 2021, Tehran, Iran
2nd International Conference on Rheology
ICOR 2021
article A-10-235-1

Investigation of Differences between Interface Viscoelastic Properties in Polyethylene/Polyethylene Blends with Montmorillonite or Joncryl ADR

Mohammadmahdi Negaresh
Master of Research and Development at Rangdaneh Sirjan Company, Postal Code 7815350837, Sirjan, Iran

*m_neg112@aut.ac.ir

Abstract
The linear viscoelastic properties of immiscible polyethylene/polypropylene blends filled with montmorillonite or compatibilized by Joncryl ADR, exhibiting droplet-matrix morphologies, have been studied. The flagrant compatibilizing effect of montmorillonite, particularly located at the interface, was attested and contrasted to the more general organic compatibilization due to the establishment of an interface. The results show that there are some resemblances between the two kinds of compatibilization, but primarily eminent remarkable differences in rheological properties of the two types of interphase involved in the compatibilization mechanisms. The major differences in interphase viscoelastic properties were evidenced not only directly from the experimental data like SEM, TEM photos and weighted relaxation spectra.

Keywords: the linear viscoelastic properties, immiscible polyethylene/polypropylene blends, montmorillonite, Joncryl ADR, compatibilizer

Introduction

Major polymer blends have a limited degree of miscibility due to the unique properties of homopolymers such as molecular weight and distribution, degree of polarity, solubility parameter, viscosity, elastic properties. Therefore, compatibility of polymer blends is one of the most important measures today to achieve engineering properties in various medical, military, transportation, packaging. Gradually, various methods such as the use of block copolymers, small molecule compatibilizers, in situ polymerization methods, using nanoparticles, etc. were developed to increase the compatibility of polymer blends [1]. The main mechanism of compatibilizer efficiency is its presence in the interface of the blends and the reduction of interfacial stress of the polymer components [2].

In this part, the claim that plate fillers cause a change in its rheological behavior due to being in the interface between the polymer components of the blend and creating an intermediate phase. Different samples behave differently in terms of the composition of the polymer components, as well as in blends containing different amounts of filler, and the intended changes either do not occur or are so small that they are negligible [3].

In this study, the main purpose is to investigate the differences in the mechanism of miscibility of blends by compatibilizers or nanoparticles. It seems that the nature and structure of the interface can be the difference between these two types of compatibility methods. Therefore, the study is performed on polyethylene/polypropylene blends in the presence of montmorillonite or in the presence of Joncryl ADR, and the results are briefly explained.

Experimental/Theoretical

Blends were prepared from two commercial immiscible polymers: a linear low density PE, 2426 K (Amir Kabir) and PP homopolymer HP 552 R (Jam). The organic compatibilizing agent used was an Joncryl ADR referenced as 18302 by Arkema. The montmorillonite used as filler in this work is an organically modified, namely C30B, supplied by Southern Korea.

The blends were prepared in an internal mixer at 50 rpm at 180° C for 6 min. The feeding of ingredients into the mixer was simultaneous. Blend samples were prepared in such a way that 20% by weight of polypropylene was present in them and montmorillonite from 0.5% to 2% by volume and Joncryl ADR from 0.5% to 5% by volume in compatible blends were used.

Results and Discussion

Initially, SEM images of the samples were prepared before and after the presence of the filler for morphological studies. The results showed matrix-droplet morphology for the blend of these two polymers, but after using 0.5 and 1% by weight of montmorillonite and Joncryl ADR, it was observed that the morphology remained matrix-droplet, with the difference that the size of polypropylene droplets. It is much smaller than the incompatible blend and the percentage composition of each of these additives increases, a decrease in size is seen in the droplet phase. The important point in the blend with the 2% volume composition of montmorillonite was that the droplets lost their spherical state as if they had taken on an elongated state and their characteristic length had increased up to 5 μm (Fig. 1).

For better analysis of SEM images, Sigma Scan program was used and changes in the size of polypropylene (Dv) droplets were prepared according to different amounts of montmorillonite and Joncryl ADR. As the percentage of Joncryl ADR and Montmorillonite increases to 1% by volume, a large decrease in droplet size is observed, but

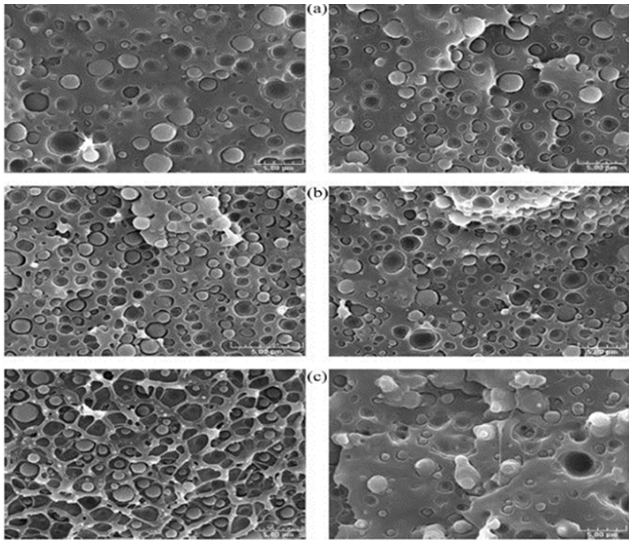

Fig. 1. SEM photographs left pictures belongs to blends containing Joncryl ADR and right one belongs to Montmorillonite: (a) 0.5, (b) 1, and (c) 2 volume fraction of each additives.

at higher amounts of these materials, the droplets tend to remain the same size, and in blends containing Joncryl ADR a linear region. It can be seen in the dimensions of 1.25 μm.

Rheological properties were determined using an oscillating shear test with an RDA-controlled strain device. The geometry of this device is two parallel plates with a diameter of 25 mm each and a distance of 2 mm. According to the strain sweep test at a constant frequency of 1 Hz, it was found that the critical strain (characteristic of the linear viscoelastic region) is 4% in the linear viscoelastic region of all samples. Therefore, all frequency sweep tests were performed in rheological examinations with this constant strain. Changes in the behavior of montmorillonite-containing blends in the composition of transfer percentage (φt), which in morphological studies indicated the beginning of morphological changes, viscoelastic studies of materials were divided in the following three categories [4].

Therefore, to investigate the viscosity and elasticity of the interface in each sample, a complex modulus and a relaxation weight function were prepared and investigated. Studies of weight distribution function showed that polyethylene has a relaxation time of 0.1 s and Polypropylene droplets have a relaxation time of 10 s. Based on this information, these properties are examined below for each of the three identified categories.

In a blend with 1% by weight of the Joncryl ADR compatibilizer, the viscosity behavior at low frequencies is such that it appears to be due to the overlap of two flow curves. The initial linear region is attributed to the viscosity of the zero shear blend phase, and the difference between this viscosity and the viscosity of the middle linear region is due to the interface phase viscosity. This behavior is not seen in the blend containing 1% of montmorillonite and is a reason for creating a discontinuous interface.

An interesting point can be seen in the diagram of the weighted relaxation spectra, the creation of a peak in longer relaxation times, which indicates the elastic behavior and intermediate phase relaxation created in both samples.

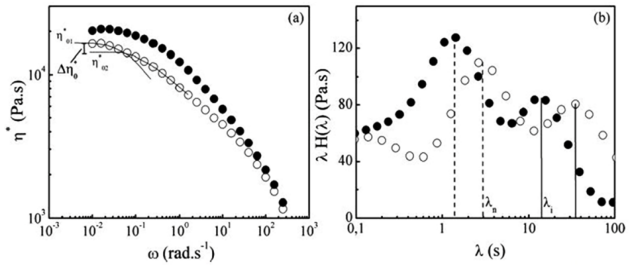

Fig. 2. (a) Complex viscosity via frequency and (b) weighted relaxation spectra; for 2% volume fraction of Montmorillonite (black circles) and 5% volume fraction of Joncryl ADR (white circles).

Final studies in this area belong to the samples with the highest amounts of montmorillonite or Joncryl ADR. In the complex viscosity diagram, the behavior changes with respect to the frequency of the sample containing the montmorillonite, and like the sample with Joncryl ADR, a slope change is seen in the initial areas of the diagram (Fig. 2). In the relaxation behavior, a sharp increase in the relaxation time of the interface has been seen, and at the same time, the relaxation effect of the polypropylene droplets has disappeared. These results indicate the creation of a fully developed interface and due to the presence of some montmorillonite in the droplet phase, the stiffness of the droplets increases and the elastic response decreases sharply [5].

Conclusion

- Similar effect of Joncryl ADR and Montmorillonite in increasing the compatibility between polyethylene and polypropylene in their blends.
- Observe the time λi as a measure of the degree of expansion of the joint phase created in the blends.
- No dependence of the length of the linear viscoelastic region on the values used by Joncryl ADR and the strong dependence of this region on the values used by montmorillonite.
- Significance of the effect of viscosity and interface relaxation in blends containing large amounts of montmorillonite compared to blends containing high amounts of Joncryl ADR.

References

[1] Salzano M., Luna D., and Filippone G., Effects of nanoparticles on the morphology of immiscible polymer blends–challenges and opportunities, *Eur. Polym. J.*, **79**, 198-218, 2016.
[2] Ville J., Médéric P., Huitric J., and Aubry T., Structural and rheological investigation of interphase in polyethylene/polyamide/nanoclay ternary blends, *Polymer*, **53**, 1733-1740, 2018.
[3] Palierne J.E., Linear rheology of viscoelastic emulsions with interfacial tension, *Rheol. Acta*, **29**, 204-214, 2019.
[4] Jacobs U., Fahrländer M., Winterhalter J., and Friedrich C., Analysis of Palierne's emulsion model in the case of viscoelastic interfacial properties, *J. Rheol.*, **43**, 6, 1495-1509, 1999.
[5] Bousmina M., Effect of interfacial tension on linear viscoelastic behavior of immiscible polymer blends,

14-15 December 2021, Tehran, Iran
2nd International Conference on Rheology
ICOR 2021
article A-10-240-1

Preparation and Evaluation of TPV Nanocomposites Based on Polycaprolactone/Ethylene Propylene Diene Monomer Rubber (PCL/EPDM) Using Dynamic Vulcanization and Presence of Sepiolite Nanoparticles

Ali Moshkriz[1], Reza Darvishi[2*], and Fatemeh Naderi[3]
1. Department of Chemical Engineering, Faculty of Engineering, Arak University, P.O. Box 38156-8-8349, Arak, Iran
2. Department of Gas and Petroleum, Yasouj University, P.O. Box 75918-74831, Gachsaran, Iran
3. Department of polymer Engineering, Faculty of Engineering, Amirkabir University, P.O. Box 15875-4413, Tehran, Iran

*r.darvishi@yu.ac.ir

Abstract
The following research is about the preparation of a nanocomposite base on polycaprolactone/ethylene propylene diene monomer rubber (PCL/EPDM) compound with 2,5-Bis(tert-butylperoxy)-2,5-dimethylhexane (DHBP)-induced dynamic vulcanization and addition of sepiolite nanoparticles (SN). The rheological behavior of the nanocomposites was investigated in order study the properties. SN were localized mostly in the EPDM droplets and at the interface where a layer of particles was formed with a small amount dispersed in the PCL matrix. The incorporation of SN or DHBP induced compatibilization, causing a significant reduction in the size of EPDM droplets in addition to improving the interfacial adhesion. On the other hand, synchronic dynamic vulcanization and SN incorporation synergistically affected the compatibilization of EPDM and PCL phases. The elongation at break and impact strength of the PCL/EPDM compound containing 5% SN showed a significant increase from 18% to 195% and 8.1 to more than 98.3 kJ/m^2, respectively as compared to the neat sample.

Keywords: compatibilization, dynamic vulcanization, SN, polycaprolactone (PCL), rheology

Introduction

Today, the wide-spreading application of common petroleum-based polymers has led to environmental contaminations, highlighting the need for novel alternative polymers with high biodegradability [1]. As a biodegradable polymer, Polycaprolactone (PCL) has been benefited from various advantages such as ease of processability, excellent biocompatibility, compared to the conventional polymers, bio-based nature, which have introduced it as a alternative to petroleum-based polymers [2]. However, PCL suffers from inherent brittleness, which has limited its commercial applications [3]. In this research, toughening of PCL has been the subject of some industrial projects. Different approaches have been developed to resolve the brittleness of PCL among which, copolymerization, and blending can be mentioned. As a cost-effective material with elastomeric nature, EPDM has been employed as a toughening agent in different polymers [4]. EPDM is also known for its high flexibility, oil resistance, weather resistance, transparency, and proper affinity toward fillers and pigments. These features have made EPDM a good option to cope with the mechanical drawbacks of PCL as reported by several researchers [5].

Experimental

The weight ratio of PCL to EPDM (PCL/EPDM) was maintained at 75/25. Four series of blends were provided including neat PCL/EPDM and SN containing blends labeled as PCL/EPDM/Nx in which x represents the weight fraction of SN (x=0, 1, 3, and 5%) with respect to the polymer content. The specimen with DHBP was showed by TPVX (x=varied from 1 to 5). The DHBP content of the compatibilized samples was set at 0.1 wt% (with respect to the total polymers). For instance, PCL/EPDM/DHBP/Nx is representative of the blend containing 75 wt% PCL, 25 wt% EPDM, 0.1 wt% DHBP, and 1 wt% SN is shown by TPV1. The melt mixing approach was utilized to obtain the specimens using a lab internal mixer (Brabender Plastirecord) at 180 °C and a rotor speed of 80 rpm for 15 min. First, PCL was incorporated into the mixing chamber. About 2 min later, the EPDM was added. After 1 min, the desired amount of SN nanoparticles was added to the samples. After about 8 min from the beginning of the mixing process, DHBP was added to initiate the dynamic vulcanization process. The samples were obtained using 5 min of compressive molding (400S Polystat model, Germany) at 190 °C.

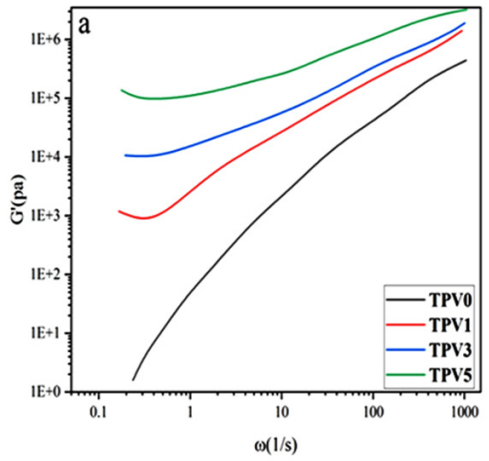

(a)

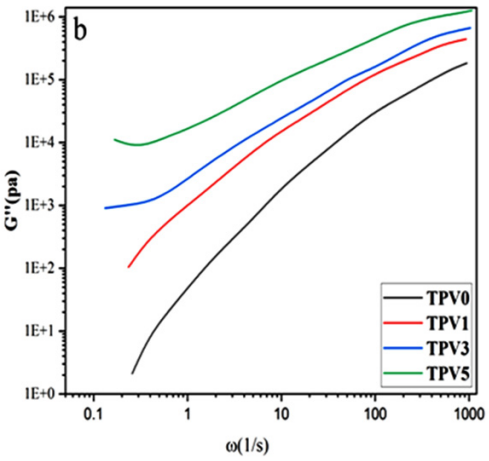

(b)

Fig. 1. Variation of: (a) storage modulus and (b) loss modulus with frequency for different samples.

Results and Discussion

Rheological Behavior

Figs. 1a and 1b shows the variation of dynamic modulus, G' and G'', with frequency for PCL/EPDM blend and crosslinked PCL/EPDM blends with and without nanoparticles. The neat PCL/EPDM sample showed terminal behavior trend by a shoulder at the storage modulus at low frequencies which could be assigned to the contribution of the interface to the blend elasticity as well as the shape relaxation of the EPDM droplets within the PCL matrix.In presence of 1 wt% nanoparticles, the modulus increased at all frequencies especially at lower values, and deviated from terminal behavior. The enhancement of both G'components and G'interface contributed to the increase of total G'. The incorporation of SN and DHBP exhibited a synergistic effect in compatibilization of the droplet and matrix phases leading to a considerable enhancement in the interfacial strength and reducing droplet size which increased G'interface. As discussed above, due to the higher affinity, the SN nanoparticles are located mainly in the EPDM droplets and some are localized in the PCL phase. Then, the G' components is also enhanced. Presence of SN in PCL phase restricts short-range dynamics of polymer chains especially in the entanglement length scales contributing to enhanced storage modulus at high frequencies. Nonetheless, SN contents above 5 wt% led to a drastic enhancement in the low-frequency storage modulus making it almost independent of frequency (a plateau). Such a trend suggests a solid-like viscoelastic feature. In other words, SN established a percolated network in the PCL matrix, spanning the sample and restraining the long range motions of polymer chain. This demonstrates that SN got "saturated" in the EPDM phase beyond 5 wt%, and the excess amount of NPs will remain in the PCL phase during the mixing process.

Conclusion

In this research, super toughened PCL/EPDM blend was successfully prepared with synchronic dynamic vulcanization and the addition of nanoparticles. At optimal loading of 5 wt% SN and 0.1% DHBP, the highest enhancement of mechanical properties was observed. However, synchronic incorporation of SN and DHBP at optimal levels led to a super toughened

PCL/EPDM blend. Rheological measurements revealed a low crosslink density induced by dynamic vulcanization. For SN contents of 5 wt% and above, a substantial increment was detected in the low-frequency storage modulus, making it almost frequency-independent (a plateau). Such a phenomenon demonstrates that NPs got "saturated" in the EPDM phase beyond 5 wt%, and the excess amounts of SN remained in the PCL phase during the mixing process.

References

[1] Han J.L., Lai S.M., and Chiu Y.T., Two way multi-shape memory properties of peroxide crosslinked ethylene vinyl-acetate copolymer (EPDM)/polycaprolactone (PCL) blends, *Polym. Adv. Technol.*, **29**, 7, 2010-2024, 2018.

[2] Burgoa Beitia A., Design and development of high-performance thermoplastic vulcanizates with vibration damping properties, 2020.

[3] Palau C.V. et al., Promotion items EPDM cheering foam hand for sports events, *Eng. Agríc.*, **38**, 6, 893-900, 2018.

[4] Deng W. et al., Adsorption recovery of phosphate from waste streams by Ca/Mg-biochar synthesis from marble waste, calcium-rich sepiolite and bagasse, *J. Clean. Prod.*, **288**, 125638, 2021.

14-15 December 2021, Tehran, Iran
2nd International Conference on Rheology
ICOR 2021
article A-10-240-2

Rheological Investigation of Binary EPDM/PA Blend Processed via Reactive Extrusion

Fatemeh Naderi[1], Reza Darvishi[*2], and Ali Moshkriz[3]
1. Department of polymer Engineering, Faculty of Engineering, Amirkabir University, P.O. Box 15875-4413, Tehran, Iran
2. Department of Gas and Petroleum, Yasouj University, P.O. Box 75918-74831, Gachsaran, Iran
3. Department of Chemical Engineering, Faculty of Engineering, Arak University, P.O. Box 38156-8-8349, Arak, Iran

*r.darvishi@yu.ac.ir

Abstract
Tough EPDM/PA blends were compatibilized by in situ reactive extrusion. This study deals with evaluation of the influences of blend composition on the rheological properties. In low frequency region, Elastic behavior of PA shifted to viscose behavior in the presence of dispersed and grafted EPDM droplets. Increasing content of EPDM in the blend, led to lower compatibility and dilatant fluid behavior moved to lower frequencies until this behavior disappeared in presence of 25% EPDM.

Keywords: in situ copatibilization, reactive extrusion, dilatant fluid, psudoductile fluid, toughness

Introduction

One of the most common engineering plastics with excellent properties is PA but its low impact strength restricts applications [1,2]. The very basic toughening method is to incorporate rubber particles [3,4]. However, their incompatibility reduces these properties. Therefore, interface interaction should be promoted. The effects of the viscoelastic behavior of blends on their final mechanical has been noticed in the past few decades [5,6]. Also, the rheology is an effective way to study morphology and the interface properties and of the blends. On the other hand, Reactive extrusion is considered as a common method to manufacture polymer blends with special properties. The rheological properties of EPDM/PA blends are investigated in this study to provide the relationship between structure and performance.

Experimental

In the conducted reactive extrusion, various amounts of EPDM was dissolved in molten CL at 160 °C under mechanical stirring and 1 wt% KOH and 0.5 wt% TDI were added to two distinct equal parts of the EPDM/CL molten mixture, following by reactive extrusion which was carried out in an co-rotating twin screw extruder at the temperatures of the 200 °C. Different blends with 5, 15, and 25 wt% contents of EPDM were produced, respectively.

Results and Discussion

Blend composition, interfacial adhesion, morphology and molecular weight are significantly affecting properties of blends. 25 the complex viscosity of the both PA and EPDM decreased as the frequency increased, and exhibited shear-thinning characteristic. However, an increase in the η* value of the reactive blends is observed at low frequencies and then decreased gradually in the high-frequency region. This diagram illustrated that this behavior us quite different from the dilatant fluid behavior in the whole-frequency region. In low frequency region, the dilatant fluid behavior attributes to the uniform distribution of EPDM droplets, and the enhanced compatibility between PA and EPDM. Gradually moving of the dilatant fluid behavior to the lower frequencies with increasing amount of EPDM is a noticeable point in the diagram. This behavior is disappeared at 25% of the EPDM based on increased diameter of droplets and decreased compatibility. Also, the complex viscosity of reactive blends increased with the EPDM content at a fixed frequency. Based on enhanced interfacial interaction, the reactive blends showed higher complex viscosities than the values predicted by linear superposition. Because of high viscosity of the reactive melting mixture of caprolactone and EPDM based on inhibited diffusion of the active ionic centers of polymerization, molecular weight decreased in the blend by increasing EPDM amount, Fig.1A.

The storage modulus (G') as PA/EPDM blends with different amounts of ABS is illustrated, Fig. 1B. As shown in the figure, the storage modulus curves for EPDM and PA followed a linear mixing rule. The storage modulus of these blends gradually increased with the increasing amount of EPDM. Notably, G' diagram showed a similar trend. As a result, the storage modulus showed an increase in the

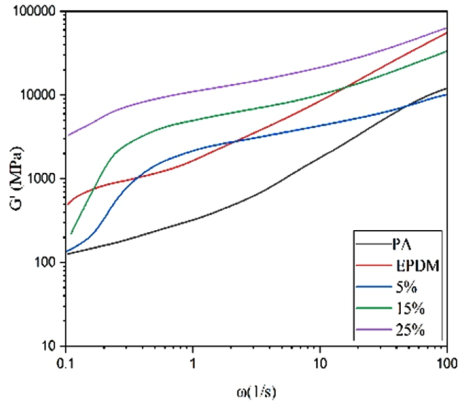

(a)

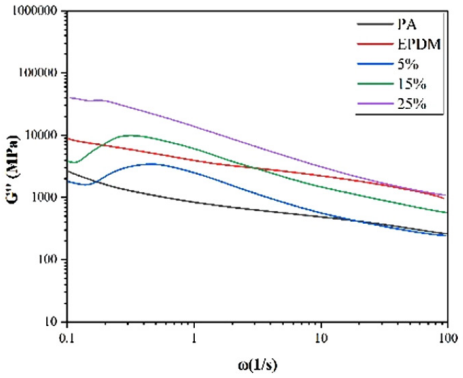

(b)

Fig. 1. Diagrams of: (a) G' and (b) G'' of different samples: (PA), (EPDM), PA with 5%EPDM (figure 5%), 15% EPDM (figure 15%) and 25% EPDM (figure 25%).

low frequency region and followed linear mixing rule in the high frequency region. Therefore, the compatibility of reactive blends is proven, which leads to an enhancement in the interfacial adhesion, Fig. 1B.

The loss modulus diagram for the reactive blends with different contents showed that the 25 wt% blends has the maximum loss modulus, indicating a higher energy dissipation that for the other blends with lower EPDM contents, Fig. 1C. The increase in EPDM or the rubber phase content increased the loss modulus of the EPDM/PA blends. Therefore, the rubbery phase in the EPDM strongly controls the viscoelastic behavior and loss modulus of the reactive blends.

Conclusion

The rheological properties of the EPDM/PA blends prepared by reactive extrusion were studied. The uniform distribution of EPDM droplets led to dilatant fluid behavior and a transition from viscous to elastic behavior in the low frequencies. Also, by increasing EPDM content, the diameter of EPDM droplets raise and the compatibility decreased, resulting in the disappearance of the dilatant behavior.

References

[1] Hale W., Lee J.-H., Keskkula H., and Paul D.R., Effect of PBT melt viscosity on the morphology and mechanical properties of compatibilized and uncompatibilized blends with ABS, *Polymer*, **40**, 3621-3629,1999.

[2] Ozkoc G., Bayram G., and Bayramli E., Effects of polyamide 6 incorporation to the short glass fiber reinforced ABS composites: an interfacial approach, *Polymer*, **45**, 8957-8966, 2004.

[3] Wu S., Control of intrinsic brittleness and toughness of polymers and blends by chemical structure: a review, *Polym. Int.*, **29**, 3, 229-247, 1992.

[4] XU C. et al., Dynamically vulcanized PP/EPDM blends with balanced stiffness and toughness via in-situ compatibilization of MAA and excess ZnO nanoparticles: preparation, structure and properties, *Compos. Part B: Eng.*, **160**, 147-157, 2019.

[5] Mungall J.E., Interfacial tension in miscible two-fluid systems with linear viscoelastic rheology, *Phys. Rev. Lett.*, **73**, 288-291, 1994.

[6] Maani A., Blais B., Heuzey M.-C., and Carreau P.J., Rheological and morphological properties of reactively compatibilized thermoplastic olefin (TPO) blends, *J. Rheol.*, **56**, 625-647, 2012.

14-15 December 2021, Tehran, Iran
2nd International Conference on Rheology
ICOR 2021
article A-10-244-2

Investigating the Degradation of PLA/PCL/ZnO Nanocomposites by Viscoelastic models

Parsa Dadashi[1] and Amir Babaei[2*]
1. School of Chemical Engineering, College of Engineering, University of Tehran, P.O. Box 14155-6619, Tehran, Iran
2. Department of Polymer Engineering, Faculty of Engineering, Golestan University, Postal Code 15759-49138, Gorgan, Iran

*a.babaei@gu.ac.ir

Abstract
For the first time, the degradation of a polymer blend in the presence of nanoparticles by considering the effect of nanoparticles on the degradation was investigated using Lee and Park model and fractional Zener model in this research. Poly(lactic acid)/poly(caprolactone)/zinc oxide nanocomposite blends were prepared by melt mixing method. Interface complex shear modulus for the neat polymer blend and its nanocomposites were calculated by using Lee and Park model in a range of frequencies. All of factors imposing elasticity on the systems including the solid-like behavior and also degradation catalytic activity of ZnO nanoparticles in the presence of polyesters were considered. Accordingly, most of the samples with a high amount of ZnO exhibited low elasticity which was attributed to the overcoming of the degradating role of ZnO. Additionally, the results obtained from the fractional Zener model was in a good harmony with the Lee and Park model analysis.

Keywords: Lee and Park model, fractional zener, hydrolytic degradation, nanocomposites, PLA, ZnO nanoparticles

Introduction

In recent decades, many researches are devoted to developing degradable polymeric systems due to the environmental pollution of petroleum-based polymers [1]. One of the most promising biodegradable polymers with extraordinarily bio-applications is poly(lactic acid) (PLA) [2]. PLA brittleness is a very important disadvantage, in spite of its bio-applications advantage [3]. Therefore, blending the PLA with other biodegradable polymer such as polycaprolactone (PCL) for improving PLA mechanical properties by toughening mechanism has been recommended [4]. Zinc Oxide (ZnO) as an antibacterial nanofiller has an effect on hydrolytic degradation on polyesters [4]. Significance of the polymer blends interface on the mechanical properties is an inevitable issue, and mechanical-microstructure correlation of the polymer blends was investigated many times but the applicability of the rheology Provide opportunities for researchers to look into various fields [5]. Accordingly, investigating the degradation was carried out with rheological emulsion models and fractional Zener model for the first time due to the role of degradation on the interfacial viscoelastic properties of PLA/PCL polymer blends.

Experimental

PLA with Ingeo 2003D trade name supplied by NatureWorks Co.Ltd. (USA), has a density of 1.24 g/cm³, a melting point of 210 °C. PCL, Capa® 6800 with melting point of 58-60 °C.g/10 min.

Samples were Melt mixed by HAAKE internal mixer model SYS 90 drive (USA). The Mixing was performed at 170 °C and 60 rpm for 8 min. Rheology assessment was performed at 170 under a Nitrogen atmosphere by instAnton Paar USD200 (Austria) rheometer. The morphology of cryo-fractured samples was investigated by using a field emission scanning electron microscope (FE-SEM) MIRA3 model from Tescan (Czech Rep).

Results and Discussion

Morphology

Fig.1a-f shows the FE-SEM micrographs of PLA/PCL blend and its nanocomposites containing 2, 4, and 6 wt% ZnO nanoparticles. FE-SEM micrographs demonstrate droplet-matrix morphology in which PLA and PCL are matrix and droplet with (80/20 w/w), respectively.

Viscoelastic Emulsion Models

Lee and Park have developed Doi and Ohta model for immiscible polymer blends. Fig. 2 shows $G^*_{interface}$ versus frequency for the PLA/PCL (80/20 w/w) samples with various ZnO nanoparticles loading obtained from Lee and park model.

As observed in Fig. 2, the following $G^*_{interface}$ values are arranged in decreasing order:

$$G^*_{i-PLAPCL} \gg G^*_{i-ZNO2} > G^*_{i-ZNO4(1)} \cong G^*_{i-ZNO4(2)} > G^*_{i-ZNO6}$$

As mentioned above, PLA/PCL sample had maximum $G^*_{interface}$ value, but by increasing ZnO contents, they almost decreased. The following results are possible reasons for this decreasing trend:

a) Probably, ZnO was migrated from PLA phase to PLA/

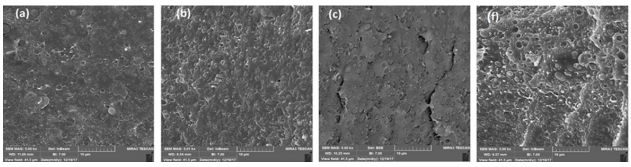

Fig. 1. FE-SEM micrographs of: (a) PLA/PCL (80:20 w/w) blend, (b) ZnO-2, (c) ZnO-4, and (f) ZnO-6.

PCL interface after degradation and play interfacial tension reduction role in non-degraded regions. Moreover, by increasing ZnO nanoparticles contents, the accumulation of nanoparticles in the interface might be increased and leads to coalescence suppression due to nanoparticles acting as barriers at the interface that results in interfacial tension decrement.

b) PLA/PCL hydrolytic degradation is associated with carboxylic acid, lactic acid, caprolactone, and other functional oligomers generation as a consequence of chain breakup. Therefore, these kinds of residues (carboxylic acid, lactic acid, and so on) could act as compatibilizers when degradation promotes through ZnO nanoparticles incorporation.

Fractional Zener Model

Fractional Zener, which is based on the standard Zener model, has been extensively applied for the evaluation of the viscoelastic properties of composite systems by fitting equation to the experimental data using the genetic algorithm for different samples were calculated, and the results are showed in Fig. 3. As it demonstrates, Ge and τ_0, from Zno-2 to Zno-4(1), ZnO-4(1) to Zno-4(2), ZnO-4(2) to Zno-4(3), and ZnO-4(3) to Zno-6 have decreasing, increasing, decreasing, increasing trend, respectively. This decreasing trend in these two parameters (Ge and τ_0) demonstrates increasing viscose nature due to the sample degradation and increasing trend in these two parameters (Ge and τ_0) attributes to increasing elastic nature in consequence of hydrodynamic interactions induced by ZnO nanoparticles. As observed, by increasing

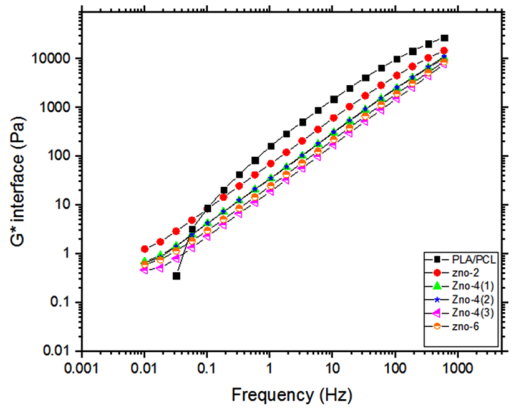

Fig. 2. $G^*_{interface}$ versus frequency for the PLA/PCL (80/20 w/w) samples with various ZnO loadings obtained from Lee and park model after modification of G^*_m values.

ZnO-NPs amounts, degradation almost increases and leads to increasing viscose nature, but Zno-6, in spite of the high amount of ZnO, has a more elastic nature than zno4(3) due to predominated hydrodynamic interactions or agglomeration or its special localization in PLA/PCL blend. In addition, G0 has an inverse trend compared to Ge that confirms mentioned phrase. It implies that increasing G0 parameter values demonstrate increasing viscose nature due to degradation of sample and decreasing trend attributes to increasing elastic nature due to hydrodynamic interactions of ZnO nanoparticles.

Conclusion

In this work is Lee and Park model and fractional Zener micromechanical models were used to describe the relationship between viscoelastic properties and hydrolytic degradation of PLA/PCL/ZnO nanocomposites. Decrement trend was almost observed in interface complex modulus by incorporation ZnO that it was ascribed to migration of ZnO to the interface as a consequence of hydrolytic degradation which interfacial tension was decreased due to compatibilizer role of ZnO or it was attributed to the compatibilization role of generated oligomer residue after degradation which interfacial tension was reduced as degradation was promoted. In addition, a fractional Zener micromechanical model was used for viscoelastic data of samples. Micromechanical model was used for viscoelastic data of samples. The model was well agreed with viscoelastic data of samples except for PLA/PCL virgin blend. Fractional Zener parameters were obtained by the genetic algorithm, which has demonstrated the order of mixing effect on degradation and consequently viscoelastic properties.

References

[1] Abdolrsaouli M.H., Babaei A., Kaschta J., and Nazockdat H., Polylactide/organoclay nanocomposites: the effect of organoclay types on the structure development and the kinetic of cold crystallization, *J. Vinyl Addit. Technol.*, **25**, 48, 2019.

[2] DeStefano V., Khan S., and Tabada A., Applications of PLA in modern medicine, *Eng. Regen.*, **1**, 76, 2020.

[3] Zhao X., Hu H., Wang X., Yu X., Zhou W., and Peng S., Super tough poly(lactic acid) blends: a comprehensive review, *RSC Adv.*, **22**, 2020.

[4] Zhang H.C., Kang B.Z., Chen L.S., and Lu X., *Polym. Test.*, **87**, 106521, 2020.

[5] Ostafinska A., Fortelny I., Nevoralova M., Hodan J., Kredatusova J., and Slouf M., Synergistic effects in mechanical properties of PLA/PCL blends with optimized composition, processing, and morphology, *RSC Adv.*, **120**, 2015.

[6] Lyu S. and Untereker D., Degradability of polymers for implantable biomedical devices, *OPEN ACCESS Int. J. Mol. Sci.*, **10**, 9, 2009.

14-15 December 2021, Tehran, Iran
2nd International Conference on Rheology
ICOR 2021
article A-10-244-3

A New Rheological Model for Investigating the Polymer/Filler Interfacial Properties for binary Polymer Blends

Parsa Dadashi[1] and Amir Babaei[2*]

1. School of Chemical Engineering, College of Engineering, University of Tehran, P.O. Box 14155-6619, Tehran, Iran
2. Department of Polymer Engineering, Faculty of Engineering, Golestan University, Postal Code 15759-49138, Gorgan, Iran

*a.babaei@gu.ac.ir

Abstract

Interfacial tension between polymer and filler is an important issue for characterizing the rheological, mechanical, electrical, thermal and optical properties in polymer blends due to the role of nanoparticles localization on the microstructure of phase segregated nanocomposites. Hence, the models that are used are not appropriate for these systems due to the negation of kinetic parameters. In this study, a new model based on Palierne emulsion model is proposed for calculating the polymer/ nanoparticle interfacial tension. The proposed model is validated for poly(methyl meta acrylate)/poly(Styrene)/multiwalled carbon nanotubes (PMMA/PS/MWCNTs) systems with droplet/ matrix morphology.

Keywords: polymer blend, palierne model, interfacial tension, LVR rheology, interphase

Introduction

Polymer/particle interface properties play a crucial role on the mechanical, electrical, optical and thermal properties specially in binary polymer blends. Interface properties are identified by a characteristic parameter that is called interfacial tension [1-4]. In this regard, Wu proposed a static model that is based on thermodynamic equilibrium state. Wu model is not appropriate in melt state that convection is dominated in these systems due to the negation of Wu model assumptions [5]. Palierne proposed a model for investigating the viscoelastic properties of emulsions based on Lorentz approach in electronic physics by accounting mechanical interactions between emulsion droplets and interface contribution [6]. However, Palierne model based on rheological assessments in dynamic states is an accurate model for calculating the polymer/polymer interfacial tensions but it's not in agreement with polymer nanocomposites rheological results due to the negation of polymer/particle interactions [6-8].

For the first time, the Palierne model (modified by pal type) was developed for binary polymer blends containing nanoparticles that is localized in droplet phase through considering the stress and strain amplification rate as polymer/particle parameters.

The model is validated for PMMA/PS/MWCNTs nanocomposites as a case study. The parameters obtained from the developed model provided information about droplets crowding effect, nanoparticles amplification rate, and nanocomposite interfacial tension in addition to polymer/particle interfacial tensions in dynamic states.

Experimental

NC-7000 MWCNTs with 90% carbon purity, 250-300 m^2/g specific surface area was provided from Nanocyl Company (Belgium). PMMA with grade of IH830 and MFI of 2.5 (g/10 min) (230 °C, 3.8 kg) was purchased from LG chemical Co. PS with grade of Solarene G114 and MFI of 8.5 (200 °C, 5 kg) was obtained from DongbuHannong Chemical Co (Korea). PMMA/PS blend with 80/20 weight percent composition containing 1 wt% MWCNTs with matrix- droplet morphology was prepared by brabender internal mixer (D-47055 model (Germany)) at temperature of 220 °C and mixing time of 12 min. Oscillatory shear rheological measurements was carried out at the temperature of 220 °C by Physica Anton Paar (MCR 301). Morphology assessments of cryo-fractured samples were carried out by FE-SEM (S-4160) made in Hitachi.

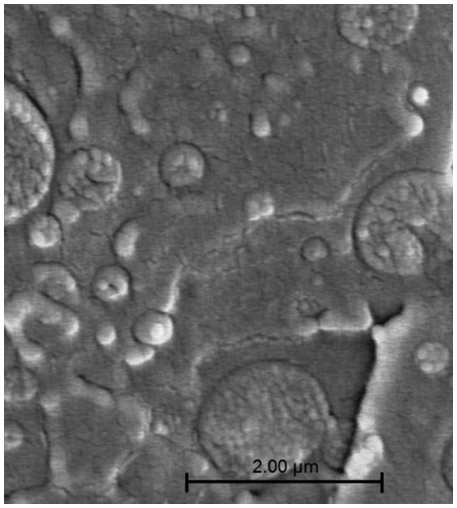

Fig. 1. FE-SEM image for PMMA/PS blend (80/20).

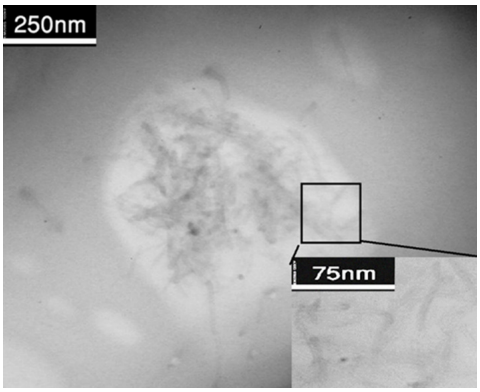

Fig. 2. TEM Image for PMMA/PS blend (80/20) containing 1 wt% MWCNTs.

Results and Discussion

Fig. 2 depicted morphology of PMMA/PS polymer blend with 80/20 weight percent composition in the presence of 1 wt% MWCNTs. According to the FE-SEM figure, the droplet-matrix morphology is dominated in this system with PMMA droplet phase. Volume average radius of droplets was obtained equal to 1570 nm from FE-SEM morphology images.

Fig. 3 demonstrated Transmission electron microscopy image of PMMA/PS polymer blend with 80/20 weight percent composition in the presence of 1 wt% MWCNTs. It is observed in Fig. 3 that MWCNTs is localized in droplet phase.

According to the Fig. 4, the developed emulsion model is proposed in Eq. (1):

$$G_C^* = G_m^*\left(\left(\frac{1+3\psi\phi H_1^*}{1-2\psi\phi H_1^*}\right)+\alpha_t\alpha_s\left(\frac{1+3\psi\phi H_2^*}{1-2\psi\phi H_2^*}\right)\right)$$

$$H_1^* = \frac{4\left(\frac{\alpha}{Rd}\right)\left[2G_m^*+5G_{d1}^*\right]+\left[G_{d1}^*-G_m^*\right]\left[16G_m^*+19G_{d1}^*\right]}{40\left(\frac{\alpha}{Rd}\right)\left[G_m^*+G_{d1}^*\right]+\left[2G_{d1}^*+3G_m^*\right]\left[16G_m^*+19G_{d1}^*\right]}$$

$$H_2^* = \frac{4\left(\frac{\alpha}{Rd}\right)\left[2G_m^*+5G_{d0}^*\right]+\left[G_{d0}^*-G_m^*\right]\left[16G_m^*+19G_{d0}^*\right]}{40\left(\frac{\alpha}{Rd}\right)\left[G_m^*+G_{d0}^*\right]+\left[2G_{d0}^*+3G_m^*\right]\left[16G_m^*+19G_{d0}^*\right]}$$

$$\psi\phi = 1-\exp\left[\frac{-\phi}{1-\left(\frac{\phi}{\phi_m}\right)}\right] \qquad (1)$$

G_m^*, G_{d1}^*, G_{d0}^*, ϕ, ϕ_m, α, R, ar and as are matrix complex shear modulus, droplet containing nanoparticles complex shear modulus, droplet without nanoparticles complex shear modulus, volume fraction, maximum packing volume, interfacial tension, and droplet radius, strain amplification rate and stress amplification rate, respectively.

Fig. 4 demonstrated the fitting result of the proposed model (Eq. (1)) with experimental results that was obtained from rheometer analysis in a graph. According to the graph, experimental results is in a good agreement with the model. $\gamma_{PS/MWCNTs}$, ϕ_m, and aras were obtained from model is equal to 1.57, 13.7, 0.37, and 1 mN/m.

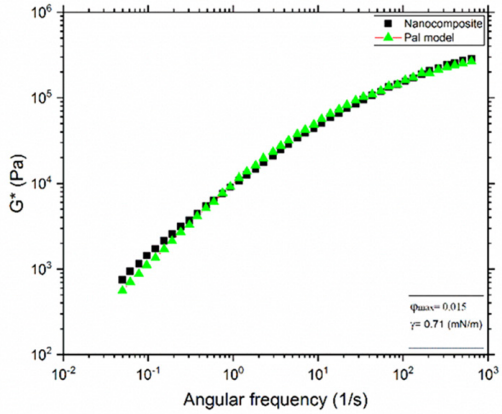

Fig. 3. Comparison between experimental viscoelastic data (complex shear modulus) and predictions of the modified palierne model (Pal model) for PMMA/PS/MWCNT nanocomposite.

Conclusion

Due to the importance of polymer/filler interphase on the mechanical, physical properties of polymer blend and lack of the accurate model for calculating the interface parameters, a new model is proposed by considering the polymer/filler and filler/filler hydrodynamic interactions in the term of stress and strain amplification rate effects. The model is validated by PMMA/PS/MWCNTs experimental data.

References

[1] Bhattacharya M. and Bhowmick A.K., Elastomer nanocomposites, *Polymer (Guildf)*, **81**, 3, 2008.
[2] Buggy M., Bradley G., and Sullivan A., Polymer–filler interactions in kaolin/nylon 6,6 composites containing a silane coupling agent, *Compos. Part A Appl. Sci. Manuf.*, **36**, 4, 437-442, 2005.
[3] Fu S.-Y., Feng X.-Q., Lauke B., and Mai Y.-W., Effects of particle size, particle/matrix interface adhesion and particle loading on mechanical properties of particulate–polymer composites, *Compos. Part B Eng.*, **39**, 6, 933-961, 2008.
[4] Mamunya E.P., Davidenko V.V., and Lebedev E.V., Effect of polymer-filler interface interactions on percolation conductivity of thermoplastics filled with carbon black, *Compos. Interfaces*, **4**, 4, 169-176, 1996.
[5] Wu S., *J. Polym. Sci. Part C Polym. Symp.*, **34**, 2007.
[6] Graebling D., Muller R., and Palierne J.F., Linear viscoelastic behavior of some incompatible polymer blends in the melt. Interpretation of data with a model of emulsion of viscoelastic liquids, *Macromolecules*, **26**, 2, 320-329, 1993.
[7] Liao H., Liao R., Li S., Liu C., and Tao G., *Polym. Bull.*, 2021.
[8] Dadashi P., Babaei A., and Rostami A., A new e for Model Emulsion M, *Iran. J. Polym. Sci. Technol.*, **34**, 83, 2021.
[9] Carriere C.J., Biresaw G., and Sammler R.L., Temperature dependence of the interfacial tension of PS/PMMA, PS/PE, and PMMA/PE blends, *Rheol. Acta*, **39**, 476-482, 2000.

14-15 December 2021, Tehran, Iran
2nd International Conference on Rheology
ICOR 2021
article A-10-246-1

Simulation of the Filler Weight Fraction Effects on Rheological Properties and Process Parameters of Polypropylene Melt in Injection Molding

Amirhosein Yazdanbakhsh* and Alireza Behzadi
School of Chemical Engineering, College of Engineering, University of Tehran, P.O. Box 14155-6619, Tehran, Iran

*a.yazdanbakhsh@ut.ac.ir

Abstract
Polypropylene (PP) is one of the most widely used plastics for the production of various parts in the injection molding process. Calcium carbonate ($CaCO_3$) is one of the most common mineral fillers that is added to PP to enhance its properties. In this study, the process of injection molding of a Toyota wheel cap was simulated by selecting PP with different weight percentages of $CaCO_3$ by Autodesk Moldflow software. The results showed that increasing the filler weight percentage affects the rheological properties of the melt and the injection process parameters. In general, with increasing filler percentage, melt viscosity, injection pressure, clamping force and shear stress had higher values.

Keywords: polypropylene, injection molding, viscosity, filler, simulation

Introduction

Polypropylene (PP) is a plastic used in the injection molding process to produce a variety of parts. Calcium carbonate ($CaCO_3$) is a common additive for PP reinforcement that increases elastic modulus, decreases yield stress, increases impact resistance, reduces crystallinity and reduces its price. PP/$CaCO_3$ composite is used in the production of plastic shelves, shoes and sandals, automotive industries, home appliances, etc. [1,2].

Dynamically, increasing the $CaCO_3$ particles, enhances the storage modulus and the loss modulus of melt and decreases the damping (tan δ). Thus, increasing the weight fraction of $CaCO_3$ changes the rheological properties of PP melt and therefore, changes the process considerations of injection molding [3]. Today, Autodesk Moldflow is the most well-known software for simulating injection molding and analyzing process conditions and defects. In this study, this software has been used to investigate the effects of increasing the weight fraction of $caco_3$ on melt rheological properties and injection conditions.

Experimental

Autodesk Moldflow software analysis is based on meshing, so the type and size of meshes are effective in the accuracy of results and analysis speed. Due to the complexity of engineering problems, numerical methods are often used. In this software, two methods of Finite Element or Finite Difference are used to perform calculations.

The meshing of the part (a Toyota wheel cap) was done according to its dimensions (140×43×135) mm of Dual Domain type and with the value of Global edge length equal to 3.99 mm. Finally, 15,690 triangular meshes were created with a maximum aspect ratio of 20.15 and a 99% mesh matching percentage. The polymer used in this work is PP, a product of Ferro Company, which once selected a grade of 20% filler ($CaCO_3$) and the next time a grade with 35% filler was selected from the software database. Gate Location, Molding Window, and Fill+Pack analyzes were performed on the mesh piece, the results of which are described below.

Results and Discussion

The simulation results showed that at the same shear rate and temperature, the viscosity of the pp melt increase with increasing weight percentage of $CaCO_3$, which is shown in Fig. 1.

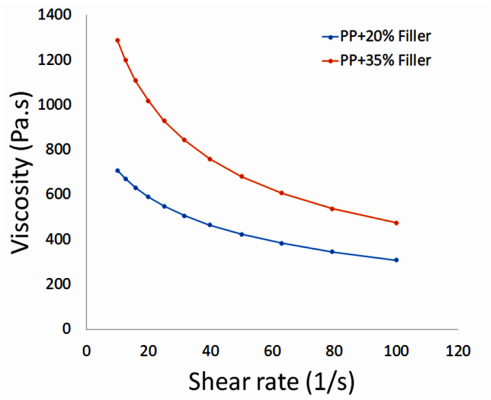

Fig. 1. Viscosity diagram vs shear rate.

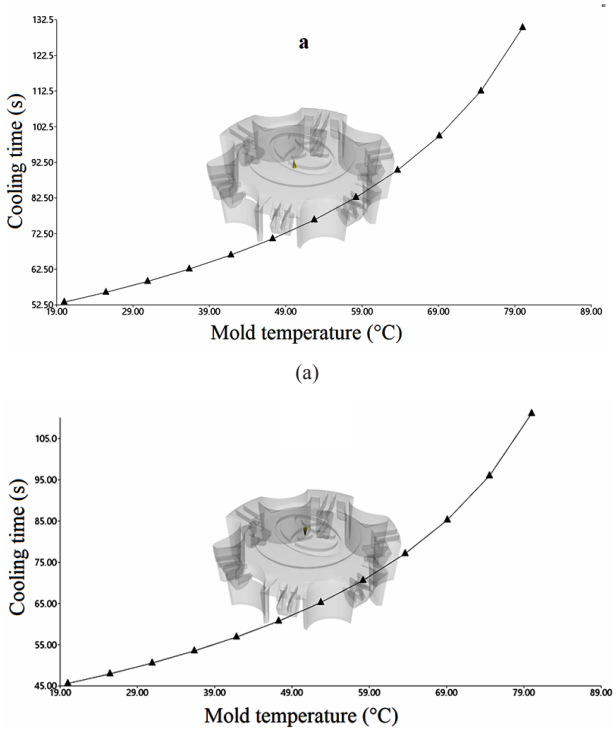

Fig. 2. Cooling time vs mold temperature: (a) PP+20% $CaCO_3$ and (b) PP+35% $CaCO_3$.

Increasing the weight percentage of filler and consequently growth the viscosity of the plastic melt can affect the injection process conditions. Table 1 compares the various important parameters in the injection molding process for the PP+20% filler and the pp+35% filler. In general, with increasing filler weight percentage, injection pressure, clamping force and shear stress showed higher values. Also, in PP with higher filler percentage, less injection time was observed, which can be related to the higher shear stress applied to this plastic by the injection machine screw, but the reduction of injection time with increasing filler percentage cannot be expressed as a general rule.

Cooling time is one of the important parameters of the injection process, which indicates the residence time of the part from the beginning of filling the mold to the ejection time. Fig. 2 shows the cooling time diagram in terms of mold temperature for plastics with different filler percentages. According to this figure, with increasing the percentage of filler in the PP+ $CaCo_3$ composite, the cooling time at different temperatures decreases. As expected, in general, the cooling time increases with increasing mold temperature.

Table 1. Injection process considerations (for different filler percentages).

Parameter	PP+20% filler	PP+35% filler
Maximum clamp force (tonne)	1.7	2.3
Maximum injection pressure (MPa)	1.8	2.5
Recommended melt temperature (°C)	278	241
Recommended mold temperature (°C)	80	80
Injection time (s)	2.5	2.3
Shear stress (MPa)	0.26	0.34

Conclusion

In this study, the process of PP injection molding with different weight percentages of $CaCO_3$ (20 and 35%) was simulated and their rheological and process parameters were compared with each other. The effect of filler increase on viscosity, injection pressure, clamping force, shear stress, melt and mold temperature, injection time and cooling time were also investigated.

References

[1] Thenepalli T., Jun A.Y., Han C., Ramakrishna C., and Ahn J.W., A strategy of precipitated calcium carbonate ($CaCO_3$) fillers for enhancing the mechanical properties of polypropylene polymers, *Korean. J. Chem. Eng.*, **39**, 1009-1022, 2015.

[2] Mao H., He B., Guo W., Hua L., and Yang Q., Effects of nano-$CaCO_3$ content on the crystallization, mechanical properties, and cell structure of PP nanocomposites in microcellular injection molding, *Polymers*, **10**, 1160, 2018.

[3] Karamipour S., Ebadi-Dehaghani H., Ashouri D., and Mousavian S., Effect of nano-$CaCO_3$ on rheological and dynamic mechanical properties of polypropylene: experiments and models, *Polym. Test.*, **30**, 110-117, 2011.

14-15 December 2021, Tehran, Iran
2nd International Conference on Rheology
ICOR 2021
article A-10-248-1

Effect of Sulfur Curing Accelerators on the Combination of Sulfur Curing and Metal Oxide in CR/CSM Rubber Blending

Farshad Taghavian and Mohammadreza Pourhossainy*
1. Malek Ashtar University of Technology, P.O. Box 1774-15875, Tehran, Iran
2. Faculty of Materials and Manufacturing Technologies, Malek Ashtar University of Technology, P.O. Box 1774-15875, Tehran, Iran

* mr_pourhossainy@yahoo.com

Abstract
In this research, preparation, description, and applications Chlorosulfonate polyethylene (CSM) and Polychloroprene (CR) rubber blend are discussed. CSM rubber is highly reactive, and reactivity is due to the SO_2Cl groups. Which have a sulfur curing. For these reasons, this type of rubber has a low scorching time, which can cause problems for subsequent processes such as molding. Polychloroprene rubber also have a metal curing and have a low scorching time too. In this research, an attempt has been made to achieve better curing by changing the curing system. The effect of using PbO instead of ZnO can also be seen in some mechanical and thermal properties.

Keywords: CSM, blend, scorch time, PbO, accelerator

Introduction

Blends of rubbers are of technological and commercial importance, since they allow the user to access properties of the final blended and vulcanized rubber that is not accessible from a single, commercially available rubber alone [1]. In reality, all blends show compositionally correlated changes in all of these properties compared to the blend components [2]. Detailed studies of the mechanisms of scorch delay have been illustrated with studies based on sulphenamide accelerators. This is probably so because this is the most popular class of accelerators in use. Sulphenamide accelerators like all other types initially furnish the necessary time period required to mix, process and shape rubber compounds. Secondly, they serve the purpose of speeding up the reaction once the crosslinking process has begun. The sulphenamides are initially converted to monomeric polysulphides followed by conversion to polymeric polysulphides (poly benzothiazole intermediates) which are the precursors to crosslinking [3]. To obtain better end use properties, rubber macromolecules are subjected to vulcanization using different type of accelerators. The chosen accelerator affects the cure rate and scorch safety as well as the number and type of the crosslink's formed. Cyclohexyl benzo thiazyl sulphenamide (CBS) is used for the crosslinking of rubbers with sulphur. Now it is starting with increasing application of ultra-accelerators like tetra methyl thiuram disulfide (TMTD) in the vulcanization of rubbers [4]. Chlorosulfonated polyethylene (CSM) is an important rubber which has been frequently used in many applications [5]. The introduction of chlorine and sulfur dioxide onto the polyethylene linking via condenzation or substitution reactions molecule destroys the crystallinity, thereby changing the thermoplastic material into an amorphous polymer, commercially known as CSM. Thus, CSM rubber is highly reactive, and reactivity is due to the SO2Cl groups [6]. Chloroprene rubber (CR) is a high-performance material with a wide diversity of applications. CR is conventionally cured with 5 phr of zinc oxide (ZnO) in the presence of 4 phr of magnesium oxide (MgO). The mechanism of CR curing is unclear. Chloroprene rubber can be cross-linked with other metal oxides, such as Lead Oxide (PbO) Such obtained CR vulcanizates are often characterized by better mechanical properties than the conventionally crosslinked CR.

Experimental

All mixing ingredients were used as received. Rubbers used for composite preparation: CR rubber, Baypren 110 from Bayer, Germany; CSM rubber, Hypalon 40S, produced by Tosoh Chemical Co. The other rubber ingredients were: stearic acid, and lead oxide (PbO); sulfur obtained from Chemmin Corporation, magnesium oxide (Merck), ethylene thiourea (ETU), TMTD, CBS. Compounding was done on a laboratory size two roll mixing mill. CRI, were calculated using Eqs. (1) and (2), respectively:

$$MDR = \frac{90(M_{Max} - M_{Min})}{100} + M_{Min} \quad (1)$$

$$CRI = \frac{100}{t_{C90} - t_{S2}} \quad (2)$$

Where, M_{Min} and M_{Max} are minimum and maximum torque; t_{S2} is the optimum cure time; and t_{C90} is the scorch time.

Table 1. The content of accelerators (phr) in different rubber compounds based on CR/CSM (50:50) rubber blend with out of any filler.

Accelerators	Sample name		
	A	B	C
CBS	1.5	0	2.5
TMTD	1	1	1
MBTS	0	0.5	0

Table 2. Curing characteristics of CR/CSM rubber blend compounds in the presence of different accelerators content.

Characteristic	A	B	C
M_{min} (dNm)	6.34	6.20	5.79
M_{max} (dNm)	21.93	22.34	19.58
ΔM (dNm)	15.59	16.14	13.79
t_{S2} (min)	0.84	0.76	1.1
t_{C90} (min)	24.2	19.64	20.8
CRI (min^{-1})	4.33	5.34	5.01

Results and Discussion

Rheographs of the mixes are given in Fig. 1. The cure characteristics are given in Table 2, in Table 1 also shows the consumption of each accelerator. The minimum torque M_{Min} in the rheograph can be taken as a measure of the viscosity of the masticated rubber and Comparison between Scorch time in blends is shown in Fig. 2. With the accelerator concentration are increasing, the M_{Max} values of CR/CSM rubber blend compounds are decreasing (By increasing the amount of CBS). Normally, the maximum torque in the rheography can be taken as the maximum viscosity of the rubber compounds, and it is a relative measure of the crosslinking density in the samples [7]. The maximum torque M_{Max} which is a measurement of the stiffness of the compound, is found that CR/CSM rubber blends with TMTD have higher values than CR/CSM compounds with CBS accelerators. The torque difference values of ΔM increase with increasing TMTD concentration and decrease with increasing concentration of CBS accelerators for CR/CSM rubber blends. The CR/CSM rubber blends with TMTD accelerator have ΔM maximum. The decrease of optimum cure time t_{C90} is extremely beneficial for real industrial processing of rubbers [7]. The scorch time t_{S2} is also improved slightly with increasing CBS (within a few seconds). that the CRI of the compounds increases with increasing accelerator concentration. The chosen accelerator affects the cure rate and scorch safety. It is clear that the tensile strength and hardness increases slightly upon the addition of accelerators, according to increase

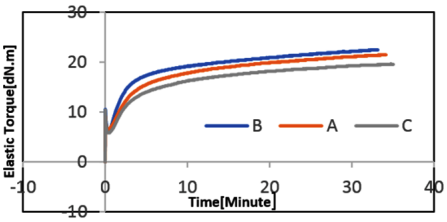

Fig. 1. Rheographs of CR/CSM rubber blend compounds cured with accelerator TMTD, MBTS, and CBS.

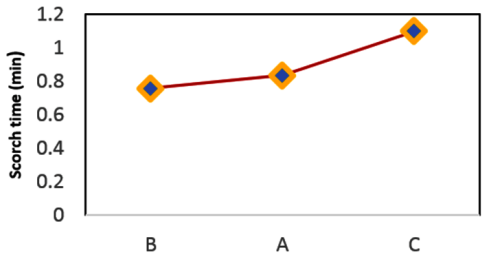

Fig. 2. Scorch time of CR/CSM rubber blend compounds.

of crosslinking density. CBS provides the best processing safety in this compound (Fig. 2). In addition, TMTD and MBTS also provide superior mechanical properties. Due to their lower reactivity, the MBTS accelerator gives a relatively low state of cure. Therefore, the vulcanizates obtained possess low modulus and hardness as well as elasticity [7].

Conclusion

The chosen accelerator affects the cure rate and scorch safety as well as the number and type of the crosslinks formed. The blends with accelerator tetra methyl thiuram disulfide accelerators possess relatively have the highest CRI and the lowest scorch time. Due to the fact that no filler is used in the compound, it can be noted that adding CBS accelerator to the compound greatly reduces the maximum torque.

References

[1] Marković G. and Jovancovic V., Curing and mechanical properties of chlorosulphonated polyethylene rubber blends, *Chem. Ind. Chem. Eng. Q.*, **17**, 3, 315−321, 2011.

[2] Marković G., Samaržija Jovanović S., Jovanović V., Marinović-Cincović M., and Budinski-Simendić J., *Chem. Ind. Chem. Eng. Q.*, **15**, 4, 291-298, 2009.

[3] Konar B.B., Studies on the effects of cyclohexyl benzothiazylsulphenamide accelerated sulphur vulcani-zation of natural rubber: Thermochemistry and oxidative aging, *J. Indian Chem. Soc.*, **82**, 7, 639–644, 2005.

[4] Konar B.B., Studies on the effects of cyclohexylbenzothiazolsulphenamide accelerated sulphur vulcanization of natural rubber. Part I: kinetics of vulcanization, *J. Indian Chem. Soc.*, **81**, 2, 141–146, 2004.

[5] Flory P.J., Effects of molecular structure on physical properties of butyl rubber, *Ind. Eng. Chem.*, **38**, 4, 417–436, 1946.

[6] Roychoudhura Y. and De P.P., Studies on chemical interactions between CSM and carboxylated nitrile rubber, *J. Appl. Polym. Sci.*, **63**, 1761–1768, 1997.

[7] Marković G. and Radovanović B., The effect of accelerators on curing characteristics and properties of natural rubber/chlorosulphonated polyethylene rubber blend, *Mater. Manuf. Proc.*, **24**, 10-11, 1224-1228, 2014.

14-15 December 2021, Tehran, Iran
2nd International Conference on Rheology
ICOR 2021
article A-10-249-1

Investigation of Effective Parameters on the Rheological Behaviors of UHMWPE/HDPE Blends

Zahra Yagoobi[1], Azam Jalali-Arani[1*], Abdolhanan Sepahi[2], and Reza Rashedi[2]
1. Polymer and Color Engineering Department, Amirkabir University of Technology, P.O. Box: 15875-4413, Tehran, Iran
2. Research and Development Center, Jam Petrochemical Co., Postal Code 1434853114, Tehran, Iran

* ajalali@aut.ac.ir

Abstract
The most common route to improve the properties of bimodal high-density polyethylene (HDPE) pipes is to add ultrahigh molecular weight polyethylene (UHMWPE), which however alters processability. Blends of HDPE and an additive-like amount of ultrahigh molecular weight polyethylene (UHMWPE) are found to offer improved sagging resistance, without compromising the melt flowability. In this study, a commercial HDPE with three types of UHMWPE differing in their molecular weights are explored. Rheological parameters (G', G", and η*) were shown that the chains of UHMWPE of 2.2 million g/mol have the highest possibility to form entanglements with the adjacent chains, confining the chain motions and increase elasticity. Such increased melt elasticity is more evident, when the UHMWPE fraction is more than 1 wt%. Furthermore, flow curve measurements and analysis of Carreau-Yasuda model indicated the incorporation of UHMWPE could result in shear thinning effect and provides the ability to arrest sagging.

Keywords: UHMWPE, rheology, entanglements, bimodal HDPE, sagging

Introduction

Bimodal HDPE offers distinct advantages compared with other piping materials because of its good mechanical properties [1]. However, bimodal HDPE lack the melt elasticity and tend to sag before hardening, due to the absence of the very high molecular weight tail [2].

Melt mixing of bimodal HDPE with UHMWPE as an engineering plastic with more of tie molecules can lead to a blend with high melt elasticity. However, a few research works have discussed the processing properties of UHMWPE/HDPE blends [3,4]. Accordingly, the form stability and sagging resistance of UHMWPE/HDPE is an interesting problem and has not been well understood up to date, although there have been few investigations to turn HDPE into an infusible network through crosslinking [5].

In this work, we explored the impact of the content and molecular weight of the UHMWPE component on the ability of HDPE to resist sagging as well as the ability of the different UHMWPE grades to mix with HDPE during melt blending.

Experimental

Materials and Sample Preparation

Bimodal HDPE resin powder provided by Jam Petrochemical Co., was used in this study (density 0.94–0.950 g/cm^3). Three UHMWPE resins of different viscosity-average molecular weights (Mv) (referred further as UH-L (2.2×10^6 g.mol^{-1}), UH-M (3.3×10^6 g.mol^{-1}), and UH-H (4.5×10^6 g.mol^{-1})) were synthesized as per procedures outlined elsewhere [6].

The HDPE and UHMWPE powders were melt-blended by a co-rotating twin screw extruder at a screw speed of 180 rpm and a temperature profile of 190-220 °C. The HDPE samples containing 0.0, 1.0, 5.0, and 10 wt%, of UH-L, UH-M and UH-H were prepared and labled according to UHMWPE content and Mw. Hence, a polymer with a code such as HU1-2.2 M has 1.0 wt% of UH-L.

Methods

Oscillatory and shear flow measurements were conducted on a modular compact rheometer (PhysicaMCR502, Anton Paar) with parallel plates (25 mm in diameter with a gap of 1 mm) at 180 ºC under nitrogen atmosphere. The dynamic frequency (ω) sweep test was carried out in the frequency range of 0.01–100 rad/s and at a strain value of 1%.

Results and Discussion

To compare the difference in melt flow behaviors of HDPE and UHMWPE/HDPE composites, dynamic frequency sweep, were carried out.

The results of storage modulus (G') and complex viscosity (η*) as a function of angular frequency (ω) at low frequency range (i.e. ω<0.1) are shown in Fig. 1a and 1b. As can be observed from the slopes of the curves, G' get much higher values when the UHMWPE fraction is increased, corresponding to the long relaxation time of UHMWPE [1].

The dynamic loss modulus (G") showed the same trend as G' (not shown here).

Interestingly, the extent of change in G' and G" showed a distinguishable difference, when the molecular weight of UHMWPE has its lowest value (i.e. 2.2 million g/mol) in each fraction of blends and the G' and G" curves of blends of UH-M and UH-H are nearly overlapped. The long chains of UH-L have fewer numbers of entanglements and are much easier to relax and overlap with the adjacent chains during the blending, however, the long chains of UH-M and UH-H are hard to relax, because of its higher entangled state [7]. Moreover, the G' of samples of UH-M and UH-H maintains nearly the similar value, when the UHMWPE fraction is further increased than 1 wt%, probably because of the decreased miscibility of the blends [6].

Table 2. Zero shear viscosity parameter of the Carreau Yasuda equation for HDPE and blend samples.

Samples	HDPE	HU1-2.2M	HU1-3.3M	HU1-4.5M	HU5-2.2M	HU5-3.3M	HU5-4.5M	HU10-2.2M	HU10-3.3M	HU10-4.5M
η_0 ($\times 10^6$)	0.536	0.698	0.601	0.586	0.844	0.795	0.745	1.850	1.400	1.540

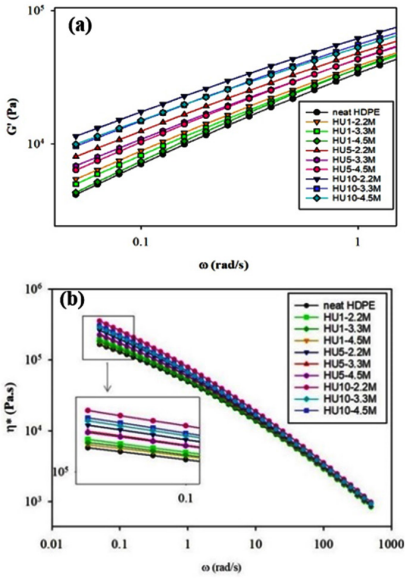

Fig. 1. The dynamic shear oscillatory measurements of the blend samples: (a) Storage modulus (G') and (b) complex viscosity (η*).

Fig. 1b shows the curves of η^* vs. ω. For HDPE, the value of η^* changes less with the variation of ω. The η^* increases gradually and becomes more dependence on the frequency, when the fraction of UHMWPE is increased. It can be registered with the increased molecular weight of the matrix. Accordingly, the slope of the curves is increased, indicating that the shear thinning phenomenon of the blends becomes apparent.

In order to evaluate the sagging resistance of blend samples, the zero-shear viscosity values were determined from the steady state flow curves (Fig. 2) using the Carreau–Yasuda model which is fitted on each curve (Eq. (1)):

$$\eta = \frac{\eta_0}{\left\{1+(\lambda\dot{\gamma})^a\right\}^{\frac{(1-n)}{a}}} \quad (1)$$

Where, η_0 is the zero-shear viscosity, $\dot{\gamma}$ is the shear rate, λ is the characteristic time and a and n are the power law exponents. The η_0 parameter shown in Table 2 indicates that the incorporation of UHMWPE up to 10 wt%, regardless of molecular weight differences, has led to a noticeable increase of the sag resistance for blends, compared with HDPE. However, it should be considered that the entanglements of UH-L, could be unfastened more easily and form new entanglements with the adjacent chains, and hence demonstrates less sagging.

Conclusion

Binary blends of UHMWPE/HDPE were prepared at various molecular weight and content of UHMWPE and evaluated for their rheological characteristics and then their sagging resistance. The rheological studies have revealed the considerable enhancement in the elastic and

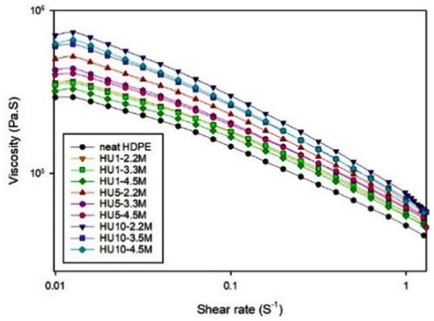

Fig. 2. Flow curves of HDPE and blend samples.

viscose parameters by up to 10% increment in UHMWPE content. In addition, at each UHMWPE content, the lowest molecular weight, i.e., 2.2 million g/mol, shows the highest value of G', G", and η* due to the ability to form new entanglements with its neighboring HDPE chains more conveniently.

Eventually, we have demonstrated from the shear flow measurements and Carreau-Yasuda model fitting that UHMWPE/HDPE blends results in shear-thinning characteristics and have higher sagging resistance. The extent of sagging variation follows the same trend as zero-shear viscosity.

References

[1] Jaggi H.S., Satapathy B.K., Ray A.R., Viscoelastic properties correlations to morphological and mechanical response of HDPE/UHMWPE blends, *J. Polym. Res.*, **21**, 482, 2014.

[2] DesLauriers P.J., McDaniel M.P., Krishnaswamy R.K., *Polym. Eng. Sci.*, **45**, 1203–1213, 2005.

[3] Lim K.L.K, Ishak Z.A.M., Ishiaku U.S., and Fuad A.M.Y., High-density polyethylene/ultrahigh-molecular-weight polyethylene blend. I. The processing, thermal, and mechanical properties, *J. Appl. Polym. Sci.*, **97**, 413-425, 2005.

[4] Aguilar M., Martín S., Vega J.F., Muñoz-Escalona A., and Martínez-Salazar J., Processability of a metallocene-catalyzed linear PE improved by blending with a small amount of UHMWPE, *J. Polym. Sci. Part B Polym. Phys.*, **43**, 2963–2971, 2005.

[5] Oliveira G.L. and Costa M.F., Optimization of process conditions, characterization and mechanical properties of silane crosslinked high-density polyethylene, *Mater. Sci. Eng. A*, **527**, 4593–4599, 2010.

[6] Bahrami H., Ramazani S.A.A., Shafiee M., and Kheradmand A., Preparation and investigation of tribological properties of ultra-high molecular weight polyethylene (UHMWPE)/graphene oxide, *Polym. Adv. Technol.*, **27**, 1172–1178, 2016.

[7] Chen Y., Zou H., Cao Y., and Liang M., Melt miscibility of HDPE/UHMWPE, LDPE/UHMWPE, and LLDPE/UHMWPE blends detected by dynamic rheometer, *Polym. Sci.-Ser. A*, **56**, 630–639, 2014.

14-15 December 2021, Tehran, Iran
2nd International Conference on Rheology
ICOR 2021
article A-10-251-1

Non-Einstein Rheological Behavior in Multiblock Copolymer Nanocomposites

Hamid Reza Heydarnezhad[1*], Naser Mohammadi[1], and Angel Alegria[2]
1. Department of Polymer Engineering and Color Technology, Amirkabir University of Technology, P.O. Box 1591634311, Tehran, Iran
2. Centro de Física de Materiales (CSIC, UPV/EHU) and Materials Physics Center (MPC), San Sebastián E-20018, Spain

*hr.heydarnezhad@aut.ac.ir

Abstract
The fundamental feasibility of the nanoparticle-induced viscosity reduction in multiblock copolymer-based nanocomposites was monitored via the shear rheological properties of segmented polyurethane/C_{60} nanocomposites (NPUs) up to 2 wt% of C_{60}. Despite the same dynamical behaviors for each matrix (PU) and its corresponding NPUs in the absence of deformation, interesting changes in the terminal rheological properties of PUs were found in the presence of C_{60} nano-filler. An anomalous terminal shear viscosity (η_0) reduction was observed for microphase-mixed PUs at low C_{60} content up to 0.5 wt%. However, the microphase-mixed NPUs having more C_{60} as well as the microphase-separated NPUs exhibited higher η_0 than their matrices. Slippage at the polymer/C_{60} interfaces was proposed as a possible mechanism behind the viscosity drop, which appeared tunable by the degree of microphase separation, the ratio of slip length to the nanoparticle size, and the stiffness of segments. Accordingly, an effective slip length, beff, was considered as the key factor in controlling the observed non-continuum effects regarding the microphase-mixed PUs.

Keywords: Multiblock copolymers, polyurethanes, nanocomposites, rheology, interfacial slippage

Introduction

As with most of homopolymer, the viscosity uprising of multiblock copolymers in the presence of nanoparticles, confirming Einstein's prediction [1], is well-known as a limiting factor in their processability. Despite numerous studies on the anomalous nanoparticle-induced viscosity reduction in the homopolymer-based nanocomposites [2-5], no systematic study was conducted regarding the phenomenon scrutinizing in the nanocomposites with multiblock copolymer matrices, to the best of our knowledge. On the other hand, substitution of homopolymers with multiblock copolymers as the matrix of nanocomposites can be accompanied with various advantages, leading to more applicability of them [6]. Thus, developing universal concepts regarding the feasibility of anomalous viscosity reduction in the multiblock copolymer-based nanocomposites appears valuable in polymer science and engineering, which were considered in our recent works [7,8]. Here, our attempt has been presented to address this complicated and poorly understood challenge through a series of multiblock polyurethane nanocomposites.

Experimental

Segmented polyurethanes (PUs) and corresponding nanocomposites (NPUs) with 40 wt% of hard segments were synthesized by three molecular weight (425, 2000, and 4000 g/mol) of poly(propylene glycol) as soft segments in a typical two-step bulk polymerization. C_{60} nanoparticles with 0.7 nm in diameter was also selected based on the requirements for achieving anomalous viscosity reduction of homopolymer-based nanocomposites. All samples were nomenclated by four sections: type of sample (PU or NPU), soft segment (SS) molecular weight, wt% of hard segment (HS), and finally wt% of nanoparticles in NPUs, which is discarded for PUs. Broad-band dielectric spectroscopy (BDS), small-angle X-ray scattering (SAXS), rheometric mechanical spectrometry (RMS), and differential scanning calorimetry (DSC) were applied as main characterization methods.

Results and Discussion

Our RMS experiments clearly show that η_0 of highly microphase-separated PUs such as PU-2000-H40 and PU-4000-H40 increases in the presence of C_{60} as a function of the nanoparticle content, while a low concentration of C_{60} nanoparticle up to 0.5 wt% decreases η_0 of the microphase-mixed PU-425-H40. These results were shown in Fig. 1 through the relaxation time spectra. However, the results of SAXS, DSC, and BDS revealed almost similar microstructural features in each group of PU and corresponding NPUs, regardless of the C_{60} loadings. In addition, apart from slowing down of αmixed process in the presence of 2 wt% of C_{60}, no

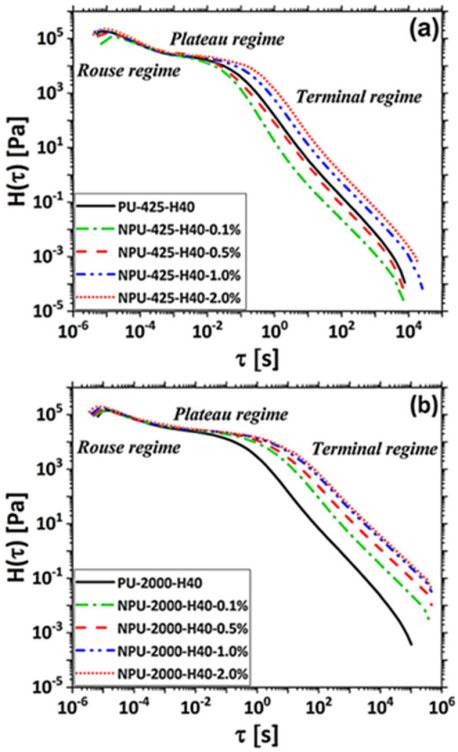

Fig. 1. Relaxation spectra for the model PUs and their corresponding NPUs at 75 °C [8].

remarkable effect of C60 nanoparticles on the dynamics of PUs was found from the BDS results, Fig. 2. Despite the failure of most possible mechanisms in interpretation of the nanoparticle-induced viscosity reduction of PU-425-H40, it seemed that the interfacial slipping under shearing conditions can be contribute to this rheological anomaly. Indeed, since no nanoparticle-induced effects were detected under deformation-free experiments such as BDS and DSC, the viscosity decrease under shearing (shear rheometry) could be assigned to the interfacial slippage through a drop in friction between C_{60} nanoparticles and surrounding polymer chains. Noteworthy, the number of possible molecular configurations of polymer chain segments in the vicinity of nanoparticles can be increased under shear flow when the friction between the nanoparticles and matrix chains is less than the friction between pure matrix chains. Hence, despite the absence of entropy increase for polymer chains under deformation-free conditions, the polymer chains under shear experience additional entropy at the interface with nanoparticles. This additional entropy leads to an increase in free volume at particle-polymer interfaces and thus induces a decrease in shear viscosity, whereas in the deformation-free conditions no increase in the free volume is observed as can be revealed from the observed constant T_g.

Conclusion

Fundamental insights on how to achieve a reduction in the shear viscosity of the multiblock copolymers using ultrafine

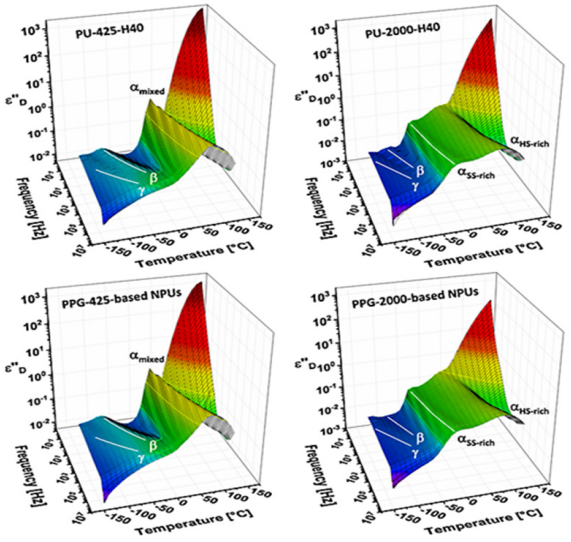

Fig. 2. Conductivity-free dielectric relaxation spectra as a function of frequency and temperature for the studied PUs and NPUs [8].

nanoparticles were provided via various investigations on a series PUs and NPUs. The results of deformation-free experiments such as SAXS, DSC, and BDS revealed no significant changes in the microstructural features and the dynamical relaxations of PUs in the presence of C_{60} nanoparticles up to 2 wt%. Under shear condition, however, the linear rheological properties of each NPU were found different from corresponding properties in its PU matrix at terminal regime. Regarding the analyses and failure of known mechanisms in describing the observed rheological behaviors, an interfacial slippage mechanism at polymer/C_{60} interfaces was considered to be responsible for the observed reductions in the shear viscosity. Hence, an effective slip length, beff, was introduced as key factor in controlling the observed non-continuum effects on the nanoparticle-induced viscosity reduction in microphase-mixed PUs.

References

[1] Einstein A., Eine neue Bestimmung der Moleküldimensionen, Annalen der Physik, 324, 371, 1906.
[2] Mackay M.E. et al., Nanoscale effects leading to non-Einstein-like decrease in viscosity, *Nature Mater.*, **2**, 762, 2003.
[3] Tuteja A. et al., *Macromolecules*, **38**, 8000, 2005.
[4] Tuteja A. et al., *Macromolecules*, **40**, 9427, 2007.
[5] Tuteja A.M.E. et al., *Nano letters*, **7**, 1276, 2007.
[6] Bockstaller M.R. et al., Block copolymer nanocomposites: perspectives for tailored functional materials, *Adv. Mater.*, **17**, 1331, 2005.
[7] Heydarnezhad H.R. et al., *Macromolecules*, **53**, 5381, 2020.
[8] Heydarnezhad H.R. et al., *Macromolecules*, **54**, 2783, 2021.

14-15 December 2021, Tehran, Iran
2nd International Conference on Rheology
ICOR 2021
article A-10-252-1

Preparation of Composite with High Damping Using Nitrile-Butadiene Rubber/Phenolic Resin

As'ad Zandi[1*], Mohadeseh Jafarzadeh[2], and Sahar Tavosi[1]
1. Polymer Engineering Department, Faculty of Chemical Engineering, Tarbiat Modares University, P.O. Box 14115-114, Tehran, Iran
2. Caspian Faculty of Engineering, College of Engineering, University of Tehran, Guilan, Iran

*asadzandi@modares.ac.ir

Abstract
Rubber is the most important damping material because of its unique viscoelastic properties. The damping principle of rubber damping material is to use the viscoelastic property of the polymer to absorb vibration energy. In this research work, NBR and phenolic resin (P55) in with a mass ratio of 80:20 and three different values of Carbon black were used. According to the resilience test the sample with 70 phr carbon black had a damping value of 91% and according to the DMA test at 10 Hz, tan δ peak showed 0.8 at a temperature of about 25°.

Keywords: rubber, viscoelastic properties, vibration energy, nitrile-butadiene rubber, phenolic resin

Introduction

Damping materials have been widely used in the vibration and noise control to reduce their harmful consequences in the military and civil areas such as their application in the aerospace and naval vessels, transportation vehicles, bridges and high buildings [1]. Polymer, especially rubber material, has unique high damping property around its glass transition temperature (Tg). During the relaxation process, part of the vibration energy dissipates as heat due to the friction between polymer chains. The loss tangent (tan δ), defined by the ratio of loss modulus (E″) to storage modulus (E′), can be a measurement of the dissipation of the vibration energy. High performance damping materials should have a high loss factor (tan δ>0.3) over a broad temperature range of at least 60–80 °C difference. However, a homopolymer usually only has effective damping performance below the room temperature with a narrow temperature range of only 20–30 °C difference. Nitrile butadiene rubber/ phenolic resin (NBR/PR [NBPR]) was selected as matrix and different amounts of carbon black (0, 10, and 70 phr) were added to this system. NBR exhibits excellent damping performance due to the presence of polar cyan functional groups in its structure [2].

Experimental

NBR with an acrylonitrile weight content of 41% (N220S) was provided by Japan Synthetic Rubber Co., Ltd (Japan). Phenolic resin granols (P55) were obtained from Wuxi Mingyang Bonding Material Co., Ltd (China). Other rubber processing additives were of analytical grade and used without further purification. The NBPR composites were obtained by mixing the NBR and PR granols (the mass ratio of NBR and PR is 80:20) in φ152.4 mm two-roll mill at room temperature. Then, the compounding and crosslinking additives were added to the above mixtures, including 5.0 phr of zinc oxide, 2.0 phr of stearic acid, 0.2 phr of tetramethylthiuram disulfide, 0.5 phr of diphenyl guanidine, 0.5 phr of dibenzothiazole disulfide, and 2.0 phr of sulfur. Three samples were prepared with carbon block values of 0, 10, and 70 phr, which were named as follows, respectively CB (0 phr), CB (10 phr), CB (70 phr). Finally, the mixtures were hot pressed and vulcanized at 160 °C and 15 MPa for their corresponding T90 (optimum

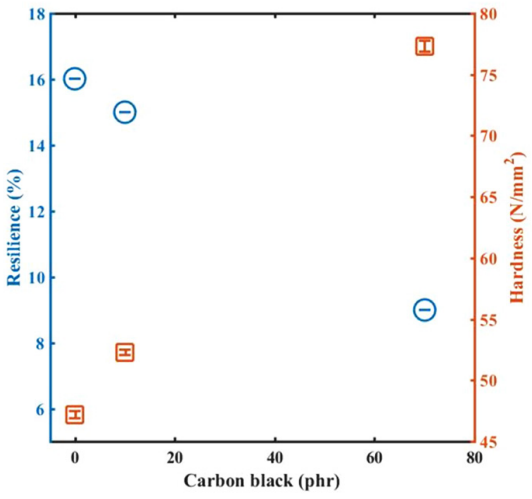

Fig. 1. Results of resilience and hardbess of CB (0 phr), CB (10 phr) and CB (70 phr) samples.

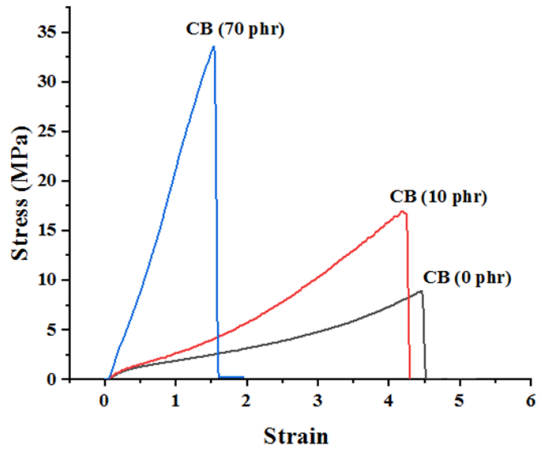

Fig. 2. Stress vs strain for CB (0 phr), CB (10 phr), and CB (70 phr) samples.

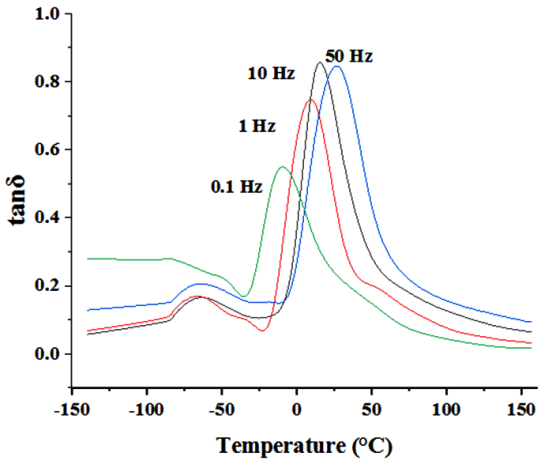

Fig. 3. Tan δ vs temperature at frequencies of 0.1, 1, 10, and 50 Hz, for example with 70 phr carbon block.

cure time). The dynamic mechanical analysis (DMA) of the cured blend is performed on a NETZSCH Dynamic Mechanical Thermal Analyzer model DMA 242 with the tension sample holder. The dimensions of the specimens are 10×5×2 mm. The dynamic force on sample is 4 N, and it is used to produce oscillating amplitude of 30 μm. If this target amplitude cannot be achieved, the measurement will run with the maximum possible force. The sample is scanned from -150 °C to 160 °C at a heating rate of 5 °C/min, and the frequencies used in the measurement are 0.1, 0.5, 1, 5, 10, and 50 Hz. Resilience , Hardness and Tensile properties It was done according to the ASTM D1054, ASTM D2240, and D412 Respectively.

Results and Discussion

Fig. 1 shows that by increasing the amount of carbon black to 70 phr, the sample dampness has become 91%. Also, with increasing carbon black, the hardness of the samples increased, which is normal. Fig. 2 shows that with increasing carbon black the modulus increased and the strain at break decreased which is reasonable. Fig. 3 shows the tan δ in terms of temperature for the 70 phr carbon block sample, showing two tan δ peaks shifting to higher temperatures as the frequency increases.

Conclusion

According to DMA and resilience tests, the sample with 70 phr carbon block has a high damping. The tan δ peak is at 10 Hz in the ambient temperature range. According to the DMA results in the range of approximately 0° to 50°, this sample has a suitable damp and can be used for applications in this temperature range. Of course, other properties should be considered according to the intended application.

References

[1] Lu X., Li X., and Tian M., Preparation of high damping elastomer with broad temperature and frequency ranges based on ternary rubber blends, *J. Polym. Adv. Technol.*, **25**, 21–28, 2014.

[2] Song M., Yue X., Wang X., Huang M., Ma M., Pan W., and Qin Q., Improved high-temperature damping performance of nitrilebutadiene rubber/phenolic resin composites by introducing different hindered amine molecules, *J. E-Polym.*, **20**, 482–490, 2020.

14-15 December 2021, Tehran, Iran
2nd International Conference on Rheology
ICOR 2021
article A-10-253-1

Tuning Pressure-Sensitive Adhesion in Blend Adhesives Using Viscoelastic Properties

As'ad Zandi and Somayeh Ghasemirad*
Polymer Engineering Department, Faculty of Chemical Engineering, Tarbiat Modares University, P.O. Box 14115-114, Tehran, Iran

*ghasemirad@modares.ac.ir

Abstract
Despite their generally high shear strength, thermoplastic polyurethane pressure-sensitive adhesives (TPU-PSAs) suffer from low tack. Herein, a synthesized TPU-PSA containing 17.5% hard segment was blended with a synthesized acrylic copolymer PSA comprised of 82 wt% butyl acrylate and 18 wt% methyl methacrylate. The purpose of the research was to control the pressure-sensitive adhesion using Chang's viscoelastic window and Chu's criteria. The blend PSAs generally demonstrated shear strengths and loop tack values in between and more than those of the pure components, respectively. The loop tack of the blend PSA was maximized at the TPU content of 40 wt% in the blend.

Keywords: thermoplastic polyurethane, pressure-sensitive adhesive, chang's viscoelastic window, loop tack, shear strength

Introduction

Pressure-sensitive adhesives (PSAs) are able to bond various substrates under light pressure in a short time, and they must be debonded without leaving residue on the substrate [1]. PSAs are used in labels, tapes, protective films, and medical products (patches, bandages, electrodes, plasters, etc.). Performance of PSAs are controlled by their viscoelastic properties due to the required balance between viscous and elastic components required for adequate bonding upon contact with the substrate and desired debonding. The performance of the PSAs are determined by three main characteristic properties, namely tack, shear strength, and peel strength.

According to the Dahlquist's criterion, an adequate tack in PSAs is obtained at G' values lower than 3×105 Pa at 25 °C and frequency of 1 Hz [2]. According to Chu, an adequate combination of adhesion (tack, peel) and cohesion (shear) properties in PSAs is expected when the G' value measured at 0.1 rad/s is (2–4) $\times 10^4$ Pa and the (G' at 100 rad/s)/(G' at 0.1 rad/s) ratio is 5 to 300 [3].

Experimental

4,4-diphenylmethane diisocyanate (MDI) was kindly donated by Karoon Petrochemical Co. (Iran) and poly(propylene glycol) (PPG) with molecular weight of 2000 g/mol was supplied by Isfahan Copolymer Co. (Iran). Dibutyl tin dilaurate (DBTDL), 1,4-butanediol (BD), and N,N-dimethyl formamide (DMF) were obtained from Merck Co. (Germany). Methyl Methacrylate, Butyl acrylate and ethyl acetate were purchased from Merck (Germany) and 2,2'-azobisisobutyronitrile (AIBN) as an initiator were purchased from daejung (Korea).

TPU-PSA was synthesized by using the prepolymer method in 250 mL flask under inert atmosphere (dried nitrogen) using an anchor impeller and overhead stirrer RZR-2102 (Germany). NCO/OH molar ratio of 1:1 were used considering also the OH groups of BD in the calculation [1]. MDI was melted at 80 °C in the flask, and the PPG, dried at 80 °C under reduced pressure (300 mbar) for 2 h, was added under stirring at 250 rpm. The reaction was continued for 30 min. Afterwards 0.02 mmol of catalyst (DBTDL) was added and the stirring was decreased to 80 rpm. The reaction lasted for 2 h and the amount of free NCO content was determined by dibutylamine titration. Then, the chain extender (BD) was added under stirring at 80 °C and 80 rpm for 5 min. DMF was used to dissolve the TPUs prior to coating on poly(ethylene terephthalate) (PET)

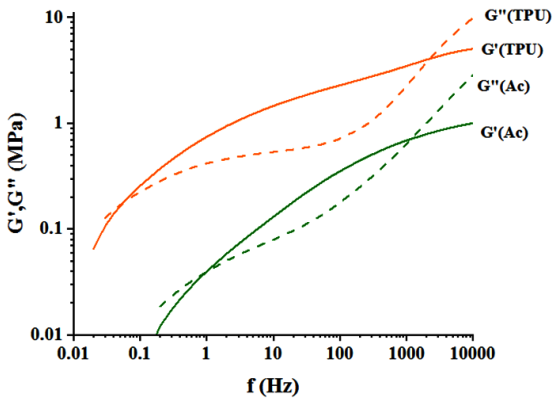

Fig. 1. Rheological mastercurve of TPU-PSA and Ac-PSA.

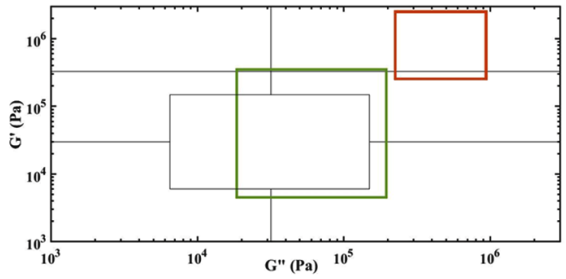

Fig. 2. Chang's viscoelastic window of TPU-PSA (orange) and Ac-PSA (green).

films. For synthesizing acrylic PSA (Ac-PSA), the reactor was initially charged with MMA and BA (18:82 by weight), ethyl acetate, and AIBN solution [4]. The polymerization was carried out in a 250-mL four-necked flask, equipped with a reflux condenser and a nitrogen inlet. The reaction was conducted at 75 °C for 4.5 h. The blends of TPU-PSA and Ac-PSA were prepared at various compositions using a magnetic stirrer at 350 rpm. The mixing was carried out at 25 °C temperature for 5 h. The blends were coded with "TPUx-Ac" where x signifies the composition of TPU in the blend in wt%.

The viscoelastic properties of the pristine TPU-PSA and Ac-PSA were measured using dynamic mechanical analysis (DMA) by Netzsch DMA 242 (Germany) at a strain of 30 µm, frequency of 0.1-50 Hz, and temperature range of -20-40 °C. The loop tack was investigated using a homemade universal testing machine using ASTM D6195-03 at a test speed of 300 mm/min. Static shear test was performed by hanging a weight of 1 kg to the PSA bonded to stainless steel in an area of 25×25 mm^2.

Results and Discussion

Using the rheological mastercurve of TPU-PSA containing 17.5% hard segment, Fig. 1, it was located in the high shear zone of the Chang's viscoelastic window, Fig. 2. Moreover, its lower low-frequency G' than 3×10^5 Pa revealed its PSA character according to the Dahlquist's criterion.

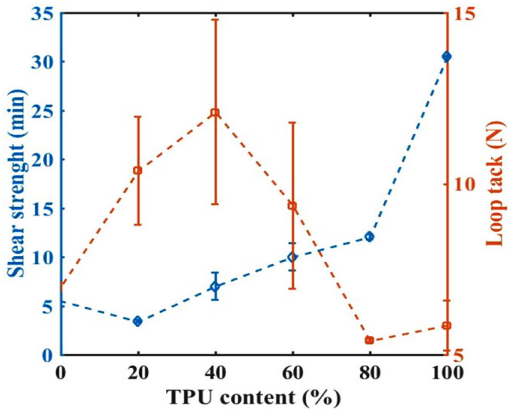

Fig. 3. Shear strength and loop tack of the PSAs versus the TPU content.

Blending of the Ac-PSA with lower storage and loss moduli with TPU-PSA led to preparation of PSAs with a generally higher shear strength than the Ac-PSA and a loop tack of interestingly higher than that of the primary components. The lower shear strength of the TPU20-Ac than the pristine Ac-PSA was probably due to the low content of TPU which could not compensate the phase separation between TPU and acrylic components. However, increase in the TPU content led to formation of interconnected microphase separated regions and an improved shear strength. The tack of the blend PSAs increased up to 40 wt% and decreased at higher TPU contents. The negative impact of the low-acrylic content in the blend, namely 20 wt%, was also observed in the tack.

Conclusion

The blend PSAs were comprised of high-shear moduli TPU and low-shear moduli acrylic copolymer. The blending of high-shear strength TPU and high-tack acrylic copolymer components showed a shear strength in between and a high synergy in tack. The blends far from the middle concentration range showed deterioration in the property expected from the lower-in-concentration component.

References

[1] Fuensanta M. and Martín-Martínez J.M., Influence of the hard segments content on the structure, viscoelastic and adhesion properties of thermoplastic polyurethane pressure sensitive adhesives, *J. Adhes. Sci. Technol*, **34**, 9, 1-20, 2020.

[2] Dahlquist C.A., Pressure-sensitive adhesives. In: Patrick R.L. (Ed.), Treatise on adhesion and adhesives, New York: Marcel Dekker Inc, 1969, pp. 219-260.

[3] Chu S.G., Dynamic mechanical properties of pressure-sensitive adhesives. In: Lee L.H. (Ed.), Adhesive bonding, New York: Plenum Press, 1991, pp. 97-137.

[4] Taghizadeh S. and Ghasemi D., Synthesis and optimization of a four-component acrylic-based copolymer as pressure sensitive adhesive, *Iran. Polym. J.*, **19**, 343-352, 2010.

14-15 December 2021, Tehran, Iran
2nd International Conference on Rheology
ICOR 2021
article A-10-254-1

Interplay between Microstructure and Nonlinear Viscoelastic Behavior of a Unique Thermo-Responsive Hydrogel

Sara Tarashi[1], Hossein Nazockdast[1*], and Saeid Shafaghsorkh[2]
1. Department of Polymer Engineering, Amirkabir University of Technology, P.O. Box 15875-4413, Tehran, Iran
2. Mechanical Engineering Department, University of Kashan, Postal Code 8731753153, Kashan, Iran

*nazdast@aut.ac.ir

Abstract
For the first time, we use the LOAS technique as a powerful tool to achieve rich information about the nonlinear response of a thermo-responsive κ-carrageenan (κ-Car)/polyacrylamide (PAm) double network (DN) system that is closely related to its structure. A strain stiffening behavior (type III) resulted from the inter-cycle viscoelasticity, which could be attributed to the deformation-induced rearrangement of unstable parts in the network structure. The intra-cycle viscoelasticity was analyzed using qualitative normalized Lissajous-Bowditch curves. The results manifested a combination of strain stiffening and shear thickening nonlinear responses. Furthermore, the temperature dependency of the DN hydrogel owing to the conformational changes of the κ-Car network encouraged us to investigate the effect of temperature on the nonlinear behaviors.

Keywords: hydrogel, carrageenan, nonlinear viscoelasticity, LAOS, strain stiffening

Introduction

Double network (DN) hydrogels have been designed as promising tough and strong soft-wet materials [1]. Considering the wide range of applications, understanding the behavior and structural changes of DN hydrogels at large deformation levels can help us to develop them, especially for load-bearing applications. As a common rheological technique, dynamic oscillatory shear measurement is a powerful tool for the evaluation of microstructure under different deformation levels ranging from small amplitude oscillatory shear (SAOS) to large amplitude oscillatory shear (LAOS). Up to now, the rheological studies on the hydrogels were mostly performed using the SAOS tests; however, in recent years, some attempts have been made to achieve additional information about the large deformation response using the LAOS technique. John *et al*. [2] tried to explore the relationship between the cross-linked structure and the nonlinear rheological behavior of pectin/calcium gels. The structural change of the chitosan/β-glycerol phosphate hydrogel as a heat-induced gelling system was studied by Lu *et al*. [3] using the LAOS tests. Goudoulas *et al*. [4] probed the microstructure of gelatin/alginate hydrogel at different concentration ratios and temperatures in the linear and nonlinear regimes. In another study, Tang *et al*. [5] used the LAOS rheology to verify the microstructures of sodium caseinate/polysaccharide hydrogels.

To our best knowledge, a comprehensive attempt on the rheological behavior of DN hydrogels, especially at large deformations is yet to be done. And only a few attempts have made a correlation between the viscoelastic results and physical behaviors. Hence, the current work aims to describe the rheological behavior of a unique thermo-responsive DN hydrogel by the SAOS and LAOS analyses and to establish a logical relationship between its properties and structural changes.

Experimental/Theoretical

Materials

κ-Carrageenan (κ-Car) in powder form was purchased from Sigma-Aldrich. Potassium chloride (KCl), acrylamide (Am), N,N'Methylenebis acrylamide (MBA) and 4'-(2-hydroxyethoxy)-2-methylpropio phenone were also purchased from Sigma-Aldrich and used as received.

Sample Preparation

The DN hydrogels was synthesized by a radical polymerization. Typically, designated amounts of κ-Car, Am, KCl, initiator and MBA were dissolved in deionized water under continuous magnetic stirring. Then, the solution was cooled and exposed to UV light to induce the photo-polymerization reaction of Am at room temperature.

Sample Characterization

Rheological experiments were performed on a DHR-3 rheometer from TA Instruments. A disposable sandblasted parallel plate with a 25 mm diameter and 1 mm gap was used for the measurements and the temperature was controlled by a Peltier plate system. The intra-cycle nonlinear response of hydrogels was performed at five strain amplitudes at two discrete temperatures (T=20 and 70 °C) and at constant

values of angular frequency (1 rad/s).

Results and Discussion

The SAOS measurement (Fig. 1a) reveals a significant temperature dependency for viscoelastic properties of the DN hydrogel, which is attributed to the conformational changes of κ-Car network. Moreover, as it can be seen in Fig. 1b, the inter-cycle nonlinearity of the DN hydrogel is categorized in type III (weak strain overshoot) viscoelastic behavior which can be explained in terms of the viscous dissipation due to the deformation-induced rearrangement of unstable parts in the network structure. The temperature dependency of the DN hydrogel owing to the conformational changes of κ-Car network at sufficiently high temperatures encouraged us to investigate the effect of temperature on the nonlinear behaviors. The strain sweep results at 70 °C, the temperature above the gel-sol transition point of the κ-Car network, are also shown in Fig. 1b. As can be seen, the length of the linear viscoelastic regime as well as the intensity of the overshoot is much lower than those at 20 °C. This is related to the reduction of crosslinks density and consequently lack of some effective interactions contributing to the viscous dissipation as a result of the dissociation of the κ-Car network.

Based on the LAOS measurements of the DN hydrogel (Fig. 2), with an increase in the strain amplitude, the elastic and viscous Lissajous-Bowditch curves change to almost quadrilateral and sigmoidal patterns, respectively, denoting an increased viscous contribution and a gradual transfer from elastic-dominated to the viscous-dominated response. It is also found that the nonlinear behavior is a combination of strain stiffening and shear thickening responses. The elastic intra-cycle strain stiffening is mainly caused by shear-induced increasing the elasticity of network chains and non-Gaussian stretching of individual chains. Although, the orientation of the κ-Car double helix segments and its enhancing effect on molecular orientation can be proposed as another possible mechanism of strain sti-ening. The viscous intra-cycle shear thickening is also interpreted by two mechanisms of shear-induced temporary structure formation and reformation of the dissociated physical

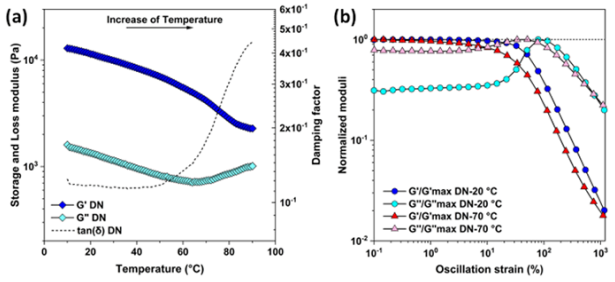

Fig. 1. (a) Changes of storage modulus (G'), loss modulus (G'') and damping factor at a fixed angular frequency (1 rad/s) and small strain amplitude of 1% during the heating process and (b) Changes of normalized G' and G'' as a function of strain at two temperature points and an angular frequency of 1 rad/s.

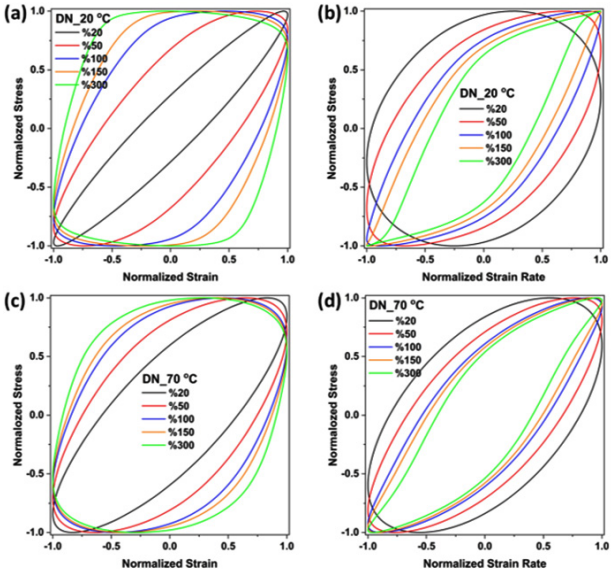

Fig. 2. Elastic (a and c) and viscous (b and d) projection Lissajous-Bowditch loops of DN hydrogel at two temperature points and at different strain amplitudes. All instantaneous stress, strain and strain rate data are normalized with respect to the corresponding maximum values of the oscillation cycle.

interactions. The intra-cycle nonlinear parameters of the DN hydrogel were also investigated at high temperature (Figs. 2c and 2d). Increasing the temperature was found to have a significant decreasing effect on the viscous nonlinearity, while its effect on the elastic nonlinearity was strongly dependent on the strain amplitude.

Conclusion

The inter-cycle nonlinearity of the DN hydrogel is categorized in type III. Based on the LAOS measurements, with an increase in the strain amplitude, the viscoelastic behavior gradually transfers from elastic-dominated to the viscous-dominated response. It is also found that the nonlinear behavior is a combination of strain stiffening and shear thickening responses. Moreover, the nonlinearity of hydrogel is investigated at high temperature.

References

[1] Matsuda T., Nakajima T., Fukuda Y., Hong W., Sakai T., Kurokawa T., Chung U.I., Gong J.P., *Macromolecules*, **49**, 1865-1872, 2016.
[2] John J., Ray D., Aswal V.K., Deshpande A.P. and Varughese S., *Soft matter*, **15**, 6852-6866, 2019.
[3] Lu S., Yang Y., Yao J., Shao Z. and Chen X., *Soft Matter*, **12**, 492-499, 2016.
[4] Goudoulas T., Germann N., *Food Hydrocolloids*, **66**, 49-60, 2017.
[5] Tang M., Lei Y., Wang Y., Li D., Wang L., *Food Hydrocolloids*, **112**, 106251, 2021.

14-15 December 2021, Tehran, Iran
2nd International Conference on Rheology
ICOR 2021
article A-10-254-2

Mechanical Behavior and Rheological Properties of Two Differently Synthesized Double Network Hydrogels: A Comparative Study

Sara Tarashi[1], Hossein Nazockdast[1*], and Saeid Shafaghsorkh[2]
1. Department of Polymer Engineering, Amirkabir University of Technology, P.O. Box 15875-4413, Tehran, Iran
2. Mechanical Engineering Department, University of Kashan, Postal Code 8731753153, Kashan, Iran

*nazdast@aut.ac.ir

Abstract
Double network (DN) hydrogels have been well recognized as new tough materials. However, a comprehensive study on the effect of synthesis methods of DN hydrogels is very critical as they influence their properties and performances. This study is aimed at investigating the effect of two different synthesis methods of thermal-curing and UV-curing on mechanical and rheological properties of the κ-carrageenan (κ-Car)/polyacrylamide (PAm) DN hydrogel. Compared to the thermal-cured DN, the UV-cured DN hydrogel has exhibited different mechanical behavior (plastic-like with localized necking vs. elastomeric-like) and excellent mechanical properties. By focusing on the rheological results, it was demonstrated that the UV-curing method has resulted in much better thermo-reversibility. An attempt was also made to explore the effect of synthesis methods on the properties of hydrogels in presence of GO nanosheets.

Keywords: hydrogel, carrageenan, mechanical behavior, rheological properties

Introduction

Hydrogels are often cross-linked through chemical bonds or physical interactions. It has been well known that both chemically and physically cross-linked single network (SN) hydrogels suffered from a poor mechanical performance. To overcome this drawback, double network (DN) hydrogels have been designed. In the physical-chemical DN hydrogels, the second chemical network is often fabricated by thermal or ultraviolet (UV) initiated radical polymerization using thermal or UV initiation source, respectively. The structure and properties of several physical-chemical DN hydrogels prepared by the thermal curing method have been studied by some research groups. Wang *et al*. [1] found superior mechanical properties and dye adsorption capacity for alginate/PAm DN hydrogel prepared by the thermal-curing method. In addition, Zhu *et al*. [2] studied the mechanical properties of thermally cured agar/PAm/GO DN hydrogel. Furthermore, the properties of UV-cured DN hydrogels have also been investigated by some research groups, i.e., Sue *et al*. [3] demonstrated that the UV-cured alginate/PAm DN shows a combination of relatively high stiffness and toughness. Also, Liu *et al*. [4] fabricated a stretchable alginate/PAm/alginate-amino graphene oxide DN hydrogel through UV-curing.

It has almost been 8 years since the first physical-chemical DN hydrogel was developed, however most efforts have been made to investigate the mechanical properties of these DN hydrogels and a comprehensive attempt on the role of the synthesis method on the mechanical and rheological properties of these hydrogels is yet to be done. Therefore, in this work, we strive to compare the effect of two different synthesis methods (thermal-curing and UV-curing techniques) of the physical-chemical DN hydrogels on mechanical and rheological properties.

Experimental/Theoretical

Materials

κ-Carrageenan (κ-Car), Potassium chloride (KCl), acrylamide (Am) and N,N'Methylenebis acrylamide (MBA) were purchased from Sigma-Aldrich. Ammonium persulfate (APS) and 2-hydroxy-4'-(2-hydroxyethoxy)-2-methylpropiophenone as thermal and UV initiators, respectively were also purchased from Sigma-Aldrich. Graphene oxide (GO) was the product of Angstron Materials.

Sample Preparation

The UV-cured DN hydrogels were synthesized by a radical polymerization. Typically, κ-Car, Am, KCl, UV-initiator and MBA were dissolved in deionized water or GO suspension under stirring. Then, the solution was cooled and exposed to UV light to induce the photo-polymerization reaction of Am. Similarly, the thermal-cured DN hydrogels were obtained by replacing the UV-initiator with APS. In this method, first, κ-Car, Am, KCl, and MBA were added into the deionized water or GO suspension under stirring, then, APS was introduced. The obtained solution was then quickly poured into a mold. The sealed mold was cooled, and then placed into an oven at 60 °C for 24 h. Samples were named as i-DN for double network hydrogel and i-DNGOx for double network containing GO. i=UV or Thermal represent the UV-curing or thermal-curing methods, and x is the weight percentage of GO.

Sample Characterization

Mechanical properties of hydrogels were measured on an Instron Machine. For tensile tests, the stretch rate of the upper clamp was kept constant. Rheological experiments were carried out by using a MCR301 rheometer with a parallel-plate system and temperature was controlled by a Peltier plate.

Results and Discussion

Tensile results (Fig. 1) have demonstrated that although the UV-cured hydrogels exhibit a plastic-like behavior with pronounced localized necking, the thermally-cured one shows an elastomeric-like behavior. Moreover, the mechanical properties of the UV-DN hydrogel (σ_f =0.42 MPa, ε_f =2079%, E=0.1 MPa, and W=3.54 MJ/m^3) are greater than those of Thermal-DN hydrogel (σ_f=0.12 MPa, ε_f=722%, E=0.069 MPa, and W=0.50 MJ/m^3), which can be explained in terms of reducing the contribution of the κ-Car physical network and also reversible interactions in favor of increasing the cross-link density of PAm chemical network through grafting reaction in the thermally-cured hydrogel. Fig. 1 also reveals that the addition of GO can have an enhancing effect on the mechanical performances of both hydrogels. The reinforcing efficiency of GO on the UV-cured hydrogel is higher than those of the thermal-cured hydrogel at the same GO content. This was attributed to the decrement in the GO interactions with individual networks as well as inter-network interactions as a result of the partial reduction of GO nanosheets in the thermal-curing method. By focusing on rheological measurements (Figs. 2a and 2b), one may notice that although the G' and G'' of the UV-cured hydrogels demonstrate a thermo-reversible behavior, the thermally-cured hydrogels exhibit no thermo-reversibility which can be due to the increasing the extent of physical network structural development caused by joining a fraction of grafted κ-Car molecules into the physical network. According to the strain sweep tests (Figs. 2c to 2f), both hydrogels have exhibited that G' is higher than G'' up to a critical strain level beyond which the G' was rapidly decreases with increasing the strain, indicating a 3D structural break down. The higher values of G' and G'' observed for thermally-cured hydrogels can be related to the enhancing effect of grafting on cross-link density of the chemical network. Interestingly, by comparing Figs. 2c and 2e with Figs. 2d and 2f, one may realize that the extent

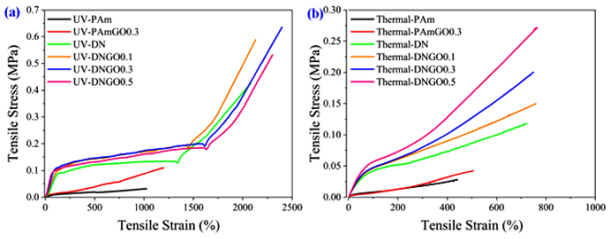

Fig. 1. Stress-strain curves under uniaxial tensile for the hydrogels prepared by: (a) UV-curing and (b) thermal-curing methods.

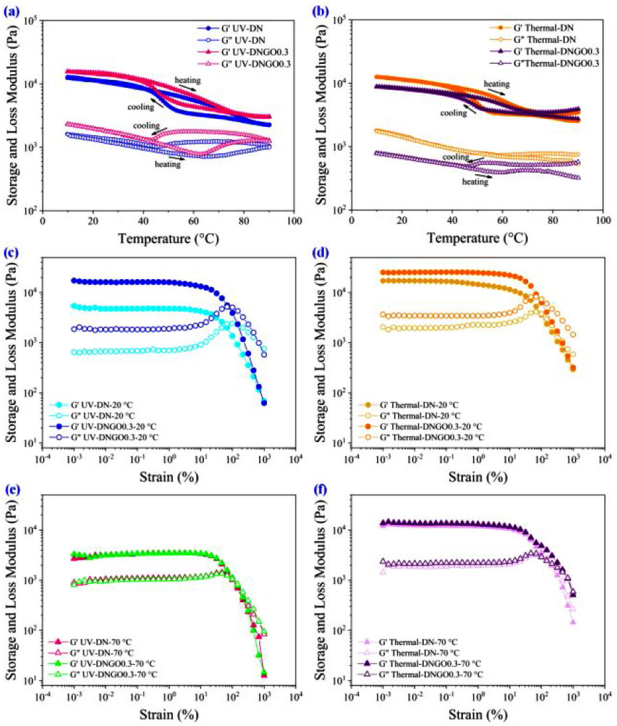

Fig. 2. Dependence of G' and G'' on temperature during a temperature sweep at a cooling and heating rate of 2 °C/min with a fixed angular frequency and strain amplitude. G' and G'' during strain sweep from 0.001% to 1000% at a constant angular frequency and at (c and d) 20 °C and (e and f) 70 °C for different hydrogels.

of reducing of G' and the overshoot associated with G'' at 70 °C are greater for the UV-cured hydrogels. On the other hand, the physical network has a considerable contribution on determining the overshoot in the G'' of the hydrogels.

Conclusion

Tensile results have demonstrated that although the UV-cured hydrogels exhibit a plastic-like behavior, the thermally-cured one shows an elastomeric-like behavior. It was also found that the mechanical properties of the UV-DN hydrogel were greater than those of Thermal-DN. Interestingly, the addition of GO can have an enhancing effect on the mechanical performances of both hydrogels. Moreover, as evidenced by the rheological results, the UV-cured hydrogels exhibited better thermo-reversibility in comparison with the thermally-cured hydrogels.

References

[1] Wang J., Su S., and Qiu J., *New J. Chem.*, **41**, 3781-3789, 2017.
[2] Zhu P., Hu M., Deng Y., and Wang C., *Adv. Eng. Mater.*, **18**, 1799-1807, 2016.
[3] Sun J.Y., Zhao X., Illeperuma W., Chaudhuri O., Oh K.H., Mooney D.J., Vlassak J.J., and Suo Z., *Nature*, **489**, 133-136, 2012.
[4] Liu S., Bastola A.K., and Li L., *ACS Appl. Mater. Interfaces*, **9**, 41473-41481, 2017.

14-15 December 2021, Tehran, Iran
2nd International Conference on Rheology
ICOR 2021
article A-10-256-1

Evaluation of PLA Functionalization Process Efficiently by Using of FTIR, DMA and Tensile Technique

Elnaz Janjan[1], Gity Mir Mohamad Sadeghi[1*], and As'ad Zandi[2]
1. Department of Polymer Engineering, Amirkabir University of Technology, P.O. Box 15875-4413, Tehran, Iran
2. Polymer Engineering Department, Faculty of Chemical Engineering, Tarbiat Modares University, P.O. Box 14115-114, Tehran, Iran

*gsadeghi@aut.ac.ir

Abstract
Poly(lactide)(PLA) has a relatively hydrophobic and neutral surface and lacks functional groups. There are different methods for functionalizition the surface. We used the chemical processing method to do this to functionalize the surface and then improve its applications by grafting heparin and so on. According to the tests performed, it was shown that the aminolysis process was performed and the PLA was functionalized.

Keywords: poly(lactide), hydrophobic, functional groups, chemical processing method, aminolysis process

Introduction

PLA is a thermoplastic material, inert, with low interaction with cells, no functionality, and is resistant to acids, alkali, and fats [1]. PLA is often used in drug-delivery systems, like carriers, for the controlled delivery of different medicines Biopolyesters, with poly(lactide) (PLA) as the most prominent representative, are an excellent alternative to fossil-based materials. Sugar-based raw materials like corn and starchcan be used for the production of PLA, which makes it sustainable. PLA is biocompatible with the human organism and can be used in the production of implants as well as in other biomedical applications. As evidenced in works regarding PLA bionanocomposites, one of the challenges in the development of functional films or medical devices is to achieve a good dispersion of active components within the polymer matrix and, at the same time, maintaining their activity. Additionally, it is essential to ensure enough surface availability of the component in order to achieve the desired activity. Two main directions can be followed in the functionalization of materials: direct incorporation of active molecules into the material and physical or chemical bonding of actives molecules onto the surface of the material. One of the possible routes can be a surface modification of active compounds using some components with better compatibility with PLA, such as the "grafting from" method of modification. The grafting of the polymer chain on a solid surface is a very adaptable method for surface modification and functionalization. Polymer chains can be grafted to the solid substrate (grafting to), or the grafting reaction can be proceeded by polymerization from the surface (grafting from). Both methods are suitable for forming a thin layer on the solid surface with the desired physical and chemical surface properties. Falling into the category of wet chemical reactions, the aminolysis is usually characterized by attacking on the backbone ester bonds by small diamine molecules at the interface between the diamine solution and bulk polyester material, endowing the polyester surface with amino (–NH2) and hydroxyl groups (–OH) [2]. The introduced –NH2 and –OH groups lay the foundation for subsequent conjugation of bioactive molecules. Compared to other surface modification methods, such as plasma or strong oxidation, the aminolysis has a clearer mechanism and predictable products. By adjusting the reaction parameters, the reaction rate and –NH2 density can be accurately tuned. In addition, as a method based on wet chemistry, the aminolysis is suitable for modifying the interior of complex structures like 3D scaffolds. Thanks to these advantages, the aminolysis has been extensively studied and used in surface modification of polyester biomaterials in various forms. The schematic of the aminolyzed PLA is shown below.

Experimental

Poly(lactide))PLA (graide 4043d was from Nature Work Co. (USA) and Ethylene diamine from Merck Co. (Germany). Chloroform from CDH Fine Chemichal Co. (Dariya Ganj Dehli India).

PLA films were prepared using solvent casting method. 3 g of PLA was mixed in 50 mL of chloroform until a homogeneous mixture was mixed using a stirrer at room temperature. The homogeneous mixture was then cast in a petri dish and allowed to stand for 24 h at ambient temperature. Then the prepared film was cut into 2cm×2cm samples and washed with ethanol. To functionalize the ethanol-washed samples in a solution containing 10 g of ethylene diamine and 100 g of ethanol at room

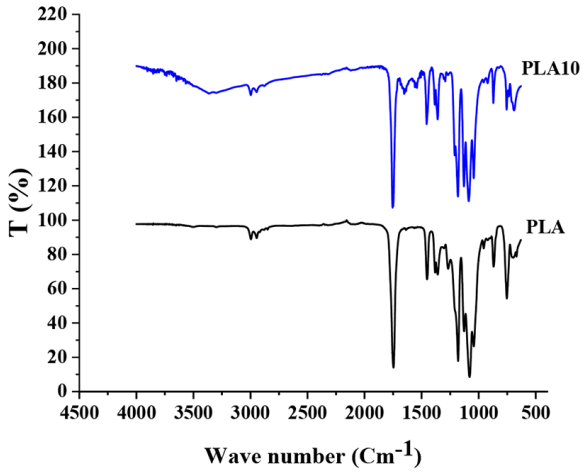

Fig. 1. Results of FT-IR of PLA and PLA10 samples.

temperature, it was stirred until the samples were finally functionalized. The functionalized samples were then washed with deionized water to remove unstable amines (it should be noted that we prepared samples with different percentages, and our optimal sample is this sample). The pure sample with code PLA and the functionalized sample with code PLA10 are shown below. For Investigation of aminolysis process using DMTA by TTDMA (England), Tensile properties, ASTM D638 and ISO 527, ATR_FTIR Tensor 27 model by Brucker (Germany).

Results and Discussion

According to Fig. 1 and the appearance of peaks 3400 cm^{-1} (amine) and 1510-1580 cm^{-1} (amide), the changes in the rheometric curves of the two samples, with differences in the curves of storage and loss modulus as well as tan δ can be seen in Figs. 2 and 3. The formation of a hydrogen bonding causes a shift in tan δ curve to higher temperatures. It can also be seen in Fig. 4 that the strength of the PLA10 sample is reduced due to the breaking of the surface chain

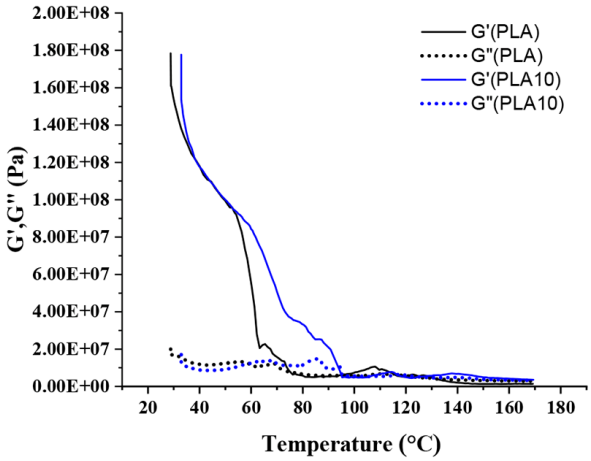

Fig. 2. Storage and loss modulus vs temperature for PLA and PLA10 samples.

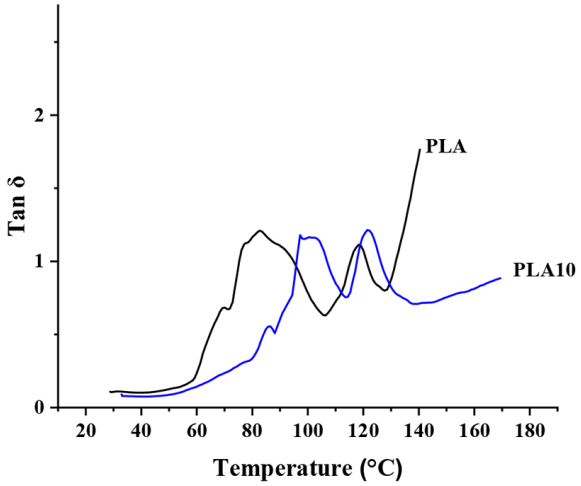

Fig. 3. Tan δ vs temperature for PLA and PLA10 samples.

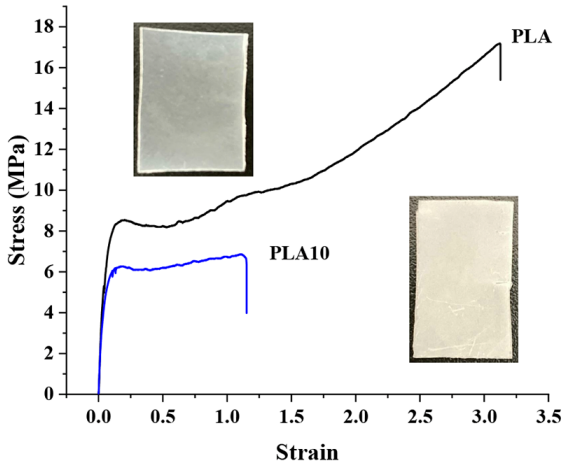

Fig. 4. Stress vs strain for PLA and PLA10 samples.

and a small amount of weight loss. The appearance of these two samples also changes. These results indicate that the Aminolysis process is performed.

Conclusion

According to FTIR, DMA, and tensile tests, it is observed that the aminolysis process has been performed for PLA and this polymer has been functionalized and can be used to grafting with heparin, etc. and expand its applications. Because for these purposes we need to functionalize the PLA.

References

[1] Mileti´c A., Risti´c I., Beatrice Coltelli M., and Pili´c B., Modification of PLA-based films by grafting or coating, *J. Funct. Biomater.*, **11**, 30, 1-16, 2020.

[2] Zhu Y., Mao Z., and Gao C., Aminolysis-based surface modification of polyesters for biomedical applications, *J. RSC Adv.*, **3**, 2509-2519, 2013.

14-15 December 2021, Tehran, Iran
2nd International Conference on Rheology
ICOR 2021
article A-10-258-1

Simulation of Print Speed Effect on Flowability and Stability of Printed Acrylonitrile Butadiene Styrene Strand in Fused Deposition Modeling Method

Nastaran Mosleh, Soheil Dariushi*, and Masoud Esfandeh
Composites Department, Iran Polymer and Petrochemical Institute, Pazhoohesh Blvd.,
Postal Code 14977-13115, Tehran, Iran

*s.dariushi@ippi.ac.ir

Abstract
3D printing is a unique and low-cost method to fabricate objects with complex geometry and low volume production. Fused deposition modeling (FDM) is one of the conventional 3D printing processesthat make parts by adding layers of molten thermoplastic filament on the build platform. The low manufacturing speed of this method in comparison to other manufacturing processes such as injection molding is one of the disadvantages of FDM. In this paper, the flowability of Acrylonitrile butadiene styrene (ABS) filament in the nozzle and during printing was simulated, and the effect of different print speeds (20, 40, and 60 mm/s) was evaluated. The results showed that the increase of print speed causes insufficient time for material extrusion and low bonding between printed strands.

Keywords: 3D printing, flowability, simulation, flow front tracking, FDM

Introduction

ABS is one of the most commonly used filaments in the FDM method. Although the higher thermal properties of ABS make it a good choice for making functional parts, increasing the printing speed leads to a more difficult flow due to its high viscosity and special molecular structure. In recent years, the simulation of heat transfer and flow in the FDM process has received much attention. Verma *et al*. [1] simulated flow behavior, heat transfer, and solidification of the deposited strand with CFD software. Kumar *et al*. [2] presented a model for heat transfer in the heat sink (before nozzle) in the filament transfer zone. Balani *et al*. [3] predicted the stability of freely extruded polymer melt and showed that the results have good agreement with the obtained experimental observations with optical microscopy. Heller *et al*. [4] presented a model to predict the strand shape of the printed strand on the build platform. In this paper, the flowability of molten ABS during printing was simulated by COMSOL Multiphysics software, and the effect of different print speeds on extruded ABS melt was investigated.

Experimental/Theoretical

To evaluate the fluid flow in the FDM process, equation of motion (1) and continuity Eq. (2) inside the nozzle and in the gap between the nozzle and build platform were considered:

$$\rho\frac{\partial u}{\partial t}+\rho(u.\nabla u)=-\nabla(pI+\mu(\nabla u+(\nabla u)^{T})+\rho g \quad (1)$$

$$\nabla u=0 \quad (2)$$

In addition, it is necessary to use the coupling of the level set function (3) with the obtained velocity field to predict the front flow interface:

$$\frac{\partial\varphi}{\partial t}+u.\nabla\varphi=\gamma\nabla.(\varepsilon\nabla\varphi-\varphi(1-\varphi)\frac{\nabla\varphi}{|\nabla\varphi|} \quad (3)$$

Boundary conditions and process conditions are shown in Fig. 1. To verify simulation results, three groups of stands were printed by ABS filament, the print condition was summarized in Table 1. The FDM printer (3D Kalla Co., Iran) with Bowden feed pipe was used to print samples.

Results and Discussion

As can be seen in Table 1, all process conditions, including temperature, the gap between the nozzle and the build plate, and feed rate are constant, and the only variable is the print speed. Results are considered for a printed strand with 4 mm length. Therefore, 0.2, 0.1, and 0.06 s are required to print this strand for 20, 40, and 60 mm/s print speeds, respectively. In Fig. 2, the fused polymer is shown with

Table 1. The experimental (print) conditions.

Print condition	Value
Layer height	0.2 mm
Layer width	0.55 mm
Feed rate	3.26 mm/s
Print speed	20, 40, and 60 mm/s
Nozzle temperature	235 °C
Bed temperature	60 °C
Nozzle diameter	0.5 mm

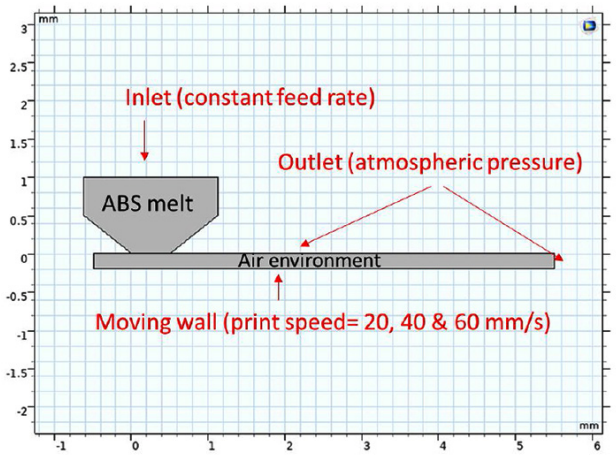

Fig. 1. Boundary conditions and material domains.

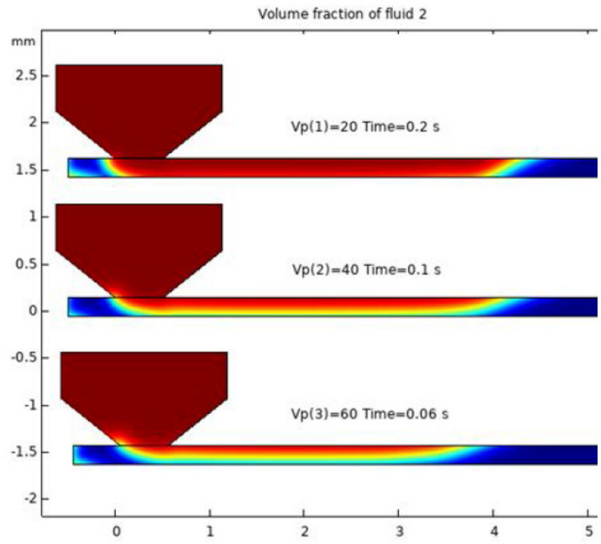

Fig. 2. Fluid flow tracking in the gap between nozzle and build platform in different print speeds.

red color, and air-filled gap between the nozel and build platform is specified with blue color. As can be seen in Fig. 2, at print speeds of 20 and 40 mm/s, the fused polymer connected to the build platform and stable printing is observed, but as the print speed increases to 60 mm/s, there is no sufficient time to fill the gap between the nozzle and the build plate. So, the strand does not print properly on the bed (unstable printing). The results are in agreement with the experimental data. (Fig. 3)

Conclusion

In this study, flow front tracking and deposition of ABS strand on the build platform in the FDM method were simulated. For modeling, the coupling of the equation of motion and the level set function was used. The simulation results showed that the increase of print speed reduces the deposition time and the gap between the nozzle and the bed

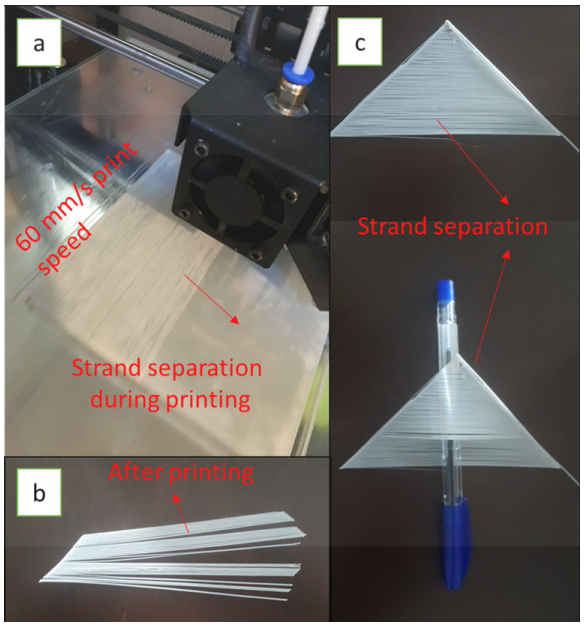

Fig. 3. Experimental observations in the high print speed and weak bonding between printed strands.

was not filled completely. Therefore, a separation of the strands from each other and unstable printing is observed. The optimal stable printing speed in this study was 40 mm/s. The results obtained are also in good agreement with the experimental data.

Acknowledgment

The authors would like to appreciate from Iran national science foundation (INSF) for its financial support. (Fund number: 99019781)

References

[1] Verma A. et al., Numerical simulation of extrusion additive manufacturing: fused deposition modeling, Informatics, *Elec. Microsyst. TechConnect Briefs*, **4**, 118-121, 2018.

[2] Munna Kumar K.S.V. and Nagpure S.K., Numerical simulation of rep-rap 3D printer liquefier to determine the thermal behavior of heat sink, in IJSRD, *Int. J. Sci. Res. Dev.*, 92-101, 2017.

[3] Balani S.B. et al., Influence of printing parameters on the stability of deposited beads in fused filament fabrication of poly(lactic) acid, *Addit. Manuf.*, **25**, 112-121, 2019.

[4] Heller B.P., Smith D.E., and Jack D.A., Planar deposition flow modeling of fiber filled composites in large area additive manufacturing, *Addit. Manuf.*, **25**, 227-238, 2019.

14-15 December 2021, Tehran, Iran
2nd International Conference on Rheology
ICOR 2021
article A-10-260-1

The Influence of Cellulose Nanoparticles on Rheology and Morphology PCL/TPU Scaffold with Cellular Structure

Hamta Kordbacheh[1], Ali Asghar Katbab*, and Nooshin Haghighipour[2*]
1. Department of Polymer Engineering, Amirkabir University of Technology, P.O. Box 15875-4413, Tehran, Iran
2. National Cell Bank of Iran, Pasteur Institute of Iran, Tehran, Iran

*katbab@aut.ac.ir

Abstract
Various nonpolymeric materials have been used for tissue engineering purposes, but polymers can be tailored to specific requirements through flexibility to design and composite. In the present study, Poly(ε-caprolactone) (PCL), thermoplastic polyurethane (TPU), and cellulose nanocrystalline (CNC) as biodegradable and biocompatible polymers are used. Compounds are prepared via a melt mixing process. Scaffolds with the cellular structure are manufactured through particle leaching and high-pressure method. Multiple test methods were used to characterize blends and nanocomposites. The positive deviation in PCL/TPU blend compare to pure polymers in the droplet-matrix morphology was observed.

Keywords: scaffold, tissue engineering, cellulose nanocrystalline, PCL, TPU

Introduction

Scaffold construction in tissue engineering aims to provide a three-dimensional environment suitable for cell culture and tissue regeneration. An ideal scaffold should have four features: highly porous and interconnected structure, biocompatible and bioresorbable, proper surface chemistry, and mechanical properties [1].

Poly(ε-caprolactone) (PCL) is one of the most attractive biocompatible and biodegradable polymers in the aliphatic polyester group with good processability because of its low melting point. Due to its slow degradation rate, PCL is a good candidate for bone-scaffolding applications [2].

TPUs are elastomeric biomaterials that are broadly employed in tissue engineering applications. The natural biodegradability of polyester-based polyurethanes has made it possible to use biodegradable scaffolds or drug delivery systems in the short term (several months) with non-cytotoxic through hydrolytic degradation mechanism [3]. Cellulose nanofiber has attracted attention in nanocomposite due to its lightweight, flexibility, biodegradability, renewability, abundance, and low cost. Nanocrystals Cellulose (CNC), because of its good mechanical properties, can be used as reinforcements in nanocomposites. Besides, They can be used as components of electronic devices, biomaterials, foams, aerogels, and textiles [4].

This study tries to investigate CNC localization in the PCL/TPU blend and its effect on morphology and rheology to create a scaffold.

Experimental

Material and methods

Poly(ε-caprolactone) (PCL) under the trade name CAPA 6500 was supplied by Solvay (Warrington, UK). Polyester-based thermoplastic polyurethane TPU with the commercial name of Desmopan 385 s and melting point of 210–230 °C, from Bayer GmbH

(Germany). NaCl (sieved 315 μm) and was purchased from Sigma-Aldrich(reagent grade). Cellulose nanocrystalline were extracted from cotton by the acid hydrolysis process [4].

PCL, TPU, and TPU/PCL (75/25) blend with/without 1% CNC were prepared. The masterbatch method was used to a better dispersion for the melt mixing [5]. All samples were prepared melt mixing in a Brabender internal mixer with a chamber volume of 60 cm^3 (Plasticorder w50 German).

The melt compounding process was carried out for 8 min at 140 °C and a rotor speed of 60 rpm. Scaffolds with cellular structure were prepared by the particle leaching method then were exposed to high pressure.

Results and Discussion

The resulting morphology and rheology are influenced by the localization of CNC. As well known, the selective localization of CNCs in polymer blends is commonly explained by the concept of wetting coefficient. The contact angles of CNC and PCL, TPU are measured and reported in Table 1. The calculated interfacial tensions between PCL, TPU, between CNC are calculated by eq. Localization nano in the blend nanocomposites can be predicted by evaluating the wetting coefficient, ω_a, using Young's equation introduced for particle-filled immiscible polymer blends Eq. (2):

$$\gamma_{12} = \gamma_1 + \gamma_2 - 2\times\left(\sqrt{\gamma_1^d\gamma_2^d} + \sqrt{\gamma_1^p\gamma_2^p}\right) \quad (1)$$

$$\omega_a = \frac{\gamma_{CNC-PCL} - \gamma_{CNC-TPU}}{\gamma_{PCL/TPU}} \quad (2)$$

γ_1, γ_2 are the surface tensions of components 1 or 2 (Table 1); $\gamma_{CNC\text{-}PCL}$ and $\gamma_{CNC\text{-}TPU}$ are the interfacial tensions

Table 1. Dispersion, polar, and total components of surface energy (mN/m).

Sample	(mN/m)	(mN/m)	(mN/m)
PCL	41.01	1.8	42.81
TPU	20.7	1.4	22.1
CNC	46.5	26.6	73.1

between CNC, and PCL and TPU, which are 14.7 and 20.94, respectively. $\gamma_{PCL-TPU}$ shows the interfacial tension between PCL and TPU that is 4.17. The wetting coefficient is most commonly interpreted in a way that, for $\omega_a < -1$, the CNC are predicted to be located in PCL, and for $\omega_a > 1$, in TPU; if $\omega_a = 1$ that means located in interphase [5].

The calculation of wetting parameters is -1.4 and shows CNC thermodynamically tends to be located in the PCL phase. Rheological properties of blend nanocomposites were examined. The strain amplitude sweep experiment was performed on nanocomposite samples at an angular frequency of 1 rad.s^{-1} in the comprehensive range of 0.001–10 (figure not shown) to determine the linear viscoelastic region. Rheological properties of blend nanocomposites were examined. The complex viscosity of PCL, TPU, PCL/TPU (75/25) blend with/without 1% CNC has been shown versus frequency in Fig. 1. The complex viscosity of the blend exhibited a positive deviation in comparison with the mixture law. Positive deviation from the pure polymers can happen in immiscible blends at low frequencies. The variation in the total interface area and relaxation process of the dispersed droplets during oscillatory shear flow leads to this behavior. According to Eq. (3), the phase inversion point was calculated; as a result, in PCL/TPU (75/25) blend, the PCL is continuous, and TPU is droplets:

$$\varphi_A / \varphi_B = \eta_A / \eta_B = \lambda \quad (3)$$

In which φ_i and η_i are the volume fraction and melt viscosity of component. Furthermore, nanoparticles have an enhancing impact on the melt elasticity of polymer nanocomposites have been considered an indicator for the degree of nanoparticles' dispersion and nanoparticle/matrix interfacial interaction. The blend containing CNCs has shown a more nonterminal performance in complex

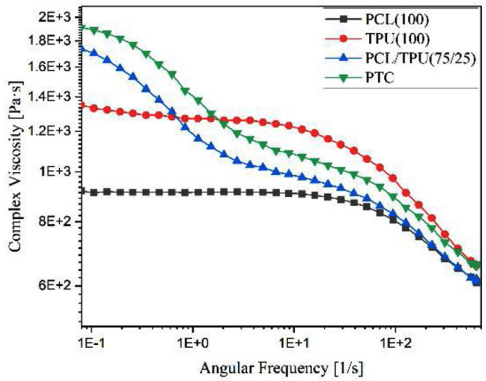

Fig. 1. The complex viscosity versus frequency for PCL,TPU, and PCL/TPU blend and blend nanocomposites (1 wt%).

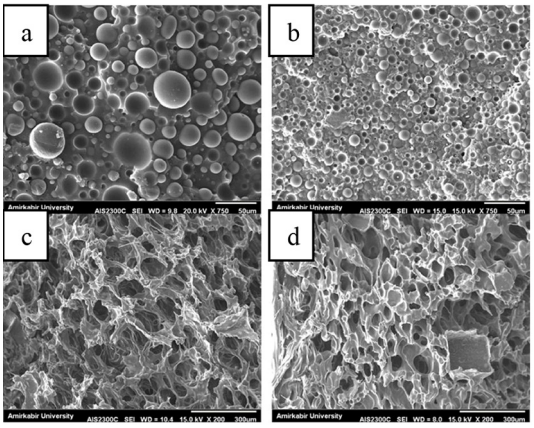

Fig. 2. (a) PCL/TPU(75/25), (b) PCL/TPU(75/25)+1 wt% CNC, (c) scaffold (75/25) + 1 wt% CNC, and (d) scaffold (75/25) .

viscosity at the low-frequency range than the PCL, TPU, and blend without CNC. These results have exhibited that nanoparticles are localized in the PCL matrix and reveal the formation of a 3D-physical network, as the results predict the contact angle analysis [5].

Sem pictures indicated that the viscosity of the melt increases, the size of the droplets decreases, and the size of the pores in the scaffold decreases to closed pores.

Conclusion

A thorough characterization of morphology and rheology CNC located in PCL matrix as predicted in contact angle measurement; CNCs improved the complex viscosity due to decreased droplet size and porosity.

References

[1] Hajiali F., Tajbakhsh S., and Shojaei A., Fabrication and properties of polycaprolactone composites containing calcium phosphate-based ceramics and bioactive glasses in bone tissue engineering: a review, *Polym. Rev.*, **58**, 1, 164-207, 2018.

[2] Taherkhani S. and Moztarzadeh F., Fabrication of a poly(ε-caprolactone)/starch nanocomposite scaffold with a solvent-casting/salt-leaching technique for bone tissue engineering applications, *J. Appl. Polym. Sci.*, **133**, 23, 19-21, 2016.

[3] Pouladzadeh F., Katbab A.A., Haghighipour N., and Kashi E., Carbon nanotube loaded electrospun scaffolds based on thermoplastic urethane (TPU) with enhanced proliferation and neural differentiation of rat mesenchymal stem cells: the role of state of electrical conductivity, *Eur. Polym. J.*, **105**, 286-296, 2018.

[4] Pracella M., Haque M.M.U., and Puglia D., Morphology and properties tuning of PLA/cellulose nanocrystals bio-nanocomposites by means of reactive functionalization and blending with PVAc, *Polymer (Guildf)*, **55**, 16, 3720-3728, 2014.

[5] Shakouri Z. and Nazockdast H., Microstructural development and mechanical performance of PLA/TPU blends containing geometrically different cellulose nanocrystals, *Cellulose*, **25**, 12, 7167-7188, 2018.

14-15 December 2021, Tehran, Iran
2nd International Conference on Rheology
ICOR 2021
article A-10-267-1

The Impact of Nano Graphene Oxide on Rheological Properties of AM-*co*-AA Hydrogel as Drilling additive

Fateme Salmani and Ahmad Rabiee*
Iran Polymer and Petrochemical Institute, Postal Code 14977-13115, Tehran, Iran

*a.rabbii@ippi.ac.ir

Abstract
Drilling mud has different properties in different stages of drilling due to various roles so it should have good behavior in terms of rheological properties. In the present study, the polymer in drilling fluid was synthesized using acrylamide (AM) and acrylic acid (AA) monomers with constant molar ratios (0.7:0.3 mole). Graphene oxide with different weight percentages (0.1, 0.3, 0.5, and 1 wt%) was added to the polymer to synthesize the nanocomposite. The polymer and prepared nanocomposite was characterized by FT-IR, DMTA, TGA, TEM, rheometer, Fluid loss test and filter cake thickness analysis. According to the rheological properties, nanocomposite with 0.5 w/w% of graphene oxide showed the best rheological properties. The addition of nanocomposite to drilling mud compared to polymer has a desirable property, such as reduction in fluid loss and thickness of mud cake which indicates a positive effect of presence of graphene oxide in drilling mud.

Keywords: drilling mud, graphene oxide, rheological behavior, nanocomposite, oil industry

Introduction

Carboxymethylcellulose (CMC) is a cellulose derivative and is used as a fluid loss reducing agent in drilling operations. It acts as an important factor in improving the quality of drilling fluid and controls fluid loss, water absorption, and retention, well wall sealing, suspension builders and concentrators. The high viscosity type is used to increase the viscosity and the low viscosity type is used as a factor in reducing the waste filtering effluent from oil drilling. Although CMC is an effective viscosifying agent, but loses its properties at high temperatures [1,2]. Graphene oxide is a combination of carbon, oxygen, and hydrogen in variable proportions, which is obtained by reacting with strong oxidizers. The ratio of carbon to the oxygen of the oxidized product is C:O=1/2 and 2.9 [3].

In this study, we focused on preparation of graphene oxide modified nanocomposite for oil well drilling application containing nanoparticles with different concentrations. The applied polymer was synthesized using acrylamide (AM) and acrylic acid (AA) monomers (0.7 molar to 0.3 molar ratio in all experiments), and nanocomposite with different amounts of Go via the free-radical polymerization technique. The results showed that the addition of nanocomposite to drilling mud compared to polymer has more desirable rheological properties, fluid loss and thickness of mud cake which is an indication of positive effect of graphene oxide in drilling mud. The copolymers with graphene oxide structure possessed better rheological properties [4].

Results and Discussion

Rheological Behavior

Fig. 1 shows the apparent viscosity of samples versus the shear rates with different amounts of graphene oxide in the nanocomposite. The apparent viscosity decrease with increasing shear rate which is an indication of shear thinning behavior. According to the results, the sample containing 0.5% of GO shows better resistance to shear and has the optimum rheological properties. Fig. 2 Shows the storage modulus of samples versus angular frequency and a gradual increase in storage modulus with increasing angular frequency with the addition of GO. The nanocomposite

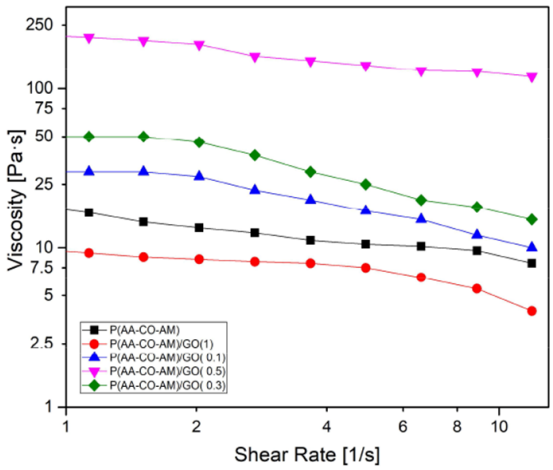

Fig. 1. The dependence of viscosity on shear rates with different amounts of Go in nanocomposite.

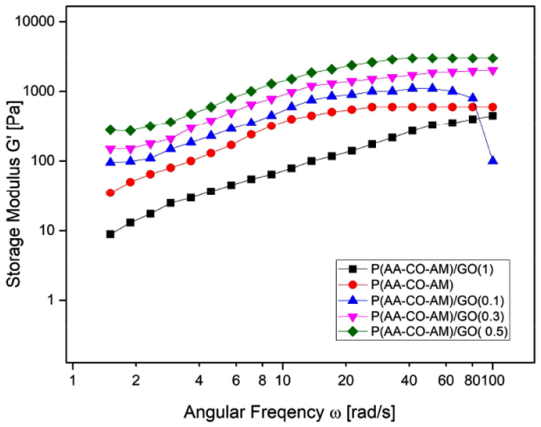

Fig. 2. The dependence of storage modulus on angular frequency with different amounts of GO in nanocomposite.

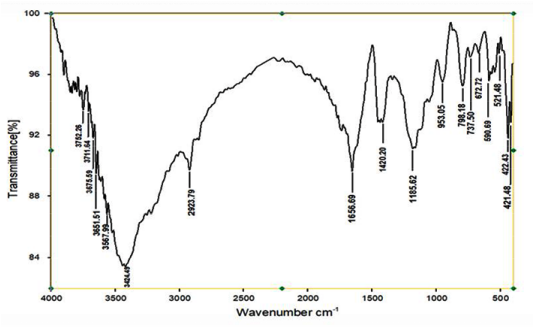

Fig. 3. FTIR spectra of copolymer (AA-*co*-AM).

containing 0.5% GO has the highest storage modulus compared to the other samples due to well dispersion of nanoparticles in the polymer matrix.

FTIR Analysis of Copolymer

Fig. 3 shows the FTIR spectra of the copolymer (AA-*co*-AM). A broad band at 3424 cm^{-1} belongs to N-H stretching vibrations of amide groups in acrylamide and overlapping with O-H stretching vibrations of acrylic acid [5]. The peak situated at 2923 cm^{-1} is assigned to the stretching vibrations of aliphatic methyl and methylene groups of polymer backbone [5]. Absorption peaks have appeared at 1656 cm^{-1} could be attributed to the carbonyl groups of the monomers [5]. The C-O stretching vibration are expected to appear at 1185.6 cm^{-1}. The peak at 1420 cm^{-1} is attributed to the in-plane bending of CH_2 groups.

Conclusion

Nanocomposite with different amount of GO (0.1, 0.3, 0.5, and 1 wt%) were prepared by free-radical polymerization technique. The sample with 0.5% nanoparticle has the optimum rheological properties. Simultaneous use of polymers and nanomaterials in the resulting composites provided a synergistic effect and led to excellent mechanical strength and very high thermal stability. According to TGA results, the addition of graphene oxide to the main copolymer chains due to dipolar interactions has increased the heat resistance of nanocomposite. The storage modulus and glass transition temperature of nanocomposite was improved .The filter cake thickness and filtrates of samples at different time intervals were reduced in nanocomposite due to presence of nanoparticles compared with the copolymer.

References

[1] Caenn R. and Chillingar G.V., Drilling fluids: state of the art, *J. Petrol. Sci. Eng.*, **14**, 3-4, 221-230, 1996.

[2] Kelessidis V.C., Poulakakis E., and Chatzistamou V., Use of carbopol 980 and carboxymethyl cellulose polymers as rheology modifiers of sodium-bentonite water dispersions, *Appl. Clay Sci.*, **54**, 1, 63–69, 2011.

[3] Hummers W.S. and Offeman R.E., Preparation of graphitic oxide, *J. Am. Chem. Soc.*, **80**, 6, 1339–1339, 1958.

[4] Ahmadi A.A. and Monjazi M., Title:investigation of the effect of nono-silica particles onheat specific properties of water based drilling fluids and rheological properties process: 1 first trial (field and check) 2 Peer review 3 editing and three trials, 554864, 2018.

[5] Wang C., Zhang M., Xu Y., Wang S., Liu F., Ma M., and Gao Z., One-of bionic and stably superhydrophobic coatings on wood surface, *Adv. Powder Technol.*, **25**, 2, 530-535, 2014.

14-15 December 2021, Tehran, Iran
2nd International Conference on Rheology
ICOR 2021
article A-10-267-2

The Improved Thermal Sealing Capability of Polyethylene Films by Grafting Lateral Branches through a Reactive Extrusion Process

Fateme Salmani, Shervin Ahmadi*, and Ghasem Naderi
Iran Polymer and Petrochemical Institute, Postal Code 14977-13115, Tehran, Iran

*Sh.ahmadi@ippi.ac.ir

Abstract
The purpose of this study is to improve the adhesion strength and increase the heat sealing ability of polyethylene films by modifying their chemical structure. For this purpose, a substrate of density polyethylene alloy low/low-density linear polyethylene (LDPE/LLDPE=30/70) with long side branches without gel formation through reactive extrusion process inside reactive twin extruder by combining different percentages of DCP primer 1-Octen and comonomer was prepared. The effect of change in the composition of the percentage of initiator and 1-Octen on the branching process and its effect on the viscoelastic behavior of polyethylene films with mechanical-rheological spectroscopic tests and dynamic properties mechanical-thermal was studied. Increased branching of the chains was accompanied by an increase in chain entanglements that caused increased elasticity of the melt was observed, in this regard, an increase in the storage modulus and viscosity of the polymer melt was observed.

Keywords: rheology, polyethylene, 1-Octane, interfacial, adhesion, thermal sewing, peel

Introduction

Ethylene/alpha-olefin copolymers with a high percentage of comonomer, known as polyolefin elastomer, are one of the most widely used thermoplastic elastomers. These materials are a relatively new proportion of poly-parents that have been industrially produced with the development of metallocene hazard catalysts in the early 1990 s. Compared to other types of thermoplastic elastomers, those thermoplastic elastomers that are based on polyolefins have attracted a lot of attention [1]. This is due to properties such as better chemical resistance, lower density, and lower price compared to similar materials. To achieve good elastomeric properties that include a low modulus against large deformations, the crystallinity of ethylene/alpha-olefin copolymer must be less than 20% by weight, which is important in the presence of alpha-olefins such as 1-propylene, butene, 1-hexene, and 1-octene. The structure of the main chain is realized. Most commercial polyolefins are elastomers of ethylene copolymers with butene or octane [1]. The accidental presence of these alpha-olefins in the chain structure prevents the crystallization of methylene sequences. Polyolefin elastomers can replace many commercial polymers such as ethylene-propylene rubber, ethylene vinyl acetate, styrene block copolymers, and polyvinyl chloride. Polyolefin elastomers have established themselves in applications such as the In general, three methods are used to create branches on polymer chains:

1. Use a suitable catalyst during the synthesis of the desired polymer.
2. Irradiation of high-energy gamma rays or high-energy gamma or electron beams to the polymer in the solid state.
3. Melt mixing using free radical scavenging agents in the presence or absence of comonomer.

In this work, the third method is used. Today, the rate of introduction of new polymers has dropped dramatically, and researchers have begun to modify existing polymers by strengthening or reactive mixing to enhance properties and fill gaps.

Experimental

Materials

LDPE (low-density polyethylene) used in this project is prepared from Bandar Imam Petrochemical Grade 020. LLDPE polyethylene (low-density linear polyethylene) used in this project is prepared from Amirkabir Petrochemical with grade 0209. (DCP) is manufactured by Merck and organic peroxides are recognized as important initiators in free radicals to modify the structure and properties of polyethylene. One of the most important common peroxides, 2,5-Dimethyl-2,5-di(tert-butylproxy) hexane.

Results and Discussion

Mechanical-Rheological Spectroscopy

Fig. 1 shows the behavior of the storage Modulus is shown in terms of the frequency of the control sample and the branched samples. As shown in the figure, none of the diagrams show the terminal behavior in the low-frequency range. In polymer alloys with interconnected morphologies, a polymer phase, such as three-dimensional lattice, is scattered throughout the alloy structure, and as a result, the behavior of the storage modulus in terms

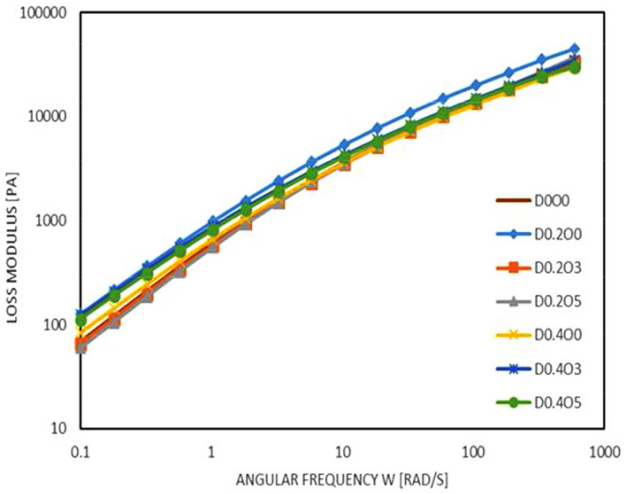

Fig. 1. Storage module behavior in terms of the angular frequency of control and branched specimens.

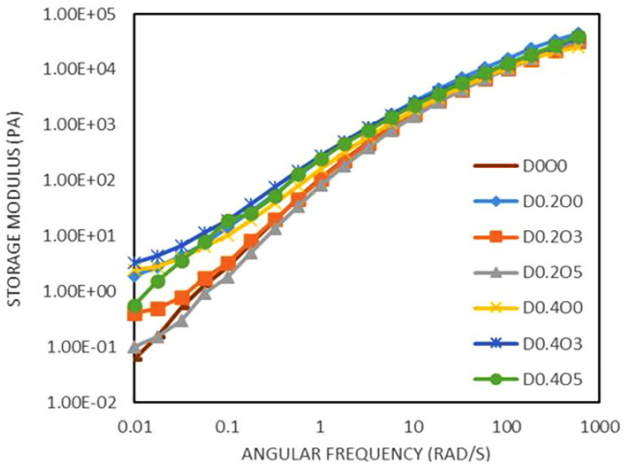

Fig. 2. Loss module behavior in terms of the angular frequency of control and branched specimen.

of angular frequency in this structure progresses to non-terminal in the low-frequency range. For all branched samples, the behavior of the storage modulus in terms of angular frequency in the low-frequency range has shifted to non-terminal [3]. When the 1-octane comonomer is added to the alloy structure with 0.2% by weight of the peroxide primer, the storage modulus of the branched polymers is slightly increased and is observed at 0.2% by weight of the peroxide primer similar to the sample. This indicates that the amount of 1-1-Octen side bonds attached to the polymer is less than the samples in which 0.4% by weight of the primer was used. In most linear polymers at low frequencies, the change in viscous behavior is greater than in the elastic state, and as a result, the dissipation modulus is greater than the storage modulus. As the modulus of branching increases, the storage and loss modulus become closer together. Increasing the storage modulus indicates an increase in the elasticity of the specimens due to branching, which restricts the movement of the polymer chains and increases the elasticity. According to table1 what was said in the analysis of the behavior of the storage module in terms of frequency, due to the increase of lateral branches, the bonding of the chains increases, and the elastic behavior of the material increases. Thus, the slope of the graph decreases in the low-frequency range. The highest slope is related to the curves of D0O0, D0.2O3, and. As mentioned, the D0.2O5 behavior deviation of the control samples from the terminal state (slope 2) is interconnected due to the proximity of the sample structure to the morphology. Also in examples, D0.2O3 and D0.2O5 Due to the lower rate of branching, less deviation from the terminal behavior occur, so the slope is higher [3].

Table 1. Loss values of storage and Loss module curves.

Sample	Storage module	Loss module
(D_0O_0)	1.13	0.74
($D_{0.2}O_0$)	0.73	0.97
($D_{0.2}O_3$)	1.11	0.77
($D_{0.2}O_5$)	1.22	0.80
($D_{0.4}O_0$)	0.93	0.73
($D_{0.4}O_3$)	0.90	0.70
($D_{0.4}O_5$)	0.99	0.71

Conclusion

1) The polyethylene branching process is a useful, efficient, and industrialized method to modify its adhesion properties in reactive extruders.
2) Rheological studies of the polymer melt showed the bonding of 1-actone comonomers to the polymer
chains and increasing the elasticity of the system without gel formation.
3) The formation of lateral branches on the chains by nucleation or regularity together was associated with increased crystallinity in branched specimens.

References

[1] Zhang K., Ye Z., and Subramanian R., Synthesis of block copolymers of ethylene with styrene and n-butyl acrylate via a tandem strategy Pd-diimine catalyst with atom transfer radical polymerization, *Macromolecules*, **41**, 3, 640–649, 2008.
[2] Wang J. and Mao Q., Methodology based on the PVT behavior of polymer for injection molding, *Adv. Polym. Technol.*, **32**, 2013, 474–485, 2012.
[3] López-Barrón C.R. and Macosko C.W., Rheological and morphological study of co-continuous polymer blends during coarsening, *J. Rheol.*, **56**, 6, 1315–1334, 2012.

14-15 December 2021, Tehran, Iran
2nd International Conference on Rheology
ICOR 2021
article A-10-269-1

Rheology and Mechanical Properties of PVC/EVA Nanocomposites Based Halloysite Nanotube

Soroush Shabani and Saman Ghaderzadeh*
1. Research Laboratory of Green Organic Synthesis and Polymers, Department of Chemistry, Iran University of Science and Technology, Postal Code 16846-13114, Tehran, Iran
2. Department of Polymer Processing, Iran Polymer and Petrochemical Institute, P.O. Box 14965/115, Tehran, Iran

*s.ghaderzadeh@ippi.ac.ir

Abstract
The innovation of this research was to study the effect of halloysite nanotube (HNT) amount on morphology, rheology and mechanical properties of the blends based on poly(vinyl chloride)/ethylene vinyl acetate copolymer (EVA). The impact resistance of PVC increased due to blending with EVA up to 90/10 while it experienced a reduction trend at the higher amount of EVA. From the rheological studies, it can be inferred that there was no strong interactions between HNT with PVC and EVA chains in the melt phase of PVC/EVA blend samples, so that the specific amount of HNT never affected on the rheological behavior and properties of the blend. It can be included from the Scanning Electron Microscopy (SEM) analysis that all the blend samples had a matrix-dispersed morphology and it was evolved by increasing HNT amount in the blend from the EVA dispersed phase size and its distribution viewpoint.

Keywords: nanocomposites, PVC, blend, HNT, impact strength

Introduction

The few studies are accomplished on thermoplastic/elastomer blend nanocomposites. Among the thermoplastics, PVC is one of the most commercial material (next to only a few more widely used plastics like PET and P.P.) which is due to its high stiffness, flame retardancy, chemical resistance and low cost [1].

In recent year, halloysite nanotubes (HNTs) have significantly been investigated as a leading nanofiller for advanced novelty of organic/inorganic composites due to their hollow structure, biocompatibility, cheap, and eco-friendly [26–28]. HNTs have been emphasized as an efficient filler to be combined with polymers for fabrication of polymer nanocomposites via performance improving. Herein we wish to report an easy and efficient approach for the preparation of PVC/EVA blend- halloysite nanocomposites by melt mixing. The structure, impact strength, thermal properties and morphology of the nanocomposites were also studied.

Experimental

PVC powder (suspension grade with K-value 65), Dioctyl terephthalate (DOTP) as plasticizer, Ba/Zn stearate and stearic acid used as thermal stabilizer and lubricant and EVA pellet (VA 28%). Ultrafine HNTs, in the form of the powder, with a density of 2.55 g/cm^3 and cationic exchange capacity (CEC) of 10 meq/100 g were supplied by Imerys Tableware Asia Limited (New Zealand). Morphological figures of natural HNT, which illustrate a transparent central area that runs longitudinally along the nanotubes, indicating hollow and open-ended structure of HNT are given in our previous works.

Table 1. Formulation of the PVC/EVA/HNT nanocomposites, unit is in phr, the abbreviations are P: PVC/E: EVA/H: HNT.

Sample code	PVC	EVA	Ca/Zn	HNT	DOTP
P95E05	95	5	4	0	25
P90E10	90	10	4	0	25
P95E05H1	95	5	4	1	25
P95E05H3	95	5	4	3	25
P95E05H5	95	5	4	5	25
P95E05H7	95	5	4	7	25

PVC powder, EVA pellet, DOTP, Ca-Zn stearate, stearic acid, and HNT were mixed according to the formulation shown in Table 1. The nanocomposites were produced by melt procedure into a two-roll mill at 170 °C for 10 min and then forced molded into sheets at 170 °C and 1000 psi for 7 min. The specimens, in dimensions 250 × 250 × 3 mm, were air cooled and obtained, then pellets were prepared for structure specification and properties measurements. Blending of PVC and EVA compared without HNT in the same process, regarding to properties the item P95E05 is chosen as an optimized blend to investigate by HNT.

Results and Discussion

Fig. 1 gives information about the variation of impact strength of PVC/EVA blends and PVC/EVA/HNT

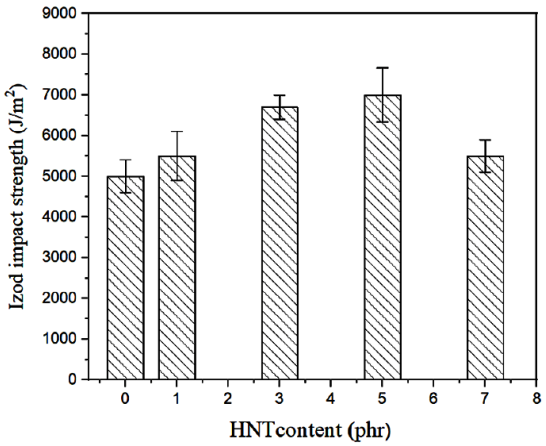

Fig. 1. Izod impact strength of PVC/EVA/HNT nanocomposites.

nanocomposites, according to ASTM D256-04. From the blends, it is noticeable when 5 phr of EVA was added to PVC, Notched Izod impact strength rose from 5.2 kJ.m^{-2} to 7.16 kJ.m^{-2} of PVC, whereas the impact strength of nanocomposites declined gradually in present of the large content of EVA loading due to some agglomeration of EVA in the PVC matrix. The nanocomposite of 95 PVC/5 EVA/5 HNT provides the highest impact strength by reaching to considerable improvement in comparison with other composites and net PVC. The notched impact strength of the nanocomposites has experienced a fall trend due to the further increase amount of HNT which cause to agglomeration of HNT in the PVC matrix, Fig. 2. However, the nanocomposite of 95 PVC/5 EVA/5 HNT exhibits a synergism effect of the EVA and HNT that enhanced the toughness of the nanocomposite.

The rheological properties of PVC/EVA/HNT nanocomposites illustrate increase in complex viscosity, Fig. 3, especially at 5 phr HNT concentrations in comparison with the PVC/EVA composite and net PVC. Therefore, the low shear rate test method in composites determines

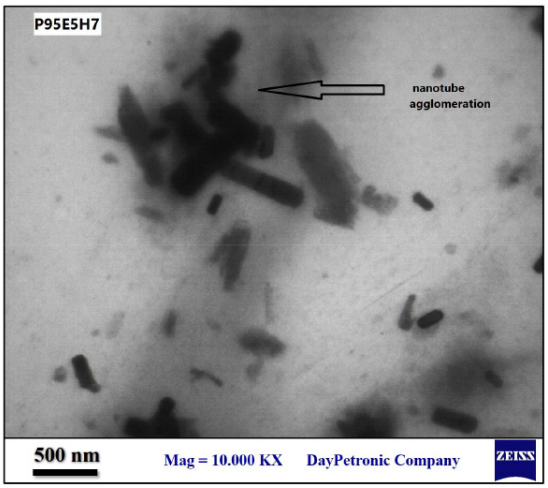

Fig. 2. TEM of agglomeration of HNT in the PVC matrix.

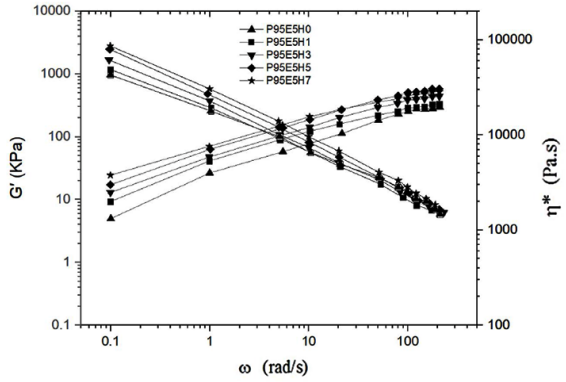

Fig. 3. Rheology properties of nanocomposites.

that the variation of viscosity for composites are growing up at low angular frequency ω values. Approximation of the viscosity trend of the investigated nanocomposites at higher ω values indicates that not only the viscosity value, but module rate rose by increasing with the amount of HNT [2,3].

Conclusion

The preparation of PVC/EVA/HNT nanocomposites was successfully carried out. The effect of EVA and HNT contents on the properties of the nanocomposites was studied. The results display that the impact test of the nanocomposites decreased with the adding of modified HNT into the PVC/EVA blend, whereas PVC was blended with 5 phr of EVA and 5 phr of HNT, synergistic improvement in notched impact strength happened. On the other hand, the EVA acts like a macromolecular plasticizer, while HNT treats as a nanoparticle reinforcing filler.

Acknowledgment

The authors gratefully acknowledge Ghazvin Granules Producing Co. for financial, material and instrument support.

References

[1] Liu C. et al., Structure and properties of poly(vinyl chloride)/halloysite nanotubes nanocomposites, *J. Macromol. Sci. Part B*, **51**, 5, 968-98, 2012.

[2] An Q.F. et al., Compatibility of PVC/EVA blends and the pervaporation of their blend membranes for benzene/cyclohexane mixture, *J. Membrane Sci.*, **222**, 1-2, 113-122, 2003.

[3] Senthilvel K. et al., Studies the effect of halloysite nanotubes on the mechanical and hot air ageing properties of nitrile-polyvinyl chloride rubber nano-composites, *Mater. Today Proc.*, **43**, 1730-1739, 2021.

14-15 December 2021, Tehran, Iran
2nd International Conference on Rheology
ICOR 2021
article A-10-270-1

Viscoelastic Study of Biopolymer Hydrogels Applicable for Additive Manufacturing

Hossein Zehtab Minooei[1] and Babak Kaffashi[2*]
1. Polymer Engineering Department, University of Tehran's Kish International Campus, Postal Code 7941639982, Kish Island, Iran
2. School of Chemical Engineering, College of Engineering, University of Tehran, Postal Code 1417613131, Tehran, Iran

*kaffashi@ut.ac.ir

Abstract
Application of biocompatible, biodegradable, inexpensive, non-toxic and edible naturally-occurring polymers in 3D printing process for biomedical and food industries are now taken into consideration. By virtue of increasing interest in 3D printing and need for the precise products with high production speed, this technology has been advancing and is considered as a state-of-the art and burgeoning technique. Keeping in view that water-soluble biopolymers behave in an intricate and time dependent way, so, predicting their rheological properties and applications in additive manufacturing process has been elusive and crucial. In this study. we investigate a novel ink made of gelatin/tragacanth hydrogel for Direct Ink Writing (DIW) and also we exhibit how formulation, preheating, amount of cross-linking agents and processing temperature influence on achieving essential time duration before clogging in nozzle. In the other hand, through study of time dependent viscoelastic measurements, we shed light on which the most optimal time for 3D printing without clogging is prior to gelation region. In fact, rheological parameters such as viscosity, storage and loss modulus, and damping factor are of vital importance to make a forecast on hydrogel behavior. In addition to assessment of printability through interconnected channels formed by filaments we suggest a new strategy by measuring the contact angle and cross-sectional area of droplet.

Keywords: biopolymer, 3D printing; ink, viscoelastic, stiffness, printability

Introduction

The application of highly hydrophilic biopolymers in the Direct Ink Writing (DIW), 3D printing process is very challenging and ambiguous. In this research, we used tragacanth gum to moderate rheological properties of gelatin. Tragacanth gum, used as a thickening agent, provides thixotropy behavior. We selected the hydrogels with an elastic modulus of about 10 kPa, which simulate tissue-like stiffness and are suitable for the culture of cells. During deposition of the hydrogel from the nozzle we encounter to serious issue of clogging in the nozzle tip due to the high rate of cross-linking and curing. Since these clumps affect the quality of the resolution and shape fidelity, therefore, we are willing to show how preheating, formulations, operating temperature, curing and preparation duration can influence the rheological and eventually, the printability properties. Through the contact angle measurement and the drop shape, one can estimate the printability of the hydrogels. It has been shown that the preheating of the gelatin and water mixture in a heat oven at 65 °C for 7 days increased the printing duration1. In this paper, we explored the preheating of the gelatin powder ca. 1 h to 2 h at 65 °C which turns out to indicate the same or even better effects.

Experimental

Preparation of Ink and Hydrogel

Gelatin type a purchased from Merck, tragacanth gum was provided from locally extracted sample from Isfahan. Since the crosslinking agents with carbonyl group such as glutaraldehide are exclusively used for crosslinking gelatin, so we introduced an equal mixture of sucrose and borax into the gelatin/tragacanth blend. Distilled water is used as solvent. Suitable composition for our work achieved by trial and error. Solutions of gelatin (17 w/w%), tragacanth (1.2 w/w%), gelatin/tragacanth mixture (17/1.2 w/w%) and gelatin/tragacanth hydrogel with 2.5 and 5 w/w% crosslink agents were prepared. 2X10 g gelatin powder preheated in the oven at 60-65 °C for 1 and 2 h. Six samples were produced and named as 17, 17/1.2, 17/1.2/2.5, 17/1.2/2.5/1 h, 17/1.2/5/1 h and 17/1.2/5/2 h.

Rheometery

A rotational Physica MCR300 (Anton Paar) rheometer was used to measure the rheological parameters such as storage modulus (G'), loss modulus (G"), damping factor (tan δ) and viscosity using a plate-plate geometry measuring geometry (25 mm). According to this, time sweep, viscosity-time and amplitude sweep measurements with the control of strain and shear rate were conducted at 37 °C.

Measurement of Contact Angle, Droplet Cross-Section Area and Printability

The images of the droplet were taken with an 8 MP camera, through the deposition of hydrogel drop on the surface of a petri dish. One equation which correctly determines the printability of the printed grid pattern formed by interconnected channels is as is as follows [2]:

$$Pr = L^2 / 16A \quad (1)$$

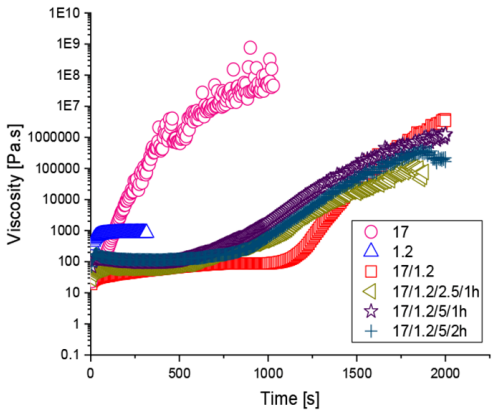

Fig. 1. Viscosity versus time semi-log curve for six samples.

Here A is the area and L is the perimeter of the interconnected channel formed by the filaments. Therefore, the acceptable printability would be from 0.9 to 1.1 in addition, we investigate cross section area of the droplet, so the printability area generally should be between being circularity (0.78) and being complete square (1).

$$\pi / 4 \le Pr \le 1 \qquad (2)$$

Results and Discussion

Rheological Analysis

Considering the viscosity versus time data on three temperatures (25, 32, and 37 °C), as the slopes of the curves indicate, the pressure required to apply on ink in order to exit the nozzle, the appropriate temperature was chosen to be 37 °C. As is indicated in Fig. 1, the wider the initial plateau region of curve was, the longer the duration of 3D printing. The amplitude sweep measurement in the range of 1% to 300% strain amplitude was also performed immediately after the time sweep measurement. The results show for all samples the both measurements equally increase until 1% then both measurements to decline which indicate a viscoelastic solid, the two moduli intersect after 100% strain. Considering the time sweep measurements, the best possible time for 3D printing will be under gelation condition. It can be said with a good approximation that

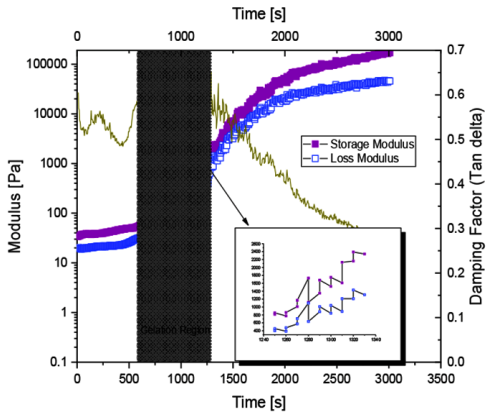

Fig. 2. Time sweep semi-log curve for hydrogel 17/1.2/5/2h.

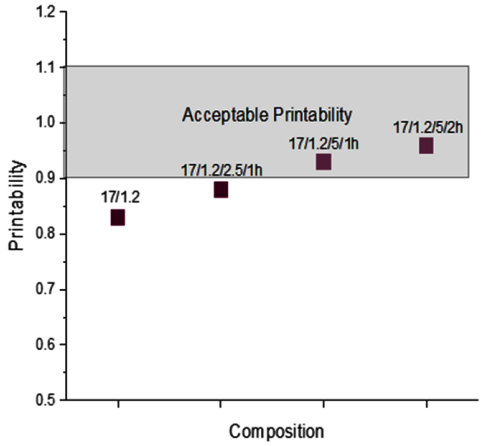

Fig. 3. Printability based on average area of interconnected channels formed by filaments after 1h deposition on the petri dish at 37 °C.

the starting time of gelation is after the plateau region, say it is a viscoelastic liquid, and the end time is where the damping factor (tan δ) reaches the highest value as close to 1 (Fig. 2).

Contact Angle and Printability

The measurement of the contact angles shows the lowest amount belongs to the pure gelatin and the highest one assigned to the hydrogel of 17/1.2/5/2h to be 21° and 89°, respectively. Furthermore, the values of cross sectional area increase from 0.4 to 0.79 for pure gelatin and hydrogel 17/1.2/5/2h, respectively. The measurement of the printability criteria was done in which printability increase from 0.83 for pure gelatin to 0.96 for hydrogel of 17/1.2/5/2h.

Conclusion

The application of hydrogels in the direct ink writing 3D printing technique is a challenging issue in the biomedical and food industries. The high rate of cross-linking during the process can be facilitated by applying practical solutions to reach an appropriate formulation, preheating and suitable processing temperature. We add two other methods for determining printability, that is, measuring contact angle and the cross-section area compared to the common methods. The best results achieved for the sample of 17/1.2/5/2 h. The whole strategies are essential but not sufficient. It may be suggested that the introduction of hydrophobic agent can improve the printability.

References

[1] Yao Tan J.J., Lee C.P., and Hashimoto M., Preheating of gelatin improves its printability with transglutaminase in direct ink writing 3D printing, *Int. J. Bioprint.*, **6**, 4, 118-129, 2020.

[2] Ouyang I., Yao R., Zhan Y., and Sun W., *Biofabrication J.*, **8**, 1-13, 2016.

[3] Zhang B., Chung S.H. et al., Direct ink writing of polycaprolactone/polyethylene oxide based 3D constructs, *Prog. Nat. Sci. Mat. Int. J.*, **31**, 180–191, 2021.

14-15 December 2021, Tehran, Iran
2nd International Conference on Rheology
ICOR 2021
article A-10-270-2

Rheology and Printabilty Studies of Crosslinked Gelatin/Tragacanth/ Lignin Hydrogels

Hossein Zehtab Minooei[1] and Babak Kaffashi[2*]
1. Polymer Engineering Department, University of Tehran's Kish International Campus, Postal Code 7941639982, Kish Island, Iran
2. School of Chemical Engineering, College of Engineering, University of Tehran, Postal Code 1417613131, Tehran, Iran

*kaffashi@ut.ac.ir

Abstract
Growing demands and dwindling non-renewable resources has prompted researchers to concentrate on more efforts on those natural polymers having advantages such as hydrophilicity and hydrophobicity simultaneously. With the advancement of additive manufacturing technique, it would lead one to apply, for instance lignin, the second-most abundant component of planted material and a complex biopolymer, as a crosslinking agent. Lignin is a non-toxic agent and can be used in the preparation of 3D printed scaffolds as a rheology and printability enhancer. We have come up with a novel ink, lignin cross-linked gelatin/ tragacanth hydrogel for direct ink writing application. The polydispersity index and molecular weight were characterized by the gel permeation chromatography. The hydrogel chemical structure was investigated by the FT-IR spectroscopy. The swelling ratio of samples in both distilled water and 1*PBS were calculated. The samples stiffness, storage and loss moduli, damping factor and viscosities obtained from the time, amplitude sweep and the time transient were carried out using a rheometer. The printability test was also conducted through the contact angle measurement, cross-section area of droplet and grid pattern channels formed by the filaments deposited via nozzle. The results shed the sample containing 4 w/w% lignin not only is in the acceptable range of printability but also has the maximum optimal time available for 3D printing process before clogging takes place in the nozzle tip.

Keywords: biopolymer, additive manufacturing, hydrogel, stiffness, printability

Introduction

Gelatin with many benefits such as non-toxicity, ediblity, biocompatibility and biodegradability has become one of the most widely used ingredients in the food, pharmaceutical and biomedical engineering industries. Tragacanth gum imparts thixotropy to solution and here we added that to gelatin in order to regulate viscosity. Lignin as a natural branched complex biopolymer exists in all terrestrial and some aquatic organisms. In this study, we have used the direct ink writing (DIW) method which on the other hand is termed extrusion-based additive manufacturing method. Here, we elaborate rheology and printability of a novel ink, lignin cross-linked gelatin/tragacanth hydrogel. Our intention is to provide practical solutions in order to predict and facilitate elusive and crunch conditions during additive manufacturing process.

Experimental

Preparation of Ink and Hydrogel

Gelatin type a purchased from Merck, tragacanth gum was provided from locally extracted sample around Esfahan. We acquired lingo-sulfonic acid sodium salt with an average molecular weight from Sigma-Aldrich. Distilled water and pure ethanol (50:50) were used as solvents. Suitable composition for our work achieved by the trial and error. Six samples with different compositions, gelatin/ tragacanth with and without preheating, gelatin/tragacanth hydrogel with 2, 4, and 6 w/w% crosslink agent lignin and gelatin/tragacanth hydrogel with 4 w/w% lignin without preheating were prepared, therefore samples are termed as 17/1.2, 17/1.2/2h, 17/1.2/2h/2, 17/1.2/2h/4, 17/1.2/2h/6 and 17/1.2/4, respectively.

Rheometery

The rotational rheometery via a Physica MCR300 (Anton Paar) rheometer was implemented to measure the rheological parameters using a plate-plate measuring geometry (25 mm). According to this, the time sweep, viscosity versus time and amplitude sweep measurements with the control of strain and shear rate were conducted at 37 °C.

Measurement of Contact Angle, Droplet Cross-Section Area and Printability

The images of the droplet were taken with an 8 MP camera, through the deposition of hydrogel drop on the surface of a petri dish. One equation which correctly determines the printability of the printed grid pattern formed by channels is as follows [2]:

$$Pr = L^2 / 16A \quad (1)$$

Here A is the area and L is the perimeter of the interconnected channel formed by the filaments. Therefore, the acceptable printability would be from 0.9 to 1.1. in addition, we investigate cross section area of the droplet, so the printability area generally should be between either circular (0.78) or complete square (1).

$$\pi/4 \leq Pr \leq 1$$

Infrared Spectroscopy

FT-IR spectra were characterized using a FT-IR

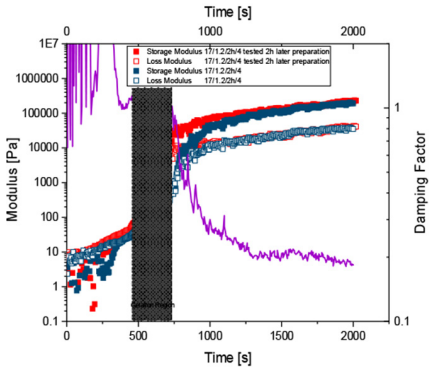

Fig. 1. Time sweep semi-log curve for hydrogel 17/1.2/2h/4 immediately after preparation (blue symbols) and 2 h after (red symbols).

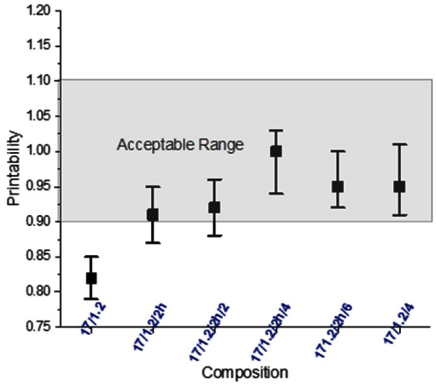

Fig. 2. Printability based on average area of interconnected channels formed by filaments after 1 h deposition on the petri dish at 37 °C.

spectrometer, Spectrum Two (PerkinElmer).

Gel Permeation Chromatography

The measurement of molecular weights and polydispersity index are conducted by Agilent 1260 Infinity.

Swelling Properties

Swelling properties of the films were measured using a method described by Mu *et al.* (2012). Films (2×2 cm in size) were immersed in 25 mL of deionized water and 1×PBS at room temperature (25 °C). The weight gain of swollen films (Ws) was measured at selected times after being dried up their surfaces with absorbent filter paper. The swelling ratio (SR) was calculated using Eq. (2):

$$\text{Swelling ratio} = (W_s - W_d) / W_d \quad (2)$$

W_d is the weight of dried samples (in grams). The measurements were repeated three times [3].

Results and Discussion

Rheological Analysis

Giving consideration to the viscosity against time measurement, the slope of the graph indicates that the essential pressure to deposit from nozzle and the extent of the plateau region is the optimal time before clogging. Based on the time sweep measurements, the time necessary before sample gets ready for 3D printing application would be the time when the formulation reaches its gelation condition. It can be said that with a good approximation that the starting time of gelation is after the plateau region where both moduli intersect, as solution become a viscoelastic liquid, and the end time is where the damping factor (tan δ) reaches a value close to unity (Fig. 1). The amplitude sweep measurement in the range of 1% to 300% of strain amplitude was also performed immediately after the time sweep measurement. The results showed for all samples both moduli advance as plateau until 1% then both decline; at the end, two moduli intersect at a ca. 100% strain indicating the network collapse.

Printability

Measuring contact angle, cross section area of droplet and grid pattern channel formed by the filaments show that the sample with 4 w/w% lignin in which the obtained data locate within the acceptable range and close to unity, has a suitable composition (Fig. 2).

FT-IR Spectrum Analysis

The FT-IR spectra of gelatin, tragacanth and lignin cross-linked gelatin/tragacanth hydrogel have been investigated. We see a strong absorbance and broad region of OH and NH at 3666, in which wider part shows functional group of OH, the narrower part likely belongs to NH stretch and the peak 3604 also is probably assigned to free OH groups. The weak band at 2324 cm^{-1} perhaps belongs to the ammonium group. The weak absorbance and partly broad at 2088. belongs to the C=C bond and 1757 cm^{-1} peak is assigned to the aromatic ketones. Therefore, crosslinking triggers hydrogen bonding (shift to left) and reduces the intensity of peaks absorbance specially under 2000 cm^{-1}.

Swelling Ratio Investigation

Preheating causes gelatin chains to be pliable, so it can absorb more water. Amount of weight gain of swollen films for 1×PBS is less compared to water. Reciprocally, the degradation in PBS is more pronounced.

Conclusion

According to high molecular weight of tragacanth and gelatin and constituent component of lignin, three mechanisms of hydrogen and covalent bonding, hydrophobic interactions and entanglements are responsible for forming hydrogels. The high rate of cross-linking during the process can be facilitated by applying practical solutions to reach an appropriate formulation, preheating and suitable processing temperature. Here, the sample with 4 w/w% lignin gives a better result. There are diverse parameters for instance the height of nozzle and speed of movement which should be investigated in this technique.

References

[1] Yao Tan J.J., Lee C.P., and Hashimoto M., Preheating of gelatin improves its printability with transglutaminase in direct ink writing 3D printing, *Int. J. Bioprint.*, **6**, 4, 118-129, 2020.

[2] Ouyang I., Yao R., Zhan Y., and Sun W., *Biofabrication J.*, **8**, 1-13, 2016.

[3]. Aadil K.R., Barapatre A., and Jha H., Synthesis and characterization of Acacia lignin-gelatin film for its possible application in food packaging, *Bioresour. Bioproc. J.*, **3**, 27, 2016.

14-15 December 2021, Tehran, Iran
2nd International Conference on Rheology
ICOR 2021
article A-10-271-1

Effect of Atmospheric Pressure Cold Plasma (ACP) Treatment on the Technological Characteristics of Quinoa Flour

Leila Zare, Sarah Sanaei Nasab, Mitra Pashaee, and Neda Mollakhalili Meybodi*
Department of Food Sciences and Technology, School of Public Health, Shahid Sadoughi University of Medical Sciences, P.O. Box 89165-564, Yazd, Iran

*neda_mabodi@yahoo.com

Abstract
Atmospheric pressure cold plasma (ACP) is considered as non-thermal treatment with potential microbial inactivation efficiencies. This study is aimed to determine the effect of cold plasma treatment on rheological characteristics of quinoa flour. Regarding, whole quinoa grains were subjected to a dielectric barrier discharge contained plasma reactor for 5 min/50 kV, 10 min/50 kV, 5 min/60 kV, and 10 min/60 kV known S1, S2, S3, and S4 respectively. Untreated sample is named as control sample. Results indicated that ACP treatment could change the rheological properties depending on the treatment exposure time and voltage. As treatment parameter determine the rheological characteristics and consequently the applicability of quinoa flour, an optimization is required.

Keywords: cold plasma, quinoa, rheological properties, nonthermal processing

Introduction

Quinoa (*Chenopodium quinoa Willd.*) as gluten-free pseudo cereal with high protein content, balanced amino acid profile, high content of dietary fiber, vitamins, minerals, and bioactive compounds has recently received increased popularity.

Considering the potential contamination of quinoa flour with microorganisms through planting, harvesting, and storage, the necessity of using effective antimicrobial treatments and their potential impacts on rheological characteristics needs also be investigated.

Plasma, an equilibrium combination of photons, free electrons and neutral atoms, as the fourth state of matter is electrically neutral despite its chemical activity [1].

Considering the ever growing importance of quinoa as a gluten-free pseudo cereal in formulation of functional foods and the necessity of being properly stored, using atmospheric pressure cold plasma treatment is recommended. Tthis study is aimed to investigate the effect of ACP treatments parameter (voltage, time of exposure) on rheological characteristics of quinoa flour [2].

Experimental

Materials and Methods

Materials

Quinoa grains (*Titicaca*) were purchased from a local retailer and were of Persian origin.

Atmospheric Pressure Cold Plasma (ACP) Treatment

Samples obtained by ACP treated whole quinoa grain at 5 min-50 kV, 10 min-50 kV, 5 min-60 kV, and 10 min-60 kV were termed as S1, S2, S3, and S4 respectively.

Fundamental Rheological Measurement

Frequency sweep test was carried out in a frequency range of 0.1-100 Hz at 30 °C using parallel plate geometry by Physica MCR 301 rotational rheometer. The rheological properties (storage modulus (G') and loss modulus (G'')) were reported.

Results and Discussion

The storage (G') and loss modulus (G'') indicate the elastic and viscose behavior of materials respectively. As shown in Figs. 1a and 1b, elastic modulus for all samples is higher than the viscous modulus (G'>G''), indicating the solid behavior of quinoa gel. As depicted, the elastic moduli of the control sample were higher than the ACP treated samples at different times and voltages. Changes in protein structure induced by active species of ACP treatment may also affect the rheological characteristics of quinoa flour. At constant treatment time of 5 min, increasing the treatment voltage increased the viscosity modulus (S3 compared to S1). Also, at constant treatment time of 10 min, the viscose and elastic moduli has been increased with increasing the treatment voltage (S4 compared to S2). The higher the amount of protein in network, the greater the strength, elastic and viscous properties will be. Also, the cross-links created between starch-starch, protein-protein, or protein-starch molecules by plasma treatment improve the systems rheological properties. This improvement may be due to the partial gelatinization of starch and the interaction between other components. In S1 sample which ACP treated at shortest exposure time and voltage (5 min, 50 kV), the rheological properties (G' and G'' moduli) had been decreased compared to control sample. This decrease

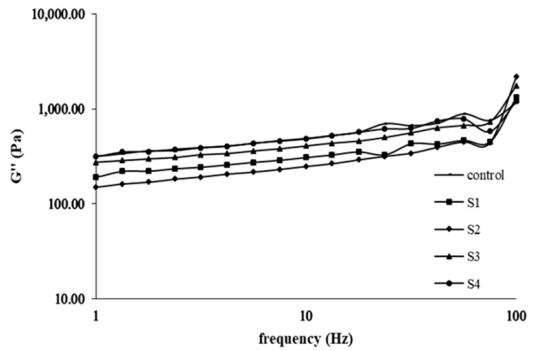

(a)

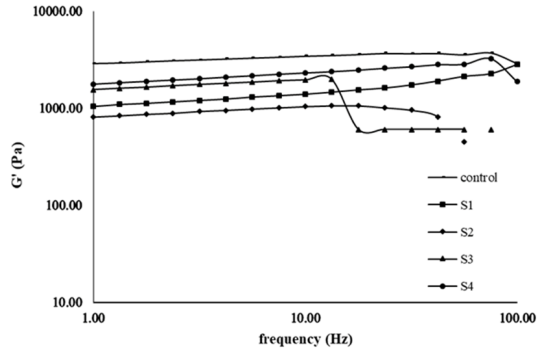

(b)

Fig. 1. (a) Rheological properties (loss modulus) of untreated sample (control) and plasma treated quinoa flour and (b) rheological properties (storage modulus) of untreated sample (control) and plasma treated quinoa flour.

may be due to starch depolymerization [3,4].

Conclusion

Results indicated that rheological characteristics of quinoa flour can remarkably be influenced by atmospheric pressure cold plasma treatment depending on its voltage and exposure time. Plasma treatment can significantly influence the protein and starch structure. Intermolecular connection like starch-starch, starch-protein or protein-protein may also be formed in quinoa flour through cold plasma treatment. The present study shows that the plasma parameters play a significant role on rheological applicability determination of quinoa flour. Applied voltage and treatment time are factors influenced the functional characteristics of food components.

References

[1] Mollakhalili-Meybodi N., Yousefi M., Nematollahi A., and Khorshidian N., Effect of atmospheric cold plasma treatment on technological and nutrition functionality of protein in foods, *Eur. Food Res. Technol.*, **1**, 1-16, 2021.

[2] Bußler S., Rumpold B.A., Fröhling A., Jander E., Rawel H.M., and Schlüter O.K., Cold atmospheric pressure plasma processing of insect flour from tenebrio molitor: impact on microbial load and quality attributes in comparison to dry heat treatment, *Innov. Food Sci. Emerg. Technol.*, **36**, 277-286, 2016.

[3] Hertwig C., Reineke K., Ehlbeck J., Knorr D., and Schlüter O., Decontamination of whole black pepper using different cold atmospheric pressure plasma applications, *Food Control*, **55**, 221-229, 2015.

[4] Hertwig C., Leslie A., Meneses N., Reineke K., Rauh C., and Schlüter O., Inactivation of salmonella enteritidis PT30 on the surface of unpeeled almonds by cold plasma, *Innov. Food Sci. Emerg. Technol.*, **44**, 242-248, 2017.

14-15 December 2021, Tehran, Iran
2nd International Conference on Rheology
ICOR 2021
article A-10-275-1

Rheological Characteristics of Wheat Dough in the Presence of Potassium Chloride and Different Fermentation Types

Mitra Pashaei, Leila Zare, Sara Sanaeinasab, and Neda Mollakhalili-Meybodi*
Department of Food Sciences and Technology, School of Public Health,
Shahid Sadoughi University of Medical Sciences, Yazd, Iran

*neda_mabodi@yahoo.com

Abstract
Overconsumption of bread as the main contributors of sodium intake plays an important role in heart disease occurrence. Regarding, its sodium chloride content is recommended to be decreased by different strategies e.g. salt substitution by sodium free mineral salts. Considering the importance of sodium chloride on technological characteristics and fermentation efficiency of wheat bread, this study is aimed to investigate of the impacts of potassium chloride (KCl) substitution level (10, 20, 30, 40, and 50%) and fermentation types (yeast and sourdough) on rheological characteristics of wheat dough, using rheometer and parallel plate geometer. Results indicated that despite the prevalence of elastic modulus (G') on viscose modulus (G") at all formulations, KCl replacement can significantly influence the rheological characteristics by decreasing the storage modulus (G'), loss modulus (G"), complex modulus (G*) parameters. Substitution of KCl up to 20 w/w% in the presence yeast provide the formulations similar to 100 w/w% NaCl containing sample.

Keywords: salt reduction, potassium chloride (KCl), rheology, sourdough (MFSD), yeast

Introduction

Wheat bread is a staple food product [1]. It is typically produced by wheat flour, water, salt, and yeast as the main ingredients. NaCl considered as a common salt in bread making that influences the technological properties such as dough development time, extensibility, yeast activity and etc. [2]. Sodium is considered as an essential nutrient for maintaining the fluid balance, cell functionality and nerve impulses in human body [3]. High sodium intake is related to cardiovascular disease [4]. Considering the high total intake of bread even low salt content of bread is important [5]. Reduction of daily intake of sodium results major health effects. Partial substitution of sodium with potassium is a popular strategy in production of low sodium foods [6-8]. Adequate daily intake of potassium has positive effects on decreasing the risk of cardiovascular diseases [9]. Despite the positive health effects of KCl, high usage of KCl in food products creates off flavor (bitterness and metal flavor). Adding food permissible flavor enhancers, such as yeast extracts, considered as a recommended strategy for masking the unpleasing tastes [10]. In addition to the ingredients, fermentation is also considered as a key step in bread baking that influences the technological and sensory characteristics of final products. Fermentation with yeast and/or MFSD is commonly used in bread making that produced different types of aroma and flavoring agents. To the best of our knowledge, no study is available on characterization of wheat bread as the effects of partial replacement of NaCl with KCl and fermentation types yeast and/or MFSD. Therefore, the purpose of this work was developing the wheat bread with different ratio of NaCl/KCl and yeast and/or MFSD and evaluating the rheological characteristics of the final products.

Experimental

Materials and Methods

Materials

Potassium chloride produced by Merk Company were purchased from scientific retail and other materials were also purchased from the local market.

Rheological Measurement

Controlled shear/stress rheometer (Anton Paar MCR301, GmbH, Germany) with parallel plate geometry was used for rheological measurement.

Results and Discussion

Viscoelastic characteristics were determined to investigate the impacts of KCl substitution level and fermentation types on technological characteristics of wheat bread. Dynamic viscoelastic characteristics of wheat bread were determined by frequency sweep test at frequency range of 0.01-10 Hz. The frequency sweep curves of wheat dough containing different KCl: NaCl ratio and fermented differently are presented in Figs. 1a to 1d as G', G", G*, and tan δ respectively. All formulations were frequency dependent with storage modulus greater than loss modulus (G'>G") at whole range of angular frequencies as an indicator of elastic-like gel formation of wheat bread as demonstrated by [11]. Elastic and viscose moduli are generally monitored as quality determining factors as high quality bread should be more elastic than viscose [11]. Alongside, the complex modulus and damping factor also provide valuable information about dough strength.

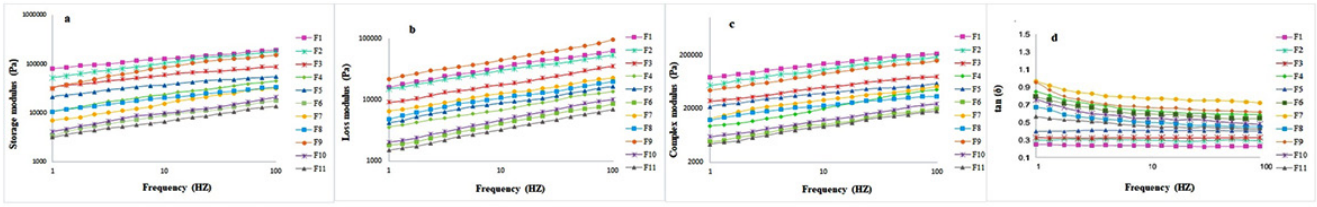

Fig. 1. Effect of yeast and MFSD on Rheological characteristics of wheat bread samples: (a) storage modulus of wheat bread samples, (b) loss modulus of wheat bread samples, (c) complex modulus of wheat bread samples, and (d) tan δ of wheat bread samples.

Considering both elastic and viscose modulus, complex modulus should be optimized as formulations with high complex modulus are generally too rigid to facilitate the growth of air bubble and those having low G* are unable to restore gases.

In yeast fermented samples, increasing the KCl incorporation level decrease G', G", and G* and increase tan δ. In other words, despite decrease observed in both elastic and viscose moduli, the G' modulus decreased more sharply in yeast fermented samples via increasing the KCl incorporation level. In MFSD fermented samples, increasing the ratio of KCl incorporation level enhance the degradation activity of lactic acid bacteria in a way that lowest G', G", and G* is found in F11 containing 50 w/w% KCl in the presence of MFSD. Furthermore, highest G', G", and G* is found in F9 containing KCl: NaCl at 30:70 ratios. The lowest frequency dependency of G* is also found in F8 confirming the formation of strong gel structure [13].

Conclusion

Results showed that although increasing the KCl incorporation level and added sourdough by inhibiting yeast activity and weakening the gluten network respectively, decreased G', G", and G*, and increased tan δ, decreasing the KCl substitution ratio, Due to the increase in glutenin level, decreased G" and increased G', which is a desirable behavior in dough products. Samples with 20% KCl with the highest elasticity and cohesion were optimal samples and in rheological evaluation were slightly different from the control sample.

References

[1] Weegels P.L., The future of bread in view of its contribution to nutrient intake as a starchy staple food, *Plant Food Hum. Nutr.*, **74**, 1, 1-9, 2019.

[2] Pasqualone A., Caponio F., Pagani M.A., Summo C., and Paradiso V.M., Effect of salt reduction on quality and acceptability of durum wheat bread, *Food Chem.*, **289**, 575-578, 12019.

[3] Cepanec K., Vugrinec S., Cvetković T., and Ranilović J., Potassium chloride-based salt substitutes: a critical review with a focus on the patent literature, *Compr. Rev. Food Sci. Food Safe.*, **16**, 5, 881-894, 2017.

[4] He F.J. and MacGregor G.A., Role of salt intake in prevention of cardiovascular disease: controversies and challenges, *Nature Rev. Cardiol.*, **15**, 6, 371-377, 2018.

[5] Avramenko N., Tyler R., Scanlon M., Hucl P., and Nickerson M., The chemistry of bread making: the role of salt to ensure optimal functionality of its constituents, *Food Rev. Int.*, **34**, 3, 204-225, 2018.

[6] Arab M., Sohrabvandi S., Khorshidian N., and Mortazavian A.M., Combined effects of salt-related variables on qualitative characteristics of probiotic fermented milk, *Curr. Nutr. Food Sci.*, **15**, 3, 234-242, 2019.

[7] Antúnez L., Giménez A., Vidal L., and Ares G., Partial replacement of NaCl with KCl in bread: effect on sensory characteristics and consumer perception, *J. Sens. Stud.*, **33**, 5, e12441, 2018.

[8] Zheng J., Han Y., Ge G., Zhao M., and Sun W., Partial substitution of NaCl with chloride salt mixtures: impact on oxidative characteristics of meat myofibrillar protein and their rheological properties, *Food Hydrocolloid.*, **96**, 36-42, 2019.

[9] Engberink R.H.O., van den Born B.-J.H., Peters-Sengers H., and Vogt L., Long-term potassium intake and associated renal and cardiovascular outcomes in the clinical setting, *Clin. Nutr.*, **39**, 12, 3671-3676, 2020.

[10] Sinesio F., Raffo A., Peparaio M., Moneta E., Civitelli E.S., Narducci V. et al., Impact of sodium reduction strategies on volatile compounds, sensory properties and consumer perception in commercial wheat bread, *Food Chem.*, **301**, 125252, 2019.

[11] Meybodi N.M., Mortazavian A.M., Mirmoghtadaie L., Hosseini S.M., Yasini S.A., Azizi M.H. et al., Effects of microbial transglutaminase and fermentation type on improvement of lysine availability in wheat bread: a response surface methodology, *Appl. Food Biotechnol.*, **6**, 3, 151-64, 2019.

[12] Belz M.C., Ryan L.A., and Arendt E.K., The impact of salt reduction in bread: a review, *Crit. Rev. Food Sci. Nutr.*, **52**, 6, 514-524, 2012.

[13] Demirkesen I., Mert B., Sumnu G., and Sahin S., Rheological properties of gluten-free bread formulations, *J. Food Eng.*, **96**, 2, 295-303, 2010.

[14] Chen G., Hu R., and Li Y., Potassium chloride affects gluten microstructures and dough characteristics similarly as sodium chloride, *J. Cereal Sci.*, **82**, 155-163, 2018.

14-15 December 2021, Tehran, Iran
2nd International Conference on Rheology
ICOR 2021
article A-10-277-1

The Role of EVA Level on Melt Viscoelasticity, Rate of Crosslinking and Morphology Development in Cross-Linked Ethylene-Vinyl Acetate/Low-Density Polyethylene/(EVA/LDPE) Blend Foams

Narges Asghari, Azizeh Javadi*, and Ali Asghar Katbab
Department of Polymer Engineering, Amirkabir University of Technology, P.O. Box 15875-4413, Tehran, Iran

*ajavadi@aut.ac.ir

Abstract
Ethylene-vinyl acetate copolymer/Low-density polyethylene (EVA/LDPE) blend foams are prepared by simultaneous crosslinking and foaming via compression molding. Effects of EVA weight fraction on gel content, melt viscosity, and morphology of foams are studied. Cell density increased with reducing cell size by EVA level due to a higher rate of EVA crosslinking, leading to the enhancement of melt viscosity. This is evidenced by an increase in gel content of the foams with the EVA weight fraction.

Keywords: EVA/LD blend, foam, crosslinking, gel content, morphology

Introduction

Foams or cellular structure materials retain the advantages of bulk materials with low-density structures, relatively high stiffness, and flexible cell structure. Due to their properties such as thermal and acoustic insulation, buoyancy, low density, high impact absorbance, long durability, and stress-cracking resistance, polymeric foams are widely used in several engineering applications, including impact energy absorption systems, sound absorbers, electrical and thermal insulators, electromagnetic wave shields [1]. The application of polymeric foam is determined by its structure, e.g., cell type, cell size, cell size distribution, and cell density. Using a Foaming agent as a gas source requires crosslinking to stabilize bubbles growth during expansion and enhance the resistance of the cellular material to thermal collapse, which is necessary for some applications [2]. Low-density polyethylene (LDPE) and ethylene-vinyl acetate copolymer (EVA) are popularly used to manufacture polymeric foams; in particular, the LDPE/EVA foam possesses higher flexibility, toughness, and impact resistance. Cross-linked EVA usually shows a better control of nucleation and formation of cells with uniform size in the foaming of EVA [3,4].

This study aims to investigate chemical crosslink and EVA content's effect on the cell morphology of the cross-linked EVA/LDPE foams.

Experimental

LDPE L2102TX00 (MFI=1.9 g/10 min) from Laleh Petrochemical Company, Iran, and EVA VS430 (MFI= 2.5 g/10 min; 18 wt% vinyl acetate content) from Lotte Company, South Korea, were supplied. Azodicarbonamide (ADC, Anhui Huishang Group, China) as a chemical blowing agent, zinc oxide (ZnO, Rangine Pars, Iran) as ADC activator, dicumyl peroxide (DCP, Di-Cup 98, Hercules) as a cross-linking agent, and stearic acid (Palmac, Malaysia) as an external lubricant were also used. EVA/LDPE blends containing compositions (100:0, 90:10, 70:30, 50:50) were prepared by melt compounding method using a laboratory batch internal mixer (Brabender Plasticorder) at starting temperature of 110 °C and with a rotor speed of 60 rpm. This temperature was chosen to avoid activation and decomposition of ADC and DCP during mixing. First, polymers including EVA and LDPE were added into the mixer and allowed to melt and mixed for 3 min. Then, ADC and ZnO were incorporated into the mixture, and mixing was continued for up to 10 min. Finally, DCP was added to the mixing chamber, and compounding was completed at 15 min. Samples were foamed in a hot-press machine at 155 °C and a pressure of 50 bar. After 25 min, the pressure was removed, and the samples were allowed to expand.

Results and Discussions

The gel content was determined by a 24 h Soxhlet extraction cycle using xylene as the solvent at a temperature of 140 °C according to ASTM D-2765.

After the extraction cycle, the remaining insoluble sample was dried in a vacuum oven at 60 °C to a constant weight. The gel fraction was calculated from the ratio of the final weight, w1, of the sample to its initial weight, w0, as follows:

$$gel\ content = \frac{w_1}{w_0} \times 100 \quad (1)$$

As shown in Table 1, at the same DCP fraction, the gel content increased with EVA content. This indicated that

Table 1. Gel content of EVA/LD foams.

Sample	Gel content (%)
EVA/LD 50/50	76.27
EVA/LD 70/30	78.86
EVA/LD 90/10	84.15
EVA/LD 100/0	89.13

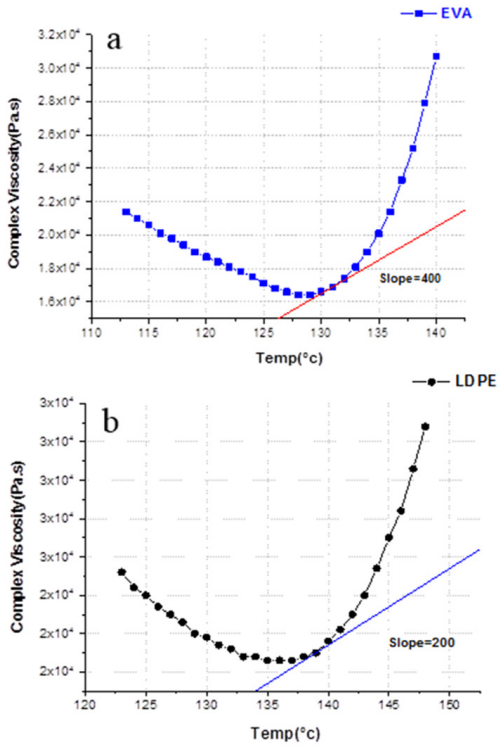

Fig. 1. Temp-sweep test of: (a) EVA and (b) LDPE cross-linked with DCP.

the presence of EVA was favorable to the crosslinking of polymer blends.

Furthermore, according to Fig. 1, the Temp-Sweep mode of the RMS result indicates that EVA starts to crosslink in fewer temperatures with a higher rate (higher fitting slope). This can lead to an increase in the gel content and melt strength with increasing EVA content.

$$N_f = \left(\frac{nM^2}{A}\right)^{3/2} \quad (2)$$

Where, n, M, and A are the number of cells in the micrograph, the magnification number of the micrograph,

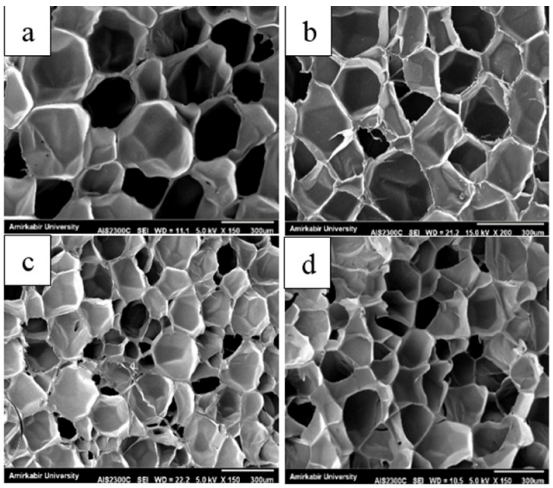

Fig. 2. SEM micrographs of EVA/LD foams: (a) 50/50, (b) 70/30, (c) 90/10, and (d) 100/0.

Table 2. Average cell diameter and cell density of foams.

Sample	Cell diameter (μm)	Cell density (*10^8 Cells/Cm^3)
EVA/LD 50/50	232.52	51.37
EVA/LD 70/30	230.56	59.34
EVA/LD 90/10	187.58	95.64
EVA/LD 100/0	183.45	98.21

and the area of micrograph (cm^2), respectively. According to the results of SEM analysis, For the cross-linked foams, as shown in Table 2, the average cell diameter decreases, and cell density increases with the increasing of EVA content. Wang *et al*. [4] reported that EVA has lower melt viscosity and melt strength, leading to larger cells and decreased cell density in non-cross-linked foams. Still, we observed that after crosslinking EVA/LDPE blends, due to the EVA higher gel content, melt viscosity and strength of the blends are enhanced by the crosslinking network in the polymer blends. The fusion and break of the cells can be restrained, and the cells can also become smaller.

Conclusion

The crosslinking in the EVA/LDPE matrix with EVA major phase improves the melt viscosity and strength, leading to a higher resistance to cell expansion and a barrier to the coalescence of the neighboring cells. Thus, the smaller cell size and a higher cell density of the foams could be obtained.

References

[1] Soriano-Corral F., Hernández-Gámez J.F., Durón-Sánchez L.H., Ramos de Valle L.F., Lozano-Estrada M., and Soto-Lara Y.A., *Key Eng. Mater.*, **779**, 64-70, 2018 .

[2] Liu H., Wu S., Tian N., Yan F., You C., and Yang Y., Carbon foams: 3D porous carbon materials holding immense potential, *J. Mater. Chem. A*, **8**, 45, 23699-23723, 2020.

[3] Pham T.H., Le T.M., and Zhang X.W., *Appl. Mech. Mater.*, **889**, 223-230, 2019.

[4] Wang B., Wang M., Xing Z., Zeng H., and Wu G., Preparation of radiation crosslinked foams from low-density polyethylene/ethylene-vinyl acetate (LDPE/EVA)copolymerblendwithasupercriticalcarbondioxide approach, *J. Appl. Polym. Sci.*, **127**, 2, 912-918, 2013.

14-15 December 2021, Tehran, Iran
2nd International Conference on Rheology
ICOR 2021
article A-10-278-1

Interfacially Reaction Compatibilization of Polyisoprene/ Polydimethylsiloxane Immiscible Blends

Jaber Nasrollah Gavgani[1], Fatemeh Goharpey[1*], and Sachin Velankar[2]
1. Department of Polymer Engineering and Color Technology, Amirkabir University of Technology, P.O. Box 15875-4413, Tehran, Iran
2. Department of Chemical Engineering, University of Pittsburgh, Pittsburgh, Pennsylvania, USA

*goharpey@aut.ac.ir

Abstract
The immiscible blends of polydimethylsiloxane (PDMS) and polyisoprene (PI) were reactively compatibilized by means of multifunctional reactive compounds capable of forming crosslinked copolymers at the interface. Interfacial chemical reaction was occurred between amine-functional PDMS and maleic anhydride-functional PI. Droplet-matrix blends of PI/PDMS with different reactive compatibilizer loadings were examined by optical microscopy and rheometry. The PI-continuous blends show double emulsion morphology including drop clusters and some drops with apparently rough interfaces. In contrast, PDMS-continuous blends displayed double emulsion with round drops that do not appear to aggregate. The rheological properties are also asymmetric: The PI-continuous blend showed gel-like behavior in oscillatory experiments, high viscosity and strong viscosity overshoots in creep experiments, all of which are likely attributable to drop clustering, whereas PDMS-continuous blends showed liquid-like behavior, and low viscosity due to drops coalescence. We consider that the observed morphological and rheological asymmetry is attributable to the asymmetry of the compatibilizer architecture on the two sides of the interface.

Keywords: reactive compatibilization, crosslinked copolymer, rheology, drops coalescence, morphology

Introduction

An interesting property of copolymers in immiscible homopolymer blends is their behavior as emulsifying agents, similar to surfactants. In this context, they are known as "compatibilizers". Block copolymers can lower the interfacial tension of incompatible homopolymers and facilitate the formation of a highly dispersed drop phase. Because the copolymers can reduce the interfacial tension, they promote drop breakup. However, it is generally believed that the more important role of copolymers in polymer blending is that they can inhibit the flow-induced drop coalescence [1,2]. Currently, two mechanisms have been proposed to explain the inhibition of drop coalescence by copolymers; (i) a Marangoni effect that immobilizes the interface [3,4] slows down the drainage process in the thin film between colliding drops, and (ii) steric repulsion between the adsorbed copolymers. A number of studies have shown that the suppression of coalescence is more effective when the molecular weight of the "exterior" block (i.e., the block in the matrix phase) is increased [5] and this seems to support the steric effect as being dominant. In this work, we further explore the effects of an interfacial crosslinked copolymer on the rheological properties of blends, and its effect on drop coalescence and aggregation.

Experimental

The principal components of the blends are PI (Kuraray) and PDMS (Rhodia). Two multifunctional compatibilizer, polyisoprene-graftmaleic anhydride (PI-MA) and poly(aminopropylmethylsiloxane-*co*-dimethylsiloxane) were received from Alderich and Gelest Co respectively. Samples will be designated by $S_{x\text{-}wcomp}$, where x is the weight fraction of the PDMS phase and wcomp is the

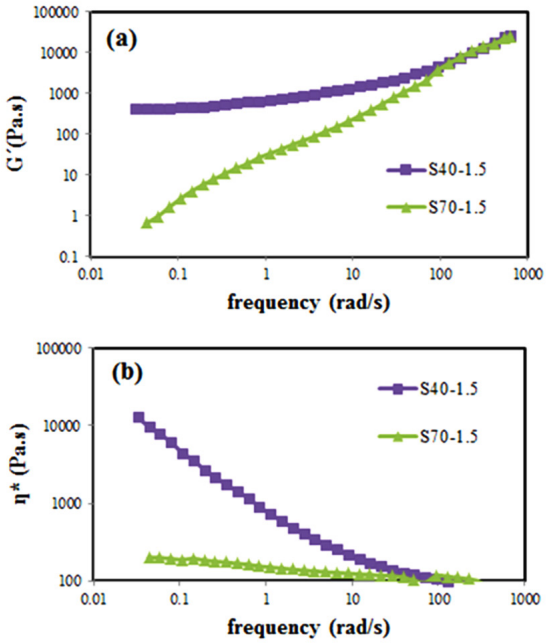

Fig. 1. (a) Storage modulus and (b) Complex viscosity as a function of frequency for S40-1.5 and S70-1.5 samples.

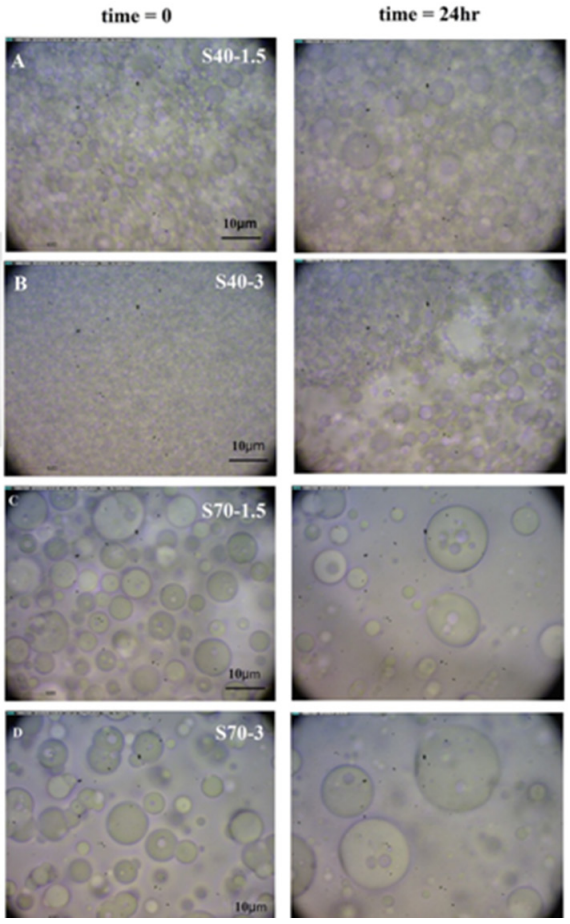

Fig. 2. Visualization of microstructure immediately after mixing (t=0) and after 24 h at quiescent conditions.

overall wt% of compatibilizer. For example, a 1 g sample of S30-3.0 contains 0.285 g PDMS, 0.685 g PI, and 0.015 g each of PI-MA and PDMS-NH_2. The blends were prepared in two steps. First, PDMS-NH_2 was mixed with the nonreactive PDMS, and PI-MA was mixed with the nonreactive PI in the appropriate ratios. Then these two phases were blended together in specific weight ratio. All blends were mixed by hand using a spatula and degassed prior to further experiments.

Results and Discussion

Increasing reactive compatibilizer loading in PI-continuous (S40) blends was found to increase the formation of drop clusters (Figs. 2a and 2b) and increase the"gel-like"behavior and viscosity of the blends (Fig. 1a). In contrast, blends of PI dispersed in PDMS (S70) showed no droplet clusters or gel-like behavior in oscillatory rheological measurements (Fig. 1b). The reasons for observed morphological and rheological asymmetry are not clear, specifically, why the cross-linked skin behaves like a soft solid when PI is the continuous phase, but not when PDMS is a continuous phase remains unknown.

Conclusion

We speculate that the differences in rheological behavior of the S40 versus S70 blends are entirely related to whether the drops stick and form clusters. The presence of clusters in the S40 blends is responsible for the gel-like behavior. In contrast, the apparently normal behavior of the S70 blends seems to arise from the lack of clustering in these blends.

References

[1] Hu Y.T., Pine D.J., and Leal L.G., Drop deformation, breakup, and coalescence with compatibilizer, *Phys. Fluids*, **12**, 484–489, 2000.

[2] Yoon Y., Hsu A.S., and Leal L.G., Experimental investigation of the effects of copolymer surfactants on flow-induced coalescence of drops, *Phys. Fluids*, **19**, 023102, 2007.

[3] Deleo C., Walsh K., and Velankar S.S., Effect of compatibilizer concentration and weight fraction on model immiscible blends with interfacial crosslinking, *J. Rheol.*, **55**, 4, 713-731, 2011.

[4] Dai B. and Leal L.G., The mechanism of surfactant effects on drop coalescence, *Phys. Fluids*, **20**, 040802, 2008.

[5] Gong Y. and Leal L.G., Role of symmetric grafting copolymer on suppression of drop coalescence, *J. Rheol.*, **56**, 2, 397-433, 2012.

14-15 December 2021, Tehran, Iran
2nd International Conference on Rheology
ICOR 2021
article A-10-279-1

Evaluation of Tribological and Rheological Characteristics of Cress Seed Gum-Xanthan Thickened Liquids Applicable for Dysphagia Diet

Parisa Poursani and Seyed Mohammad Ali Razavi*
Center of Excellence in Native Natural Hydrocolloids of Iran, Ferdowsi University of Mashhad,
P.O. Box 91775-1163, Mashhad, Iran
*s.razavi@um.ac.ir

Abstract

The physical properties of a bolus (tribology and rheology) affect the bolus transmission behavior in the pharynx, which is important for predicting the swallowing behavior of dysphagia. The tribological (coefficient of friction) and rheological (hardness, adhesiveness, cohesiveness) properties of xanthan gum (XG)-cress seed gum (CSG) thickened fluids at the concentrations of 0, 0.5, and 1%. It was found that the high lubricating capacity of the selected thickeners can help in the management of dysphagia and prevent the feeling of the unpleasantness of the network's stickiness. The results confirmed that increasing the thickeners' concentration lead to increasing cohesiveness from 0.11 to 0.38 as well as aspiration risk reduction.

Keywords: Cress seed gum, Dysphagia, Texture, Tribology, Xanthan gum

Introduction

Dysphasia, the difficulty of swallowing, is one of the challenging problems after stroke. According to the statistics, about 8% of the world's people have dysphasia [1]. To better understand the texture and consistency of dysphagia patients, the level of concentration of consolidated fluids can be classified. More sophisticated laboratory techniques such as tribology and rheology play an important role in the design and development of new products for dysphagia management. On the other hand, these tests may provide a better understanding of the fluid flow characteristics. In summary, one of the major challenges in addressing dysphagia diet management is the tribological-rheological characteristics of the product. So far, few studies have been performed on the tribological properties of commercial hydrocolloids in the diet of dysphagia, but still not well characterized in recent works [2], and the findings reveal a need for further studies on this subject to create an interconnection between these properties. Therefore, this study aimed to classify the concentration levels of hydrocolloids in the presence of artificial saliva based on tribological and rheological properties. This research also aimed to categorize the lubrication or tribological properties of boluses concerning different thickeners' concentrations.

Experimental

Tribological Test

Tribological measurements were conducted on a Physica MCR 301 tribometer (Anton Paar, Graz, Austria) at 37 °C using a ball-on-three-pins test configuration. The tribopair in this setup consisted of a rotating glass ball (12.7 mm diameter) and three pins (6 mm diameter and height) that are fixed into the sample holder. Each sample was placed on the plate, and then the upper tool was reduced to a 1 N normal force for each tribological test. The in-mouth force was estimated to be about 0.01-10 N during oral processing [3]. Afterward, the friction factors were measured when the sliding speed was raised from 0.1 mm/s to 1000 mm/s. The speed of the human tongue has been assessed in the range of 10-200 mm/s. All tribological tests were performed in at least three replicates. Sliding speed (ϑ, m/s) and friction coefficient (μ, dimensionless) were determined by using Eqs. (1) and (2), respectively:

$$\vartheta = R\omega \quad (1)$$

$$\mu = M / (RF_N) \quad (2)$$

Where, R(m), ω(rad/s), F_N (N), and M (N.m) are the radius between the pivot point and the ball, rotational speed of the spindle, normal force, and torque, respectively.

Mechanical Test

The solid rheological properties of the samples was evaluated by using a texture analyzer (CT3 Texture Analyzer, Brookfield, USA). First, the 25 mL of the sample in a special cylindrical container (height 50 mm; and diameter 30 mm), designed based on the geometry of the mouth and throat, poured and using a cylindrical probe with a diameter of 19 mm, the leading forward extrusion test (FE), at a speed of 50 mm/s, according to the average velocity of the fluid in the throat, was performed. The diameter of the outlet opening is 2 mm according to the average diameter of the esophagus when swallowing a drink. Three parameters including hardness (the peak force (g) during the penetration of the sample), adhesiveness (the negative surface area (g.s) during withdrawal), and cohesiveness (the positive surface area (g.s) during loading) were determined from the force-deformation data [4].

Results and Discussion

Tribological Properties

Oral tribology deals with the oral process during food consumption that provides knowledge of how the bolus behaves during swallowing [5]. The coefficient of friction in tribology can be related to some sensory properties [6]. The Stribeck curves results from tribology measurements for all samples are shown in Fig. 1. It can be seen that the friction coefficient decreased to a minimum with increasing speed in the mixed regime, then it increased at increasing values of the sliding speed in the hydrodynamic regime. The 0.0XG-0.0CSG and 0.0XG-0.5CSG samples showed the least lubricating and the highest frictional resistance in the intermediate sliding velocity range (mixed regime), while 1.0XG-1.0CSG was the most lubricant. Within the intermediate sliding velocity regime, the curves showed a similar trend. For all samples, there was only a minor increase in friction factor when saliva was added to the

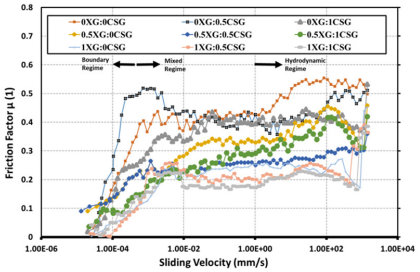

Fig. 1. The Stribeck curves of the xanthan-cress seed gum thickened fluids at T=37 °C.

sample (data not shown). In contrast to the 1.0XG-0.5CSG and 1.0XG-1.0CSG samples, the Stribeck curves for the low concentrations of thickeners showed stick-slip events at intermediate sliding velocities. The results of Vieira, Oliveira Jr [7] demonstrated that the coefficient of friction was decreased with increasing xanthan gum concentration. In other words, it offered more lubrication capacity at higher concentrations. It was also concluded that the properties of the food matrix and the interactions between the polymers were effective in the lubrication capacity of the sample. The threshold concentration forms a complete barrier against surface contact by forming a layer of particles, and a further increase in threshold concentration and the number of particles does not affect the coefficient of friction [8].

Rheological Properties

The rheological parameters such as hardness, adhesiveness, and cohesiveness are demonstrated in Table 1. Hardness is defined as the resistance of a product to target deformation applying an external force. The results showed that the hardness value among the samples enhanced with increasing the amounts of CSG and XG. The hardness of hydrocolloid solutions depends on their macromolecular structure. Since with increasing amount of gum, the amount of absorbed water and consequently the fluid viscosity also increases.

Adhesiveness is the force required to separate food from the surface of other materials, such as the probe of a device or the tooth and tongue [4]. There was a significant increasing adhesion trend, with increasing the amount of gum ($P < 0.05$). Nevertheless, increased adhesion of the bolus during the swallowing process can increase the residual risk in the esophagus [9].

Cohesiveness is defined as the work of forces acting on the structure of food [4]. The results showed the highest cohesion was observed compared to other samples at the levels of 1.0XG-0.5CSG and 1.0XG-1.0CSG ($P < 0.05$) due to water molecules' binding ability of gums. As a result, more force will be required for the rupture of the samples' texture by the device probe. It is worth highlighting that the report from Nakagawa, Matsuo [10] confirmed that excessive dietary cohesion increases the risk of aspiration and easy swallowing has been reported for foods with connective texture in the range of 0.2 to 0.9 [11].

Table 1. Rheological characteristics of xanthan-cress seed gum thickened fluids.

Treatments	Hardness (g)	Adhesiveness (g.s)	Cohesiveness (g.s)
0.0XG-0.0CSG	$1.44^{h}\pm0.37$	$0.02^{h}\pm0.01$	$0.11^{g}\pm0.01$
0.0XG-0.5CSG	$3.68^{g}\pm0.10$	$0.18^{g}\pm0.01$	$0.12^{g}\pm0.01$
0.0XG-1.0CSG	$7.24^{f}\pm0.93$	$0.24^{f}\pm0.02$	$0.19^{f}\pm0.02$
0.5XG-0.0CSG	$12.11^{e}\pm0.33$	$0.31^{e}\pm0.01$	$0.28^{e}\pm0.02$
0.5XG-0.5CSG	$15.24^{d}\pm0.23$	$0.40^{d}\pm0.02$	$0.30^{d}\pm0.04$
0.5XG-1.0CSG	$20.34^{c}\pm0.53$	$0.47^{c}\pm0.01$	$0.33^{c}\pm0.03$
1.0XG-0.0CSG	$17.11^{d}\pm1.93$	$0.46^{c}\pm0.03$	$0.32^{c}\pm0.01$
1.0XG-0.5CSG	$21.15^{b}\pm2.50$	$0.51^{b}\pm0.02$	$0.35^{b}\pm0.03$
1.0XG-1.0CSG	$24.05^{a}\pm3.13$	$0.54^{a}\pm0.01$	$0.38^{a}\pm0.03$

Conclusion

In this research, the tribological and rheological properties of a typical food bolus including CSG and XG, were investigated. It was found that the high lubricating capacity of the selected thickeners can help in the management of dysphagia and prevent the feeling of unpleasant stickiness. The tribological and rheological results demonstrated that CSG could be used as a potential food thickener for dysphagia patients combined with commercial xanthan gum (XG). Moreover, CSG may contribute to develop a more complete formulation of a product aimed at dysphagic patients, hence assisting in the mitigation of the current treatments' side effects.

References

[1] Cichero J.A., Steele C., Duivestein J., Clavé P., Chen J., Kayashita J. et al., The Need for international terminology and definitions for texture-modified foods and thickened liquids used in dysphagia management: foundations of a global initiative, *Curr. Phy. Med. Rehabil. Rep.*, **1**, 280-291, 2013.

[2] Munialo C.D., Kontogiorgos V., Euston S.R., Nyambayo I., Rheological, tribological and sensory attributes of texture-modified foods for dysphagia patients and the elderly: a review, *Inst. Food Sci. Technol.*, **55**, 5, 1862-1871, 2019.

[3] Miller J.L. and Watkin K.L., The influence of bolus volume and viscosity on anterior lingual force during the oral stage of swallowing, *Dysphagia*, **11**, 117-124, 1996.

[4] Szczesniak A.S. JFS.28, 385-9, 1963.

[5] Stokes J.R., Boehm M.W., and Baier S.K., Oral processing, texture and mouthfeel: from rheology to tribology and beyond, *Curr. Opin. Colloid Interf. Sci.*, **18**, 4, 349-59, 2013.

[6] Marconati M., Engmann J., Burbidge A., Mathieu V., Souchon I., and Ramaioli M., A review of the approaches to predict the ease of swallowing and post-swallow residues, *Trend. Food Sci. Technol.*, **86**, 281-97, 2019.

[7] Vieira J., Oliveira Jr F., Salvaro D., Maffezzolli G., de Mello J., Vicente A. et al., Rheology and soft tribology of thickened dispersions aiming the development of oropharyngeal dysphagia-oriented products, *Curr. Res. Food Sci.*, **3**, 19-29, 2020.

[8] Yakubov G., Branfield T., Bongaerts J., and Stokes J.J., Tribology of particle suspensions in rolling-sliding soft contacts, *Biotribology*, **3**, 1-10, 2015.

[9] Sungsinchai S., Niamnuy C., Wattanapan P., Charoenchaitrakool M., Texture modification technologies and their opportunities for the production of dysphagia foods: a review, *Compr. Rev. Food Sci. Food Saf.*, **18**, 1898-912, 2019.

[10] Nakagawa K., Matsuo K., Shibata S., Inamoto Y., Ito Y., Abe K. et al., Efficacy of a novel training food based on the process model of feeding for mastication and swallowing—A preliminary study in elderly individuals living at a residential facility, **5**, 72-78, 2014.

[11] Wada S., Kawate N., and Mizuma M., What type of food can older adults masticate? evaluation of mastication performance using color-changeable chewing gum, *Dysphagia*, **32**, 636-643, 2017.

14-15 December 2021, Tehran, Iran
2nd International Conference on Rheology
ICOR 2021
article A-10-282-1

Effect of Carbon Black Levels on Magic Triangle of Tire Treads Based on SSBR/BR/Silica

Mohammad Barghamadi, Mohammad Karrabi*, Mir Hamid Reza Ghoreishy, and Ghasem Naderi
Polymer and Petrochemical Institute, P.O. Box 14965-115, Tehran, Iran
*m.karabi@ippi.ac.ir

Abstract
In this study, the effects of carbon black (CB) on the wet grip, rolling resistance and abration resistance behavior of compounds based on solution styrene butadiene rubber (SSBR)/butadiene rubber (BR)/silica were investigated. By increasing the CB in the compounds, the damping factor in 0 °C (tan $\delta_{0°C}$) and 60 °C (tan $\delta_{60°C}$) were decreased and increased, respectively. Another effective parameter in the tread compounds of green tires is the abrasion resistance, which was studied for different samples containing 10, 20, and 30 phr of carbon black contents. The results showed that adding 10 phr of carbon black improved this criterion.

Keywords: green tire, ssbr, br, silica, hybrid filler

Introduction

In recent years, with the stricter requirements for tire performance, shortage of petroleum resources, and people's attention to environmental protection, better wet grip property as well as lower rolling resistance are demanded when rubber is applied to tire tread [1–3]. A well-known industrial and practical method for achieving optimum properties is the use of SSBR with silica and CB and also the use of butadiene rubber (BR) with a high cis percentage. Recently, the concept of hybrid fillers has been considered by many researchers. It has been shown that multi-phase hybrid fillers is able to maintain the properties of each filler and also has shown a synergistic effect on processability due to compatibility and effective interactions [4].

In these tires, by changing the reinforcing filler from carbon black to silica as the reinforcing agent, the wet grip and rolling resistance of the tire treads are improved. Therefore, at present, the passenger car tire industry uses silica as a filler in the tire tread formulations. Apart from improving rolling resistance, tire wear properties are also important criteria for tire safety and performance. The abrasion resistance of tire tread rubber directly determines the service life of tire.

The most stubborn problem in the research and development of high-performance tires is that there are contradictions among the abrasion resistance, rolling resistance and wet traction of rubber materials, which is called "magic triangle" in industry [5].

The ratio of loss modulus to storage modulus is defined as the damping factor (tan δ) and is a measure of the performance of wet grip and rolling resistance of tires. The values of the damping factor at two temperatures i.e. 0 and 60 °C have so far been considered as the most suitable indicator for the wet grip and rolling resistance of the tire tread [6].

In the present study, rolling resistance and wet grip for tread compound with the base of SSBR/BR/Silica/CB were evaluated by Dynamic mechanical thermal analysis (DMTA) on a laboratory scale. Abrasion characteristic was also measured by abrasion test.

Experimental

Solution styrene butadiene rubber with 53% vinyl content, 23% styrene content, 24% oil content, Mooney viscosity ML (1+4)@100 °C of 53 and glass transfer temperature of -25 °C was purchased from KUMHO (South Korea). The amount of SSBR used in the mixes was 100 phr. 30 phr of polybutadiene rubber with a cis content of 97% and Mooney viscosity ML (1+4)@100 °C of 45 was provided from Arak Petrochemical (Iran). Carbon Black by grade of N330 with DBP adsorption of 125 mL/100 g, initial particle size of 28 nm and iodine adsorption number of 120 mg/g and three different amounts of 10, 20, and 30 phr were perchased from Pars Industrial Co. (Iran). 60 phr of sedimentary silica with a BET surface area of 180 m^2 was produced by Gujarat Multi Gas Company (India). Other additives was Zinc oxide (ZnO) and stearic acid are used as curing system activators, paraffin wax as processing aid, cyclohexyl benzothiazole (CBS) sulfonamide and diphenyl guanidine (DPG) as accelerator, isopropyl phenylphenylenediamine (IPPD) as antioxidant and sulfur as curing agent.

Initially, all components except the curing agent and accelerators were fed into Banbury mixer along with half of the silica. Mixing was continued for 3 min at a rotational speed of 80 rpm until a temperature of 100 °C. At this temperature the remaining silica was added to the system and mixing was continued for 3 min until reaching a temperature of 150 °C with a rotational speed of 80 rpm. Sulfur and accelerators were then added to the mixes, and the mixes were rolled for 5 min with the curing system. Curing was performed at a pressure of 150 kg/cm^2 and a temperature of 150 °C.

DMTA test was performed by a mettler device (England) according to ASTM D 5026 standard.

The abrasion resistance of the samples was measured according to DIN 53516 using Abrasion Meter by Frank (Germany).

Results and Discussion

Fig. 1 shows a schematic representation of tan δ versus temperature. The tan δ is the result of dividing the storage modulus (G') by the dissipation modulus (G") at each temperature (tanδ=G'/G"). The level of the tan δ at 0 and 60 °C is a measure of wet grip and rolling resistance, respectively. Therefore, the amount of tan δ at the mentioned

temperatures is compared for the rubber compounds filled with hybrid of carbon black and silica, which indicate the two characteristics of green tires, namely wet grip and rolling resistance.

Fig. 2 shows the damping factor at 0 °C (tan $\delta_{0°C}$) of the samples filled with three different amounts of carbon black i.e. 10, 20, and 30 phr. As can be seen, the highest damping factor occurred for the carbon black-free sample. In fact, with the addition of carbon black, the probability of forming a wide filler network increases and the number of rubber chains trapped in the filler networks increases and the effective volume of the rubber chains decreases, leading to a lower amount of dissipation at this temperature. Therefore, increasing the carbon black level to the compounds causes a decrease in wet grip in green tire treads.

It is widely accepted that the loss factor values in 60 °C (tan δ60 °C) are a measure of the tread rolling resistance. Compounds with a high dissipation factor at 60 °C show high rolling resistance and therefore require more energy and fuel to drive. Therefore, to achieve low fuel consumption, the ideal tire tread should have a lower loss factor value at 60 °C. The amount of dissipation factor at 60 °C for compounds containing different amounts of carbon black is shown in Fig. 3. As can be seen, by increasing the amount of carbon black, the rolling resistance increases. It is believed that at high temperatures, the inter-filler frictions causes exotherm and damping raise.

Table 1 shows the abrasion loss of the compounds. Abrasion loss is a function of two mechanisms: energy dissipation and coefficient of friction. Initially, the abrasion resistance improves with increasing energy dissipation, but the coefficient of friction also increases with increasing sample temperature due to the increase in energy dissipation in the form of heat, and finally overcomes the energy

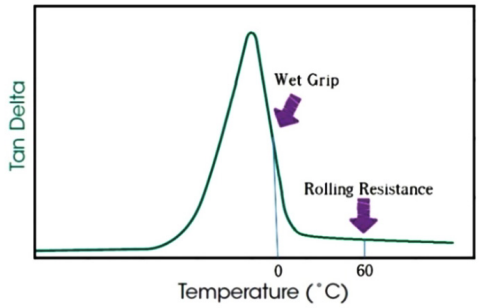

Fig. 1. Schematic representation of determining the wet grip and rolling resistance criteria in green tires.

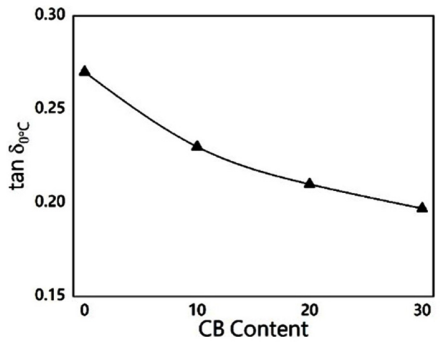

Fig. 2. Tan $\delta_{0°C}$ of samples filled with various CB content.

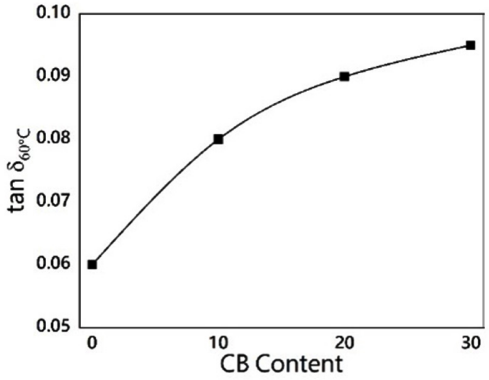

Fig. 3. Tan $\delta_{60\,°C}$ of samples filled with various CB content.

Table 1. Abrasion loss of compounds.

CB Content	Abrasion loss (mm^3)
0	117.4
10	99.3
20	164.2
30	195.0

dissipation mechanism and reduces abrasion resistance. Therefore, by adding carbon black to the compounds, the abrasion loss is reduced by adding 10 phr, but by adding more carbon black due to high friction, the highest carbon black loss is obtained.

Conclusion

Adding CB to the rubber compounds, resulted in an decrease in tan δ0 °C and increase in tan δ60 °C. This means that by the incorporation of CB, the wet grip and rolling resistance characteristics were weakened. But on the other hand, adding 10 phr soot significantly improved abrasion resistance. Therefore, the optimum amount of CB increase of 10 phr was considered.

Acknowledgment

This work was supported by Iran National Science Foundation (INSF) under grant No. 99028742. The authors would like to thanks to INSF for the financial support of this study.

References

[1] Morton M., Rubber technology, Springer Science and Business Media, 2013.
[2] Whelan A. and Lee K.S., Developments in rubber technology-2: synthetic rubbers, Springer Science and Business Media, 2013.
[3] Chandra A.K., Current topics in elastomers research, Boca Raton, 2008, pp. 919–933.
[4] Tian Q., Tang Y., Ding T., Li X., and Zhang Z., *Compos. Commun.*, **10**, 190–193, 2018.
[5] Dominic M., Joseph R., Begum P.M.S., Kanoth B.P., Chandra J., and Thomas S., Cellulose nanofibers isolated from the cuscuta reflexa plant as a green reinforcement of natural rubber, *Carbohyd. Polym.*, **230**, 115620, 2020.
[6] Mao Y., Tian Q., Zhang C., Tang Y., Wang Y., Li X., and Ding T., *Polym. Eng. Sci.*, **59**, 1270–1278, 2019.

14-15 December 2021, Tehran, Iran
2nd International Conference on Rheology
ICOR 2021
article A-10-282-2

Experimental Data and Modeling of Storage and Loss Moduli for SSBR/BR Filled with Hybrid Filler

Mohammad Barghamadi, Mohammad Karrabi*, Mir Hamid Reza Ghoreishy, and Ghasem Naderi
Polymer and Petrochemical Institute, P.O. Box. 14965-115, Tehran, Iran
*m.karabi@ippi.ac.ir

Abstract
In this research, the effects of carbon black (CB) on viscoelastic behaviors of compounds based on solution styrene butadiene rubber (SSBR)/butadiene rubber (BR)/silica were investigated. Results illustrated that by increasing the CB in the compounds, the storage and loss moduli (G' and G") were increased, respectively. In order to evaluate the viscoelastic behavior of compounds containing different amounts of CB, rubber processing analyzer (RPA) in the form of strain sweep test was applied. Viscoelastic parameters were calculated using Kraus model and the G' and G" versus strain curves from Kraus model were plotted along with the experimental results.

Keywords: SSBR, BR, storage and loss moduli, viscoelastic, Kraus model

Introduction

The tire is one of the most important components of the car as its performance has a great impact on the performance of the vehicle [1]. The tire is composed of various components, among which, the tire tread as the only part that is in contact with the road surface, is responsible for transferring forces and torques from the car to the tire and vice versa. Therefore, the performance of a tire depends to a large extent on the response of the tire to the stresses and strains. The tire tread is the most effective part of the tire on its three important functional characteristics, namely rolling resistance, wet grip and abrasion resistance. A well-known industrial and practical method for achieving optimum properties is the use of solution styrene butadiene rubber (SSBR) with silica and carbon black and also the use of Butadiene rubber (BR) with a high cis percentages [2]. Theoretical studies and experimental findings indicate that in order to achieve an optimum compound, having sufficient, comprehensive and in-depth knowledge of the filler performance, especially the interaction between the filler-polymer and the filler network at different temperatures, frequencies and strains is absolutely necessary. The two fillers most commonly used in the tire industry are silica and carbon black [3]. Undoubtedly, the addition of carbon black and silica during mixing increases the mechanical properties of the neat rubber. Recently, the concept of hybrid fillers has been considered by many researchers [4]. carbon black-reinforced rubber has a higher modulus than silica-reinforced rubber. However, silica offers an extraordinary combination of abrasion resistance, tear resistance and aging resistance. Because carbon black and silica have several advantages, a combination of both may give rubber properties superior properties. The mechanism of the filler network in carbon black is to form an interconnected network. When the sample strains, the rubber stores energy and the carbon black network is destroyed, releasing energy in the form of heat. By removing the strain of energy stored in the tire, it forms the filler network again. The mechanism of the Payne effect is in the cases of silica and CB are filler network and polymer adsorption, respectively [5]. Due to the fact that the structure of the filler and trapped rubber is higher in the carbon black system, so the storage modulus is much higher than in the silica system.
In this study, the effect of carbon black content on the tread tire hybrid filler compounds based on SSBR/BR/silica by RPA was investigated.

Experimental

SSBR with 23% styrene from KUMHO, South Korea, BR with a cis content of 97% from Arak Petrochemical, Iran, CB with the grade of N330 from Pars Industrial Co., Iran, silica with surface area of 180 m^2 by Gujarat CO., India were used that the values of each materials are given in Table 1.

All materials except the curing system were mixed into Banbury for 3 min at 80 rpm and a temperature of 100 °C. Finally, Sulfur and accelerators were added to the mixture for 5 min. Curing was applied at a pressure of 150 kg/cm^2 at 150 °C.

A rubber processing analyzer (RPA 2000) from Alpha Technologies Co. (United Kingdom) was used to evaluate the viscoeastic characteristics of composunds in format of strain sweep test (temperature=50 °C, frequency= 60 Hz) after curing (temperature=150 °C, strain=6.98% and frequency=1.68 Hz).

With Origin 2021, the fitting functions are created as user-defined functions through the Non-linear Curve Fit box.

Results and Discussion

Fig. 1 shows the storage modulus (G') versus strain for the compounds reinforced with various content of CB. The non-

Table 1. Formulation of rubber nanocomposites.

Ingredients	Content (phr)		
	SBN0	SBN10	SBN20
SSBR	100	100	100
BR	30	30	30
Silica	60	60	60
CB	0	10	20
S	2	2	2
CBS	1.4	1.4	1.4
Other	3	3	3

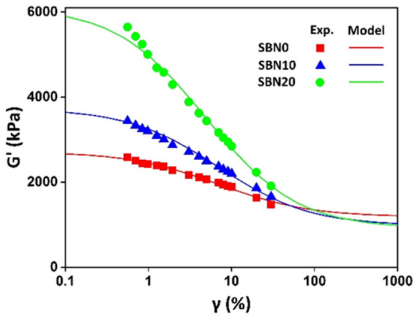

Fig. 1. Storage modulus versus strain for various compounds.

linear behavior of the G′ by increasing the strain amplitude at a constant temperature is called the Payne effect. As can be seen, by increasing of CB, the storage modulus increases and the Payne effect occurred at lower strains. In the presence of CB and silica, filler–rubber interactions lead to an increment in the stiffness and modulus. This result is due to the entrapment of rubber chains in the networks formed by CB and silica, this networking has been intensified by increasing the amount of CB.

Fig. 2 illustrates the the loss modulus (G″) is attributed to the energy dissipated during deformation due to molecular slips (rubber-rubber and filler-rubber frictions). Therefore, with increasing shear strain, the elastic modulus decreases and the loss modulus increases. At low strains, with increasing strain, the energy dissipation of compounds increases rapidly because there are many bonds to break. At higher strains, bonds are broken and the number of intact bonds is lower, thus reducing the rate of energy loss. As can be seen, the G″ increases with increasing CB content. So, as the CB load increases, the filler network develops and the molecular slip strongly increases.

The Kraus model [6] was applied to predict the storage and loss moduli (G′ and G″) vs strain curves. The Kraus model can be expressed by the following:

$$G'(\gamma) = G'_{\infty} + \frac{G'_0 - G'_{\infty}}{1 + (\frac{\gamma}{\gamma_c})^{2n}} \quad (1)$$

$$G''(\gamma) = G''_{\infty} + \frac{2(G''_m - G''_{\infty})(\frac{\gamma}{\gamma_c})^{n}}{1 + (\frac{\gamma}{\gamma_c})^{2n}} \quad (2)$$

Where, γ_c is the characteristic value of the strain, at maximum loss modulus G''_m. G'_0 is the storage modulus for small strains; G'_∞ and G''_∞ are the plateau values of the

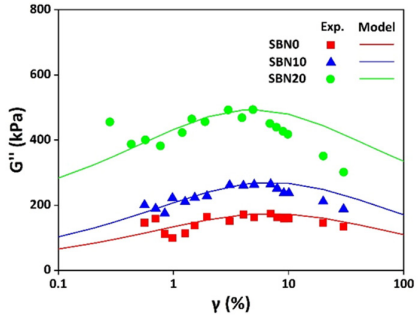

Fig. 2. Loss modulus versus strain for various compounds.

Table 2. Kraus model parameters.

Ingredients	Content (phr)		
	SBN0	SBN10	SBN20
G'_∞	1183.26	976.01	908.86
G'_0	2715.58	3730.76	6120.77
γ_c	6.98	6.98	4.9
G''_∞	5.82	11.12	141.19
G''_m	174.18	264.35	493.03

storage and loss modulus at large strains, respectively; n is a exponent to fit the data which is assumed to be 0.4.

As can be seen in Figs. 1 and 2, the model fits well with the experimental data but deviates from the data by increasing the amount of CB.

Table 2 shows the model parameters of different hybrid compounds. As can be seen, SBN20 shows the highest initial storage modulus (G'_0), final loss modulus (G''_∞) and maximum loss modulus (G''_m). This is because of the the increased stiffness of the compound due to the networking of fillers inside the rubber matrix, trapping the chains and thus reducing their mobility. Also, as mentioned earlier, as the amount of CB increases, the critical strain and the linearity of the compound decreases. The inability of the model to predict the final storage modulus (G'_0) is probably due to a sharp decrease in the G′ at higher CB levels and a deviation in the curve fitting.

Conclusion

Incorporation of CB to the SSBR/BR/Silica compounds, resulted in an increase in storage and loss moduli (G′ and G″). Viscoelastic curves were fitted to the Kraus model using Origin 2021 software. Fitting of the samples was done well, but at higher CB values, a slight deviation from the experimental data was observed.

Acknowledgment

This work was supported by Iran National Science Foundation (INSF) under grant No. 99028742. The authors would like to thanks to INSF for the financial support of this study.

References

[1] Ridha R.A. and Curtiss W.W., Developments in Tire Technology. In: Rubber Products Manufacturing Technology, Routledge, 533–564, 2018.
[2] Shen M., Zhao F., Wang S., and Zhao S., *J. Macromol. Sci. Part B*, **52**, 398–406, 2013.
[3] Kim I.J., Ahn B., and Kim D., Vulcanizate structures and mechanical properties of rubber compounds with silica and carbon black binary filler systems, *Rubber Chem. Technol.*, **94**, 339–354, 2021.
[4] Thaptong P., Jittham P., and Sae-oui P., Effect of conductive carbon black on electrical conductivity and performance of tire tread compounds filled with carbon black/silica hybrid filler, *J. Appl. Polym. Sci.*, **138**, 50855, 2021.
[5] Yang R., Song Y., and Zheng Q., Payne effect of silica-filled styrene-butadiene rubber, *Polymer*, **116**, 304–313, 2017.
[6] Wu J., Chen L., Su B.L., and Wang Y.S., Evolution of Payne effect of silica-filled natural rubber in curing process, *J. Rubber Res.*, **22**, 127–132, 2019.

14-15 December 2021, Tehran, Iran
2nd International Conference on Rheology
ICOR 2021
article A-10-283-1

Colloid-Polymer Mixtures: Effects of Polymer Depletant Topology

Esmaeel Moghimi, Parvin Kiany*, Daniele Parisi, and Dimitris Vlassopoulos
IESL-FORTH, and Department of Materials Science and Technology,
University of Crete, Heraklion, Crete, Greece

*p.kiany@iesl.forth.gr

Abstract
Recent Monte-Carlo simulations and mean-field density functional theory demonstrate that ring polymers are stronger depletants compare to their linear counterparts. This is due to the stronger repulsion between ring-ring and ring-walls. Here, we examine this theoretical finding and explore further the role of macromolecular architecture of the depletant. We use the established PMMA hard spheres at an intermediate volume fraction (0.44). By adding linear, ring and star polymers of the same size and molecular weight as depletant and systematically increasing its concentration, we investigate the formation of gel and assess its viscoelastic properties by means of linear and nonlinear shear rheological measurements. We focus in particular on probing the onset of gelation and the strength of the resultant gel. Our results indicate that in the presence of rings, gelation occurs at smaller concentrations and the resulting gels are much stronger than the respective gels based on linear and star polymers. Our unambiguous results point to the importance of polymer molecular structure in influencing interactions and consequently gelation in colloid-polymer mixtures and open the route for further investigations using branched polymers and soft colloids, which we currently pursue.

Keywords: ring polymer, star polymer, colloid system, depletion

Introduction

Depletion forces are ubiquitous in soft materials that contain hard particles and smaller flexible macromolecules, [2] such as colloid–polymer and colloid–surfactant mixtures. Practical applications of depletion forces are initiating flocculation of impurities in water treatment, promoting aggregation of DNA and crystallization of proteins, [3] and controlling stability and dynamical properties of many consumer products, such as paints, foods and pharmaceuticals [2].

Attempts to interpret experimental or simulation data of depletion forces in colloid–polymer mixtures typically treat the polymer size and concentration as free parameters [3]. The impact of polymer conformation on relative stabilities of hard-sphere colloidal crystals has been addressed [6-9]. A very recent theoretical study also showed that the ring polymers are stronger depleting agents compared to their linear counterpart [1].

In this work, we evaluate the effects of polymer topology as a depletant agent.

Experimental

The polymer stock solution was mixed with the particle stock suspension to prepare final colloid-polymer mixtures with particle volume fraction of 0.44 and varying polymer concentrations (c_p/c_p^*) where c_p^* is the polymer overlap concentration: $c_p^*=3Mw/4\Pi N_A R_g^3$ with NA being the Avogadro's number. We used polystyrene (PS) with three different architectures as the depletant: (i) linear PS with two different molecular weights: Mw=50 kDa, Mw/Mn =1.140, and hydrodynamic radius RH=5.8 nm and Mw =10 kDa Mw/Mn=1.140 and RH=2.8 nm. (ii) Rings with Mw=50 kDa, Mw/Mn=1.24 and R_H=3.1 nm (iii) Stars with f=8 arms with Mw=8000 per arm, Mw/Mn=1.14) and R_H=5.7 nm. We used model hard spheres PMMA particles with R=132 nm, which are sterically stabilized by a short grafted layer, 10 nm, of poly-hydroxystearic acid (PHSA) chain and dispersed in the dioctyl phthalate (DOP). DOP has a high boiling point (385 °C) that minimizes evaporation and allows long-time rheological measurements.

Rheological experiments were performed with an ARES-HR strain-controlled rheometer with a force balance transducer using homemade rough cone-plate geometries of diameter 15 mm, cone angle 0.0415 rad. The temperature was set to 30 °C using a Peltier element. As the standard protocol before each experiment, the sample was rejuvenated at a shear rate of γ=200 s^{-1} for a duration of 200 s, which is sufficient to reach steady-state shear flow. Subsequently, the flow was stopped, and the sample was allowed to age for 4000 s. This time is enough to achieve constant values of the linear viscoelastic moduli.

Results and Discussion

Here, we report the experimental linear and Nonlinear rheology of colloidal gels formed from well-dispersed suspensions of hard spheres at the same volume fraction ϕ=0.44 and varying depletant concentrations. We first interrogate the role of depletants in the linear response rheology of colloidal gels. In Fig. 1, we show the full experimental linear viscoelastic response from dynamic frequency sweeps (DFS) measurements for colloid-polymer mixtures of different depletant architectures. Samples

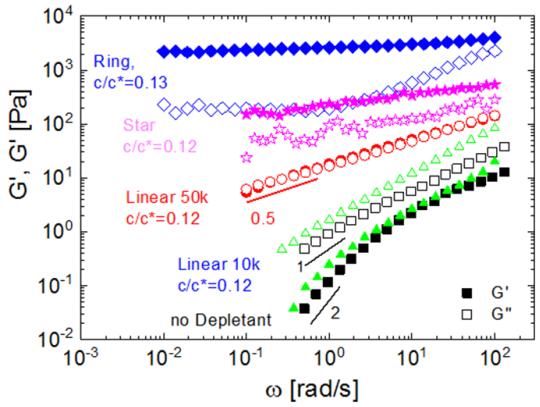

Fig. 1. Experimental dynamic frequency sweeps (with G′ as solid and G″ as open symbols) were performed at a strain of 0.05 and 3 for Linear 10 k after rejuvenation.

containing Ring and Star polymers as the depletant show the typical viscoelastic behavior expected for colloidal gels with G′>G″ in the whole frequency regime indicative of a solid-like response. G′ increases weakly with frequency and G″ exhibits a minimum in the case of the ring polymer. In comparison, linear 10 k depletant did not cause a gel structure at low c/c^*=0.12. To study the concentration effect of depletants, steady-state values of G′ at ω=1 rad/s were compared as a function of c/c^*. At all concentrations, ring depletant forms a stronger gel, suggesting a stronger depletant force than linear and star polymer topologies. As expected, star polymers are stronger depletants compared to linear chains since they are harder objects. Surprisingly, below gelation, Linear 10 k exhibits a weaker elasticity compared to other depletants; however, above gelation it shows a larger G' compared to Linear 50 k due to its smaller size and hence a stronger depletion force.

Nonlinear rheological response during start-up shear flow measurements exhibited the typical yield stress peak. In star and linear polymers, the broadness of the stress peak decreased with shear rate. In contrast, for the ring polymer it was unchanged. The ring polymer has the largest yield stress and a less yield strain, indicating stronger attraction but a lower range, respectively.

Conclusion

At the same c/c*, gels based on rings depletant exhibit larger elasticity and larger yield stress indicating a stronger attractive forces and a lower yield strain due to a smaller attraction range.

References

[1] Chubak et al., Ring polymers are much stronger depleting agents than linear ones, *Mol. Phys.*, **116**, 2911-2926, 2018

[2] Pusey P.N., Colloidal suspensions, in Liquids, Freezing and Glass Transition, Les Houches Session 51, edited by J.-P. Hansen, D. Levesque, and J. Zinn-Justin (North-Holland, Amsterdam, 1991), Vol. 2, 1991, pp. 763-931.

[3] Kulkarni A. and Zukoski C., Depletion interactions and protein crystallization, *J. Cryst. Growth*, **232**, 156 -164, 2001.

[4] Rudhardt D., Bechinger C., and Leiderer P., Direct measurement of depletion potentials in mixtures of colloids and nonionic polymers, *Phys. Rev. Lett.*, **81**, 1330-1333, 1998.

[5] Milling A. and Biggs S., Direct measurement of the depletion force using an atomic force microscope, *J. Colloid Interface Sci.*, **170**, 604-660, 1995.

[6] Lin K.H., Crocker J.C., Zeri A.C., and Yodh A.G., Colloidal interactions in suspensions of rods, *Phys. Rev. Lett.*, **87**, 088301, 2001.

[7] Mahynski N.A., Kumar S.K., and Panagiotopoulos A.Z., Stabilizing colloidal crystals by leveraging void distributions, *Nat. Commun.*, **5**, 4472, 2014.

[8] Mahynski N.A., Kumar S.K., and Panagiotopoulos A.Z., Relative stability of the FCC and HCP polymorphs with interacting polymers, *Soft Matter*, **11**, RSC, 280-289, 2015.

[9] Mahynski N.A., Kumar S.K., and Panagiotopoulos A.Z., Stabilizing colloidal crystals by leveraging void distributions, *Soft Matter*, **11**, 5146-5153, 2015.

14-15 December 2021, Tehran, Iran
2nd International Conference on Rheology
ICOR 2021
article A-10-284-1

Rheological Properties and Crystallization Behavior of Polyethylenes Used in Drip Irrigation Tapes

Sina Haghparast and Gholamreza Pircheraghi*
Polymeric Materials Research Group (PMRG), Department of Materials Science and Engineering,
Sharif University of Technology, Postal Code 1458889695, Tehran, Iran
*pircheraghi@sharif.ir

Abstract
This study was done with the aim of distinguishing the main structural features of polyethylene grades using for drip irrigation tape application. In this regards, two different commercial drip irrigation tape polyethylene grades (DB and MD samples) with different microstructural features were fully characterized by means of thermal, mechanical and different rheological measurements. A set of DSC measurements revealed that DB sample has faster crystallization kinetics probably due to its higher crystallizable length and broader molecular weight distribution. It was also found that, the type of co-monomer used in the DB sample is 1-hexene and in the MD sample is 1-butene, also given the fact that the amount of co-monomer in DB is higher than the MD sample. With special attention to various rheological methods including frequency sweep test in linear viscoelastic region, thermo-rheological measurements and extensional rheological properties, the presence of long chain branches in DB sample was confirmed. The presence of special long chain branches in accompany with short chain branches originated from 1-hexene comonomer has dramatic effects on melt strength dependent rheological properties including increased dynamic moduli, prolongation of the G´-G" crossover, significant thermo-rheological complexity and strong strain-hardening during extension. In addition, microscopic observations show that long chain branches cause the separation of amorphous and crystalline regions at the molecular scale in DB sample, and this special morphology affects the long term properties confirmed by mechanical measurements.

Keywords: drip irrigation tapes, melt strength, long chain branches, thermorheology, extensional rheology

Introduction

The drip irrigation is a precise irrigation method by which water is uniformly and slowly dripped into the soil near the crops roots via low pressure pipeline system and drip irrigation tapes. Compared with the traditional irrigation, the drip irrigation technology can save plenty of freshwater resources [1]. The production process of drip irrigation tapes is done as a tensile field and at high speeds (approximately 200 m/min). For this reason, the polyethylene grade of drip irrigation tape must have a high melt strength for being economical for producers in downstream industries [2]. It is well accepted that microstructural features affect the melt strength-dependent rheological properties of polyethylene, these include molecular weight, molecular weight distribution, type and amount of co-monomer, and most important of all long chain branches [3,4]. Although extensive research has been done on the relationship between microstructure, properties, and processing in polyolefins, there are still challenges that we cannot accurately assess the microstructure of matter. In this regard, in rheological tests, because the change in viscoelastic functions due to changes in microstructural features are in one direction, it is not possible to study the effect of each independently [4-6]. Studies conducted by Maddah *et al*. [7] and Kessner *et al*. [8] show that by using thermorheological methods and plotting the diagram of activation energy (E_a) as a function of the loss angle (δ), the presence of long chain branches (LCBs) in polyethylene can be detected. Based on these researches, if E_a shows no dependency on Loss angle, this is an indication of linear structure and in opposite, dependency of E_a on loss angle is due to the structure with long chain branches. Herein, we investigated and characterized the microstructure of two different commercial Irrigation tape Polyethylene grades by means of various rheological, thermal methods and try to correlate them to mechanical properties.

Experimental

Two different commercial drip irrigation tapes PE grades, include one medium density Polyethylene (MD) and one High density Polyethylene (DB) were supplied from Jam Petrochemical Company and Versalis company, respectively (Table 1).

The Oscillation rheological tests were performed using a rheometric spectrometer (Anton paar MCR502) in oscillatory shear mode with parallel plates at a wide frequency range from 0.01 rad/s to 1000 rad/s. It is worth mentioning that measurements were performed at two different temperatures (170 and 190 °C). The extension measurements were also done using the lab scale AERS G2 extensional rheometer at 180 °C over various strain rates, namely 0.05 and 0.5 s^{-1}.

Table 1. Some characteristics of Polyethylene samples.

Sample	Density (g/cm^3)	MFI (g/10min)
DB	0.94	0.25
MD	0.935	0.38

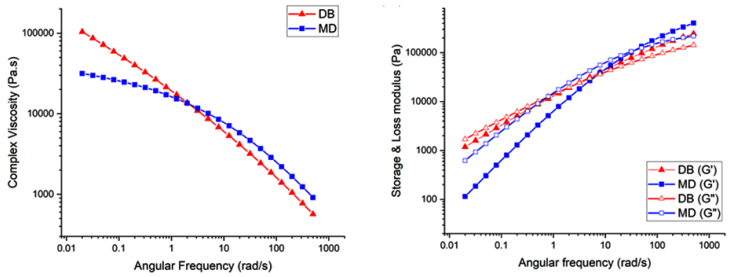

Fig. 1. Frequency sweep rheological measurements: (a) complex viscosity vs angular frequency and (b) storage and loss modulus for PE samples.

Results and Discussion

Fig. 1a demonstrates severe shear thinning behavior as well as higher viscosity at zero shear rate (μ_0) for DB specimen, which is characteristic of high molecular weight polymers with broad distribution. In contrast, MD exhibits more plateau behavior at low frequencies and we see viscosity depression at high frequencies similar to LLDPE resin with short chain branches. In addition, in Fig. 1b, the lower slope of the storage modulus in terminal zone for DB is another reason for the existence of microstructural features that cause such elastic behavior.

Since the main objective of the current work is to distinguish the microstructural features that cause high melt strength in irrigation tape grades, we tried to use activation energy-based thermo-rheological methods to characterize the LCBs. By paying attention to Fig. 2, we observe the complex thermo-rheological behavior in DB, which is well expressed in its nonlinear, δ-dependent behavior. In contrast, the Ea behavior is much more linear and independent of for MD sample, which is due to the absence or presence of negligible amounts of LCBs in this sample. Thus, it is assumed that the main distinctive microstructural feature in DB is the existence of these LCBs, which has led to higher melt strength in this sample during processing.

In addition, the curves of extensional viscosity of DB and MD samples at various stretch rates are presented in Fig. 3. It is clear that DB sample exhibits strong strain-hardening behavior for both stretch rates presented due to its special comb structure. Also az expected, since MD sample doesn't have LCBs, no hardening happens for both investigated rates.

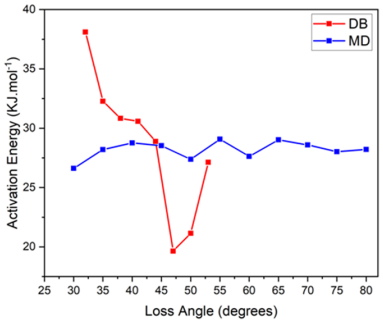

Fig. 2. Calculated activation energy (Ea) vs. loss angle (δ) of PE samples.

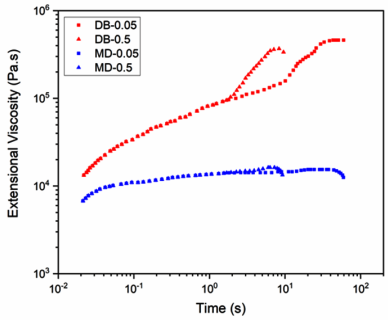

Fig. 3. Extensional viscosity versus time for PE resins at 180 °C.

Conclusion

In this study, we showed that Long chain branches is the most important molecular feature in desirable drip irrigation PE grades, which is resulted in high melt strength in theses grades during processing.

References

[1] Phocaides A., Handbook on pressurized irrigation techniques, 2nd Edition, 2007.
[2] Joseph V., EP16200547, 2017.
[3] Tong Wu T. et al., Effect of molecular weight distribution on rheological, crystallization and mechanical properties of polyethylene-100 pipe resins, *J. Polym. Res.*, **20**, 271, 2013.
[4] Wood-Adams P.M. and Dealy J.M., Using rheological data to determine the branching level in metallocene polyethylenes, *Macromolecules*, **33**, 20, 7481–7488, 2000.
[5] Savas G. et al, Long chain branching and polydispersity effects on the rheological properties of polyethylenes, *Polym. Eng. Sci.*, **40**, 11, 2279-2287, 2000.
[6] Stadler F.J., Influence of type and content of various comonomers on long-chain branching of ethene/α-olefin copolymers, *Macromolecules*, **39**, 4, 1474-1482, 2006.
[7] Maddah Y. et al., Control over branching topology by introducing a dual catalytic system in coordinative chain transfer polymerization of olefins, *Macromelcules*, **53**, 11, 4312–4322, 2020.
[8] Kessner U. et al., Thermorheological behavior of various short- and long-chain branched polyethylenes and their correlations with the molecular structure, *Macromolecules*, **43**, 17, 7341–7350, 2010.

14-15 December 2021, Tehran, Iran
2nd International Conference on Rheology
ICOR 2021
article A-10-288-1

Investigation of the Effect of In-Situ Microfibril Formation on Creep-Recovery Behavior of Polypropylene/Polyethylene Terephthalate Polymer Composites

Elahehossadat Hejazi* and Mahmood Masoomi
Polymer Group, Chemical Engineering Department, Isfahan University of Technology, Postal Code 8415683111, Isfahan, Iran
*es.hejazi@ce.iut.ac.ir

Abstract
In this study, Microfibrillar Composites (MFCs) based on polypropylene/polyethylene terephthalate were prepared in different amounts of dispersed phase, and the effect of in-situ microfibrils formation on creep-recovery behavior was examined. In-situ reinforced microfibrillar composites were prepared during three stages of melt mixing by extrusion, hot drawing immediately after leaving the extruder die and isotropization of the matrix at a temperature lower than the dispersed phase melting temperature using the compression molding method. The fibrillar morphology formed after the hot drawing process was confirmed using scanning electron microscopy (SEM). Fiber-induced elasticity was investigated as a distinct behavior by creep-recovery test, and it was observed that after formation of mature fibrils, the elasticity of the composites increased significantly. The results of creep-recovery test also showed that the resistance of microfibrillar samples to deformation increases and show stronger recovery after stress removal.

Keywords: microfibrillar polymer composites, creep recovery, fiber, polymer blends, rheology

Introduction

Today, the presence of polymers in daily life seems necessary, but these materials are also a major source of environmental pollution. Recyclable polymeric materials have received much attention to reduce pollution caused by polymer waste. A new generation of recyclable polymeric materials are “Micro-Fibrillar Composites (MFC)”. In the processing of MFCs by blending two immiscible polymer components, the reinforcing component, which at first appears in the form of spherical elements, takes the fibril form through appropriate thermal and mechanical treatments. Because reinforcing microfibrils are formed in this two-component blend during the process, some researchers call these composites “in-situ microfibrillar composites”. By introducing this technique, Fakirov claimed that the problem of aggregation and agglomeration of microfibrils could be solved.

MFCs with a polyolefinic matrix have received a great deal of attention due to their availability, ease of processing, and expansion of the processing window due to their relatively low melting temperature, as well as their low cost. One of the most studied microfibrils in the polyolefin matrices is polyethylene terephthalate (PET) due to the good fibril formation and its availability due to the recycled PET obtained from bottles. For reinforcing polypropylene (PP), which is a hydrophobic thermoplastic with excellent chemical resistance and relatively poor mechanical properties, strong PET seems to be a good choice.

In order to evaluate the viscoelastic behavior, oscillating rheological tests, stress relaxation and creep tests are used. The creep test involves applying a constant shear stress over a period of time and measuring the resulting shear strain. The recovery step includes the removal of applied stress and the monitoring of the strain during relaxation from the stored elastic stresses. Only the elastic deformation of the sample can be fully recovered and its viscous deformation is permanent.

The aim of this study was to investigate the effect of in-situ formation of PET fibrils in PP matrix on creep-recovery behavior of their blend using transient rheological technique. In order to evaluate the formed fibrous morphology and its effect on the final properties, scanning electron microscopy and nonlinear creep-recovery rheological test were used. The results of creep-recovery test showed that with the formation of PET fibrils within the matrix, the composite tends to recover the applied stress more.

Experimental

Polypropylene (grade C30S Maroon Petrochemical Company, with a density of 0.9 g/cc) was used as a matrix, and TG641 grade polyethylene terephthalate, a product of Tondgooyan Petrochemical Company, (with intrinsic viscosity of 0.64 dl/g) was used as the dispersed phase. Extruded samples of PP/PET blends in a single-screw extruder with a screw speed of 50 rpm in a composition of 7, 10, and 13% by weight of PET were prepared by melt mixing. The temperature profile of the extruder was set at 190, 270, 280, and 280 °C from the hopper to the die. To prepare the microfibrillar samples, the output strands of the die was passed through a water bath and entered a take-up device. All samples were subjected to a constant DDR of 8. After the drawing step, the strands were compression molded at 190 °C.

The morphological characteristics of the in-situ formed microfibrils after extraction of the matrix by boiling xylene were performed by the XL30 electron microscope made by Philips Company.

A MCR 502 parallel plate rheometer made by the Anton Paar with plates with a diameter of 25 mm was used for creep-recovery test. Creep recovery test was performed at constant stress (1 and 100 Pa for extruded samples/100 Pa for MFC samples) and after stress removal, strain changes were recorded over time. How the system recovers by removing stress will reflect its viscous and elastic parts.

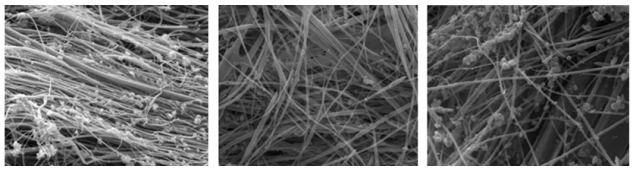

Fig. 1. The SEM images of the MFC samples after extracting the matrix at magnification of 50 micron from left to right at 7, 10, and 13 wt% PET, respectively.

Results and Discussion

The microscopic images taken from the in-situ formed PET microfibrils, after selective extraction of the PP matrix, are shown in Fig. 1. It should be noted that any loss of fibril orientation observed in the micrographs is due to the effect of floating fibrils during the extraction of the PP phase. As shown in Fig. 1, the hot drawing step has led to the formation of fibrous morphology in composite samples.

The creep recovery test is used to analyze the material resistance to deformation. By creep-recovery measurements, the contribution of fibrillar structure to the elasticity of PP/PET composite was determined. In addition, the sample recovery response can be considered as a reflection of the evolution of the fibrillar network. Strain changes over time for extruded samples during constant stresses of 1 and 100 Pa (for a duration of 300 s) and up to 600 s after stress removal are shown in Figs. 2a and 2b. In order to prevent droplet stretching and fibril formation, the extruded samples were subjected to creep test at 240 °C. In both amounts of stress, it is observed that with increasing the dispersed phase concentration, strain decreases and the recovery after stress removal increases. The extruded sample containing 7 wt% of PET shows the highest creep, while the sample consisting of 13 wt% of PET shows the highest resistance to deformation and stronger recovery. In addition, increasing the applied constant stress from 1 Pa to 100 Pa (Fig. 2b) causes a large deformation of the extruded samples due to incompatibility and poor interaction at the interface, and by removing the stress, they show a weak recovery. These results indicate that the spherical regions of the dispersed phase are not able to improve the elasticity of the polymer composite, and polymer composites with matrix-dispersed phase morphology show viscous behavior, especially at high stresses.

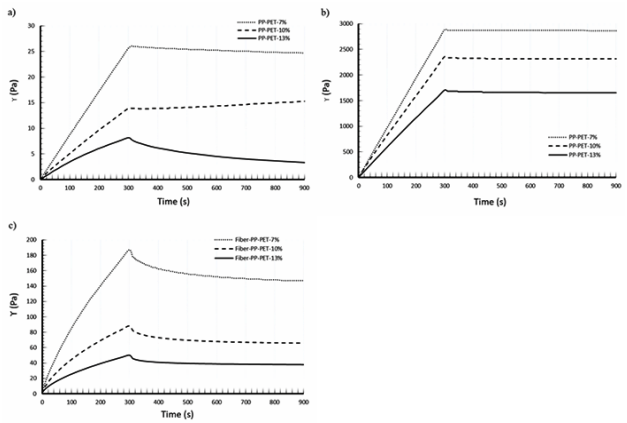

Fig. 2. Creep recovery test: (a) and (b) extruded samples experienced stress of 1 and 100 Pa, respectively, at 240 °C, and (c) MFC samples experienced stress of 100 Pa at 200 °C.

The creep-recovery behavior of MFC samples at 200 °C (far below the melting point of the PET) is shown in Fig. 2c. The creep of MFCs under constant stress decreases with increasing dispersed phase content, and samples with a higher amounts of PET microfibrils show higher resistance to deformation. Compared to extruded samples, samples of microfibrillar composites show less deformation and stronger recovery. In addition, the evolution of the physical fibrillar network with increasing the PET content can be considered effective in improving the recovery behavior in microfibrillar composites. This behavior was also observed for PP/PA6 spun blend fibers.

Conclusion

Scanning electron microscopy results showed that by increasing the dispersed phase concentration in MFCs, the fibril diameter increases and samples containing 13 wt% of PET have fibrils with larger diameter and elongated morphology than other samples. In this study, creep-recovery test was used to determine the contribution of in-situ fibrils on the elasticity of the composite. Samples containing a high amount of PET microfibrils show the lowest creep rate and a sudden recovery, which indicates the high contribution of fibrils to the elasticity of the composite. Increasing the fibrils content increases the interface surface area of these fibrils with the matrix and, as a result, increases the friction at the interface, which results in a higher strength of the composite containing high volume fraction of in-situ microfibrils. In addition, as the fibrils content increases, the interaction of the fibrils dominates, leading to the formation of an interconnected physical network within the matrix. This network distributes the applied force to the composite, resulting in solid-like behavior and stronger recovery by eliminating the applied stress.

References

[1] Mishra R.K., Thomas S., and Kalarikkal N., Micro and nano fibrillar composites (mfcs and nfcs) from polymer blends, Woodhead, 2017.

[2] Fakirov S., Nano- and microfibrillar single-polymer composites: a review, *Macromol. Mater.d Eng.*, **298**, 9, 2013.

[3] Fakirov S., Nano-/microfibrillar polymer–polymer and single polymer composites: the converting instead of adding concept, *Compos. Sci. Technol.*, **89**, 211, 2013.

[4] McCardle R., Bhattacharyya D., and Fakirov S., Effect of reinforcement orientation on the mechanical properties of microfibrillar pp/pet and pet single-polymer composites, *Macromol. Mater. Eng.*, **297**, 7, 711-23, 2012.

[5] Mezger T., The rheology handbook, Vincentz Network, 2020. https://doi.org/10.1515/9783748603702

[6] Hajiraissi R., Jahani Y., and Hallmann T., Investigation of rheology and morphology to follow physical fibrillar network evolution through fiber spinning of PP/PA6 blend fiber, *Polym. Eng. Sci.*, **58**, 8, 1251-1260, 2018.

[7] Hajiraissi R., Linear and nonlinear melt viscoelastic properties of fibrillated blend fiber based on polypropylene/polytrimethylene terephthalate, *Polym. Bull.*, **77**, 5, 2423-42, 2020.

14-15 December 2021, Tehran, Iran
2nd International Conference on Rheology
ICOR 2021
article A-10-290-2

Effect of Concentration and Temperature on the Steady Shear Flow Behavior of Nettle Seed (Urtica Pilulifera) Gum

Zahra Zamani and Seyed Mohammad Ali Razavi*
Division of Food Engineering, Department of Food Science and Technology, Ferdowsi University of Mashhad, P.O. Box 91775-1163, Mashhad, Iran

*s.razavi@um.ac.ir

Abstract
The steady shear flow behavior of Nettle seed gum (NSG) was investigated between 3 and 5% (w/w) concentration and temperatures of 10–70 °C. NSG showed shear thinning behavior at all concentrations and temperatures. The Herschel–Bulkley model was employed to characterize the flow behavior of NSG solutions at the shear rate of 14–400 s^{-1}. When the concentration increased from 3% to 5%, the flow behavior index decreased significantly from 0.927±0.021 to 0.686±0.065 with increasing concentration, indicating more thickening, stabilizing, and pseudoplasticity functions at higher concentrations. The dependence of viscosity on temperature was evaluated by applying the Arrhenius-type model. The activation energy for the NSG was calculated as 18.88 kJ/mol at 3% concentration, which was almost equal to values reported for Nettle seed (*Urtica dioica*) gum. When the shear rate increased, the NSG flow behavior became more the same as Newtonian behavior, and No gelling influence was seen by increasing the temperature.

Keywords: hydrocolloid, pseudoplasticity, rheology, shear viscosity, Urtica pilulifera seed gum

Introduction

Natural hydrocolloids, as functional biological macromolecules (mainly polysaccharides and proteins), are widely used in food and pharmaceutical products [1]. Seeds are generally regarded as a traditional source of different hydrocolloids, mucilage, and gums [2]. *Urtica pilulifera* L. is a plant sorted in *Urticaceae* family. Seeds are obtained from the mature fruits of U. pilulifera. When the seeds are soaked in water, mucilaginous layers appear in the water [3]. In our recent research, based on the numerical optimization method, the optimal conditions for extraction of Nettle seed (*Urtica pilulifera*) gum (NSG) were determined [4]. The purpose of this study was to characterize the steady shear flow properties of NSG solution as well as to study the effect of concentration and temperature on the rheological behavior of NSG solution. Characterizing the rheological properties NSG is crucial and in turn, permits food manufacturers to better implement the functionality of this novel gum in different products.

Experimental

Steady Shear Rheological Measurements

Nettle seed gum was provided under the optimized conditions as described by Zamani et al., (2020). Measurement of rheological properties of NSG dispersions was carried out by a rotational viscometer (Visco 88; Bohlin Instruments, UK) equipped with a bob and cup (C30) geometry according to the viscosity of the samples and a thermal circulator (Julabo, model F-12-MC, Julabo Labortechnic, Germany) to equilibrate the desired temperature.

Shear Rate Dependence

The influence of shear rate on the rheological behavior of the specimens in the shear rate of 14 s^{-1} to 400 s^{-1} was investigated. To describe flow behavior, test data (shear rate-shear stress) was fitted by the Herschel-Bulkley model and the rheological parameters were reported as the mean of two replications [5]:

$$\tau = \tau_{OH} + K_H(\dot{\gamma})^{n_H} \quad (1)$$

Concentration Dependence

The influence of NSG concentration (C%) was evaluated at five levels (3, 3.5, 4, 4.5, and 5%). The apparent viscosity of every solution was quantified at a shear rate of 50 s^{-1} and 25 °C. The concentration dependency of the apparent viscosity of NSG was determined by applying the power model (Eq. (2)), the exponential model (Eq. (3)), and the polynomial model (Eq. (4)) [6]:

$$\eta_a = a_1 C^{b_1} \quad (2)$$

$$\eta_a = a_2 e^{b_2} \times C \quad (3)$$

$$\eta_a = 1 + a_3 C + b_3 C^2 \quad (4)$$

Temperature Dependence

The consistency coefficient dependence of NSG on the temperature at five levels (10, 25, 40, 55, and 70 °C) and constant shear rate (50 s^{-1}) and concentration (3, w/w%) was determined by using the Arrhenius-type model as follows:

$$k = k_0.e^{(\frac{Ea}{RT})} \quad (5)$$

Results and Discussion

Effect of Shear Rate

Flow behaviors, e.g. the apparent viscosity variation with shear rate, of the NSG dispersions for different concentrations from 3% to 5% (w/w%) at 25 °C are shown in Fig. 1a. Accordingly, NSG exhibited a non-Newtonian shear-thinning behavior at all concentrations. Similar behavior was observed for most hydrocolloids including Nettle seed (Urtica dioica) gum [7]. The Herschel-Bulkley equation displayed higher efficiency than two other models (the Power-law and Casson) to fit the shear stress-shear rate data. Based on this model, the consistency coefficient (k), flow behavior index (n), and yield stress (τ_0) of NSG were in the range of 0.009-0.495 Pa.sn, 0.686-0.927, and 0.148-0.630 Pa, respectively.

Effect of Concentration

Based on the results of Herschel-Bulkley model, The consistency coefficient and yield stress of NSG increased from 0.009±0.001 Pa.s^n to 0.495±0.083 Pa.s^n and from 0.148±0.028 Pa to 0.630±0.083 Pa, respectively, when the concentration increased from 3% to 5%, however, the flow behavior index decreased significantly from 0.927±0.021 to 0.686±0.065 with increasing the concentration, indicating more thickening, stabilizing and pseudoplasticity functions at higher concentrations. The results of fitting three empirical models (power, exponential, and polynomial models) on the Herschel-Buckley model parameters as well as apparent viscosity-concentration data showed that the power model was considered as the best model to predict the apparent viscosity of NSG as a function of concentration.

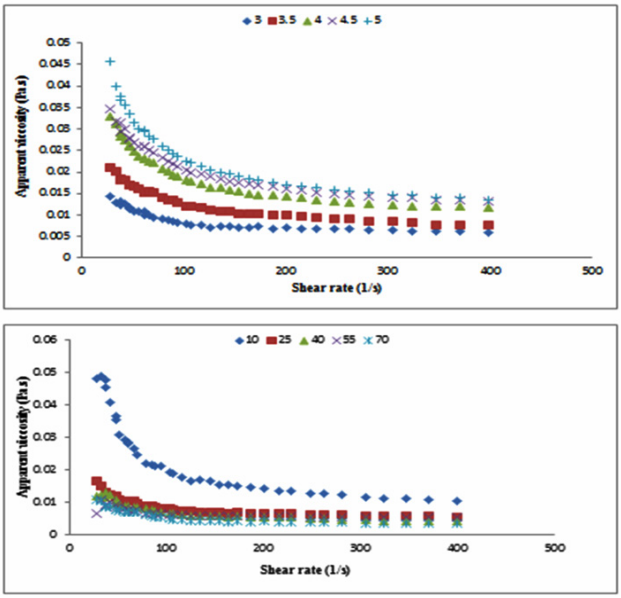

Fig. 1. Apparent viscosity of Nettle seed gum; (a) at different concentrations (3%, ♦; 3.5%, ■; 4%, ▲; 4.5%, ×; and 5%, +) and constant temperature (25 °C) and (b) at different temperatures (10 °C, ♦; 25 °C, ■; 40 °C, ▲; 55 °C, ×; and 70 °C, Ж) and constant concentration (3%).

Effect of Temperature

The effect of temperature on the apparent viscosity of NSG is shown in Fig. 1b. Typically, the apparent viscosity of the gum dispersions decreased by elevating the temperature. This behavior may be due to an increase in motility and movement of macromolecules in Nettle seed gum, which caused less resistance to flow with increasing temperature. At all temperatures, NSG indicated a shear-thinning behavior, especially at low shear rates and 10 °C (Fig. 1b). Nonetheless, when the shear rate increased, the NSG flow behavior became more the same as Newtonian behavior. No gelling influence was seen by increasing the temperature. The dependence of viscosity on temperature was evaluated by applying the Arrhenius-type model. The activation energy for the NSG was calculated as 18.88 kJ/mol at 3% concentration, which was almost equal to values reported for Nettle seed (*Urtica dioica*) gum (17.99 kJ/mol) [7].

Conclusion

Time-independent rheological studies showed the Herschel-Bulkley model is the most appropriate model to describe the steady shear flow behavior of the NSG. At all the concentrations and temperatures, NSG indicated a shear-thinning behavior, especially at low shear rates and 10 °C. Besides, the rheological properties of NSG were severely affected by concentration and temperature.

References

[1] Razavi S.M.A., Emerging natural hydrocolloids: rheology and functions, John Wiley and Sons Publisher, Chichester, England, 2020.

[2] Cui W., Eskin N.A.M., and Biliaderis C.G., Chemical and physical properties of yellow mustard (Sinapis alba L.) mucilage, *Food Chem.*, **46**, 169-176, 1993.

[3] Baytop T., Türkiye'de Bitkilerle Tedavi Nobel Tıp Kitapevleri, Baskı, istanbul, 1999.

[4] Zamani Z., Razavi S.M.A., and Amiri M.S., Molecular parameters and intrinsic viscosity of nettle seed (*urtica pilulifera*) gum as a function of temperature, *Res. Inno Food Sci. Tech.*, **9**, 143-160, 2020.

[5] Steffe J.F., Rheological methods in food process engineering, Freeman, 1996.

[6] Rao M.A., Rheology of fluid and semi-solid foods (principles and applications), Aspen Publication, 1996.

[7] Kutlu G., Bozkurt F., and Tornuk F., Extraction of a novel water-soluble gum from nettle (Urtica dioica) seeds: optimization and characterization, *Int. J. Biol. Macromol.*, **162**, 480-489, 2020.

14-15 December 2021, Tehran, Iran
2nd International Conference on Rheology
ICOR 2021
article A-10-292-1

Effect of Gamma Irradiation Treatment on the Rheological Characteristics of Quinoa Flour

Sarah Sanaei Nasab, Leila Zare, Mitra Pashaee, and Neda Mollakhalili Meybodi*
Department of Food Sciences and Technology, School of Public Health,
Shahid Sadoughi University of Medical Sciences, Yazd, Iran

*neda_mabodi@yahoo.com

Abstract
This study aimed to investigate the effect of gamma irradiation on the rheological properties of quinoa flour using six different doses of irradiation (0.5, 1, 2.5, 5, 7.5, and 10 kGy). The changes in rheological properties using frequency tests were evaluated. Where decreased in the storage modulus (G′), loss modulus (G″), and complex modulus (G*) after the treatment was observed. Results also revealed that there is an increase in damping factor (tan δ) after the treatment. Thus, gamma irradiation treatment can be one of the physical modification methods for changing the rheological properties of quinoa.

Keywords: gamma irradiation, quinoa, rheological properties, loss modulus, storage modulus

Introduction

Quinoa (*Chenopodium quinoa*) is a gluten-free grain that has a high protein content (more than 15%) with a balanced combination of essential amino acids as well as significant amounts of lipids, dietary fiber, vitamins, minerals, antioxidants and bioactive compounds [1,2]. Quinoa unlike other cereals, is rich in lysine and with high amounts of sulfur amino acids is considered a high protein quality food. Quinoa contains significant amounts of vitamins (e.g riboflavin and pyridoxine) and is a rich source of minerals (Ca, Mg, Fe, Cu, and Zn) compared to other grains [1]. Contamination of quinoa with microorganisms such as Fuma Exigua during different stages of planting, holding, harvesting, and storage requires using effective antimicrobial treatments [2]. Food irradiation is a beneficial, cost effective, and environmentally friendly technology [3] to reduce microbial load, maintain quality and improve food safety [4]. Gamma irradiation alters food carbohydrates and proteins. Free radicals generated by irradiation break down large starch polysaccharides into small dextrin fractions by hydrolyzing glycoside bonds [5] and these effects eventually cause physical, textural, and rheological changes in food. Hence, due to the increasing importance of quinoa in the production of functional foods and, the ionizing nature of gamma rays, which besides reducing microbial load, may affect the protein, and starch to change the rheological properties of cereal flour in a way to affect its performance in subsequent applications, This study aims to investigate the effect of gamma irradiation on the rheological characteristics of quinoa flour.

Experimental

Materials

The white Quinoa seeds (*Titicaca*) were purchased from a trade market (Elia trade, Mashhad, Iran) and packed into airtight polyethylene bags. All chemicals and reagents used were of analytical grade.

Gamma Irradiation Treatment

Irradiation treatments of samples using Gamma source Co-60 at doses of 0.5, 1, 2.5, 5, 7.5, and 10 kGy (1.15 Gy/s, 23±2 °C) were done at NSTRI of Iran and un-irradiated sample used as control.

The Oscillatory Rheological Analysis

Frequency sweep test (0.1-100 Hz, 30 °C) was carried out using Physica MCR 301 rotational rheometer and the storage modulus (G′) and loss modulus (G″) were reported. Parameter damping factor (tan δ) and complex modulus (G*) were calculated respectively using the following formula:

$$\mathrm{Tan}\delta = G'' / G' \quad (1)$$

$$G^* = \sqrt{G'^2 + G''^2} \quad (2)$$

Results and Discussion

In frequency sweep tests the values of storage modulus (G′; elasticity) were higher than loss modulus (G″; plasticity) for all samples (Fig. 1); which shows a gel-like viscoelastic behavior of quinoa flour. Similar results have

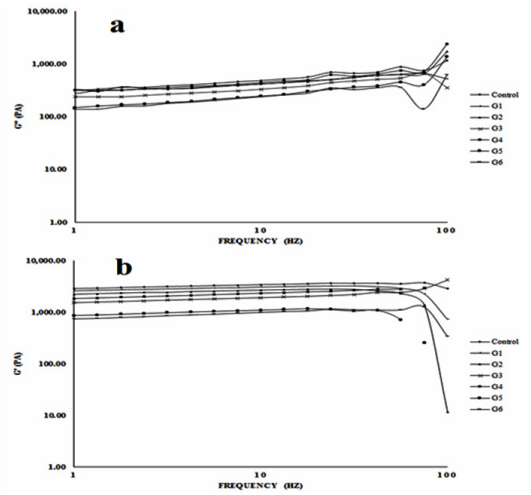

Fig. 1. Frequency sweep test: (a) loss modulus and (b) storage modulus of irradiated and un-irradiated (control) quinoa flour.

been reported by Ye et al. (2016) and Bashir et al. (2017). Higher values of both moduli (G′ and G″) were found in un-irradiated flour, whereas the lowest values were found in the 10 kGy (G6) irradiated flour as similar as Zhu (2016). The decreasing trend of G′ and G″ as increasing the irradiation dose can be attributed to interaction between particles in quinoa flour and starch, degradation of the starch molecules and the structural breakdown at higher doses which lead to the formation of weaker gel network [6-8]. Also Higher frequencies led to an increase in the patterns of G′ and G″ as in Kong et al. (2009). The complex modulus (G*) and damping factor (tan δ) of samples at constant frequency of 10 Hz (Table 1.) Shows significant reduction in complex modulus of irradiated samples compared to control sample indicating the formation of weaker gel in irradiated quinoa flour [6]. Gel formation with higher complex modulus may be due to the polymerization of proteins and the formation of disulfide bonds [9]. Damping factor (tan δ) significantly increased in irradiated sample compared to control, validating the predominant solid-like character of quinoa flour structure [7]. The rheological characteristics results, thus, might be due to the cleavage and rearrangement of the starch granules after irradiation [10].

Table 1. Effect of gamma irradiation on complex modulus (G*) and Parameter damping factor (tan δ) of quinoa flour in 10 Hz.

Sample	G*	Tan d
Control	$3.47\times10^{3}\pm0.03^{a}$	$1.37\times10^{-1}\pm0.02^{f}$
G1	$3.11\times10^{3}\pm0.01^{b}$	$1.42\times10^{-1}\pm0.01^{f}$
G2	$2.72\times10^{3}\pm0.05^{c}$	$1.56\times10^{-1}\pm0.01^{e}$
G3	$1.95\times10^{3}\pm0.02^{e}$	$1.74\times10^{-1}\pm0.02^{d}$
G4	$2.38\times10^{3}\pm0.02^{d}$	$1.91\times10^{-1}\pm0.03^{c}$
G5	$1.13\times10^{3}\pm0.03^{f}$	$2.25\times10^{-1}\pm0.01^{b}$
G6	$1.02\times10^{3}\pm0.05^{g}$	$2.43\times10^{-1}\pm0.05^{a}$

*Values followed by different letters in each column are significantly different ($P<0.05$).

Conclusion

Gamma irradiation treatment of quinoa resulted in decreasing the viscoelastic nature of its gel (G′ and G″) as well as complex modulus (G*) and increasing damping factor (tan δ) significantly and induced changes in the rheological properties of quinoa flour. Results indicated that this treatment can cause the degradation of starch molecules and the structural breakdown besides changing gel network. Therefore, can be used to change rheological properties of quinoa.

References

[1] Sohaimy S.A.E., Mohamed S., Shehata M., Mehany T., and Zaitoun M., Compositional analysis and functional characteristics of quinoa flour, *Annu. Res. Rev. Biol.*, 1-11, 2018.
[2] Wang S. and Zhu F., Formulation and quality attributes of quinoa food products, *Food Bioprocess Technol.*, **9**, 1, 49-68, 2016.
[3] Filho A.M.M., Pirozi M.R., Borges J.T.D.S., Pinheiro Sant'Ana H.M., Chaves J.B.P., Coimbra J.S.D.R., Quinoa: nutritional, functional, and antinutritional aspects, *Crit. Rev. Food Sci. Nutr.*, **57**, 8, 1618-1630, 2017.
[4] Danielsen S., Bonifacio A., and Ames T., Diseases of quinoa (*Chenopodium quinoa*), *Food Rev. Int.*, **19**, 1-2, 43-59, 2003.
[5] Sá A.G.A., Moreno Y.M.F., and Carciofi B.A.M., Food processing for the improvement of plant proteins digestibility, *Crit. Rev. Food Sci. Nutr.*, 1-20, 2019.
[6] Ito V.C., Bet C.D., Wojeicchowski J.P., Demiate I.M., Spoto M.H.F., Schnitzler E. et al., Effects of gamma radiation on the thermoanalytical, structural and pasting properties of black rice (Oryza sativa L.) flour, *J. Therm. Anal. Calorim.*, **133**, 1, 529-537, 2018.
[7] Bhat N.A., Wani I.A., Hamdani A.M., Gani A., and Masoodi F., Physicochemical properties of whole wheat flour as affected by gamma irradiation, *LWT-Food Sci. Technol.*, **71**, 175-183, 2016.
[8] Bashir K., Jan K., and Aggarwal M., Thermorheological and functional properties of gamma irradiated wholewheat flour, *Int. J. Food Sci. Technol.*, **52**, 4, 927-935, 2017.
[9] Kong X., Kasapis S., Bao J., and Corke H., Effect of gamma irradiation on the thermal and rheological properties of grain amaranth starch, *Radiat. Phys. Chem.*, **78**, 11, 954-60, 2009.
[10] Du Z., Li Y., Luo X., Xing J., Zhang Q., Wang R. et al., Effects of electron beam irradiation on the physicochemical properties of quinoa and starch microstructure, *Starch Stärke*, **72**, 11-12, 2020.
[11] Thirumdas R., Trimukhe A., Deshmukh R., and Annapure U., Functional and rheological properties of cold plasma treated rice starch, *Carbohyd. Polym.*, **157**, 1723-1731, 2017.
[12] Zhu F., Impact of γ-irradiation on structure, physicochemical properties, and applications of starch, *Food Hydrocolloids*, **52**, 201-212, 2016.

14-15 December 2021, Tehran, Iran
2nd International Conference on Rheology
ICOR 2021
article A-10-294-1

Non-Linear Rheological Responses and Tribological Behaviors of Model Reduced-Fat O/W Emulsion Using High Pressure-Treated Corn Starch as a Novel Fat Replacer

Ali Heydari and Seyed Mohammad Ali Razavi*
Center of Excellence in Native Natural Hydrocolloids of Iran, Ferdowsi University of Mashhad,
P.O. Box 91775-1163, Mashhad, Iran
*s.razavi@um.ac.ir

Abstract
The main objective of this study was to evaluate the influence of high hydrostatic pressure (HHP) treated corn starch (HPCS) with different concentrations (10 and 15%) as a fat replacer on the large amplitude oscillatory shear (LAOS) and tribological properties of reduced-fat O/W emulsions at various fat reduction (FR) levels (25 and 50%). The obtained results from rheological essays revealed that by increasing FR level, greater nonlinearity, higher friction factor, and shear-thinning were observed for the HPCS-contained samples. Using HPCS with higher concentration at each FR level, the extent of nonlinearity (regardless of elastic or viscous) and friction factor decreased meaningfully.

Keywords: emulsion, fat replacer, large amplitude oscillatory shear, rheology, tribology

Introduction

High hydrostatic pressure (HHP) as a non-thermal, green, and primary technique has been frequently used to modify the functional properties of different starch sources [1,2]. HHP-treated starches show the modified crystalline structure, lower viscosity, and considerably lower retrogradation tendency, which can be applied as a good fat replacer [3]. The storage stability of numerous O/W emulsions relates to the rheological features of the element phases.

Some rheological researches have currently focused on examining large amplitude oscillatory shear (LAOS) and tribological behavior of various food systems, mostly because of their capability for supplying helpful information about micro-/macro-structural characteristics of foods under large deformations, and frictional properties between two interacting surfaces, respectively [19]. Consequently, the LAOS behavior and tribological properties of model reduced-fat O/W emulsions in three fat reduction levels (25 and 50%) prepared with HPCS at different concentrations (10 and 15 w/w%) as fat replacer were scrutinized by comparison with the full-fat O/W emulsion.

Materials and Methods

Materials

Corn starch was purchased from Sigma-Aldrich Company [1]. Sunflower oil was bought from an accessible market.

Samples Preparation

High hydrostatic pressure (HHP)-treated starches were produced by applying the mentioned methods of Heydari *et al*. [1]. Also, all reduced-fat and full-fat emulsions were made according to the procedures described by Heydari *et al*. [2] and Heydari and Razavi [6].

Large Amplitude Oscillatory Shear (LAOS) Measurements

Elastic and viscous characteristics of the emulsions in the non-linear (n-LVE) regions were assessed by applying a physica MCR 301 rheometer (Anton Paar, Austria) with amplitude sweep in the range of 0.01–1000% at a constant frequency of 1 Hz and 25 °C. Elastic and viscous Lissajous plots were employed to scrutinize the n-LVE response of the emulsions.

Tribological Analysis

By applying a Physica MCR 301 rheometer (Anton Paar, Austria) at 36.6 °C with a ball-on-three-pins test geometry at the normal force of 1 N in the range of 0.1 mm/s to 1000 mm/s sliding speed tribological characteristics of prepared emulsions were evaluated.

Statistical Analysis

Two-way analysis of variance (ANOVA), followed by Duncan's multiple range test to compare means ($p \leq 0.05$) of gained data were performed. Using the curve fitting toolbox and Levenberg–Marquardt algorithm of MATLAB software, the given data were fitted.

Results and Discussion

LAOS Characteristics

The shape of the elastic Lissajous-Bowditch plots of the HPCS-contained emulsions was semi-rectangular, which depicts the gel-like structure of these emulsions. However, by increasing the FR level, the enclosed area of the Lissajous plots was increased (Fig. 1). By using HPCS with higher concentrations (15 and 20%) at each FR level, the shape of elastic Lissajous plots almost changed to elliptical shapes with lower confined area, which shows dominant elastic behavior of reduced-fat emulsions (strain-stiffening).

The viscous Lissajous-Bowditch curves, Fig. 2, depicted very nonlinear viscoelastic behavior as well as intense intra-cycle shear-thinning at high shear rate values, as proved by the approximately S-shape of the loops [7]. Also, by increasing the concentration of HPCS, the confined area of viscous plots increased, demonstrating dominant elastic properties of reduced-fat emulsions.

Tribological Investigation

The magnitudes of friction coefficient (μ) of all samples were in the range of 0.1-1.0 for all examined sliding

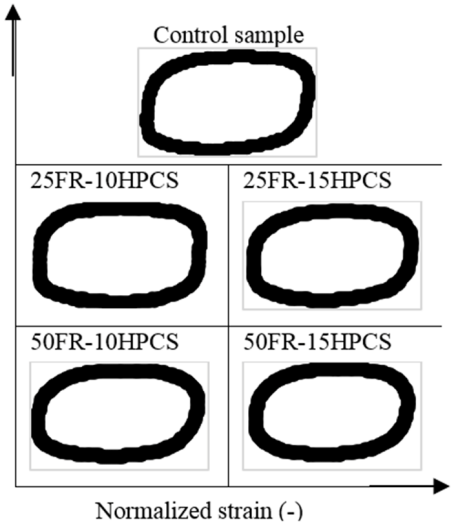

Fig. 1. Elastic Lissajous-Bowditch plots (stress (y-axis) versus strain (x-axis) (τ (γ)) of the control (containing 80% oil) and reduced-fat O/W emulsions at a fixed frequency of 1 Hz, 1000% strain amplitude and 25 °C. FR, fat replacement level; HPCS, high pressure-treated corn starch concentration.

velocities, and the shape of friction curves differed based on the defined factors applied for making the samples. Nonetheless, according to the friction curve shapes, Fig. 3, all prepared samples depicted the boundary to the mixed regime at all inspected sliding speeds, which was in accordance with the previous researches [8].

With augmenting FR level, the μ value of prepared samples increased significantly ($P<0.05$) which can be attributed to the greater size droplet, more dissimilarity (non-homogeneity), and more viscous dominant behavior of the samples at higher FR levels [2,6]. But, using HPCS with higher concentration, the friction value of reduced-fat samples decreased. The reason for this observation can be highly attributed to the smaller droplet size, lower polydispersity index (PDI), greater hardness, and elasticity of prepared reduced-fat samples with a higher concentration of HPCS [2,6].

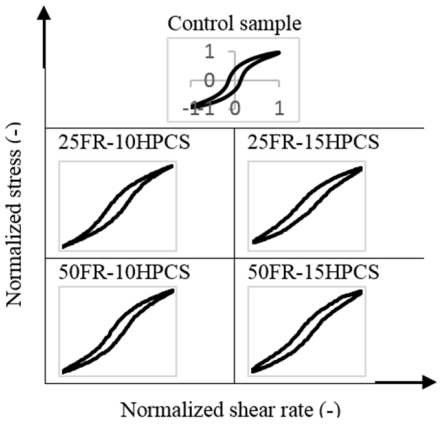

Fig. 2. Viscous Lissajous-Bowditch plots of the control (containing 80% oil) and reduced-fat O/W emulsions at a fixed frequency of 1 Hz, 1000% strain amplitude, and 25 °C. FR, fat replacement level; HPCS, high pressure-treated corn starch concentration.

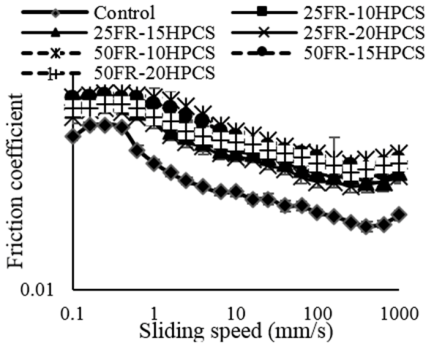

Fig. 3. Stribeck curves of the control (containing 80% oil) and HPCS-contained samples. FR, fat replacement level; HPCS, high pressure-treated corn starch concentration.

Conclusion

LAOS and tribological characteristics were measured for reduced-fat O/W emulsions which were made by HPCS as a fat replacer. Increasing fat reduction (FR) levels caused an increase in the nonlinear behavior and friction factor. Using HHP-treated starches with higher concentrations at each FR level, the values of friction factor decreased and dominant elastic behavior of reduced-fat emulsions was observed.

References

[1] Heydari A., Razavi S.M.A., Hesarinejad M.A., and Farahnaky A., New insights into physical, morphological, thermal, and pasting properties of hhp-treated starches: effect of starch type and industry-scale concentration, *Starch-Stärke*, 2000179, 2021.

[2] Heydari A., Razavi S.M.A., and Farahnaky A., Effect of high pressure-treated wheat starch as a fat replacer on the physical and rheological properties of reduced-fat O/W emulsions, *Innov. Food Sci. Emerg. Technol.*, 102702, 2021.

[3] Kim S., Yang S.-Y., Chun H.H., and Bin Song K., High hydrostatic pressure processing for the preparation of buckwheat and tapioca starch films, *Food Hydrocolloid*, **81**, 71, 2018.

[4] Anvari M. and Joyner H.S., Effect of fish gelatin and gum arabic interactions on concentrated emulsion large amplitude oscillatory shear behavior and tribological properties, *Food Hydrocolloid*, **79**, 518-525, 2018.

[5] Hyun K., Kim S.H., Ahn K.H., and Lee S.J., Large amplitude oscillatory shear as a way to classify the complex fluids, *J. Nonnewton. Fluid Mech.*, **107**, 51-65, 2002.

[6] Heydari A. and Razavi S.M.A., Evaluating high pressure-treated corn and waxy corn starches as novel fat replacers in model low-fat O/W emulsions: a physical and rheological study, *Int. J. Biol. Macromol.*, 2021.

[7] Ewoldt R.H., Hosoi A.E., and McKinley G.H., New measures for characterizing nonlinear viscoelasticity in large amplitude oscillatory shear, *J. Rheol.*, **52**, 1427-1458, 2008.

[8] Joyner H.S., Pernell C.W., and Daubert C.R., Impact of oil-in-water emulsion composition and preparation method on emulsion physical properties and friction behaviors, *Tribol. Lett.*, **56**, 1, 143-160, 2014.

14-15 December 2021, Tehran, Iran
2nd International Conference on Rheology
ICOR 2021
article A-10-295-1

Rheological Properties of Bovine Serum Albumin-Cress Seed Gum Complex Coacervates

Fatemeh Hamedi and Seyed Mohammad Ali Razavi*
Center of Excellence in Native Natural Hydrocolloids of Iran, Ferdowsi University of Mashhad,
Postal Code 9177948974, Mashhad, Iran
*s.razavi@um.ac.ir

Abstract
The intermolecular interactions between the bovine serum albumin (BSA) and cress seed gum (CSG) were investigated by rheological characterization as a function of pH (7.0- 2.0), and concentrations of BSA (0.1, 0.5, and 1 %w/w) and CSG (0.01, 0.05 and 0.1 %w/w). Dominant storage modulus (G') over loss modulus (G") demonstrated the formation of a weak gel-like structure. Moreover, the complex viscosity (η*) of the complex coacervate decreased linearly in a small range of frequency (0.1-10), implying the shear-thinning behavior of the coacervates. These results reflect that CSG-BSA complex coacervate could be a suitable biopolymer carrier for sensitive and bioactive compounds.

Keywords: biopolymer, complex coacervation, rheology, protein, polysaccharide

Introduction

In the food industry, proteins and polysaccharides are the most important structure-forming ingredients (Tolstoguzov, 1991). Both are important in controlling the stability and rheology of food colloids. Interactions between proteins and polysaccharides are the basis for many important biological processes. In this regard, mixed systems can improve or modify their functional behavior (Dickinson & Galazka, 1991). Protein–polysaccharide complexes have better mechanical, thermal, and emulsifying properties than either of the individual biopolymers with an advantage of modulating electrostatic interactions and in consequence, their complex properties (Ye, 2008). Lepidium sativum, known as garden cress, which belongs to the Brassicaceae family, is a fast-growing annual herb native to Iran, Egypt, and West Asia. When soaked in water, cress seeds swell and get covered with transparent colorless mucilage. Cress seeds contain a significant amount of mucilage (6.5-15 wt%) with outstanding functional properties comparable to commercial gums such as xanthan, guar, and locust bean gum.

Experimental/Theoretical

Materials

The biopolymers used in this study were bovine serum albumin (BSA) and cress seed gum (CSG). Sodium azide, hydrochloric acid (HCl), and sodium hydroxide (NaOH) were obtained from Merck (Darmstadt, Germany). Deionized water was used in all experiments.

Complexes Formation

Binary mixtures of CSG-BSA (0.1-0.1, 0.05-0.1, and 0.1-0.5 %w/w) were prepared by adding appropriate proportions of the two biopolymer dispersions then stirred at 300 rpm for about 1h at ambient temperature (25±2 °C). All samples were made in triplicate.

Rheological Tests

Dynamic shear rheological properties of the dispersions of complexes and also the BSA and CSG dispersions separately were determined by a Physica MCR 301 rheometer (Anton Paar, GmbH, Graz, Austria) equipped with a coaxial cylinder system (ME21/T200/Q1; bob diameter of 21 mm and cup diameter of 22.158 mm). BSA, CSG, and CSG-BSA complexes at pH=3.5 were analyzed, while each sample was equilibrated at 25 °C for at least 5 min before testing. Strain sweep tests were performed over a strain range of 0.01-100% in the controlled rate mode and 1 Hz to determine the linear limit of strain (γ_L) and the critical strain value (γ_c). Furthermore, elastic modulus at LVR (G'_{LVR}), loss modulus at LVR ($G"_{LVR}$), the flow point stress or τ_f, and loss tangent (tan δ), were extracted from the strain sweep data. Frequency sweep measurements were carried out at a 0.5% strain (which was within the linear viscoelastic region, LVR) over a frequency range of 0.01-10 Hz (Alghooneh, Razavi, and Behrouzian, 2017). The empirical power-law model was used to describe the frequency dependence of the storage modulus (G′) and loss modulus (G″) (Rao, 1999).

Results and Discussion

Dynamic Rheological Properties

Rheological properties can be related to structural elements in materials and oscillatory shear measurements monitor structures in weak gels and viscoelastic fluids (Behrouzain *et al*., 2020). Because of the Newtonian behavior of the BSA

Table 1. Strain sweep parameters determined for CSG-BSA coacervates at pH 3.5, 25 ºC and f=1 Hz.

CSG-BSA	G'_{LVE}	G''_{LVE}	Tan δ_{LVE}
0.2 – 0	9.28±0.44c	4.23±0.09c	0.46±0.02c
0.1 - 0.1	123.30±3.11a	62.2±1.52a	0.50±0.05b
0.05 - 0.1	25.69±1.37b	13.24±1.25b	0.51±0.03b
0.1 - 0.5	12.23±0.16c	6.58±0.34c	0.54±0.01a

solution (0.5 %w/w), the BSA results were omitted here. The obtained results of the strain sweep are represented in Table 1. Within the linear viscoelastic region, the G'_{LVE} dominated over the G''_{LVE} at all samples, showed a solid-like behavior primarily ($G'_{LVE}>G''_{LVE}$), but after the flow point (crossover point), the samples revealed a liquid-like behavior ($G'_{LVE}<G''_{LVE}$) and the moduli values reduced at strains greater than the critical strain. The characteristic value of loss tangent (tan $\delta_{LVE}= G''_{LVE}/G'_{LVE}$) is applied for evaluation of the viscoelastic behavior, the low value of tan δ (tan δ<1) represents a predominantly elastic behavior, while tan δ>1 shows a predominantly viscous behavior. Also, the Tan δ value lower than 0.1 means that the sample is a true gel while the value between 0.1 and 1 shows the structure is a weak gel (Mandala, Savvas, and Kostaropoulos, 2004). Tanδ_{LVE} values of the CSG dispersion (0.46) and the CSG-BSA mixtures (0.50-0.54) were lower than 1 but higher than 0.1, which shows the presence of predominant elastic structure in the weak biopolymer gel. Beyond the crossover point, the stress is considered a good indicator of yield stress, while the structure ruptured and the flow behavior started (Rafe *et al.*, 2013).

Frequency sweep spectra of the CSG and 0.05CSG-0.1BSA complex coacervate at pH 3.5 are shown in Fig. 1. As is seen, a gel-like network structure with mainly elastic behavior was observed for the samples, as both moduli (G′>G″) were slightly frequency-dependent without any crossover point in the selected frequency range (0.1-10). Besides, the complex viscosity (η*) decreased almost linearly with increasing frequency, which indicates the general shear-thinning behavior. The dispersions of cress seed gum and its fractions with random coil conformation

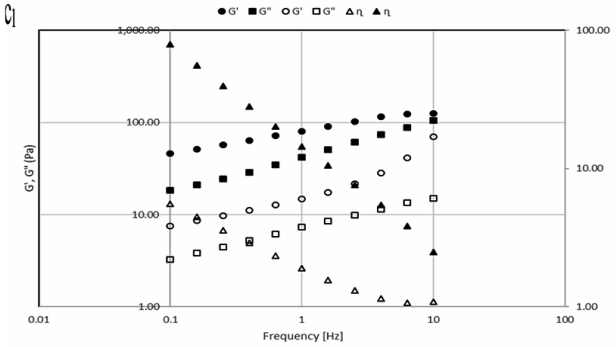

Fig. 1. Frequency sweep of the CSG (open symbols) and 0.05%CSG-0.1%BSA (filled symbols) complex coacervate (pH 3.5) at 0.5% strain amplitude and 25 ºC.

showed solid-like behavior and were classified as weak gels in the concentrate regime, which might impact the behavior of the CSG-BSA complex coacervates. The gel-like behavior of the CSG-BSA coacervates implies that the BSA molecules and the CSG chains form a more strongly entangled network structure.

Conclusion

The present study showed that interactions between BSA and CSG could produce complex coacervates, depending on the protein or polysaccharide content and the pH level. The dominant G' over G'' values in the frequency range of 0.1-10 Hz revealed the highly interconnected gel-like network structure of the complex coacervates, which mainly results from the electrostatic interactions between BSA molecules and CSG chains. Regarding the amorphous structure in the CSG-BSA complex coacervate and also the gel-like network structure, it could be a suitable biopolymer carrier for sensitive and bioactive compounds.

References

[1] Tolstoguzov V.B., *Food Hydrocolloids*, **4**, 6, 429–468, 1991.
[2] Dickinson E., and Galazka V.B., (1991). *Food Hydrocolloids*, **5**(3), 281–296.
[3] Ye, A. (2008). *International Journal of Food Science & Technology*, **43**(3), 406–415.
[4] Karazhiyan H., Razavi S.M.A., and Phillips G.O., Extraction optimization of a hydrocolloid extract from cress seed (Lepidium sativum) using response surface methodology, *Food Hydrocolloid.*, **25**, 5, 915–920, 2011.
[5] Alghooneh A., Razavi S.M.A., and Behrouzian F., Rheological characterization of hydrocolloids interaction: a case study on sage seed gum-xanthan blends, *Food Hydrocolloid.*, **66**, 206–215, 2017.
[6] Behrouzian F., Razavi S.M.A., and Alghooneh A., Evaluation of interactions of biopolymers using dynamic rheological measurements: effect of temperature and blend ratios, *J. Appl. Polym. Sci.*, **134**, 5, 2017.
[7] Rao M.A., Rheology of fluid and semisolid foods—principles and applications aspen, 1999.

14-15 December 2021, Tehran, Iran
2nd International Conference on Rheology
ICOR 2021
article A-10-296-1

Properties of Styrene Butadiene Rubber (SBR) Nanocomposites Filled with Modified Silica

Masoumeh Kalantari, Ali Asghar Katbab*, and Hossein Nazokdast
Department of polymer Engineer, Amirkabir University of Technology, P.O. Box 15875-4413, Tehran, Iran

*katbab@aut.ac.ir

Abstract
The traditional method for directly compounding rubber, silica, and bis(3-triethoxysilylpropyl) tetrasulfide (TESPT) by shear force, which we called it One-Step Method (OSM), results in a modification of mechanism: indicated that the TESPT hydrolyzed firstly to generate the silanol (Si–OH), and the silanol reacted with the hydroxyl groups on the surface of silica, which characterized by FTIR. The properties of modified silica were studied. Furthermore, the SBR nanocomposites filled with modified silica by OSM were prepared and the properties comparisons were carried out. The obtained results exhibited the advantages of TESPT.

Keywords: nanocomposite, surface treatment, nanoparticles, coupling agents, BR

Introduction

Silica is widely used to improve the static and dynamic mechanical properties of rubber, such as wet skid resistance and rolling resistance.

Furthermore, silica is also independent of oil resources and environmentally friendly filler used as a replacement for carbon black [1]. Because of the poor compatibility between silica and the rubber matrix and the severe agglomeration resulting from the surface hydroxyl groups of silica, the applications of silica are limited. So the surface modification must be introduced in application of silica and silane coupling agents, such as bis(3-triethoxysilylpropyl) tetrasulfide (TESPT), are most commonly used to modify the silica [2]. About the method for the surface modification of the silica. The rubber matrix, silica, and TESPT are compounded in a two-roll mill or an internal mixer. TESPT reacts in situ with the surface hydroxyl of the silica by shear force in the compounding process, and then the sulfur of TESPT reacts with the unsaturated bonds of the rubber matrix during the curing process. Sae-oui *et al*. [3] used this method to prepare a silica/TESPT/polychloroprene nanocomposite in a Haake Rheomix mixer. They suggested that TESPT improved the processability of the compound, mechanical properties of the vulcanizates, and dispersion of silica in the vulcanizates. However, it is not clear whether the interaction between silica and TESPT is simple physical absorption or the chemical bonding during the condensation reaction of the hydrolyzed hydroxyl of TESPT and surface hydroxyl of silica. As is well known the deep chemical bonding of silica and silane favors the dispersion of silica and interfacial interaction between the rubber and silica during mixing.

Materials

Styrene butadiene rubber was from Lanxess Chemical Industry Co., Ltd. (Germany). Precipitated silica of Tixosil 383 (median diameter is 13.7 nm, DOP oil absorption is 2.66 mL/g, CTAB specific surface area is 163 m^2/g) was produced by Rhodia France (Qingdao, China).

Bis(3-triethoxysilylpropyl) tetrasulfide (TESPT) was obtained from Nanjing Shuguang Chemical Group Co., Ltd. (China). The other materials are all commercially available.

Preparation of Rubber Nanocomposites

The formulation of modified silica filled SBR compounds is shown in Table 1. First, because silica is a fan of silica, we put it in the oven for 24 h to absorb its moisture. The mixture is first prepared in laboratory rollers at room temperature. In order to reduce the viscosity and to completely wet the reinforcements with the matrix, we masticated the rubber several times and then add the reinforcements with oil.

Table 1. The formulation of modified silica filled SBR compounds.

	N35	N15
SBR1500	100	100
N550	35	15
Silica	15	35
TESPT(si69)	5	5
Naphtenic oil	10	10
ZnO	5	5
Stearic acid	1/5	1/5
Sulfur	1/7	1/7
TMTD	0/015	0/015
MBTS	1	1

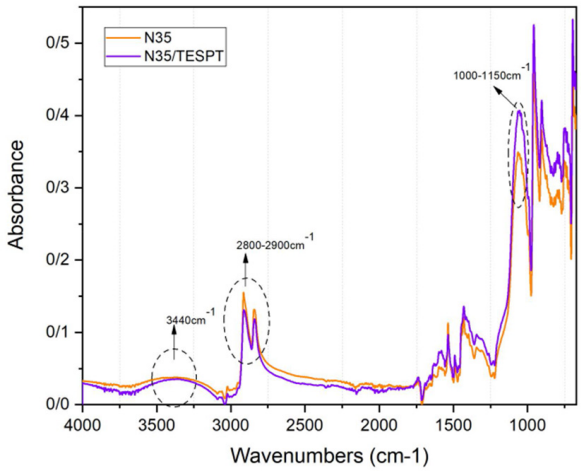

Fig. 1. FT-IR spectra of nanocomposites.

When fully dispersed, add zinc oxide and stearic acid. We should note that if the silane modifying agent was present in the formulation, it should be added directly to the silica in the same second step to perform the in situ correction operation. The optimum cure time (t_{90}) of the compounds was determined by a Disc Vulkameter (Beijing Huanfeng ChemicalMachinery Trial Plant, Beijing, China). The compounds were vulcanized at 160 °C for t_{90} in a standard mold to form the nanocomposites.

Results and Discussion

According to the results obtained in Fig. 1, it can be seen that. The peaks appearing in the wave numbers 3411 and 1100 cm^{-1} were the main characteristics of silica and belongs to OH and Si-O-Si groups, respectively. Poor peak for C-H bond tension around 12811 cm^{-1} Approves surface modification of silica with silane. Simultaneously decreasing the peak intensity of the OH group and increasing the peak intensity related to Si-O-Si tension in the modified sample confirms the surface correction reaction. In other words, the amount of hydroxyl groups on the silica surface decreases after activation by Si69, thus destroying the hydrogen bonds on the silica surface as much as possible [4].

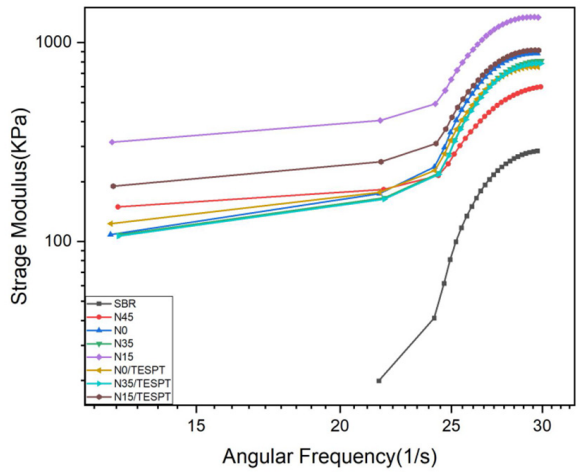

Fig. 2. G' versus frequency for nanocomposites at varying weight percentages.

The frequency dependence of viscoelasticity of storage modulus for the silica/SBR vulcanizates is shown in Fig. 2. The storage modulus of the vulcanizates in the rubbery state can be used to evaluate filler–filler interaction. The low frequency storage modulus was increased for each sample compared to pure styrene butadiene. Storage modules are similar at higher frequencies. Low frequencies are associated with rolling resistance [5]. Rolling resistance is the energy that is lost when the tire is rotated by the constant deformation of the tire. If desired, the material's ability to return more stored energy reduces the tire's rolling resistance.

Conclusion

The primary objective of this research was to explore polymer and nanoparticle interactions that effect rheological properties related to increasing grip while decreasing rolling resistance in tires. The chemical bond formed after grafting reaction between silica and TESPT was generated, which was confirmed by FTIR experiments. and For vulcanizates, the rheological properties associated with rolling resistance were improved. At low frequencies that correspond with rolling resistance, the storage modulus was significantly improved. Additionally, greater improvements of several orders of magnitude was observed at higher weight percentages of silica.

References

[1] Gerspacher M., O'Farrell C.P., Nikiel L., Yang H.H., and Le Méhauté F., High frequency viscoelasticity of carbon black filled compounds, *Rubber Chem. Technol.*, **69**, 5, 786–800, 1996.

[2] Zou H., Wu S., and Shen J., Polymer/silica nanocomposites: preparation, characterization, propertles, and applications, *Chem. Rev.*, **108**, 9, 3893–3957, 2008.

[3] Sae-Oui P., Sirisinha C., Thepsuwan U., and Hatthapanit K., Roles of silane coupling agents on properties of silica-filled polychloroprene, *Eur. Polym. J.*, **42**, 3, 479–486, 2006.

[4] Tian Q., Tang Y., Ding T., Li X., and Zhang Z., Effect of nano-silica surface-capped by bis[3-(triethoxysilyl) propyl] tetrasulfide on the mechanical properties of styrene-butadiene rubber/butadiene rubber nanocomposites, *Compos. Commun.*, **10**, 190–193, 2018.

[5] Lowrie W.G., Rheology of polymer nanocomposites for advanced tire tread compounds, Ohio State University, 2016.

14-15 December 2021, Tehran, Iran
2nd International Conference on Rheology
ICOR 2021
article A-10-298-1

Graphene Oxide Decoration for Enhancement of Rheological Performance of Nanocomposites

Fahimeh Shahsavar and Amir Babaei*
Department of Polymer Engineering, Faculty of Engineering, Golestan University, Postal Code 15759-49138, Gorgan, Iran
*a.babaei@gu.ac.ir

Abstract
The present study explores the effect of the incorporation of graphene oxide-chitosan nanohybrid on the rheological properties of the polycaprolactone matrix. To this end, firstly, covalently functionalized graphene oxide sheets were successfully synthesized by grafting chitosan. Afterward, the effect of the addition of various amounts of GO-CS nanohybrid on the rheological properties of PCL-based nanocomposites was investigated. The result indicated that GO-CS nanohybrid has an interesting dual role based on the amount of addition. It was found that GO-CS is a candidate for enhancing the processability of polymer matrices.

Keywords: graphene oxide, nano-hybrid, rheological properties, nanocomposites

Introduction

Among numerous kinds of degradable polymers, polycaprolactone (PCL) as a biopolymer is currently one of the popular materials with a bright development prospect and is considered as the 'green' eco-friendly polymer [1]. Nonetheless, despite the unique properties of PCL, its limitations in some of the applications [2]. Graphene oxide (GO) nanoparticles can dramatically improve the properties of PCL-based composites. However, the high surface energy and relatively low biocompatibility of GO puts some limits on the wide application, especially in the bio-applications, which potentially can be resolved through functionalization. One of the best candidates for this approach is chitosan (CS). CS, a bio-sourced natural polymer, has generated enormous interest due to several unique physicochemical properties and biological functions [3]. Hence, the formation of organic-inorganic hybrids by a covalent conjugation between GO and CS is an effective approach for improving their valuable properties. In this regard, the performance of PCL/GO and also PCL/GO-CS nanocomposites were investigated in terms of rheological properties. To this aim, firstly GO-CS nanohybrid is synthesized and, subsequently, the effect of the addition of various amounts of GO-CS nanohybrid on the rheological properties of PCL-based nanocomposites was investigated.

Experimental

GO was prepared by modification the Hummers method [4]. GO-CS nanohybrid was synthesized via the covalent linkage between GO sheets CS chains, according to the previously published method in the presence of catalysts [5]. The films were obtained through the solvent-casting method with various concentrations of nanoparticles.

Result and Discussion

The complex viscosity (η*) for PCL-based nanocomposites is shown in Fig. 1. The results indicate that the presence of 0.5 wt% of GO into the polymer matrix, due to network-like structures of GO sheets in the nanocomposite, the complex viscosity increased [6]. On the other hand, in the case of PCL/GO-CS 0.25% and 0.5 wt%, the complex viscosity increased, while in the PCL/GO-CS 1 wt%, the complex viscosity significantly decreased. It can be explained that, after covalently grafted GO with CS, the number of layers

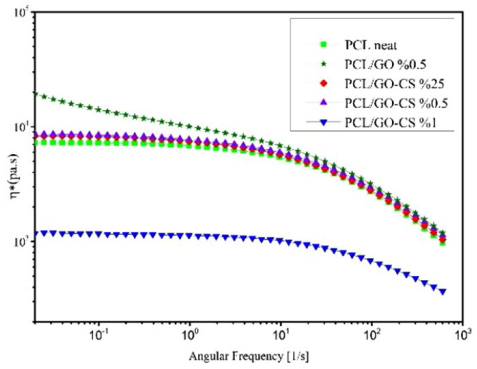

Fig. 1. Complex viscosity of PCL neat and PCL based nanocomposites with frequency sweep.

increased [7,8]. Moreover, CS covered the GO layers, thus, the surface chemistry of nanoparticles changed, resulted in the interaction of PCL chains with the functional groups of GO nanosheets is reduced. It can be interpreted that, the GO-CS nanohybrid exhibited a dual role according to the amount of addition: motion-limiting role and the lubricating role. It can be interpreted that a homogenous distribution in the case of PCL/GO-CS 0.25 and 0.5 wt% can be realized, hence, dual roles of nanohybrid are relatively neutralized. On the contrary, the PCL/GO-CS 1 wt% nanocomposite,

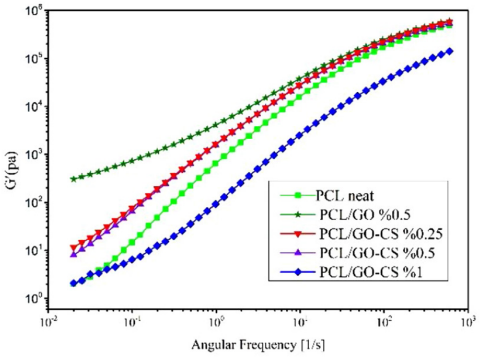

Fig. 2. The storage modulus of PCL neat and PCL based nanocomposites with frequency sweep.

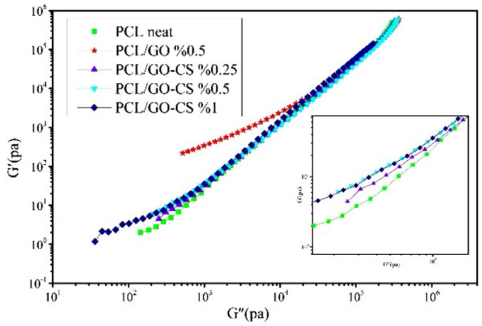

Fig. 3. Han plot of loss modulus (G´) versus storage modulus (G˝) for PCL neat and PCL based nanocomposites.

the quality of distribution changed and the lubrication role is dominated [9,10]. Fig. 2 gives the storage modulus (G´) for neat PCL and PCL-based nanocomposites. The results imply that the addition of GO to the PCL matrix increased the storage modulus, which can be assigned to 'pseudo-solid'-like behavior and a percolating network. It can be deduced that there is an interconnected GO network and strong interfacial interaction between nanoparticle and PCL chains [11]. In the case of PCL/GO-CS 0.25 wt% and PCL/GO-CS 0.5 wt% nanocomposites, the storage modulus increased it can be attributed to the high elasticity. Nevertheless, in the PCL/GO-CS 1 wt% the lubricating role of nanohybrid layers is dominant and, a decrease in the elasticity can be observed. The Han plots for the samples are shown in Fig. 3. The results imply that the slopes of the samples are almost close to each other and fairly lower than that of the pure PCL. One can conclude that PCL/GO-CS nanocomposites follow a nearly straight line, indicating a moderate physical network and, subsequently, induced elasticity linked with the added nanohybrids. Alternatively, the Han plot of PCL/GO 0.5 wt% nanocomposite exhibited a remarkable deviation, signifying the formation of nanolayer networks within the PCL. Weighted relaxation spectra of samples can be clearly detected in Fig. 4. The results imply that the relaxation spectra of the PCL-GO 0.5%, PCL/GO-CS 0.25%, and PCL/GO-CS 0.5 wt%, are shifted toward higher relaxation times, as compared to a neat PCL system. This confirms that mobility is limited by the nanoparticles or the interaction between the nanoparticles and the matrix [12]. It should be mentioned that the lower relaxation time of the PCL/GO-CS 1 wt% chain in comparison to others is due to the lubricating role of nanohybrid, which ultimately facilitates the movement of polymer chains.

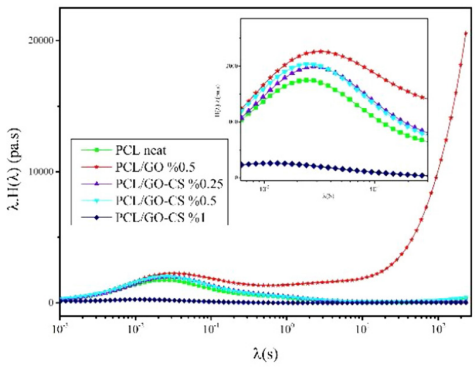

Fig. 4. Weighted relaxation spectrums of the pure PCL and their nano-composites.

As was discussed above, the higher solid-like behavior of nanocomposites is assigned to the formed nanoparticles and nanohybrid network in the nanocomposites. Therefore, GO sheets and GO-CS nanohybrid have a different effects on the nanocomposite microstructure and properties.

Conclusion

This work aimed to investigate the effect of GO-CS nanohybrid as a nanofiller on the rheological properties of the PCL matrix. The GO-CS nanohybrid has a lubricant role and motion limiting the role. It was found that GO-CS is a candidate for enhancing the processability of polymer matrices.

References

[1] Mohamed R.M. and Yusoh K., A review on the recent research of polycaprolactone (PCL), *Adv. Mater. Res.*, **1134**, 249-255, 2016.
[2] Ahmed J., Luciano G., Schizzi I., Arfat Y.A., Maggiore S., and Thai T.L.A., Non-isothermal crystallization behavior, rheological properties and morphology of poly(ε-caprolactone)/graphene oxide nanosheets composite films, *Thermochim. Acta*, **659**, 96-104, 2018.
[3] Hu H., Wang X., Wang J., Liu F., Zhang M., and Xu C., Microwave-assisted covalent modification of graphene nanosheets with chitosan and its electrorheological characteristics, *Appl. Surf. Sci.*, **257**, 7, 2637-2642, 2011.
[4] Hummers Jr W.S. and Offeman R.E., Preparation of graphitic oxide, *J. Am. Chem. Soc.*, **80**, 6, 1339-1339, 1958.
[5] Zuo P.-P., Feng H.-F., Xu Z.-Z., Zhang L.-F., Zhang Y.-L., Xia W., and Zhang W.-Q., Fabrication of biocompatible and mechanically reinforced graphene oxide-chitosan nanocomposite films, *Chem. Cent. J.*, **7**, 1, 39, 2013.
[6] Kim J.Y., Kim D.K., and Kim S.H., Effect of modified carbon nanotube on physical properties of thermotropic liquid crystal polyester nanocomposites, *Eur. Polym. J.*, **45**, 2, 316-324. 2009.
[7] Emadi F., Amini A., Gholami A., and Ghasemi Y., Functionalized graphene oxide with chitosan for protein nanocarriers to protect against enzymatic cleavage and retain collagenase activity, *Sci. Rep.*, **7**, 42258, 2017.
[8] Bao H., Pan Y., Ping Y., Sahoo N.G., Wu T., Li L., Li J., and Gan L.H., Chitosan-functionalized graphene oxide as a nanocarrier for drug and gene delivery, *Small*, **7**, 11, 1569-1578, 2011.
[9] Alzari V., Nuvoli D., Scognamillo S., Piccinini M., Gioffredi E., Malucelli G., Marceddu S., Sechi M., Sanna V., and Mariani A., Graphene-containing thermoresponsive nanocomposite hydrogels of poly(N-isopropylacrylamide) prepared by frontal polymerization, *J. Mater. Chem.*, **21**, 24, 8727-8733, 2011.
[10] Kinoshita H., Nishina Y., Alias A.A., and Fujii M., Tribological properties of monolayer graphene oxide sheets as water-based lubricant additives, *Carbon*, **66**, 720-723, 2014.
[11] Wu D., Wu L., Sun Y., and Zhang M., Rheological properties and crystallization behavior of multi-walled carbon nanotube/poly (ε-caprolactone) composites, *J. Polym. Sci. Part B: Polym. Phys.*, **45**, 23, 3137-3147, 2007.
[12] Sodeifian G., Nikooamal H.R., and Yousefi A.A., Molecular dynamics study of epoxy/clay nanocomposites: rheology and molecular confinement, *J. Polym. Res.*, **19**, 6, 9897, 2012.

14-15 December 2021, Tehran, Iran
2nd International Conference on Rheology
ICOR 2021
article A-10-300-1

Magnetically Superhydrophobic Sawdust Powder for Removal of Oil from Water Surface

Fateme Rezaei and Shadi Hassanajili*
School of Chemical and Petroleum Engineering, Shiraz University, Postal Code 84334-71964, Shiraz, Iran

*ajili@shirazu.ac.ir

Abstract
Because of frequent oil spill pollution and resulting immeasurable harm to the environment and human health, it has attracted a wide concern in recent years. Magnetic bio-sorbents are effective materials for collecting and removing oil from the surface of water. In this work magnetically superhydrophobic green oil sorbent was fabricated through precipitating of $CoFe_2O_4$ magnetic nanoparticles on the surface of sawdust and subsequently chemically modification with low surface energy fluorosiloxane. This prepared sorbent shows a great superhydrophobicity (water contact angle of 156°), and acceptable oil sorption capacity (4.2 g/g). Scanning electron microscope (SEM) and Fourrier transform infrared (FT-IR) were employed to characterize this composite sorbent. This magnetic bio-sorbent can be dispersed in oil as carrier fluid and magnetize the oil which could effectively remove the oil slicks under magnetic field. In this regard rheological properties of this fluid have been investigated. The results show that in the presence of magnetic field, increasing magnetic strength, viscosity increased and MR fluid exhibits solid-like behavior.

Keywords: oil-water separation, $CoFe_2O_4$ magnetic nanoparticles, magnetorheological, superhydrophobicity

Introduction

Due to the importance of oil spill pollutions and their serious problems, more attention has been paid to effective and efficient ways to remove the oil slicks. In some cases, preference is magnetic bio sorbents because of eco-friendly and low-cost properties. Also, magnetic separation is another advantage of magnetic bio-sorbent [1]. Inherently, bio-sorbents are low hydrophobicity materials, so different kind of modification can be applied in order to enhance this feature. Modification of magnetic bio sorbent with low surface chemicals improves their adsorptive capabilities [2]. In the present work, environmentally-friendly, economical and recyclable bio material was employed in order to fabricate versatile magnetic superhydrophobic $CoFe_2O_4$/sawdust oil sorbent.

Experimental

The reduced size sawdust was washed with abundant water and ethanol and dried in an oven for 24 h. First, 1 g pretreated sawdust was added to $CoCl_2.4H_2O$ and $FeCl_2.6H_2O$ solution at 80 °C for 1 h. Then, NaOH as the precipitation agent and KNO_3 added to the mixture until pH 12 and stirred for 3 h at 80 °C. The black precipitate was collected by a magnet and washed with DI water and dried. To modify $CoFe_2O_4$/sawdust composite, it was immersed in FAS, ammonia and ethanol solution under magnet stirring for 12 h at ambient temperature. After passing through filter paper and washing with distilled water, it was dried at 60 °C for 6 h, superhydrophobic sawdust powder was successfully obtained. The surface morphology and chemical structure of magnetic bio-sorbent was examined by scanning electron microscopy (SEM) and Fourier transform infrared (FTIR), respectively. To analyze the MR behavior of the fabricated magnetic bio-sorbent with the weight percent of 10% was dispersed in N-500 oil as carrier fluid. Rotation rheometer equipped with a magnetic field generator was employed to determine the MR properties.

Results and Discussion

SEM images of raw and modified sawdust are shown in Fig. 1. It is obvious that the surface of pristine sawdust is smooth and clear. After chemical modification a layer of aggregate magnetic particles precipitated on the surface of the sawdust. This modification results a rough morphology on the surface. Finally, superhydrophobic surface was obtained by roughening and modifying with low surface energy fluorosiloxane [3].

In order to show the successful modification of sawdust surface with $CoFe_2O_4$/FAS the FTIR spectra of raw and modified sawdust are presented in Fig. 2. By comparing, adsorption peaks were observed at 559 and 467 cm^{-1} in modified spectra attributed to Fe-O bond which indicate favored coating of $CoFe_2O_4$. The strong peaks at 935 and 848 cm^{-1} conform the existence of CF_2 and CF_3 in modified sawdust. Also, the adsorption peak at 1219 cm^{-1} indicated C-F stretching bond.

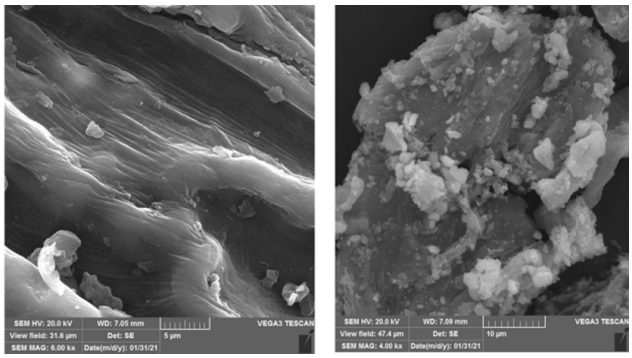

Fig. 1. Scanning electron microscopy image of raw sawdust powder and modified sawdust powder.

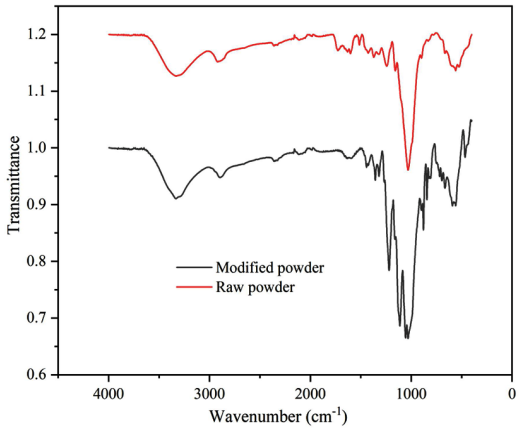

Fig. 2. FT-IR spectra of the raw sawdust and modified powder.

The variation of viscosity versus shear rate for the prepared MR fluids under different magnetic fields is shown in Fig. 3. According to the results at low shear rates the MR fluid shows a non-Newtonian behavior. Under magnetic field, MR fluid exhibited Bingham-like behavior. By increasing magnetic strength, viscosity increased which is due to the formation of strong chain-like structure of magnetic particles along the direction of magnetic field [4]. The orientation of MR fluid under magnetic field results the oil movement along the direction of field. This property causes to better oil sorption of the prepared magnetic sawdust.

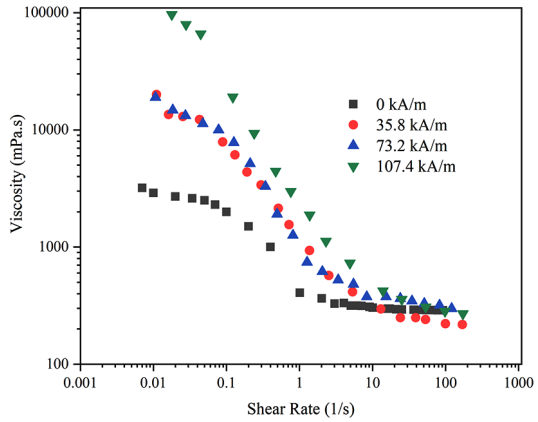

Fig. 3. The MR behavior of modified bio-sorbent at different magnetic fields.

Conclusion

In the present study magnetically superhydrophobic green oil sorbent was fabricated through precipitating of $CoFe_2O_4$ magnetic nanoparticles on the surface of sawdust and subsequent chemically modification with low surface energy fluorosiloxane. Magnetic nanoparticles and subsequent modification result a rough morphology and superhydrophobic magnetic bio-sorbent. This magnetic bio-sorbent can be dispersed in oil as carrier fluid and magnetize the oil which could effectively remove the oil slicks under magnetic field.

References

[1] Soares S.F., Fernandes T., Trindade T., and Daniel-da-Silva A.L., Recent advances on magnetic biosorbents and their applications for water treatment, *Env. Chem. Lett.*, **18**, 151-164, 2020.

[2] Fan S., Pei S., Shen T., Xu G., Li Y., and Fan W., Fabrication of superhydrophobic magnetic sawdust as effective and recyclable oil sorbents, *Materials*, **12**, 3432, 2019.

[3] Ma M. and Hill R.M., Superhydrophobic surfaces, *Curr. Opin. Colloid Interface Sci.*, **11**, 193-202, 2006.

[4] Kamgar A., Hassanajili S., and Unbehaun H., Oil spill remediation from water surface using induction of magnetorheological behavior in oil by functionalized sawdust, *Chem. Eng. Res. Des.*, **160**, 119-128, 2020.

14-15 December 2021, Tehran, Iran
2nd International Conference on Rheology
ICOR 2021
article A-10-301-1

Rheological Study of Injectable Biomimetic Hydrogel Based on Carboxymethyl Chitosan-*g*-Poly(N-isopropylacryamide)

Sina Ahmadi[1], Shadab Bagheri-Khoulenjani[1*], Sarah Rajabi[2], Sverre Arne Sande[3], and Bo Nyström[4]
1. Polymer and Color Engineering Department, Amirkabir University of Technology, Tehran, Iran
2. Department of Cell Engineering, Cell Science Research Center, Royan Institute for Stem Cell Biology and Technology, ACECR, P.O. Box 16635-148, Tehran, Iran
3. School of Pharmacy, Department of Pharmaceutics, University of Oslo, P.O. Box 1068, Blindern, N-0316 Oslo, Norway
4. Department of Chemistry, University of Oslo, P.O. Box 1033, Blindern, N-0315 Oslo, Norway

*s.bagheri@aut.ac.ir

Abstract
Biopolymers of various natures are produced by integrated cells and function to sustain human life. This study aims to generate temperature-responsive injectable hydrogel that assesses the extra cellular matrix (ECM) mimetic and self-healing characterization for cardiac tissue engineering. The carboxymethylchitosan-*g*-poly(N-isopropylacryamide) (CMC-*g*-PNIPAAm) is synthesized by reaction of 1-ethyl-3-(3-dimethylamino-propyl-carbodiimide) (NHS) group from PNIPAAm and NH_2 group of CMC. The proton nuclear magnetic resonance (^{1}H NMR) spectroscopy was utilized for the characterization of synthesized graft copolymer and the result indicates that the grafting-to reaction was successful. The almost complete and reversible self-healing behavior without the need for any external stimuli or cross-linker was scrutinized through a rheological recovery test. With these outstanding characteristics, the synthesized hydrogel in this study could open a new horizon within the injection cell based therapy for cardiac tissue engineering.

Keywords: chitosan, poly(*N*-isopropylacrylamide), injectable hydrogel, self healing, rheology

Introduction

Due to the pivotal role of cardiac tissue in human body health, and the significant obstacles of organ transplantation, which is a major socioeconomic burden, the need for opening a new horizon within the introduction of the novel therapeutic for enhancing the regeneration functions of injured cardiac tissue is tremendous abundant [1]. Chitosan, the highly abundant cationic polysaccharide and biocompatible, is among one of the most promising biopolymers due to its exquisite efficiencies in regenerative medicine. However, in aqueous media chitosan suffers from low solubility at physiological pH. Hence, hydrophilic functionalization of the surface characteristics of chitosan with suitable functional groups, such as carboxymethyl in an adjustable manner is necessary to enhance its solubility and functionality at physiological pH [2]. Direct injection of cells to the infarcted region deals with numerous limitations, the most important of which is the high mortality rate of injected cells after injection. Thus, injectable hydrogels offer a three-dimensional (3D) microenvironment platform to enhance the regeneration functionality of injected cells. The injectable hydrogel for cardiac tissue repair should have the in-situ gelation properties after injection [1]. Temperature-responsive injectable hydrogels are specially designed for in situ gelation. Poly(N-isopropyl acrylamide) (PNIPAAm), because of its physiological proximal to the lower critical solution temperature (LCST=32 °C) is one of the most studied biocompatible polymers. At temperatures far below the LCST, PNIPAAm is stabilized by hydrogen bonds and exhibits no tendency to self-associate, but at higher temperatures the isopropyl groups give PNIPAAm a hydrophobic character and self-assembling occurs with increasing temperature [3]. In this study, we aimed to synthesize the CMC-*g*-PNIPAm and investigate its self-healing behavior through rheology analysis. For the grafted polymer (CMC-*g*-PNIPAAm), the hydrophobic interactions from PNIPAAm groups provide the connectivity in the gel-network at elevated temperatures, while the CMC block is responsible for the swelling. To obtain a hydrogel it is necessary to be a balance between the connecting and swelling forces.

Experimental

Carboxymethyl chitosan (CMC) was synthesized through the reaction of chitosan with chloroacetic acid. The graft of temperature-responsive PNIPAAm-NHS (48.8 mg) side chains on the CMC (156.2 mg) backbone was accomplished using the NHS and NH_2 reaction at pH 8 in buffer solution. The reaction was performed for 2 h at 4 °C. The solution was dialyzed against DI water (MWCO 14,000 Da) for three days. The final product CMC-*g*-PNIPAAm was obtained by freeze-drying. For the rheology measurements, CMC-*g*-PNIPAAm aqueous solutions at the concentration of 3% were prepared.

Result and Discussion

The 1HNMR spectra were recorded on samples dissolved in deuterium oxide and this technique was utilized to

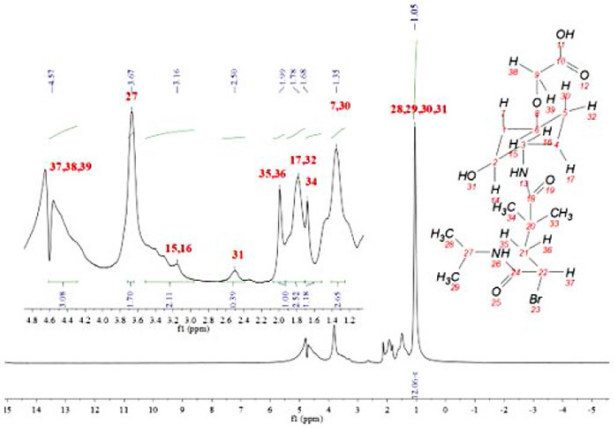

Fig. 1. [1]HNMR spectrum of CMC-g-PNIPAAm.

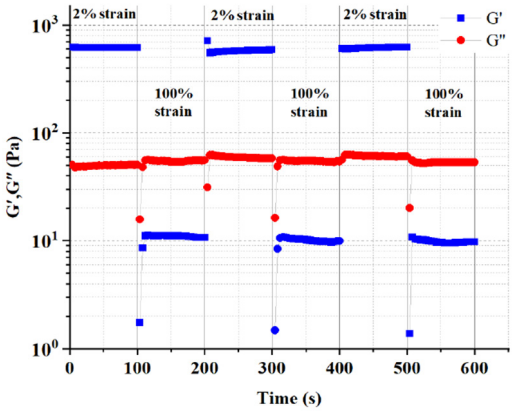

Fig. 3. Time sweep with step strain from 2 to 100% at a fixed angular frequency (10 s^{-1}) and 37 °C.

characterize the synthesized graft copolymer. The results of peak analysis and peak assignment to the corresponding protons are shown in Fig. 1. As observed, almost all expected peaks were detected. In the graft copolymer spectrum, the peak observed at 4.57 ppm corresponds to the carboxymethyl group of CMC. On the other hand, protons of the methyl group of grafted side chains were observed at 1.68 ppm. Additionally, the peak at 3.67 ppm is related to the carbon proton attached to the amide group of the PNIPAAm side chain. Other peaks of the PNIPAAm side chain were observed at 1.05 and 1.99 ppm. Although they overlapped with CMC's protons, the integral of observed peaks indicate that the grafting of the PNIPAAm side chain to CMC backbone was successful. To gain insight into the influence of grafted side chains on the gel characteristics, such as mechanical response and self-healing behavior, rheological features of the designed system in the course of gelation beyond the LCST of the PNIPAAm side chain and oscillatory shear responsiveness were investigated. Firstly, strain sweep analysis was conducted to quantitatively investigate the linear and non-linear viscoelastic region of the prepared hydrogel upon external strains (Fig. 2a). The pronounced drop of the storage modulus (G′) with increasing strain amplitude suggests disruption of the network and a gradual transition to a viscous response. The intersection of G′ and the loss (G″) modulus at a strain of 17.3% indicates that beyond this point the viscous response (liquid-like) dominates over the elastic (solid-like) response. The gel

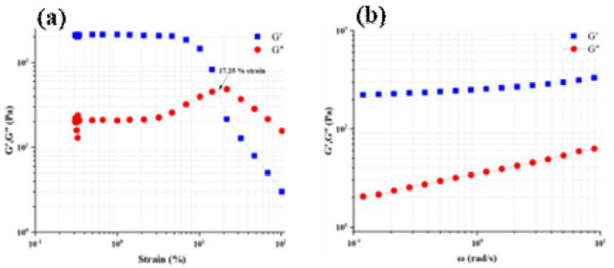

Fig. 2. (a) Strain amplitude sweep (γ=1%–100%) at a fixed angular frequency (1 s^{-1}) and (b) frequency sweep of the hydrogel at 37 °C.

behavior and the viscoelastic properties of the system was also studied through frequency sweep experiments at 37 °C and at a constant strain amplitude of 1% (Fig. 2b). As it can be seen easily, the G′ observed higher than G″ at all frequencies. This behavior indicates that the designed system is at a gel state at 37 °C. Additionally, to assess the injectability of the hydrogel and self-healing characteristic, based on strain sweep analysis, the rheological recovery test was performed at 2% (linear regime) and 100% (nonlinear regime) at a constant temperature of 37 °C. As it can be seen in Fig. 3, as the shear strain stepped from 2% to 100% and maintained for 100 s, G′ dropped from 632 Pa to 11 Pa when subjected to the 100% strain while achieved almost complete recovery within a second upon the strain returning to 2%. This fully reversible and recoverable behavior as observed at three cycles, indicating that the formulated hydrogel has self-healing characteristics.

Conclusion

In summary, we developed a chitosan-based self-healing CMC-*g*-PNIPAAm hydrogel. The NHS and NH_2 groups coexist on CMC and PNIPAAm, enabling a reaction between two functional groups at pH of 8. The excellent injectability characteristic and high healing efficiency of CMC-*g*-PNIPAAm hydrogel indicating that it could be potentially used as a cell-laden injectable hydrogel.

References

[1] Abandansari H.S., Ghanian M.H., Varzideh F., Mahmoudi E., Rajabi S., Taheri P., Nabid M.R., and Baharvand H., *Biomaterials*, **170**, 12-25, 2018.
[2] Bagheri-Khoulenjani S., Taghizadeh S.M., Mirzadeh H., *Carbohyd. Polym.*, **78**, 4, 773-778, 2009.
[3] Dashtimoghadam E., Salimi-Kenari H., Forooqi Motlaq V., Hasani-Sadrabadi M.M., Mirzadeh H., Zhu K., Knudsen K.D., and Nyström B., *Eur. Polym. J.*, **97**, 158-168, 2017.

14-15 December 2021, Tehran, Iran
2nd International Conference on Rheology
ICOR 2021
article A-10-302-1

On the Use of MHD Mechanism for Pumping Viscoplastic Fluids in Microfluidic Systems: A Numerical Study

Babak Jalali*, Saman Kosar, Mohammad Pourjafar, and Kayvan Sadeghy
School of Mechanical Engineering, College of Engineering, University of Tehran, P.O. Box 14155-6619, Tehran, Iran
*babak.jalali@ut.ac.ir

Abstract
In the present work, the effects of a fluid's yield stress is numerically investigated on the performance of MHD micro-pumps. It is assumed that the test fluid obeys the bi-viscous model. For ease of analysis, a two-dimensional planar geometry was used in this study. The geometry comprises two parallel plates of infinite span equipped with two opposing electrodes of finite length while the other parts of the channel are electrically non-conductive. Having assumed that the isothermal flow generated by the Lorentz force is occurring under creeping condition, the equations governing the two-dimensional flow was solved numerically using the finite-volume method. Based on the obtained numerical results, it is predicted that wall jets are dramatically suppressed for sufficiently large Bingham numbers. The maximum wall shear stress, however, is predicted to increase the larger the Bingham number and this can have some consequences when pumping physiological fluids.

Keywords: MHD, bingham-papanastasiou model, microfluidics, micropump, numerical modeling

Introduction

Transporting physiological fluids in microfluidic systems is not an easy task. A major problem is the small length scales involved as it normally means that the use of centrifugal systems have to be ruled out. A variety of novel techniques have been developed over the years for the transport of physiological fluids with MHD mechanism being one of the most attractive ones. These pumps feature no moving parts and enjoy having a simple and a robust design. The device relies on the interaction between an electrical current and a transverse magnetic field, which pump an electrolyte through the rise of Lorentz force [1-7]. A key feature of MHD mechanism is formation of unwanted wall jets Formation of such jets should be avoided because they make velocity profiles M-shaped and the inflection points of such profiles make them vulnerable to instability. Wall jets can also damage bio-particles suspended in fluid such as blood. In the present work, it will be shown that for by inducing yield stress in a fluid, formation of such wall jets can be suppressed.

Mathematical Development

Fig. 1 shows the flow geometry. It constitutes two parallel plates of infinite width a gap distance of 2 h. Thanks to symmetry, only the upper half of the channel is used as the computational domain [8].

For purely-viscous non-Newtonian fluids, the equations governing the flow are continuity equation and the variable-viscosity variation of the Navier-Stokes equations [8]:

$$\frac{\partial u}{\partial x}+\frac{\partial v}{\partial y}=0. \tag{1}$$

$$\rho\frac{Du}{Dt}=-\frac{\partial p}{\partial x}+\frac{\partial T_{xx}}{\partial x}+\frac{\partial T_{yx}}{\partial x}+f_x \tag{2}$$

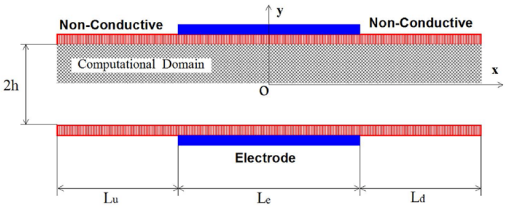

Fig. 1. Schematic showing the flow geometry.

$$\rho\frac{Dv}{Dt}=-\frac{\partial p}{\partial y}+\frac{\partial T_{xy}}{\partial x}+\frac{\partial T_{yy}}{\partial x}+f_y \tag{3}$$

Where, the electromagnetic source terms are [8]:

$$f_x=\sigma\left(-uB_0^{\,2}-\frac{\partial\varphi}{\partial y}B_0\right);\quad f_y=\sigma\left(-vB_0^{\,2}+\frac{\partial\varphi}{\partial x}B_0\right) \tag{4}$$

Where, σ is the electric conductivity of the fluid, φ is the electric potential, and B_0 is the magnetic field strength. The stress tensor for the viscoplastic fluid is modelled using the Bingham-Papanastasiou model:

$$T_{ij}=\left(\eta_\infty+\frac{\tau_y}{|\dot\gamma|}\left(1-e^{-m|\dot\gamma|}\right)\right)2d_{ij} \tag{5}$$

Where, τ_y is the material's yield stress and "m" is the regularizing parameter, which should be sufficiently large (say, 10^3). In this rheological model, η is called the plastic viscosity. Based on this model, at a given shear rate, fluid's apparent viscosity is increased the larger the yield stress

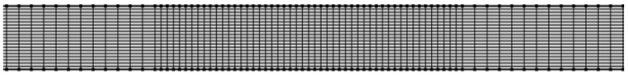

Fig 2. Typical mesh used for the simulations.

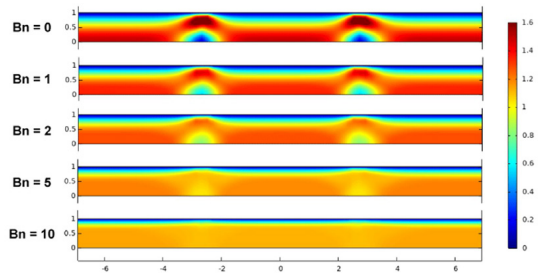

Fig. 3. Effect of Bingham number on the velocity contour.

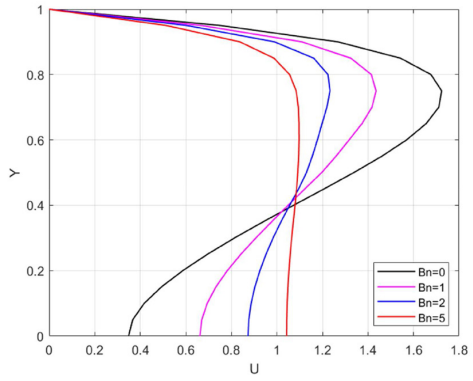

Fig. 4. Effect of Bingham number on the velocity profile at inlet section of the electrodes.

to numerically solve these equations, we have relied on COMSOL which is a finite-element package. Fig. 2 shows the structured mesh with clustering near the electrodes.

Results and Discussion

We have been able to obtain converged mesh-independent results under steady conditions using 20,000 elements. Fig. 3 shows the effect of Bingham number on the axial velocity contour. In this figure, the electrodes are extended from to The strong effect of Bingham number on the flow kinematics is evident in this figure. The effect is predicted to be stronger at the two extremes of the electrode. This notion can better be seen in Fig. 4 which shows the effect of Bingham number on the velocity profile at the inlet section of the electrodes. This figure clearly shows that the wall jet is weakened the larger the Bingham number. For Bn=5, the wall jet is seen to have been completely eliminated by becoming U-shaped.

Fig. 5 shows that shear stress is increased in the whole

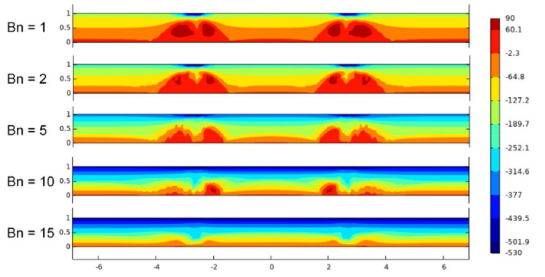

Fig. 5. Effect of Bingham number on the shear stress field.

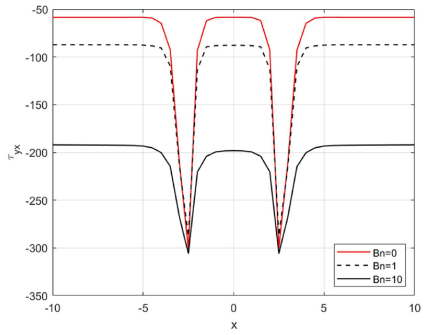

Fig. 6. Effect of Bingham number on the velocity contour.

domain the larger the Bn number. At Bn=10, Fig. 6 shows that the wall shear stress is increased by four times. The effect can be attributed to a rise in the apparent viscosity when Bn is increased although a change in the velocity gradient contribute to the effect.

Conclusion

From the results presented in this work, it can be concluded that a fluid's yield stress can indeed suppress formation of wall jets in MHD flows. Our numerical results suggest that at sufficiently large Bingham numbers the velocity profiles become U-shaped instead of M-shaped suggesting that a fluid's yield stress has a stabilizing effect on MHD flow. But, there is a four-fold increase in the maximum shear stress and this can be troublesome for physiological fluids carrying bi-particles such as RBC. For fluids which are not viscoplastic, the results obtained in this work suggests that it would be a good idea to make them viscoplastic (say, through the use of appropriate additives) if the higher shear stress incurred is none of our concern.

References

[1] Woias P., Micropumps-past, progress and future prospects, *Sens. Actuator. B*, **105**, 28–38, 2005.
[2] Abhari F., Jaafar H., and Yunus N.A., A comprehensive study of micropumps technologies, *Int. J. Electrochem. Sci.*, **7**, 9765–9780, 2012.
[3] Jang J. and Lee S.S., Theoretical and experimental study of MHD (magnetohydrodynamic) micropump, *Sens. Actuators*, **80**, 84–89, 2000.
[4] Qian S. and Bau H.H., Magneto-hydrodynamics based microfluidics, *Mech. Res. Commun.*, **36**, 1, 10–21, 2009.
[5] Ramos J.I. and Winowich N.S., Finite difference and finite element methods for mhd channel flows, *Int. J. Numer. Method. Fluid.*, **11**(6) 907-934, 1990.
[6] Papanastasiou T.C., Flows of materials with yield, *J. Rheol.*, **31**, 385-404, 1987.
[7] Moghaddam S., MHD micropumping of viscoelastic fluids: an analytical solution, *Korea-Aust. Rheol. J.*, **33**(2), 93-104, 2021.
[8] Pourhjafar M., Malmir F., Bazargan S., and Sadeghy k., Magnetohydrodynamic flow of Bingham fluids in a plane channel: a theoretical study, *J. Non-Newton. Fluid Mech.*, **264**, 1–18, 2019.

14-15 December 2021, Tehran, Iran
2nd International Conference on Rheology
ICOR 2021
article A-10-303-1

Effect of Fat Content, Iodine Value and Solid Fat Content (SFC) on the Rheological Properties of Margarine

Mohammad Fallahasgari, Darya Abolghasem, and Kooshan Nayebzadeh*
Department of Food Science and Technology, Faculty of Nutrition Science, Food Science and Technology/National Nutrition and Food Technology Research Institute, Shahid Beheshti University of Medical Sciences, Postal Code 1983969411, Tehran, Iran
*knayebz@sbmu.ac.ir

Abstract
The rheological properties of two commercial margarines with different fat content and iodine value was evaluated. Margarine A with lower iodine value showed higher solid fat content (SFC). Higher SFC resulted to higher storage (G'), loss (G") modulus and viscosity in this sample. Although margarine B had more fat content compared with margarine A, higher level of unsaturated fats (higher iodine value) in this sampled caused lower rheological properties.

Keywords: margarine, rheology, storage modulus, loss modulus, viscosity

Introduction

Margarine invented by a French chemist named Me`ge Mourie`s in 1896 as a low-cost alternative to butter. This product is a water in oil (w/o) emulsion which aqueous phase keep separated by fat crystals. The fat phase consists of a blend of triglycerides, emulsifiers and antioxidants. β-carotene usually added to the formulation as yellow color agent. The aqueous phase involves water, salt, skim milk powder, flavor and preservatives [1,2].

Rheological properties are one of the most important characteristics to study margarine's desirability [3]. Any changes in margarine's formulation could be investigation by rheological measurements. Fat content and saturation level, effect the rheological properties of the margarine. Margarine from the rheological point of view is a non-Newtonian pseudoplastic material with apparent yield stress. This product has also been reported to show thixotropic behavior, where apparent viscosity decreases with time under constant shear [4].

The aim of this study was to compare the rheological properties of two commercial margarines and evaluate how these properties are affected by fat content, iodine value and Solid fat content (SFC) and.

Experimental

Materials and Methods

Materials

Two commercial margarines with 60% (marked by A) and 70% (marked by B) fat content purchased from a local supermarket (Iran). The iodine value of the margarine A and B labeled as 75 and 90 g I/100 g. All chemicals and reagents used analytical grade.

Extraction of Margarine Fats

The fat phase of the commercial margarines separated as per Kim *et al*. [5]. Each margarine fat heated at 80 °C for melting the fat phase was. for separation the fat from the water phase, the supernatant fat transferred to a separatory funnel and washed five times with warm water. The fats filtered through an anhydrous sodium sulfate layer with a Whatman No. 1 filter paper under vacuum, to remove remaining moisture. The separated fats stored at 4 °C before further analysis.

SFC Determination

A Bruker wideline NMR (Minispec-mq20, Germany) used for measurment of samples SFC values. To remove the fat crystals from the mixture, each sample heated at 80 and 60 °C for 15 and 10 min, then the samples kept for 60 min at 0 °C and finally at each measuring temperature for 30 min before analysis. The SFC evaluated at 10, 20, 30, and 35 °C.

Rheological Properties

A physical MCR 301 Rheometer (Anton Paar, GmbH, Ostfilden, Germany) used for rheological tests. Temperature controlled at 25 °C. A serrated parallel plate geometry (PP35) with the geometry gap of 1 mm employed. Strain sweep test carried out at 0.01-600% strain and a constant frequency of 1 Hz. The storage modulus (G') and loss modulus (G") obtained during this test. The apparent viscosity of samples evaluated at a 0.1–600 1/s shear rate.

Results and Discussion

SFC

SFC associated to several physical and textural properties of margarine [6]. The SFC of margarine A and B as a function of temperature shown in Fig. 1. Margarine A shown greater SFC than margarine B at all temperatures. This is due to the fact that triglycerides in sample A are more saturated and thus more solid. The iodine value used to determine the degree of saturation in fats and oils. The lower the iodine value, the more saturated the fatty acids present in a fat are. It mentioned earlier that margarine A had lower iodine value than margarine B.

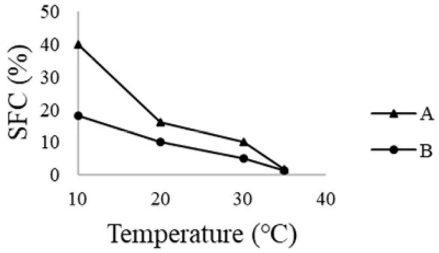

Fig. 1. Solid fat contents (SFC) of margarine A and B.

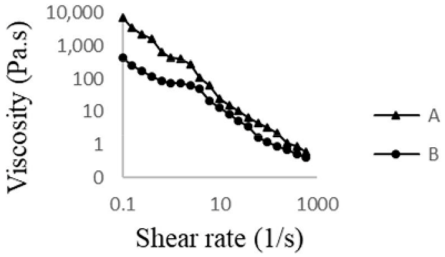

Fig. 3. Apparent viscosity of margarine A and B.

Rheological Properties

Strain Sweep

Fig. 2 shown strain sweep parameters of margarine A and B. In both samples, G' was higher than G", indicating the solid-like behavior of margarines. Changes in G' controlled by SFC and the microstructure of fats [7]. In other words, G' linked to the internal power of the aggregated systems. The G' in margarine A was higher than margarine B. It discussed in SFC section that margarine A had more solid fat. In fact, higher SFC value in this sample cause stronger structure and thus higher G'.

Dadali *et al*. reported that increase of fat content in margarine cause an increase in G' [8]. The results of this study was against their findings. Higher fat content in margarine B (70%) could not cause higher G' values compared with margarine A (60%). It seems that higher amount of solid fats in margarine A caused higher G', although it's lower fat content.

Linear viscoelastic region (LVR) is an essential rheological property which for sample structure [9]. Margarine B shown greater LVR than margarine A. So, margarine A with more solid fat has more brittle in high strains and has more narrow LVR.

Apparent Viscosity

The apparent viscosity of samples shown in Fig. 3. The viscosity declined with increase in shear rate in both samples. This known as pseudoplastic behavior which has reported in margarines [10]. Margarine A showed greater viscosity compared with margarine B in all shear rates. This is due to the higher solid fats in this sample. It seems that the interactions between microstructural parts in margarine, leads to increase solid fat in the formulation and viscosity. Mousazadeh et al. shown that increment in cocoa butter as a saturated fat in low fat spreads, leads to reduce viscosity. So, addition of pistachio oil to the formulation of the spreads, leads to reduction in viscosity. This was due to the fact that pistachio oil is a source of unsaturated fats with low solid fats [4].

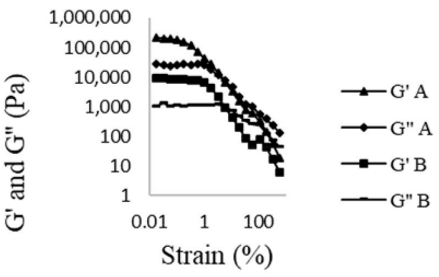

Fig. 2. Strain sweep parameters of margarine A and B.

References

[1] O'Brien R.D., Fats and oils: formulating and processing for applications, 3rd Ed., Boca Raton: CRC, 2009, pp 680.

[2] Liang Z., Li L., Xu Z., and Li B., Influence of lipid composition, solid fat content and temperature on hardness of margarines, 3rd Ed., *International Conference on Nutrition and Food Sciences*, 2014.

[3] O' Dwyer S.P., O' Beirne D., Ní Eidhin D., Hennessy A.A., and O' Kennedy B.T., Formation, rheology and susceptibility to lipid oxidation of multiple emulsions (O/W/O) in table spreads containing omega-3 rich oils, *LWT- Food Sci. Technol.*, **51**, 2, 484-491, 2013.

[4] Mousazadeh M., Mousavi S.M., Emam-Djomeh Z., HadiNezhad M., and Rahmati N., Stability and dynamic rheological characterization of spread developed based on pistachio oil, *Int. J. Biol. Macromol.*, **56**, 133-139, 2013.

[5] Kim B.H., Lumor S.E., and Akoh C.C., Trans-free margarines prepared with canola oil/palm stearin/palm kernel oil-based structured lipids, *J. Agr. Food Chem.*, **56**, 17, 8195-8205, 2008.

[6] Podchong P., Sonwai S., and Rousseau D., Margarines produced from rice bran oil and fractionated palm stearin and their characteristics during storage, *J. Am. Oil Chemists' Soc.*, **95**, 4, 433-445, 2018.

[7] Saadi S., Ariffin A.A., Ghazali H.M., Abdulkarim M.S., Boo H.C., and Miskandar M.S., Crystallisation regime of w/o emulsion [eg multipurpose margarine] models during storage, *Food Chem.*, **133**, 4, 1485-1493, 2012.

[8] Dadalı C. and Elmacı Y., Influence of fat and emulsifier content on volatile release of butter aroma used in water phase and physical attributes of model margarines, *Eur. J. Lipid Sci. Technol.*, **122**, 7, 2000036, 2020.

[9] Cheong L.Z., Tan C.P., Long K., Yusoff M., and Lai O.M., Physicochemical, textural and viscoelastic properties of palm diacylglycerol bakery margarine during storage, *J. Am. Oil Chem. Soc.*, **86**, 8, 723-731, 2009.

[10] Sellami M., Ghamgui H., Frikha F., Gargouri Y., and Miled N., Enzymatic transesterification of palm stearin and olein blends to produce zero-trans margarine fat, *BMC Biotechnol.*, **12**, 1, 1-8, 2012.

14-15 December 2021, Tehran, Iran
2nd International Conference on Rheology
ICOR 2021
article A-10-304-1

Shear Thickening Behavior and Hysteresis in Non-Brownian Suspension

Mohamadreza Mahmoudian[1*], Fatemeh Goharpey[1], Zahra Daneshfar[2], and Morteza Behzadnasab[3]
1. Department of Polymer Engineering, Amirkabir University of Technology, P.O. Box 15875-4413, Tehran, Iran
2. Department of Chemical and Polymer Engineering, Yazd University, Postal Code 8915818411, Yazd, Iran
3. Iran Polymer and Petrochemical Institute, Postal Code 13115-14977, Tehran, Iran
*m.mahmoudian@aut.ac.ir

Abstract
In this work, the flow of non-Brownian suspension of methacrylate sphere dispersed into Newtonian silicon oil over a wide volume fractions are investigated. Suspension exhibit a shear thinning behavior at low shear stress, a shear thickening behavior at the intermediate range of shear stress which can be attributed to the transition between the lubricated contact and frictional ones. The frictionless and frictional jamming packing fractions were predicted by the Krieger-Dougherty model with viscosity data at low and high shear stress limits, respectively. Step up-down measurements also reveal a shear history hysteresis effect which can be attributed to the different spatial structure of the particle assembly arises from particle rotation and clustering.

Keywords: non-Brownian suspension, shear thickening, hysteresis loop, frictional interaction

Introduction

Flows of suspensions (solid particles immersed in a fluid) are ubiquitous in nature, everyday life and industry such as chemical, biochemical, aerospace and environmental engineering: water-saturated sediments, muds, concrete, silica suspensions [1]. Non-Brownian suspensions exhibit a wide range of rheological behavior, including shear-thinning, shear thickening and hysteresis. Shear thickening corresponds to an increase of the viscosity with the shear rate even if the suspending fluid is Newtonian, which is a particularly intriguing phenomenon. In the absence of inertia, the origin of shear thickening is the role of contact forces. Under high shear rates, transient form lubricated to frictional interactions occurs [2], and different behaviors like CST and DST (continuous shear thickening & discontinuous shear thickening) are predicted depending upon the value of the volume fraction, ϕ. In addition, suspension exhibit the flow hysteresis loop sensitive to shear history due to the structural dynamics of particles [1]. In this paper, we investigated the shear thickening behavior and flow hysteresis loop of non-Brownian suspension of methacrylate particles in silicone oil at different volume fractions.

Experimental

The spherical particles, are synthesized by photopolymerization method using photo curable methacrylate resin (Maancure 2500, Maanbaspar Co). First resin was dispersed in an aqueous medium containing sodium dodecyl sulfate (SDS) by mechanical stirrer. After about 3 min, the mixtures were exposed to UV radiation for 2 min to initiate polymerization and the droplets begins to solidify due to crosslinking. The produced particles were post-cured by UV irradiation for future 1 h to complete the gelling and remove of unreacted monomers. The density of particles were determined via He-picnometry ρ=1.22 g/cm^2. Then, the synthesized particles, were dispersed in silicon oil (η=1.062 Pa.s, ρ=0.97 g/cm^2) by the vortex mixer. Rheological measurements were performed using strain-controlled rheometer (MCR302, Anton Paar Physica) with parallel plate geometry at temperature of 25 °C. The steady state viscosity curves were measured by shear stress descending and then ascending with sweep rate of 600 s per decade of stress [3]. Pre-shear has been applied for 200 s at shear rates above the shear thickening regime.

Results and Discussion

The Fe-SEM micrograph and particle size distribution of unmodified synthesized methacrylate micro particles are shown in Fig. 1. As seen the methacrylate micro particles are nearly spherical and uniform in size with average diameter of about 80 μm and polydispersity of 0.05. Fig. 2 shows the steady relative viscosity, in descending and ascending mood at different volume fractions. As can be seen, all suspensions exhibit a shear-thinning behavior can be interpreted as a decrease of the effective volume fraction upon shear stress through the lubricated interaction between particles. As the shear stress is increased, the mild shear thickening was observed at low volume fraction. Upon increasing volume fraction, shear thickening becomes stronger which is probably due to the stronger frictional contacts between neighboring particles. To distinguish the type of shear thickening regime a power law $\tau \propto \dot{\gamma}^{\alpha}$ is fitted to obtain the exponent α. For maximum volume fraction ϕ=0.499, α=1.86 that shows CST regime [4]. We employed Krieger-Dougherty-type relation to predict maximum

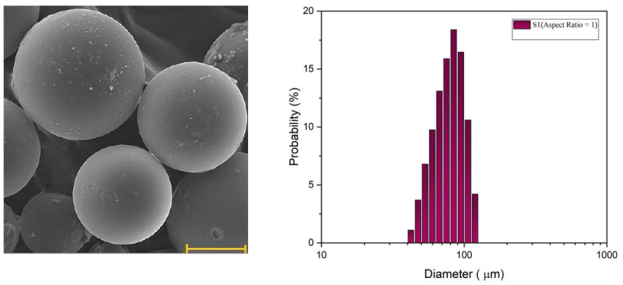

Fig. 1. Left: FE-SEM images of dry spherical particles fabricated by suspension photopolymerization method. Right: particle size analyze with an average diameter of 80 μm. Scale bar shows 50 μm.

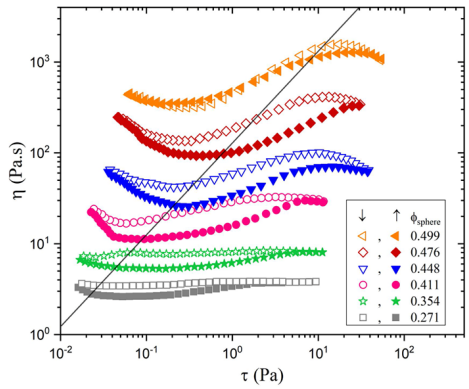

packing fraction, as follows:

$$\eta_r = (1-\frac{\phi}{\phi_J})^{-\beta} \quad (1)$$

Where, η_r is the suspension viscosity rescaled by the suspending solvent's viscosity, ϕ_J is the jamming packing fraction of interest and the exponent β is a fitting parameter: ϕ_0 in the frictionless low-shear limit or ϕ_m in the frictional high-shear limit. Using β =1.7 as the value that best fitted the data in plot (as shown Fig. 3), this leads to ϕ_m=0.500 and ϕ_0=0.518. In ascending and descending sweep experiments, the shear thickening transition behavior is reversible for all samples with hysteresis loop. That's why we investigated the dependency of shear on its history in step up-down shear test in Fig. 3. After the first change of shear rate (from

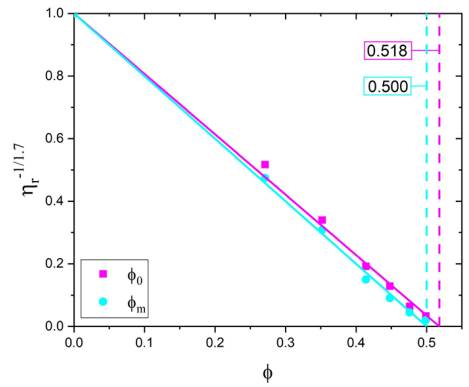

Fig. 3. Rescaled maximum high-shear and low-shear viscosities as a function of packing fraction, enabling the determination of the frictional and frictionless jamming point from Krieger-Dougherty model.

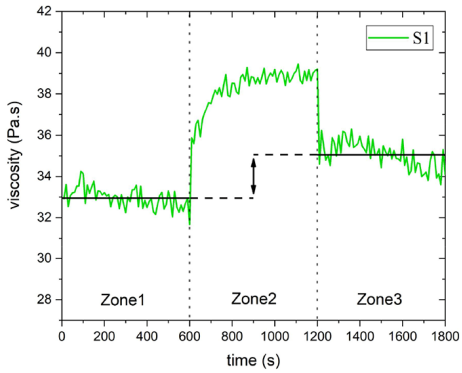

Fig. 4. Fluctuations in viscosity of the suspension as a function of time. the applied shear rate changed between 0.05 in zone 1, 0.1 in zone 2, and back to 0.05 in zone 3. ϕ = 0.431.

0.05 to 0.1), the relative apparent viscosity of the suspension retains its previous value (≈33) before it gradually increases to ≈39. This indicates that the suspension temporarily remembers its previous shear history before it reaches a new configuration in zone 2. When the shear rate decreases back to its initial value, the suspended particles attain a different equilibrium viscosity (≈35) in zone 3 than at the end of zone 1. The end state of the suspended particles in each zone is the initial configuration for the next shear rate. The reason for a different viscosity in zone 3 is that the spatial structure of the particle assembly differs from that of zone 1, which started with a random distribution.

Conclusion

The rheological behavior (shear thinning, shear thickening and hysteresis loop) has been studied in non-Brownian suspension over a wide volume fractions. All suspension exhibit CST shear thickening behavior which can be attributed to the frictional contacts between neighboring particles. Step measurements reveal a shear history hysteresis effect which can be attributed to the different spatial structure of the particle assembly arises from particle rotation and clustering.

References

[1] Srinivasan S., Van Den Akker H.E.A., and Shardt O., International journal of multiphase flow shear thickening and history-dependent rheology of monodisperse suspensions with finite inertia via an immersed boundary lattice Boltzmann method, **125**, 2020.

[2] Chatté G. et al., Shear thinning in non-Brownian suspensions, *Soft Matter*, **14**, 6, 879–893, 2018.

[3] Brown E. and Jaeger H.M., The role of dilation and confining stresses in shear thickening of dense suspensions, *Soft Condens. Matter*, 2012.

[4] Brown E. and Jaeger H.M., Shear thickening in concentrated suspensions: phenomenology, mechanisms and relations to jamming, *Rep. Prog. Phys.*, **77**, 4, 2014.

14-15 December 2021, Tehran, Iran
2nd International Conference on Rheology
ICOR 2021
article A-10-305-1

The Effect of Activator on Rheological Properties of Inorganic Polymers used for 3D Printing

Mahdi Madelatparvar[1*] and Chunwei Zhang[2]
1. Department of Material Science and Engineering, School of Civil Engineering, Qingdao University of Technology, Qingdao 266033, China
2. Center for Infrastructure Engineering Kingswood Campus, University of Western Sydney University, Australia Locked Bag 1797 Penrith NSW, Australia
*mahdi@qut.edu.cn

Abstract
Designing the rheological properties of alkali-activated materials (AAM) used for 3D printing are of important challenge for material designers. During the process, AAM are pumped, extruded and placed layer by layer to form a structure without any mold as supporter. The lower viscosity and pumpability are required before extruding materials. In contrast, higher thixotropic properties are desirable after placing the material to tolerate the own weight and the next layer weight. This characteristic is compatible to Bingham model. The sustainability of materials after printing is mainly related to the static yield stress. This parameter can be calculated through multiplying the critical shear strength and extrapolation storage modulus against time. Static yield stress then compared with the weight of layers to investigate the sustainability of the products against gravitational forces. None of the specimens could resist the own weight in this study.

Keywords: inorganic polymer, alkali activated materials, 3D printing, rheology

Introduction

Alkali activated materials (AAM) are inorganic polymers made from the chemical activation of silicate materials and alkaline activators. The consumption of geopolymers including alkali activated materials instead of common cementitious concrete has been raised due to reducing the carbon dioxide emission and other green construction activity. Every day new types of geopolymers are being developed from waste materials with different properties. On the other hand, 3D printing of building has gained many attentions and is projected to replace the common labor and time-consuming construction method in the near future. Indeed, 3D concrete printing uses minimum material wastage, and there is no need for molds and frameworks. The process of concrete 3D printing contains pumping, extruding and positioning materials at the certain place based on CAD file, layer by layer. Materials are used for 3D printing should meet certain mechanical and rheological properties in each process level. The shear stress required for concrete flowing called dynamic yield stress and plastic viscosity are the key properties of the materials in the pumping and extrusion stages. Also, at the positioning state, static yield stress which increases after positioning play an important role in material design for printability [1]. Stress growth test and flow curve test have been used for static yield stress and dynamic yield stress measurement respectively. The appropriate material has to own low viscosity at the time of pumping and high viscosity and high thixotropy during the printing. Hence, the rheological properties of material before and after extrusion is in contrast.

The aim of this study is to find a relationship between the type of AAM and those rheological properties of the specimens which are related to printing.

Experimental/Theoretical

The components of the material consisted of granulated blast furnace slag (GBFS), the commercial by-product of Isfahan Steel Company Sodium hydroxide was purchased from Bandar Imam Petrochemical Company and diluted to two different molarities with tap water. Silica sand with mesh size of 0-0.3 mm was purchased from Taban powder Malayer Company located in Hamedan, Iran. Chemical analysis through XRF is shown in Table 1. Anton Paar 300 was employed for determination the rheological behavior of the AAM.

Table 1. Raw materials analysis.

Material	SiO_2	CaO	Al_2O_3	MgO	MnO	FeO
GBFS	37.5	36.4	9.3	7.3	1.9	0.0
Silica Sand	99.51	3.0	0.1	0	0	>0.01
Material	TiO_2	V_2O_5	Na_2O	LOI		
GBFS	3.2	1.9	4.2	>0.01		
Silica Sand	>0.01	0	>0.01	>0.01		

Table 2. AAM samples components and G'_0.

Sample	NaOH/slag	Silica sand	Activator molarity	Storage modulus (Pa)
M35	0.35	0	3.5	163
M85	0.35	0	8.5	127
M85S	0.35	20	8.5	1990

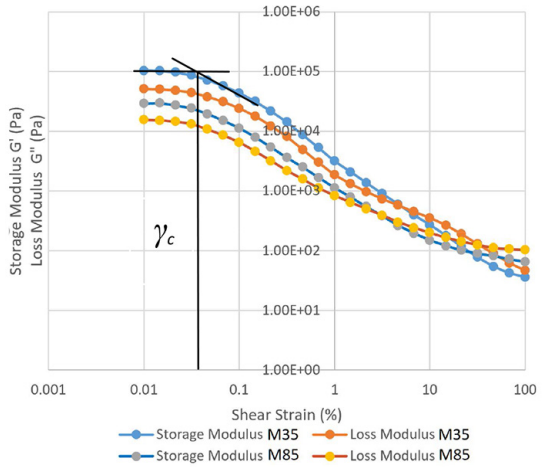

Fig. 1. Storage and loss modulus of samples with different activators molarity.

The samples properties were also shown in Table 2. The relationship for calculation static yield stress is $\tau_0=G'_0\times\gamma_c$ where τ_0 is static yield stress, G'_0 is storage modulus which is gained through extrapolation of storage modulus against time, and γ_c is the critical shear strain. Samples mixed 10 min with hand and rested for 10 min then tested.

Results and Discussion

In order to investigate the printability of the material static shear strength has been calculated for 3 samples and have been shown in the Table 2.

The loss modulus and storage modulus of two samples with two different activator molarities were measured and were depicted against shear strain in Fig. 1.

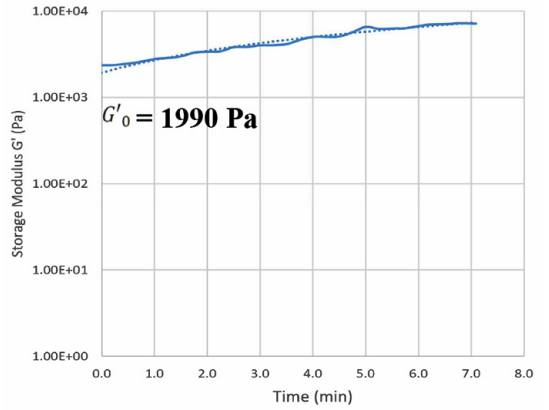

Fig. 2. The evolution of the storage modulus of M85s after printing and G'_0 extrapolation.

The critical shear strain γc was obtained from the interaction of two fitted line on storage modulus plot. The first line is the tangential of linear elastic stage whereas the second line is fitted to the viscoelastic phase. The critical shear strain was approximately 0.03% for those two samples. Fig. 1 also shows that the storage modulus of AAM decreased with increasing the molarity of the activator. The differences between critical shear strain of other samples can be neglected. Results show that by increasing the molarity of activator to slag ratio, the storage and loss modulus of the printed inorganic polymer is decreased.

This is mainly because of the interaction forces between particles which leads to formation and cessation of 3D gel of C-S-H bonds inside the AAM.

Table 3 shows the increase in molarity of activator led to decrease the storage modulus of samples. As the critical shear strength in two samples with different molarity was approximately the same, the static yield stress of high activator molarity sample is lower than low activator sample.

Addition of silica sand also increased the storage modulus of the AAM to more than 1 order of magnitude. The result of static yield stress was lower than the stress level of the printed layer which is calculated through the ρgh where ρ is 1800 kg/m^3, g is 9.8 m/s^2 and h is 0.01 m. Print (176.4 Pa >> τ_0=0.597 Pa).

Although addition of silica sand increased the storage modulus to a considerable amount, it is still lower than being sustainable to print.

Conclusion

Static yield stress was calculated as the main parameter of the material printability. Results show that by decreasing the molarity of the activator and adding silica sand, the static yield stress has been increased. In this case the very low static yield stress shows that this material is not printable.

References

[1] Ranjbar N., Mehrali M., Kuenzel C., Gundlach C., Pedersen D.B., Dolatshahi-Pirouz A., and Spangenberg J., Rheological characterization of 3D printable geopolymers, *Cement Concrete Res.*, **147**, 106498, 2021.

[2] Panda B., Unluer C., and Tan M.J., Investigation of the rheology and strength of geopolymer mixtures for extrusion-based 3D printing, *Compos. Part B: Eng.*, **176**, 2019.

14-15 December 2021, Tehran, Iran
2nd International Conference on Rheology
ICOR 2021
article A-10-306-1

Study of Uniformity and Diameter Variation of Electrospun PVDF/CNC Fibers by Rheology

Zohreh Solouki* and Fatemeh Goharpey
Amirkabir University of Technology, P.O. Box 15875-4413, Tehran, Iran
*z.solouki@gmail.com

Abstract
We prepared poly (vinylidene fluoride) (PVDF)/cellulose nanocrystals (CNC) nanocomposites using the electrospinning process and investigated the effects of PVDF concentration and varying the CNC content on the rheological behavior, uniformity and diameter of the fibers obtained. The diameter and uniformity of the nanofibers were evaluated by scanning electron microscopy. By using rheometry technique, complex viscosity and storage modulus were measured and it was found by CNC increasing, storage modulus increases monotonically up to 3 wt%, while complex viscosity hasn't specific trend. Also, the result from extensional rheometry depicts increase of extensional viscosity with adding CNCs up to 3 wt%.

Keywords: electrospinning, polyvinylidene fluoride (PVDF), cellulose nanocrystals (CNC), nanocomposite, rheological behavior

Introduction

Factors affecting the formation of fibers resulting from the electrospinning process are solution properties such as concentration, polymer molecular weight, viscosity and conductivity. A minimum concentration is required to form fibers in polymer solutions, below which electrospinning is converted to electrospraying [1]. For a polymer solution, the higher polymer concentration, the higher entanglement density, resulting in an increase in apparent viscosity and an increase in fiber diameter. Addition of nanoparticles to the polymer solution, due to the interaction of nanoparticles with polymer chains and nanoparticles network formation; the viscosity and storage modulus increase [2].

In this work, the changes in fiber diameters resulting from the electrospinning of PVDF/CNC solution in different content of CNC are investigated.

Experimental

Material

Poly(vinylidene fluoride) (PVDF) (Kaynar 720 molecular weight 250,000 g/mol), DMF, acetone and cellulose nanocrystals (length range of 200-300 nm and a diameter of 20-30 nm) was used.

Preparing the Electrospun PVDF/CNC Fiber

PVDF/CNC solution (23%) with different percentages of CNC (0, 1, 3, and 5% by weight of the polymer) and DMF/acetone ratio of 50.50 was prepared. The CNC and PVDF granules were added in to the solvent and magnetized for two hours at 60 °C. The solutions were exposed to 15 kV at 25 °C, feed rate of 1 mL/h and a distance of 18 cm from the nozzle tip to the collector plate.

Table 1. Mean diameters of PVDF/CNC electrospun fibers with different CNC loadings.

PVDF/CNC nanocomposit	CNC 0	CNC 1	CNC 3	CNC 5
Mean diameter (μm)	0.206	0.250	0.310	0.149

Characterization

By using the abeload viscometer, Intrinsic viscosity was obtained. Morphology and mean diameter of electrospun nanofibers were analyzed by scanning electron microscopy (SEM). The complex viscosity and storage modulus of PVDF/CNC have been measured by using RMS. Extensional viscosity obtained from extensional rheometry.

Results and Discussion

Minimum concentration required for uniform fiber formation is 2-2.5 Ce. Also, considering that Ce=10 C* and C*=0.77/[η] [3]. Intrinsic viscosity calculated from the extrapolation of the Kramer-Huggins equations obtained from abeload, which is equal to 0.79 dl/g. According to this result, 23 wt% solution of PVDF/acetone/DMF was obtained from uniform polymer fibers. Also, with increasing PVDF, due to the increase of entanglement, the diameter of the fibers increases (Fig. 1) [4].

Fig. 2 shows the SEM images of electrospun nanocomposites. The mean diameters of fibers with different CNC content are measured and are tabulated in Table 1. By increasing CNC, the fiber diameter increases up to 3 wt%, but at 5 wt%, in addition to decreasing the diameter, heterogeneity is also observed.

In Fig. 3, it was observed that by adding 1 wt% CNC, complex viscosity decreases and then by adding 3% CNC, increases. Therefore, viscosity cannot be responsible for the increase in diameter. The storage modulus was shown in Fig. 3. By addition CNCs up to 3 wt%, the storage modulus increases at low frequencies and decreases at 5 wt% due to agglomeration formation. Adding 1 wt% CNC may increase the free volume, which facilitates movement and thus reduces viscosity. Another possibility is that the long chains interacted with the CNCs, which reduced

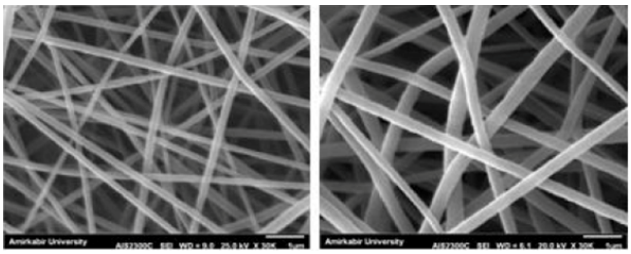

Fig. 1. SEM images of nanofibers produced from solutions with: (a) 23 wt% and (b) 27 wt% of PVDF.

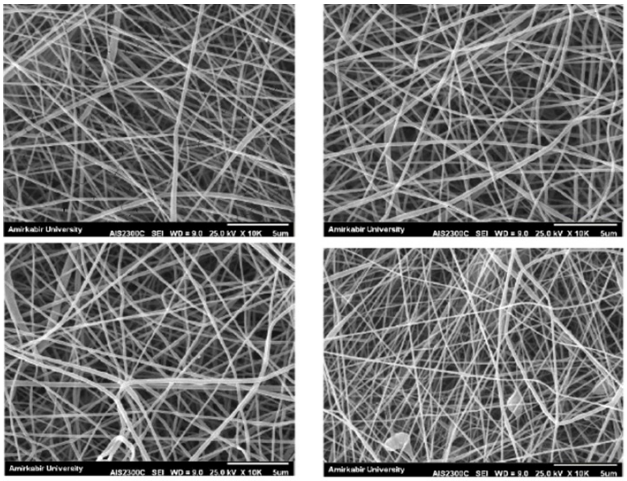

Fig. 2. SEM images captured from PVDF/CNC electrospun nanocomposites with different CNC contents with respect to PVDF weight: (a) 0% CNC, (b) 1% CNC (c) 3% CNC, and (d) 5 % CNC.

the bulk viscosity. The reason of modulus increasing is formation of nanoparticles network [2]. Therefore, it is possible that increasing the storage modulus in the lower regions, because of the solid-like of the jet during the electrospinning process, could be responsible for diameter

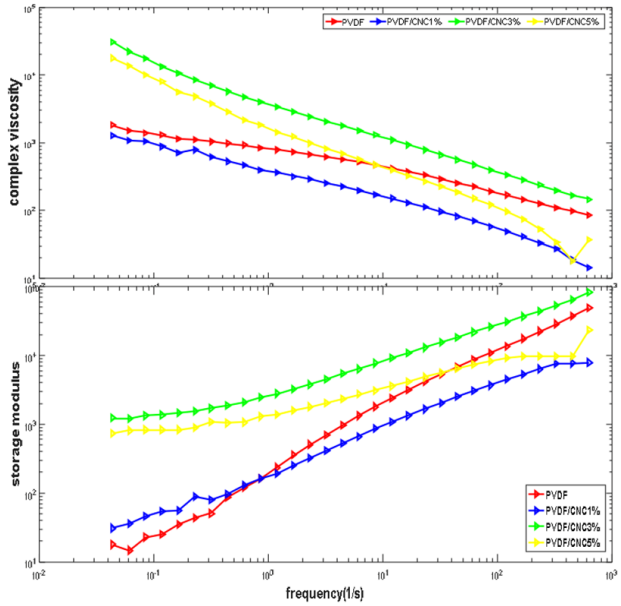

Fig. 3. complex viscosity and storage modulus of samples with different CNC contents.

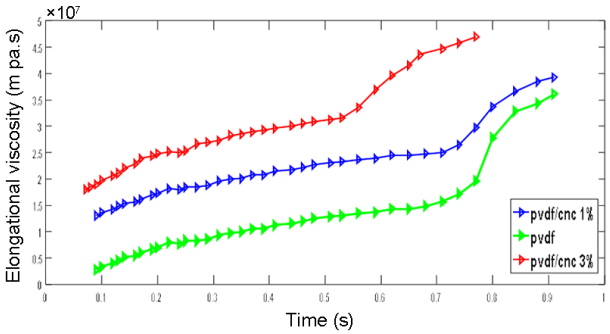

Fig. 4. Extensional viscosity of PVDF and 1 and 3 wt% PVDF/CNC with 1 1/s elongational rate.

increase.

Extensional viscosity of PVDF and 1 and 3 wt% PVDF/CNC samples is shown in Fig. 4. By adding CNC, the Extensional viscosity increases and strain hardening occurs earlier. The Extensional stress forces fluid to arrange in direction of tension. The presence of CNCs and their interaction with polymer chains requires more stress for this arrangement, so viscosity increases. Moreover, Because of this interaction adding CNCs reduces the slope of the line related to the sudden increase in viscosity. This slope is proportional to the inverse of chains relaxation time. Increasing the relaxation time means that fluid elasticity increases, resulting in the fiber diameter increase [5].

Conclusion

The optimum concentration for uniform fiber formation was 23 wt% PVDF. The fiber diameter also increased with increasing polymer concentration. The addition of nanoparticles increases the fiber diameter by up to 3 wt%. The viscosity of the complex does not increase monotonically with adding CNC. While increasing the modulus and extensional viscosity by adding nanoparticles has a trend similar to increasing diameter.

References

[1] Li S. et al., Uniform high-molecular-weight polylactide nanofibers electrospun from a solution below its entanglement concentration, **44853**, 1–7, 2017

[2] Chee Y. et al., Rheological properties of cellulose nanocrystal-embedded polymer composites: a review, *Cellulose*, **23**, pp. 1011–1030 , 2016.

[3] Wang C. and Wang Y., Impact of entanglement density on solution electrospinning: a phenomenological model for fiber diameter, *Macromolecules*, **49**, 20, 7985–7996, 2016.

[4] Bera B., Literature review on electrospinning process (a fascinating fiber fabrication technique), *Imper. J. Interdi. Res.*, **2**, 8, 972–984, 2016.

[5] Zell A., Gier S., Rafaï S., and Wagner C., Is there a relation between the relaxation time measured in caber experiments and the first normal stress coefficient?, *J. Nonnewton. Fluid Mech.*, **165**, 1265-1274, 2010.

14-15 December 2021, Tehran, Iran
2nd International Conference on Rheology
ICOR 2021
article A-10-311-1

Gel Structure of PVC Plastisol Used as Automotive Underbody Coatings

Malihe Pishvaei* and Behrouz Eftekhari
Department of Resin and Additives, Faculty of Surface Coating and Novel Technologies,
Institute for Color Science and Technology, Tehran, Iran

*pishvaei@icrc.ac.ir

Abstract
The PVC plastisol is a dispersion of fine particles of resin in a liquid plasticizer in which the particle interactions lead to the formation of microstructures. Depending on how such structures respond to the shear stress, one observes different types of flow behavior. Given the change of flocculation structure and shear-thinning behavior during the shear period, the Herschel-Bulkley model is more suitable for calculating the static yield stress of these materials. In this study, static yield stress changes along with the thixotropy (hysteresis area) are investigated for various industrial PVC plastisol used as automotive underbody coatings (UBC). The results show that with increasing the thixotropic behavior in different samples the yield stress increases. On the other hand, the gel like behavior is observed for all samples at room temperature as the storage modulus are higher than loss modulus over the entire experimentally accessible frequency range, and both are nearly constant.

Keywords: plastisol, static yield stress, viscosity, thixotropy, hysteresis area

Introduction

The PVC plastisol is a dispersion of fine particles in a liquid plasticizer to produce a fluid like mixture that can be spread on a substrate. The coated substrates (Fig. 1) are then heated in an oven to gel and fuse the plastisol in to the final rubbery products [1].

The aging characteristics or the change in viscosity of a plastisol with time during the storage are very important. The mechanisms involved in plastisol aging include particle deagglomeration, particle swelling, particle dissolution, particle solvation, and plastisol structure development [2]. In this work, static yield stress changes along with the thixotropic properties (hysteresis area) were investigated for various industrial plastisols, both of freshly prepared samples and aged plastisols as well. Furthermore, the viscoelastic properties of samples were studied at the room temperature.

Experimental

Different commercial plastisols were examined as presented in Table 1. Anton-Paar MCR 300 rheometer with cone and plate geometry was used to measure the rheological properties. The viscosity of the samples were measured from shear velocities of 0.001 1/s to 1000 1/s with a rest time of 300 (s) at 1000 1/s and return velocity in the same range at 25 °C. The frequency sweep tests were performed in the linear viscoelastic area of samples.

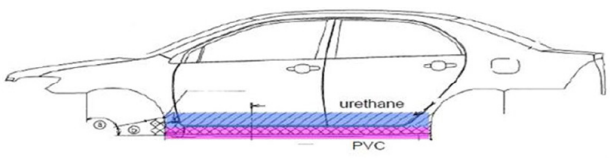

Fig. 1. Automotive underbody coatings (UBC).

Results and Discussion

Flow tests were performed for various industrial PVC plastisol samples. Thixotropy can be defined as a (reversible) decrease of viscosity of the material in time when the material is made to flow. Yield stress is an important term to describe the flowability of paste materials. The static yield stress was calculated based on the experimental data and using the Herschel-Bulkley equation from the shear rate-shear stress diagram for each sample.

Generally, the yield stress appears when the particle repulsions are strong enough to induce a regular arrangement of particles or a sort of "macrocrystallization". The

Table 1. Commercial PVC Plastisol Samples.

Sample	Application	Company
1	UBC	Henkel
2	UBC	Daghigh shimi
3	Sealer (S.)	Henkel
4	Sealer	Daghigh shimi
5	UBC (aged sample 1)	Henkel
6	UBC (aged sample 2)	Gama thinner
7	S. (aged sample 3)	Henkel
8	UBC	Daghigh shimi
9	UBC	Gama thinner
10	Sealer	Gama thinner
11	UBC (aged sample 8)	Daghigh shimi
12	UBC (aged sample 9)	Gama thinner
13	S. (aged sample 10)	Gama thinner

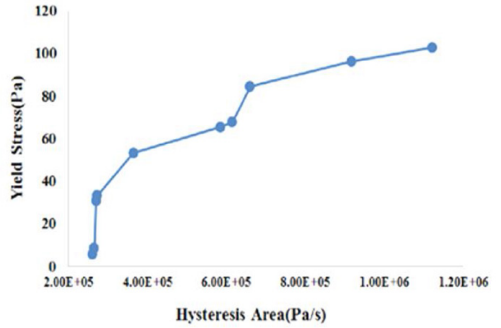

Fig. 2. Experimental values of yield stress and thixotropy for 10 different PVC plastisols.

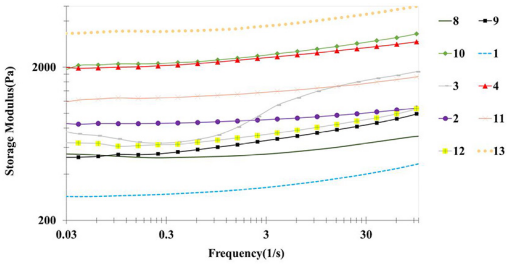

Fig. 3. Storage modulus versus frequency for 10 different PVC plastisols.

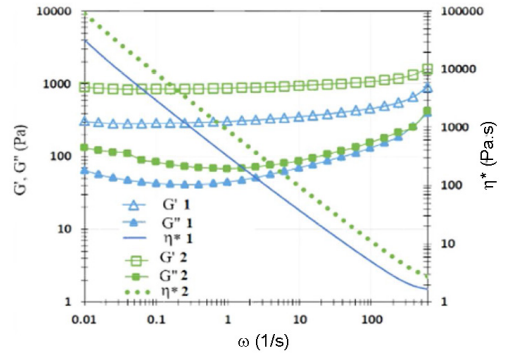

Fig. 4. Viscoelastic properties of 2 plastisols: G'' solid points, G' open points and complex viscosity: solid line and dashed line.

hysteresis area (Pa/s) was also obtained from the shear rate-shear stress diagram. The area within the hysteresis loop represents the energy consumed in structure breakdown. Fig. 2 shows the changes in the hysteresis area in terms of static yield stress. Samples with a larger hysteresis area show greater yield stress and vice versa. The results confirm that the yield stress and the thixotropy in PVC plastisols are caused by the same fundamental physics and this may be related to the microstructure-strength [3]. Beyond the gel point, the materials behave like viscoelastic Hookean solids at low frequencies or large scales [4]. However, the rubbery plateau as an evidence for gel like behaviour were observed for all samples in this study for PVC plastisols at room temperature (Figs. 3 and 4).

Conclusion

1- PVC plastisols behave like an elastic solid i.e. with G'>G'' over the entire experimentally accessible frequency range, and where both of modulii are nearly constant (i.e. independent of frequency).

2- The results confirm that the yield stress and the thixotropy in PVC plastisols are caused by the same fundamental physics and this is related to the microstructure-strength.

References

[1] Rasteiro M.G., Toma´s A., Ferreira L., and Figueiredo S., *J. Appl. Polym. Sci.*, **112**, 2809-2821, 2009.

[2] Hoffmann D.J., and Garcia L.G., *J. Macromol. Sci. Phys.*, **20**, 335-348, 1981.

[3] Jarni S. et al., *Cement and concrete research*, **35.10**, 1873-1881, 2005.

[4] Pishvaei M., Graillat C., McKenna T.F., and Cassagnau P., *Polymer*, **46**, 1235-1244, 2005.

14-15 December 2021, Tehran, Iran
2nd International Conference on Rheology
ICOR 2021
article A-10-312-1

An Experimental Study on the Rheological Effect of Silica and Modified Silica-IL in PU Nanocomposites

Shadi Hasansanjili*, Abed Khavand, Ghazal Azangou, and Fatemeh Omraninasab
School of Chemical and Petroleum Engineering, Shiraz University, Postal Code 84334-71964, Shiraz, Iran
*ajili@shirazu.ac.ir

Abstract
The rheological behavior of polymer melt has a significant role in polymer processing as it describes the deformation and flow behavior of the material. In this work, the rheological and viscoelastic properties of three Polyurethane (PU) based nanocomposite samples were investigated in oscillatory rheometer in molten state. The samples are 1. pure PU, 2. PU/silica nanocomposite, and 3. PU/silica-IL nanocomposite. The effect of silica nanoparticles on rheological properties of PU/silica nanocomposite has been investigated. The second sample has a larger cross over in modulus compared to the other two samples, in fact, the crossover is shifted to lower frequency. The parameters for shear viscosity models obtained and the effect of nano particles on viscosity models are described. In addition, the twin Maxwell elements model has been used to describe the stress relaxation behavior in linear viscoelastic region approximately for these three samples.

Keywords: polyurethane/silica-IL, viscosity model, non-Newtonian fluid, linear viscoelastic, Twin Maxwell elements model

Introduction
Rheological investigation on polymer melts is widely used for quality control and the optimization of processing. Polyurethanes (PU) have a wide range of chemical and rheological properties. Polyurethane composites (PUC) have attracted much attention because of their high potential to achieve great improvement in properties including good processability, mechanical and physical properties by adding a small amount of nanoparticles in the polymer matrixes [1,2]. In this study Polyurethane nanocomposite with silica and silica/IL have been studied. Silica is hydrophilic due to the presence of the silanol (Si-OH) group on the surface of the particle and does not show a tendency to non-polar polymers, for this reason, adding silica nanoparticles have no positive effect on properties and do not disperse homogeneously [2]; so, we modified silica nanoparticles with IL that is increase their compatibility with polymeric matrix [2].

Experimental
I. Preparation of Samples:
Pure PU sample was made by 10 wt% of polyether urethane in dimethylformamide (DMF) as a solvent. For composite samples, at first modified commercial silica with [BMIM][PF6] and non-modified silica should disperse for an hour in DMF at 70 °C then PU granules added to the solution and mixed enough for better dispersion. Three samples were made from pure PU and two different silica nano particles (modified and non-modified). The silica nanoparticles concentration in 2 samples are 5% (wt/wt). Ultrasonication must be done to prevent nanoparticles agglomeration. [3,4]

II. FTIR Analysis of Samples:
Molecular interaction identification can be observable in FTIR spectra.

III. Viscosity Analysis of Samples:
An oscillatory rheometer has been used in molten state of samples (185 °C). The cone and plate disks with 2.5 cm diameter and 0.034 mm height were applied on rheometer [4].

IV. Frequency Sweep Test of Samples:
The same device in the last experience has been used for frequency sweep tests in molten states. To study on the viscoelastic region, 1% of shear strain was applied in all points of 3 tests [4].

Results and Discussion
I. FTIR Analysis of Samples:
In Fig. 1, FTIR peaks shows N-H bonds in the range of 3200-3500 cm^{-1}, C=O in 1600-1800 cm^{-1} and C-O-C between 1000-1200 cm^{-1}. Stretching Si-O-Si peaks can be observed between 1010-1190 cm^{-1} in samples No. 1 and No. 2. Around 850 cm^{-1} in sample No. 3 we have P-F peaks to prove the presence of IL in PU/silica-IL.

II. Viscosity Analysis of Samples:
The Power-low (Eq. (1)) and Carreau viscosity equations (Eq. (2)) have been used to find the viscosity behavior of samples. All the samples behave like pseudoplastic fluid (Fig. 2) and viscoplastic fluid behavior not seen, so the

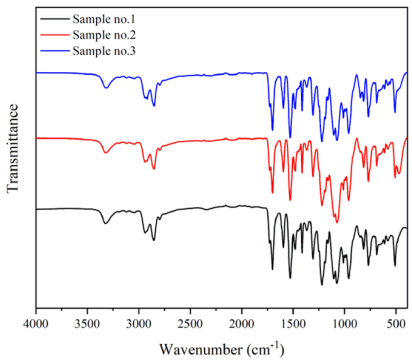

Fig. 1. FTIR spectra of samples: 1. PU, 2. PU/Silica, and 3. PU/silica-IL.

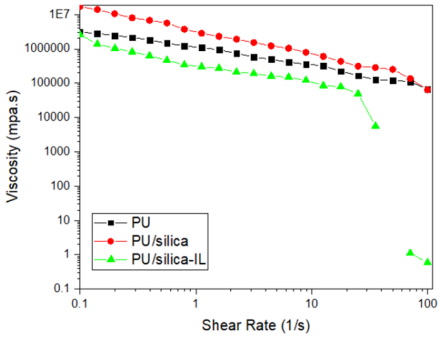

Fig. 2. Pseudoplastic behavior of samples.

Table 1. Viscosity parameters.

Sample	Eq.	Parameter	Value
Pure PU	1	m	1229
		n	0.3979
		R^2	0.9656
	2	λ	5.18
		n	0.3608
		R^2	0.9951
PU/silica	1	m	3786
		n	0.2267
		R^2	0.7968
	2	λ	6.046
		n	0.08246
		R^2	0.9823
PU/silica–IL	1 (γ =0.0998 - 25.1 1/s)	m	391.5
		n	0.4029
		R^2	0.9521
	2	λ	9.259
		n	0.0265
		R^2	0.9135

Herschel-Bulkley and other same equations did not used [6,7]. The viscosity parameters are reported in Table 1.

$$\tau_{yx} = m.\dot{\gamma}_{yx}^{\ n} \quad (1)$$

$$\frac{\mu-\mu_\infty}{\mu_0-\mu_\infty} = (1+(\lambda.\dot{\gamma}_{yx})^2)^{\frac{n-1}{2}} \quad (2)$$

III. Frequency Sweep Test of Samples:

The storage modulus of the samples versus frequency are reported in Fig. 4. As it is obvious adding unmodified silica into PU increase G' at low frequencies due to solid-like network structure and filler aggregation. But adding IL modified silica with the same percent has reduced storage G' in this region due to better silica dispersion. The frequency sweep data used to obtain a linear viscoelastic model. The Maxwell parameters reported in Table 2. For better calculations we are able to use more elements, so the modeling gets closer to better fitting on experimental

Table 2. Maxwell model parameters.

Sample	i	G_i	λ_i	R^2
1. Pure PU	1	4236.65	0.052	0.9996
	2	1.112e5	0.0021	
2. PU/silica	1	1.23e4	0.080	0.9964
	2	8.956e4	0.029	
3. PU/silica-IL	1	3.5e4	0.012	0.9997
	2	8.809e4	0.003	

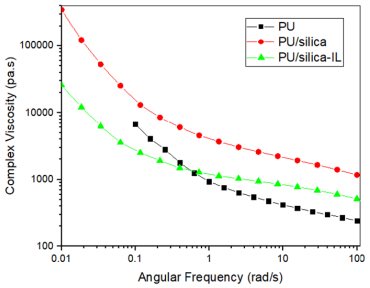

Fig. 3. Complex viscosity comparison.

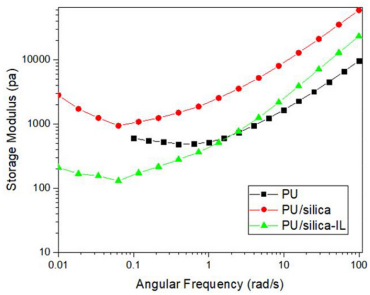

Fig. 4. Storage modulus comparison.

data, but it can be more difficult and time consuming.

Conclusion

Nanoparticles and modifier have a negative effect on functionality of viscosity specially in high shear rates, the Carreau model is able to use in nanocomposites. The silica nanoparticles caused the viscosity shifted to high values, but the modified silica had inverse effect and intensified the pseudoplastic behavior. In low frequency, PU and PU/silica nanocomposite are closer in complex viscosity (Fig. 3), storage modulus (Fig. 4) and loss modulus compared to modified nanocomposite, but in high frequency both of nano composites (modified and non-modified) get closer to each other, and PU modulus make a difference with other samples.

References

[1] Vaithylingam R., Ansari M.N.M., and Shanks R.A., Recent advances in polyurethane-based nanocomposites: a review, *Polym.-Plast. Technol. Eng. J.*, **56**, 2017.
[2] Hassanajili S. and Sajedi T., Fumed silica/polyurethane nanocomposites: effect of silica concentration and its surface modification on rheology and mechanical properties, *Iran Polym. J.*, **25**, 2016.
[3] Sasikumar B., Arthanareeswaran G., and Ismail A.F., Recent progress in ionic liquid membranes for gas separation, *J. Mol. Liq.*, **226**, 330-341, 2018.
[4] Hassanajili S., Masoudi E., and Karimi G., Mixed matrix membranes based on polyether urethane and polyester urethane containing silica nanoparticles for separation of CO_2/CH_4 gases, *Sep. Purif. Technol.*, **116**, 1-12, 2013.
[5] Dealy J.M. and Wissbrun K.F., Melt rheology and its role in plastics processing: theory and application, *Spring. Sci. Bus. Media*, 2012.
[6] Chhabra R.P. and Richardson J.F., Non-Newtonian flow and applied rheology, Elsevier, 2008.
[7] Crawford R.J., Plastic engineering, 3rd Edition, 1998.

14-15 December 2021, Tehran, Iran
2nd International Conference on Rheology
ICOR 2021
article A-10-314-1

Investigation of Cure characteristics of Silicon Rubber/SEBS Blends by Moving Die Rheometer

Ehsan Alikhani and Mohsen Mohammadi*
Department of Polymer Engineering, Faculty of Engineering, Qom University of Technology,
P.O. Box 37195-1519, Qom, Iran

*mohammadi@qut.ac.ir

Abstract
In this study, silicon rubber (SR)/styrene-ethylene butylene-styrene (SEBS) blends with different ratios were prepared for the first time. Then, cure characteristics of SR/SEBS blends by moving die rheometer (MDR) were investigated. The results showed that the curing time of SEBS is longer than SR. In addition, the cross-link density of SEBS is significantly lower than SR. Mixing was evaluated and performed through a lab torque rheometer as internal mixer and the obtained diagrams of torque and melt temperature were analyzed. Steady trend in torque over time confirmed that the blends were not cross-linked during mixing with peroxide.

Keywords: silicone rubber, SEBS, rheometer, curing, mixing

Introduction

Because of higher properties of silicone rubber (SR) in biomedical and industrial issues, it has been interested extensively [1]. Styrene-ethylene butylene-styrene copolymer (SEBS) is one of the most important TPEs that has thermal stability, aging resistance and good electrical properties [2]. In the past, SR blends systems with polyolefins have been investigated [1,3]. However, the SR/SEBS blend system and its properties have not been studied, so far. SEBS has an olefin component in its chain, which usually contains more than 50% of each chain. So that, the study of the SR/SEBS blend system seems to be an interesting research topic.

Experimental

Commercial Silicone rubber (NE-5280) with a hardness of 80 (Shore A) having density 1.25 g/cm^3 was obtained from Djsilicone Co., Ltd. (China). Commercial tri-block copolymer SEBS (Globalprene-7550U), with 30 wt% styrene units and density 0.91 g/cm^3, was supplied by LCY Co., Ltd (Taiwan), peroxide curing agent BIPB (bis(tert-butylproxy isopropyl) benzene) was purchased from Rhein Chemie Co., Ltd. (China).

Silicone rubber and SEBS were melt mixed into a Rheosens Lab Torque Rheometer, IPPI Co., Ltd (Iran) as internal mixer. The mixing was performed at 190 °C at a rotor speed of 60 rpm for 8 min. First SEBS was added, and it was melted for 2 min. Silicone rubber was then added and mixed for 6 min. Then the obtained blend was mixed with the peroxide agent for 5 min at 70 °C and 60 rpm using the internal mixer. The given low mixing temperature for adding peroxide was chosen to ensure that the peroxide was not degraded. The samples were then compression molded for T90+2 min at 175 °C under 30 tones in an electrically heated hydraulic press (SPH-300, Santam Co., Ltd. Iran). Samples were designated as B1, B2, B3, B4, B5, and B6 containing 0, 10, 25, 75, 90, and 100 wt% of silicone rubber, respectively.

The cure characteristics of the samples were studied by a moving disk rheometer (MDR) (SMD-200, Santam Co., Ltd., Iran). About 5 cm^3 of samples were used to perform the tests. This test was performed at a frequency of 1.68 Hz, a temperature of 175 °C and amplitude of 0.5° for 20 min.

Results and Discussion

The samples rheograms are shown in Fig 1. The rheograms of all the samples show an initial decrease in their torque. The initial reduction in torque is due to the softening of the polymer as it heats up, which reduces the viscosity and thus the torque required to move the rheometer disc. Then, with the activation of the curing agent and the generation of the first cross-links, the resistance of the chains to movement increases and then the torque increases until it finally reaches a constant value. According to Fig. 1, and the information in Table 1, the following results are inferred:

- As the amount of SEBS increases, the scorch time (Ts2) increases. As a result, scorch safety is improved.
- As the SR content increases, the cure time (T90) of the blends decreases.
- Increasing the content of SR increases the cure rate.
- Increasing the content of SR increases the ΔM of blends. Since this difference is directly related to the cross-link density, increasing the SR content increases the cross-link

Table 1. Cure paprameters of the samples.

Name	Ts2	T90	ML	ΔM	Rate of cure
	(min)	(min)	(dN.m)	(dN.m)	(dN.m/min)
B1	2.50	8.01	1.35	4.18	0.35
B2	2.23	7.95	1.35	5.30	0.48
B3	1.42	7.78	1.54	8.23	0.93
B4	0.53	5.15	1.77	23.19	4.07
B5	0.38	3.03	1.61	29.13	9.18
B6	0.38	2.22	1.25	33.66	15.43

density of the blends.

o There is a significant difference between the cure characteristics of SR and SEBS.

The same behavior was observed in the SR blend with EVA [1] and the SR blend with polyurethane rubber [4]. In those blends, increasing the content of SR reduced the scorch time and curing time. Also, increasing the content of SR increased the cure rate and ΔM. It should be noted that the difference in solubility of the curing agent in elastomers can cause significant differences in their curing speed and the amount of their crosslinking [1]. In addition, it should be noted that the nature of each polymer, the energy of the chains and the type of chemical bonds in each polymer, cause differences in its cure characteristics. But there are other reasons for the difference in SR and SEBS cure characteristics. In the present study, the mixing temperature of the samples with peroxide was set at 70 °C. When polymers are mixed inside the internal mixer, the friction caused by the polymer chains with each other as well as with the wall of the internal mixer generates additional heat. The excess heat generated also causes the temperature of the polymer in the internal mixer to be slightly higher than the set temperature. Fig. 2 shows the changes in torque, middle zone temperature (set temperature) and melt temperature of the polymer while mixing with peroxide (melt temperature refers to the temperature of the polymer in the internal mixer). This diagram is obtained from the Rheosens Lab Torque Rheometer, for B1. Mixing diagrams of other samples follow a similar procedure.

Changes in torque over time (Fig. 2) confirm that the presence of peroxide and mixing with SEBS for 5 min did not cause the polymer to cure, as torque did not increase

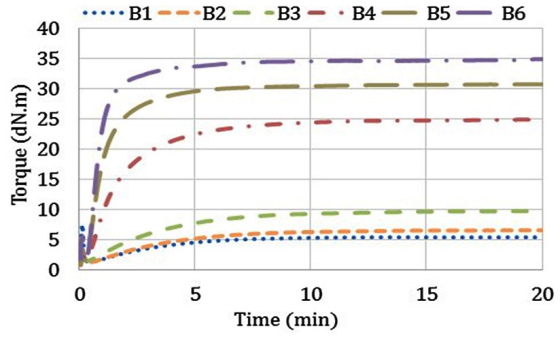

Fig. 1. Rheogrms of the SR/SEBS blends.

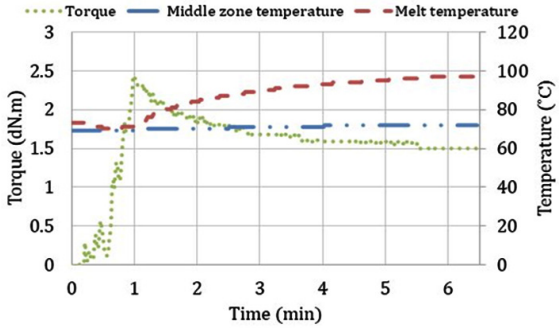

Fig. 2. The mixing diagrams of B1, obtained from the Rheosens Lab Torque Rheometer.

during SEBS mixing with peroxide. Therefore, at the mixing temperature and time most of peroxide was not activated. It should be noted that peroxide was added to SEBS after 1.5 min. A comparison of the middle zone temperature and the melt temperature shows that the middle zone temperature, which was considered as the mixing temperature, remained almost unchanged at about 70 °C. The melt temperature has risen from 70 °C to 97 °C. Therefore, the PS blocks were close to their glass transition temperature when mixing with the peroxide. In this case, there is weak possibility of penetrating peroxide into the PS blocks. Because PS blocks are still solid, while EB blocks are very soft and fluid at this temperature.

Conclusion

The rheograms revealed that as the SR content increases, the cure time (T90) of the blends decreased and ΔM and cross-link density of the blends increased. There was a significant difference between the cure characteristics of SR and SEBS. When the blends prepared, after adding peroxide into the internal mixer, because of friction the melt temperature rose from 70 °C to 97 °C, but torque was steady, which confirms no curing occurred during the mixing time.

References

[1] Ganesh B. and Unnikrishnan G., Cure characteristics, morphology, mechanical properties, and aging characteristics of silicone rubber/ethylene vinyl acetate blends, *J. Appl. Polym. Sci.*, **99**, 3, 1069-1082, 2006.

[2] Wu Y., Shentu B., and Weng Z., Synergistic effect of SBS and trimethylopropane trimethacrylate (TMPTMA) on dynamically vulcanized SEBS/PP blends, *J. Appl. Polym. Sci.*, **134**, 5, 1-7, 2017.

[3] Serenko O.A., Pryakhina T.A., Vasil'ev V.G., Buzin, M.I., Volkov, I.O., Kotov, V.M., and Muzafarov A.M., Effect of reactionary capable siloxane compatibilizer on the properties of blends of ethylene propylene diene and siloxane rubbers, *Russ. Chem. Bull.*, **70**, 5, 960-966, 2021.

[4] Gan L.M., Ni H.Y., Zhou Y.J., and Chen J., *J. Macromol. Sci., Part B*, **50**, 8, 1491-1499, 2011.

14-15 December 2021, Tehran, Iran
2nd International Conference on Rheology
ICOR 2021
article A-10-315-1

Rheological Hysteresis in Complex Fluids

Zahra Daneshfar*
Department of Chemical and Polymer Engineering, Faculty of Engineering, Yazd University,
Postal Code 8915818411, Yazd, Iran
*daneshfar@yazd.ac.ir

Abstract
Rheological hysteresis has been studied combining global flow curve and local velocity profiles measurements. This behavior is not unique to thixotropic materials either, it also occurs in other complex fluids. The surface area of the hysteresis loop depends on several parameters; such as the shear history prior to the test, the sweep time and the maximum value of shear rate. Indeed, transient and time-dependent shear band affected the loop area and the range of hysteresis. This review summarizes the most important aspects covered in the rheological hysteresis in different complex fluids.

Keywords: rheological hysteresis, thixotropy, shear banding, complex fluids

Introduction

In the rheological literature, the first mention of hysteresis loops reported by E.L. McMillen in paints [1]. The rheological hysteresis in different complex fluid [2-8] can be studied from apparent flow curve measurements by applying ascending and descending shear rate (stress) sweep. For a given material, the hysteresis loop will depend on test conditions such as the shear history prior to the start of the experiment, the maximum shear rate and the sweep rate [9]. In addition, hysteresis appears in the measured velocity profiles, with profiles at any given shear rate differing between the descending and ascending sweeps. The experimental and simulation studies reported that hysteresis is often also accompanied by the spatial heterogeneous flows such as shear banded or plug flows [10,11]. This review summarizes the most important aspects covered in the rheological hysteresis in different fluid complex.

Hysteresis in Thixotropic Systems

Thixotropy defines as the continuous decrease of viscosity with time when flow is applied to a sample that has been previously at rest, and the subsequent recovery of viscosity when flow is discontinued. The excellent reviews of thixotropy are already available; namely, those of Mewis [9], Larson et al. [12]. The observed hysteresis often demonstrate the existence and extent of the thixotropic behavior in complex fluids. The shape and area of the hysteresis loops have been used to evaluate the thixotropic degree i.e., larger area means larger thixotropic degree. However, due to the simultaneous change of two variables of shear rate and time during the experiment, hysteresis in flow curves represents nonequilibrium behavior. The shapes of the hysteresis loop in the flow curve of the complex fluid are shown in Fig. 1. In ordinary thixotropic fluids, stress in ascending sweep is higher compared to descending ones (Fig. 1a). Fig. 1b illustrates a system where breakdown of the initial structure after starting up dominates the time evolution of the stress, resulting in a stress overshoot. In ascending sweep measurements, a reduction of stress can cause shear banding and heterogeneous shear rate distributions in the sample. When shear at relatively low shear rates induces structure formation the hysteresis loop can take a shape as the one in Fig. 1c [13]. Zhu et al. [14] observed flow hysteresis loop in Al_2O_3 colloidal gels, and suggested that the rates of agglomeration and breakdown of flocs which determined by the rate of collision of them lead to the time-dependent colloidal structure and thixotropy. In literature, the area of the hysteresis loop from flow curve (A_σ) and velocity profiles (A_v), defined as follows:

$$A_\sigma = \int_{\dot{\gamma}_{min}}^{\dot{\gamma}_{max}} \left| \Delta \langle \bar{\sigma} \rangle (\dot{\gamma}) \right| d(\log(\dot{\gamma})) \quad (1)$$

$$A_v = \int_{\dot{\gamma}_{min}}^{\dot{\gamma}_{max}} \int_0^L \left| \Delta v(\dot{\gamma}, y) \right| dy\, d(\log(\dot{\gamma})) \quad (2)$$

Divoux et al. [11] demonstrated that the A_σ and A_v depend on the sweep time, δt. For thixotropic materials such as mayonnaise, laponite and carbon black suspensions exhibit a robustly reproducible bell-shape dependence hysteresis loop area on the sweep time δt. In simple yield stress fluids such as carbopol microgel, this time scale is very small, and thus, A_σ and A_v decrease monotonically as δt increases. Recently, Radhakrishnan et al. [15] showed that the fluidity models and the soft glassy rheology model can reproduce such hysteresis loops. According to the simulation results, different tendencies to form shear bands in simple and time-dependent yield stress fluids during the sweeps cause to two different form of dependence hysteresis loop on sweep time. Simple yield stress fluid exhibit the homogenous flow response during the descending sweep in shear rate, followed by shear banding triggered by stress overshoot in the ascending sweep. While in time-dependent yield stress fluids, shear banding formed during descending weeps. In particular, Puisto et al. [16] suggested that a coupling between hysteresis measured from the local velocity profiles and that measured from the global flow curve. They predicted a monotonic decrease of the hysteresis loop areas A_σ and A_v with increasing sweep time δt, for inelastic fluids. However for viscoelastic materials they demonstrated more complicated dependences, in some cases resembling the bell-shaped plots. These experimental measurements and simulation results has been limited to the macroscopic measurements of a system and indicated that there is a characteristic time scale in different thixotropic fluids. Jamli et al. [17] determined a characteristic hysteresis time in attractive colloidal suspensions based on the hysteresis areas calculated at three different length scales:

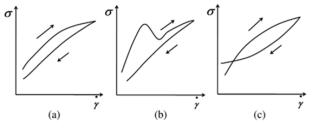

Fig. 1. Different shapes of hysteresis loops [9].

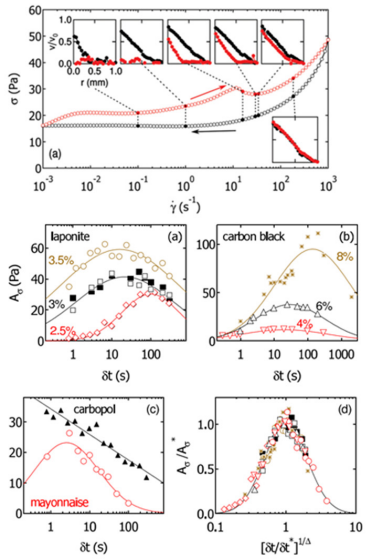

Fig. 2. Flow curve of a 2.5 wt% laponite suspension: descending sweep in 90 logarithmically spaced steps of duration δt=15.5 s (black symbols), ascending sweep (red symbols). Insets: Velocity profiles during the descending (black), ascending (red) sweeps. Area of the hysteresis loop as a function of δt for: (a) laponite suspensions, (b) carbon black gels, (c) a carbopol microgel and a commercial mayonnaise, and (d) Normalized data [11].

from particle-level local measurements of coordination number (microscale), to the appearance of density and velocity fluctuations (mesoscale), and up to the shear stress response to an imposed deformation (macroscale). At all length scales, the characteristic hysteresis time become shorted upon increasing the strength of the inter particle attraction, and also the maximum hysteresis area increases due to the formation of bonds, clusters and spanning networks between particles. Moreover, they suggested that suspension with stronger attractions exhibit larger sensitivity to the history of flow.

Hysteresis in Different Systems

System with thermal behavior showed rate dependent hysteresis due to the competition between the driving and the relaxation rates [18]. Nguyen et al. [19] reported hysteresis phenomenon in Al_2O_3-water and CuO water nanofluids beyond a critical temperature which the particle suspension properties seem to be drastically altered. This critical temperature has been found to be strongly dependent on both particle size and concentration. Demirkır et al. [20] found that the graphene-water nanofluids with relatively higher particle concentration and at higher temperatures exhibit more pronounced shear thinning behavior in descending sweep rather than ascending ones, and thus showed hysteresis.

Conclusion

We have reviewed the experimental and simulation studied on rheological hysteresis in complex fluids. Hysteresis phenomena as a rate and time dependent relaxation time can be described by a measurement of flow curve in ascending and descending stress (shear) rate sweep and the local velocity profiles measurements. In addition, hysteresis is often also accompanied by the spatial heterogeneous flows such as shear banded or plug flows.

References

[1] McMillen E., Thixotropy and plasticity. iii—the effect of thixotropy upon plasticity measurements, *J. Rheol.*, **3**, 179, 1932.
[2] Labanda J. and Llorens J., A structural model for thixotropy of colloidal dispersions, *Rheol. Acta*, **45**, 305-314, 2006.
[3] Fourmentin M., Ovarlez G., Faure P., Peter U., Lesueur D., Daviller D., and Coussot P., Rheology of lime paste-a comparison with cement paste, *Rheol. Acta*, **54**, 647–656, 2015.
[4] Mendes R., Vinay G., Ovarlez G., and Coussot P., Reversible and irreversible destructuring flow in waxy oils: An MRI study, *J. NonNewton. Fluid Mech.*, **220**, 77–86, 2015.
[5] Adams J., Fielding S., and Olmsted P., The interplay between boundary conditions and flow geometries in shear banding: hysteresis, band configurations, and surface transitions, *J. Non-Newton. Fluid Mech.*, **151**, 101, 2008.
[6] Sollich P., Rheological constitutive equation for a model of soft glassy materials, *Phys. Rev.*, **E58**, 738, 1998.
[7] Stickel J.J., Knutsen J.S., and Liberatore M.W., Response of elastoviscoplastic materials to large amplitude oscillatory shear flow in the parallel-plate and cylindrical-Couette geometries, *J. Rheol.*, **57**, 6, 1569-1596, 2013.
[8] Visintin A., Rheological models and hysteresis effects, *Rend. Semin. Mat. Univ. Padova*, **77**, 213-243, 1987.
[9] Mewis J.and Wagner N.J., Thixotropy, *Adv. Colloid Interface Sci.*, **147–148**, 214–227, 2009.
[10] Divoux T., Tamarii D., Barentin C., and Manneville S., Transient Shear Banding in a Simple Yield Stress Fluid, *Phys. Rev. Lett.*, **104**, 208301, 2010.
[11] Divoux T., Grenard V., and Manneville S., Rheological Hysteresis in Soft Glassy Materials, *Phys. Rev. Lett.*, **110**, 018304, 2013.
[12] Larson R.G. and Y.Wei, A review of thixotropy and its rheological modeling, *J. Rheol.*, **63**, 477, 2019.
[13] Kanai H. and Amari T., Negative thixotropy in ferric-oxide suspensions, *Rheol. Acta*, **34**, 303-310, 1995.
[14] Zhu C., and Smay J.E., Thixotropic rheology of concentrated alumina colloidal gels for solid freeform fabrication, *J. Rheol.*, **55**, 3, 655–672, 2011.
[15] Radhakrishnan R., Divoux T., Manneville S., and Fielding S.M., Understanding rheological hysteresis in soft glassy materials†, *Soft Matter*, **13**, 1834–1852, 2017.
[16] Puisto A., Mohtaschemi M., Alava M.J., and Illa X., Consistency tests of classical and quantum models for a quantum annealer, *Phys. Rev. E*, **91**, 042314, 2015.
[17] Jamali S., Armstrong R.C., McKinely G.H., Multiscale Nature of Thixotropy and Rheological Hysteresis in Attractive Colloidal Suspensions under Shear, *Phys. Rev. Lett.*, **123**, 248003, 2019.
[18] Bertotti G. and Mayergoyz I., The science of hysteresis, Academic, New York, 2006.
[19] Nguyen C.T., Desgranges F., Galanis N., Roy G., Maré T., Boucher S., Angue Mintsa H., *Int. J. Therm. Sci.*, **47**, 103–111, 2008.
[20] Demirkır HE., A review of heat transfer deterioration of supercritical carbon dioxide flowing in vertical tubes: Heat transfer behaviors, identification methods, critical heat fluxes, and heat transfer correlations, *Int. J. Heat Mass Transfer*, **149**, 119113, 2020.

14-15 December 2021, Tehran, Iran
2nd International Conference on Rheology
ICOR 2021
article A-10-325-1

Synthesis of Rough Particles and Investigation its Rheological Behavior in a Newtonian Matrix

Sheyda Khazaee[1*], Fatemeh Goharpey[1], and Reza Foudazi[2]
1. Polymer and Color Engineering Department, Amirkabir University of Technology, Tehran, Iran
2. Chemical, Biological and Materials engineering, the University of Oklahoma, Norman, Oklahoma

*khazaeesheida2@gmail.com

Abstract
A reason for the recent surge of interest in studying the rheological behavior of rough particles in suspensions is that the proving of the relationship between shear thickening behavior and frictional contact among the particles due to the asperities on the surface of the particles. Surface roughness has emerged as an essential design parameter for the thickening response. For instance, one can increase the solid loading and delay undesired shear thickening by introducing a small number of particles displaying lower friction into the system be of interest for slurry processing, for example. Conversely, increasing surface roughness enables a significant reduction of the volume fraction, while retaining extreme thickening but having lower viscosities in the unthickened region of the flow curve, which could be of interest in fluid materials for vibration or impact absorption. In this project, we try to use different volume fraction of rough particles in dilute till concentrated suspension to calculate the critical shear stress in each volume fraction. And so in practical with tuning the roughness of the surface and its volume fraction, one can reach to the most proper behavior of the suspension.

Keywords: rough particles, colloidal suspension, frictional contact, rheology, shear thickening behavior

Introduction

Concentrated suspensions (volume fraction $\phi \geq 0.40$) have an essential contribution in a broad range of engineering applications and physical aspects, from past to present.
A number of researchers investigated the effect of particle surface roughness on the rheology of their suspension, by using a variety of rough particles.

Hsiao *et al*. [1] investigated the effect of roughness on the suspension shear thickening and dilatancy behavior by using PMMA particles with varying surface roughness length scales up to 10% of the particle radius. They use AFM equipment to characterized surface asperities. They observed that in smooth particle suspension, the critical shear stress is independent of ϕ and only in very large amounts of volume fraction and also shear rate the system shows a weak shear thickening. However with appearance of roughness on the surface, shear thickening behavior intensified and on the other hand critical shear stress in a certain amount of roughness decreases with increasing ϕ [2].

In this article, at first, we present a new method for synthesis of raspberry-like poly(styrene-*co*-acrylic acid)/ silica nanocomposite, then prepare dilute-concentrated suspensions of synthesized nanoparticles to investigate the effect of roughness on the rheology of the suspensions compared to a smooth one.

Experimental

Materials

Styrene (UN2055, Merck Co.) was passed through a column of basic alumina to remove inhibitor, poly(acrylic acid) (PAA, Merck) as an auxiliary monomer and stabilizer, potassium peroxydisulfate (KPS, Merck) as initiator, tetraethoxysilane (TEOS, 99.9%, Merck Co.) as a silica source, poly(ethylene glycol) (PEG400, Sinchem, South Korea) as continuum fluid, absolute ethanol (EtOH, 99.5%, Merck Co.) as a solvent, ammonia solution (25 wt% ammonia, Merck Co.) as a catalyst and deionized water were used without any further purification.

Synthesis of Smooth PS Nanoparticles

PS nanoparticles were synthesized by soap-free emulsion polymerization [3] For this goal, 15 g styrene monomer with 100 g deionized water was mixed in a 250 cc flask equipped with reflux system for 30 min. Then 1 g acrylic acid was added to the reactor, and the reaction was mixed for 30 min. At last the reactor was put in a 70 °C-oil bath and KPS solution (0.1 g KPS in 15 g water), was added to the reaction medium, simultaneously. The reaction had been completed in 24 h, and finally, poly(styrene-*co*-acrylic acid) latex was directly achieved.

Sol-Gel Process

The sol-gel process was used for coating the poly(styrene-*co*-acrylic acid) spherical nanoparticles with silica. 3 cc TEOS, 40 cc EtOH and 5 g PS latex were dispersed with a stirrer, and then 7 cc ammonia was added to the system to activate the hydrolysis reaction of TEOS. The hydrolysis-condensation reaction had been completed in 50 °C for 24 h, and after centrifuge the raspberry-like PS/SiO_2 nanoparticles were obtained.

Results and Discussion

FE-SEM and TEM images of synthesized raspberry-like silica nanoparticles with PS cores are shown in Fig. 1 with a average diameter about 500 nm.

In Fig. 2 as can be seen, in all samples in the volume fraction of about ϕ = 20%, almost quasi-Newton behavior can be seen. Only in the range of $10^{-3} < Pe < 10^{-1}$, due to some weak structures in the system, some discrepancies are observed in the diagrams. It is noteworthy that this amount of deflection increased in the quite rough sample, and also the flow curve shows a plateau at higher Pe. This behavior can be attributed to the presence of surface roughness resulting in more frictional contacts and more particles colliding with each other. On the other hand, in the volume fraction of ϕ = 34% in all samples, we see shear thinning in almost the entire range of Pe. Here it can be said that increasing the percentage of rough particles has

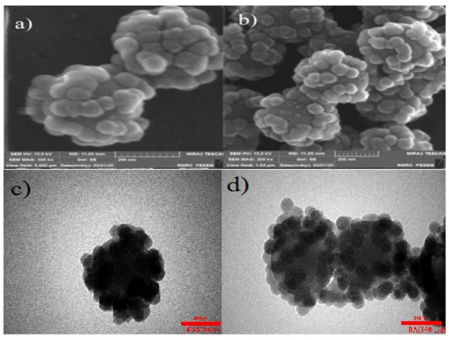

Fig. 1. (a, b) FE-SEM and (c, d) TEM images of images of synthesized nanoparticles. The scale bar is equal to 200 nm in all nanographs.

somewhat increased the viscosity of the system. In fact, in this percentage combination, with an increasing the percentage of rough particles in the system, the resulting structures become more robust, and this causes that by increasing the shear rate on the suspension, the structures are broken, and the shear thinning is somehow occur stronger in the system. In other words, in this case, it can be said that the hydrodynamic forces overcome the Brownian forces as well as the existing structures, leading to the arrangement of particle [4]. In this way, we see a decrease in the viscosity of the system. This behavior is seen in all samples with different shear rates, but in a perfectly smooth sample with relatively high Pe values, we see plateau in the diagram, while the occurrence of plateau in other samples is either not seen or it is minimalon. The other hand, fragile shear thickening behavior can be observed in 8/2 and quite rough samples. Therefore, it can be said that the presence of a high percentage of roughness in the system, leads to an increase in frictional contacts and thus increase energy loss in the system and consequently increase the viscosity in the system [5,6].

In the volume fraction of ϕ = 49% in all samples, at low Pe numbers, shear thinning behavior occurs without

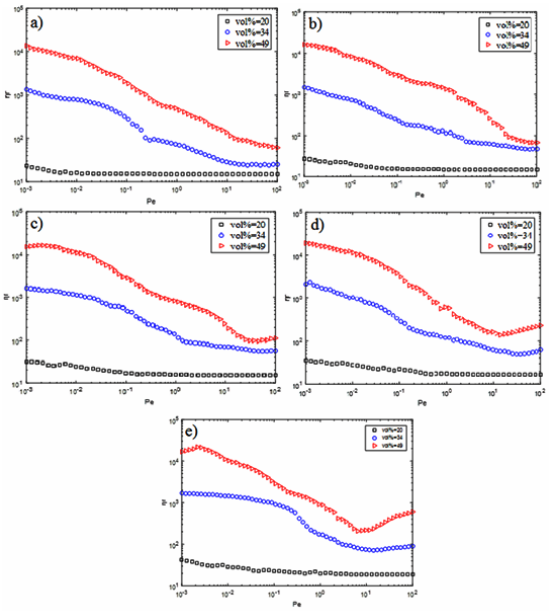

Fig. 2. Relative viscosity curve as a function of Peclet number for samples: (a) smooth, (b) 80/20, (c) 50/50, (d) 20/80, and (e) rough.

any constant viscosity at a low shear rate. However, with increasing the roughness percentage, from the sample 5/5-0.49 and above, the shear thickening behavior is seen. This behavior becomes more visible and intensified by increasing the percentage of rough particles.

In fact, as the percentage of roughness increases, the hydroclusters created by the particles, as a result of their solid-solid frictional contacts and the roughness of the surface particle, locking together and loss more of the shear stress in the system. It moves and thus further increases the viscosity of the system [7]. Although the shear thickening behavior also had be seen in samples containing a higher percentage of smooth particles, such as sample 5/5, this behavior can be more attributed to hydrodynamic forces in the system. The morphology of hard spherical suspensions in this area is in the form of hydrocluster. In this way, the fluid between the two particles is compressed due to the increase in hydrodynamic pressure. In this case, the lubricating forces are most significant and have brought the particles closer together. The resulting hydrocarbons have more stress and lead to energy loss or increased viscosity in the system. Therefore, in hard spheres, the formation of hydroclusters leads to shear thickening behavior without thixotropy and significant residuals [8,9], it can be concluded that surface roughness has also been effective in intensifying this behavior in addition to the effect of lubricating hydrodynamic forces [3,10].

References

[1] Hsiao L.C., Jamali S., Glynos E., Green P.F., Larson R.G., and Solomon M.J., Rheological state diagrams for rough colloids in shear flow, *Phys. Rev. Lett.*, **119**, 15, 1–6, 2017.

[2] Smith M.I., Besseling R., Cates M.E., and Bertola V., Dilatancy in the flow and fracture of stretched colloidal suspensions, *Nat. Commun.*, **1**, 8, 2010

[3] Pinto F. and Meo M., Design and manufacturing of a novel shear thickening fluid composite (STFC) with enhanced out-of-plane properties and damage suppression, *Appl. Compos. Mater.*, **24**, 3, 643–660, 2017.

[4] Jiang T. and Zukoski C.F., Role of particle size and polymer length in Rheology of colloid-polymer composites, *Macromolecules*, **45**, 24, 9791–9803, 2012.

[5] Tapia F., Pouliquen O., and Guazzelli É., Influence of surface roughness on the rheology of immersed and dry frictional spheres, *Phys. Rev. Fluids*, **4**, 10, 04302, 2019.

[6] Peters I.R., Majumdar S., and Jaeger H.M., Direct observation of dynamic shear jamming in dense suspensions, *Nature*, **532**, 7598, 214–217, 2016.

[7] Hsu C.P., Ramakrishna S.N., Zanini M., Spencer N.D., and Isa L., Roughness-dependent tribology effects on discontinuous shear thickening, *Proc. Natl. Acad. Sci. U. S. A.*, **115**, 20, 5117–5122, 2018.

[8] Maranzano B.J. and Wagner N.J., The effects of interparticle interactions and particle size on reversible shear thickening: Hard-sphere colloidal dispersions, *J. Rheol. (N. Y. N. Y).*, **45**, 5, 1205–1222, 2001.

[9] More R.V.and Ardekani A.M., Effect of roughness on the rheology of concentrated non-Brownian suspensions: a numerical study, *J. Rheol. (N. Y. N. Y).*, **64**, 1, 67–80, 2020.

[10] Hoyle C., Dai S., Tanner R., and Jabbarzadeh A., Effect of particle roughness on the rheology of suspensions of hollow glass microsphere particles, *J. Nonnewton. Fluid Mech.*, **276**, 2019, 104235, 2020.

14-15 December 2021, Tehran, Iran
2nd International Conference on Rheology
ICOR 2021
article A-10-328-1

Effects of Cellulose Nanowhiskers on Rheological Properties of Polycaprolactone/Poly(lactic acid) Cellulose Nanowhisker Composites

Golnaz Haghgoo and Amir Babaei*
Department of Polymer Engineering, Faculty of Engineering, Golestan University, Postal Code 15759-49138, Gorgan, Iran

*a.babaei@gu.ac.ir

Abstract
Cellulose nanowhisker (CNW) was used as a nanofiller in the polylactic acid (PLA)/polycaprolactone (PCL) blend prepared by the solution casting method. Its effect on the rheological properties of the blend was studied by rheological methods. 0.5 wt% of CNW had the highest effect on the rheological properties due to its good dispersion and network formation while 1 wt% failed due to agglomeration and network collapse.

Keywords: nanocomposite, rheology, cellulose nanowhisker, polycaprolactone, polylactic acid

Introduction

In recent years, CNW has attracted a lot of attention due to its good physicochemical properties and strength [1]. They were used as nanofillers to reinforce plastics and their application in biology is being researched thoroughly [2]. Rheology is an in-depth analysis method for investigating polymer blends and nanocomposites [3-6]. By using this method, rheological properties of PLA/PCL/CNW nanocomposites were studied in the linear region to analyze the effect of nanoparticles on the blend and their dispersion state. The results are shown in Figs. 1-3.

Experimental

Nanocomposite Preparation

CNW was first synthesized based on a method from another paper [7]. The synthesized nanoparticles were added to dissolved solutions of PLA/PCL (10 mg/mL) in 250 mL dimethylformamide (sigma) with respect to their specific weight percentage and were probe ultrasonicated for 10 min. Table 1 shows the composition of the prepared samples.

Results and Discussion

Fig. 1 shows the complex viscosity of the as-prepared samples. The addition of CNW resulted in an increase of complex viscosity for all the samples in all the frequencies. Between the samples, CNW-0.5 proved to be the most effective and also displayed a huge decrease in the low-frequency region which could be due to a network of nanoparticles [4-6] Meanwhile, CNW-0.25 had a decreased effect compared to CNW-0.5 which indicates its worse dispersion state and agglomeration. The storage modulus of the nanocomposites is shown in Fig. 2. These plots also agree with the findings for Fig. 1. The addition of CNW resulted in an increase of G′ for all the samples. Frequency independent behavior (indicated by the slope becoming lower) was also displayed in low frequencies which also implies the formation of a network for CNW-0.5 [3].

Han plot of the nanocomposites was also studied. The slope of the Han plot in the low frequencies usually

Table 1. Sample composition.

Sample	Composition
CNW-0	Pure PLA/PCL
CNW-0.25	PLA/PCL+0.25 wt% CNW
CNW-0.5	PLA/PCL+0.5 wt% CNW
CNW-1	PLA/PCL+1 wt% CNW

Table 2. Slope of Han plot

Sample	Slope
CNW-0	0.805
CNW-0.25	0.916
CNW-0.5	0.628
CNW-1	0.901

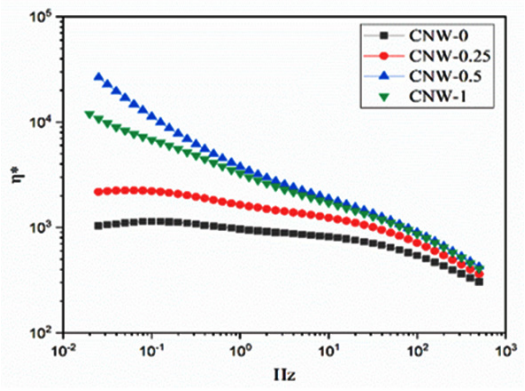

Fig. 1. Complex viscosity plot of the samples.

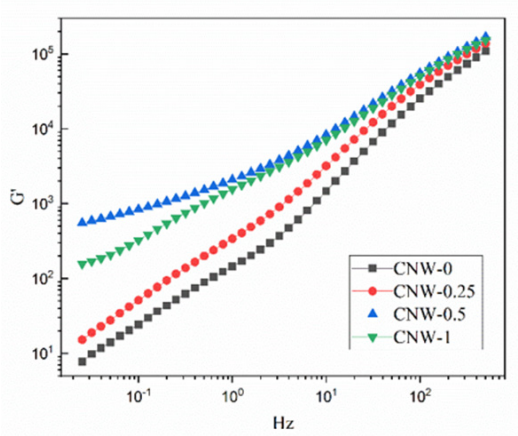

Fig. 2. Storage modulus plot of the blend and nanocomposites.

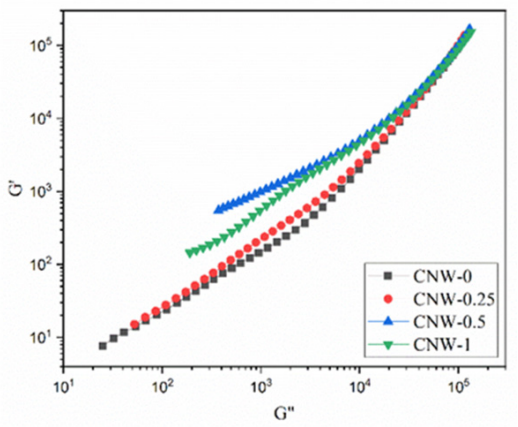

Fig. 3. Han plot of the prepared samples.

indicates whether the sample is homogenous or not (slope 2 for a homogenous polymer). CNW-0 itself is a blend that is given away here with its slope diverging from that of 2. The slope table for other samples is shown in Table 2. Interestingly, a peculiar trend for the slope can be seen in the table. Both the CNW-0.25 and CNW-1 generally showcase a more viscous response compared to the pure blend. This could be due to a bad dispersion state and more strengthening for one phase rather than both. However, CNW-0.5 shows a lower slope compared to the neat blend, indicating a more elastic response and the formation of a network-like structure [5,6].

This phenomenon could be due to a good dispersion state of this sample and more importantly, nanoparticles being placed in the interface of the two-phase and acting like a compatibilizer between them [8].

References

[1] Eichhorn S.J., Cellulose nanowhiskers: promising materials for advanced applications, *Soft Matter*, **7**, 2, 303-315, 2011.

[2] Dash R. and Ragauskas A.J., Synthesis of a novel cellulose nanowhisker-based drug delivery system, *RSC Adv.*, **2**, 8, 3403-3409, 2012.

[3] Noroozi N., Schafer L.L., and Hatzikiriakos S.G., Thermorheological properties of poly(ε-caprolactone)/ polylactide blends, *Polym. Eng. Sci.*, **52**, 11, 2348-2359, 2012.

[4] Dogan S.K., Reyes E.A., Rastogi S., and Ozkoc G., Reactive compatibilization of PLA/TPU blends with a diisocyanate, *J. Appl. Polym. Sci.*, **131**, 10, 2014.

[5] Gholizadeh A., Babaei A., and Ziaratban M., Analysis of dual role of nanographene on the microstructure-properties correlation of TPU/NG nanocomposite, *Polym. Adv. Technol.*, **32**, 3, 1150-1161, 2021.

[6] Ahmadzadeh Y., Babaei A., and Goudarzi A., Assessment of localization and degradation of ZnO nano-particles in the PLA/PCL biocompatible blend through a comprehensive rheological characterization, *Polym. Degrad. Stabil.*, **158**, 136-147, 2018.

[7] Capadona J.R., Shanmuganathan K., Trittschuh S., Seidel S., Rowan S.J., and Weder C., Polymer nanocomposites with nanowhiskers isolated from microcrystalline cellulose, *Biomacromolecules*, **10**, 4, 712-716, 2009.

[8] Walha F., Lamnawar K., Maazouz A., and Jaziri M., Rheological, morphological and mechanical studies of sustainably sourced polymer blends based on poly(lactic acid) and polyamide 11, *Polymers*, **8**, 3, 2016.

14-15 December 2021, Tehran, Iran
2nd International Conference on Rheology
ICOR 2021
article A-10-330-1

A Molecular Dynamic Simulation Study of the Rheological Behaviour Jamming in Densely Packed and Shear Thickening Shape Nanoparticles in Polyethylene Glycol

Mehdi Zojaji[1], Amir Hydarinasab[1*], Seyed Hasan Hashemabadi[2], and Milad Mehranpour[3]
1. Department of Chemical Engineering, Science and Research Branch, Islamic Azad University, Postal Code 1477893855, Tehran, Iran
2. CFD Research Laboratory, School of Chemical Engineering, Iran University of Science and Technology, Postal Code 16846-13114, Tehran, Iran
3. Department of Polymer Engineering, Science and Research Branch, Islamic Azad University, Postal Code 1477893855,Tehran, Iran
*a.heidarinasab@srbiau.ac.ir

Abstract
In this computational study, the effect of the shape of graphene oxide (GO) and SiO_2 nanoparticles on the shear thickening Behaviour of the fluids was reported with the molecular dynamics (MD) approach. For this purpose, the viscosity of fluids with C, Si, O, and H atomic arrangements was determined by Tersoff and Lenard-Jones (LJ) interatomic force fields. Atomic stability of the simulated structures was detected after 1.000.000 time-steps, demonstrating the validity of the PEG-400-based STF. Additionally, MD simulation results indicated that addition of zigzag GO and cubic SiO_2 nanoparticles to the pristine fluid would maximize the viscosity of this atomic structure. Numerically, by adding these nanostructures, the viscosity of the simulated fluid was converged to 88 and 94 Pa.s, respectively.

Keywords: shear thickening fluids (STFs), nanoparticle, jamming, rheology, molecular dynamics (MD)

Introduction

According to the reported description, MD simulations in this study were performed in two main steps [1]:

Step A: Initial PEG-400-based STF in the presence of GO and SiO_2 nanoparticles is simulated with UFF, DREIDING, and Tersoff force fields. After this process, simulated structures were equilibrated by the NPT ensemble for 100.000-time steps. For this purpose, the MD simulation was set at T=300 K, P=0 bar, and the atomic behavior of simulated structures was reported by the temperature and potential energy calculations.

Step B: Next, external tension was inserted into equilibrated structures by the NVE ensemble implemented in the MD simulation box. For the rheological study of defined atomic systems, physical parameters, such as viscosity and radial distribution function of the PEG-400-based STF, were reported. In this step of our computational study, the effects of a) shape of GO nanosheets, b) shape of SiO_2 nanoparticles on the PEG-400-based STF were reported.

Experimental

Simulation Method

In our MD simulations, Si, C, O, and H atoms interacted with each other for 3.000.000-time steps (Δt= 1 fs). This atomic process demonstrates the rheological behaviour of polyethylene glycol 400 -base fluid by adding GO and SiO_2 nanoparticles utilizing the Large Scale Atomic Molecular Massively Simulator (LAMMPS) software. Fig. 1 depicts polyethylene glycol 400 base fluid, GO, and SiO_2 nanoparticles in the simulation box. The atomic structures were visualized by Open Visualization Tool (OVITO) software [2,6]. This atomic structure size was 200 Å in x, y, and z directions. The periodic boundary conditions were used in x, y, and z directions [3,4]. Furthermore, GO nanosheets with armchair/zigzag edge added to pristine PEG 400 structure. The size of these nanosheets was identical, and their shape was square. Atomically, carbon atoms in these nanosheets were arranged in an ideal honeycomb lattice. Next, an NVT ensemble was used to equilibrate the system [5,7].

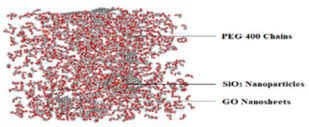

Fig. 1. Atomic structure of PEG 400-based STF with SiO_2 and GO nanoparticles.

Results and Discussion

Effect of GO Nanosheets Shape on the Viscosity of STFs

In this phase of the MD simulations, we study the effect of the GO nanosheets shape on the rheological behavior of the PEG-400-based fluid. For this purpose, GO nanosheets

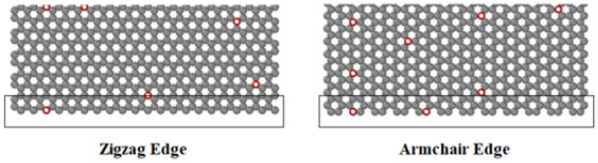

Fig. 2. Schematic of various edges in graphene-based (GO) nanostructures.

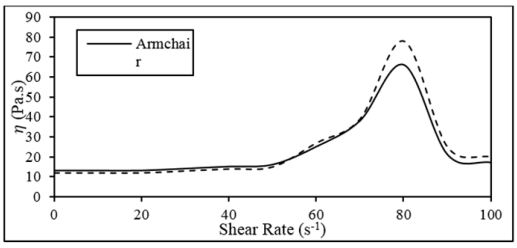

Fig. 3. The viscosity of PEG 400-based STF as a function of GO nano sheets type at T=300 K.

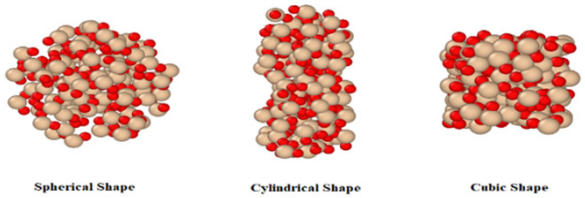

Fig. 4. SiO_2 nanoparticles with cylindrical, spherical, and cubic structures.

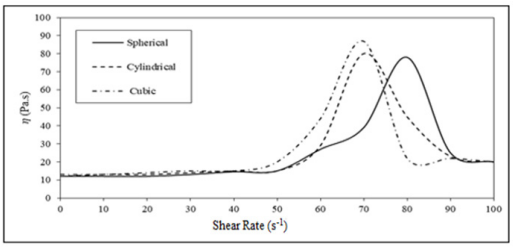

Fig. 5. Viscosity of PEG 400-based STF as a function of SiO_2 nanoparticles shape at T=300 K.

with armchair and zigzag edges in Fig. 2 (by a 5% atomic ratio) are added to the base fluid in the presence of 0.05% SiO_2 nanoparticles (see Fig. 3). For the rheological test's conductance, the external shear rate value inserted on fluids varied from 0 s^{-1} to 100 s^{-1}. This figure shows that the viscosity of the PEG-400-based STF reached its maximum value (78 Pa.s) adding the zigzag GO nanosheet. This rheological converges to 66 Pa.s. In the presence of armchair nanosheets. Such atomic behavior can be assigned to the higher mechanical strength of the zigzag GO compared to the armchair one.

Effect of SiO_2 Nanoparticles Shape on the Viscosity of STFs

In the final step of our MD study, we changed the shape of SiO_2 nanoparticles. To report SiO_2 nanoparticles shape effect on the rheological behavior of the pristine fluid, these nanoparticles were inserted into the pristine fluid with cylindrical, spherical and cubic shapes as depicted in Fig. 4. The results showed that the viscosity of fluid was maximized upon adding cubic Nanoparticles (see Fig. 5). Numerically, the jamming viscosity of STFs increased from 78 Pa.s to 87 Pa.s as the shape of nanoparticles changed from cylindrical to cubic. This atomic behavior can be assigned to a larger contact area between SiO_2 nanoparticles and the pristine PEG-400 fluid. Structurally, in cubic structures, the typical surface between the base fluid and nanoparticles reaches a maximum ratio.

Conclusion

This computational work investigated the effect of the shape of graphene oxide (GO) and SiO_2 nanoparticles on the rheological behavior of the PEG-400-based STF. According to our previous studies, DREIDING and Universal force fields can simulate shear-thickening fluids and correctly estimate their rheological behavior [1]. All atomic structures were simulated by the LAMMPS molecular dynamics package at T=300 K and P=1 bar. Moreover, in all simulated fluids, an external shear rate is implemented in the range of 5 s^{-1} to 55 s^{-1}. Then, the viscosity was reported after 2 ns to viscosity changes detection in the MD simulation box. The results can be summarized as follows:

A. UFF, DREIDING, and Tersoff interatomic force fields are the appropriate MD simulation functions of PEG-400-based STFs.

B. The shape of GO nanoparticles is an essential parameter in the rheological behavior of the PEG-400-based STF. Numerically, the optimization of this atomic parameter can increase the maximum viscosity of the pristine fluid to 78 Pa.s. In addition, the Darcy friction factor (fD) in simulated structures reaches 45 and 52 values for armchair and zigzag GO nanosheets.

C. By enlarging the GO nanosheets length from 10 Å to 50 Å, the maximum viscosity of PEG- 400-based STF varied from 78 Pa.s to 88 Pa.s.

D. PEG-400-based STF reached its maximum atomic viscosity (87 Pa.s) upon adding cubic SiO_2 nanoparticles.

References

[1] Zojaji M., Hydarinasab A., Hashemabadi S.H., and Mehranpour M., Rheological behaviour of shear thickening fluid of graphene oxide and SiO_2 polyethylene glycol 400-based fluid with molecular dynamic simulation, *Mol. Simulat.*, **47**, 4, 1-9, 2021.

[2] Haynes W.M., CRC Handbook of Chemistry and Physics, CRC , 2011.

[3] Liu A.J. and Nagel S.R., Jamming and rheology: constrained dynamics on microscopic and macroscopic scales, Taylor and Francis, 2001.

[4] Rapaport D.C. and Rapaport D.C.R., The art of molecular dynamics simulation, Cambridge University Press; 2004.

[5] Mayo S.L., Olafson B.D., and Goddard W.A., Dreiding: a generic force field for molecular simulations, *J. Phys. Chem.*, **94**, 8897-8909, 1990.

[6] Tersoff J., Modeling solid-state chemistry: interatomic potentials for multicomponent systems, *Phys. Rev. B.*, **39**, 5566-5568, 1989.

[7] Rappé A.K., Casewit C.J., Colwell K., Goddard III W.A., and Skiff W.M., UFF, a full periodic table force field for molecular mechanics and molecular dynamics simulations, *J. Am. Chem. Soc.*, **114**, 10024-10035, 1992.

14-15 December 2021, Tehran, Iran
2nd International Conference on Rheology
ICOR 2021
article A-10-331-1

Similarities in Electrical and Rheological Percolation of the Nanocomposites Comprising Hybrid of Nanoparticles

Mohammad Heydarnejad Moghadam* and Fatemeh Goharpey
Department of Polymer Engineering, Amirkabir University of Technology, P.O. Box 15875-4413, Tehran, Iran
*m.heydarnejad.moghadam@gmail.com

Abstract
The evolution of electrical conductivity and melt state storage modulus by increment in the weight percentage of nanoparticles is described by the scaling law of the percolation theory. Consistent with the percolation theory, the phenomenon transport experiences a sudden jump-like transition at the critical weight percentage of the percolation threshold and increases by power-law near the percolation threshold via a critical exponent. Herein, it is shown that the charge and mechanical load transport experience a similar percolation behavior due to the identical trend for percolation threshold and critical exponent, when the utilized nanoparticles are electrically conductive and mechanically stiff. Also, it was indicated that the composites of hybrid particles are more complex and more efficient than the composite of the single-kind nanoparticle. Interestingly, stitching hybrid components can make particles' networks extremely structured; however, it can also increase the percolation threshold.

Keywords: hybrid, percolation theory, electrical conductivity, linear rheology, critical exponent

Introduction

It is well known that the evolution trend of many phenomena such as electrical and thermal conductivity, Young's modulus, viscosity, storage modulus in melt state by the fraction of particles can be described by the percolation theory [1]. Percolation theory claims an exponential increment of phenomenon Φ by particle fraction of φ after a critical fraction of φ_c, percolation threshold, via an exponent t, critical exponent (Eq. (1)):

$$\Phi_\infty(\varphi-\varphi_c)^t \quad (1)$$

Both φ_c and t are under the impression of the microstructure of particles, and improvement in dispersion state leads to a decrement in φ_c, and exponent t is an indicator of the networks' dimensionality of particles [1]. Utilizing multi-walled carbon nanotube (MWCNT) and/or graphene for the fabrication of polymer nanocomposite makes the employment of percolation theory for the investigation of the contributor networks in electrical and rheological percolation feasible as a result of the conductive and stiff nature of these particles [2].

In this study, the electrical and rheological percolation of the polymer nanocomposites comprising MWCNT, graphene, and they physically mixed and chemically stitched hybrid of them are studied to a comprehensive insight of particles' microstructure is achieved.

Experimental

The styrene-*b*-(ethylene-*co*-butylene)-*b*-styrene (grade G-1652 Kraton) is used as the polymeric matrix in this study, and the nanocomposites containing octadecyl amine (ODA) modified MWCNT (NC7000 Nanocyl) and graphene (N002 PDR angstron) and their physically mixed hybrids are obtained by the solution casting method. Furthermore, the chemically stitched hybrid is obtained by stitching MWCNTs' ends to graphenes' edges via ethylene diamine through a nucleophilic substitution reaction. Nanocomposites samples nomenclature is presented in Table 1.

The AC conductivity measurements are done by an Autolab PGSTAT302N apparatus, and the nanocomposites' rheological behavior is tested by an Anton Paar Rheometer MCR 302. The values of the real part of AC conductivity and shear modules at the lowest frequency (1 and 0.007 Hz for ac conductivity and storage modulus, respectively) are used for percolation behavior studies.

Result and Discussion

Fig. 1 shows the FE-SEM images of the physically incorporated and chemically stitched hybrids of MWCNT and graphene and their corresponding nanocomposites. As is evident, in the case of in the physically-mixed hybrid, Graphenes are distinct from MWCNTs' bulk, and it is manifest that there is no junction amongst them (Fig. 1a). However, in the case of chemically stitched hybrid, a unified structure of MWCNT@graphene, where MWCNTs accompany the standing graphene, is visible (Fig. 1b). The unified and hierarchical structure of nanoparticles in

Table 1. Nanocomposites samples nomenclature.

Sample name	Fraction of MWCNT	Fraction of graphene	Type of hybrid's preparation
G-x	0	1	-
C-x	1	0	-
HG-x	1	3	Physically incorporated
HC-x	3	1	Physically incorporated
CHC-x	3	1	Chemically stitched

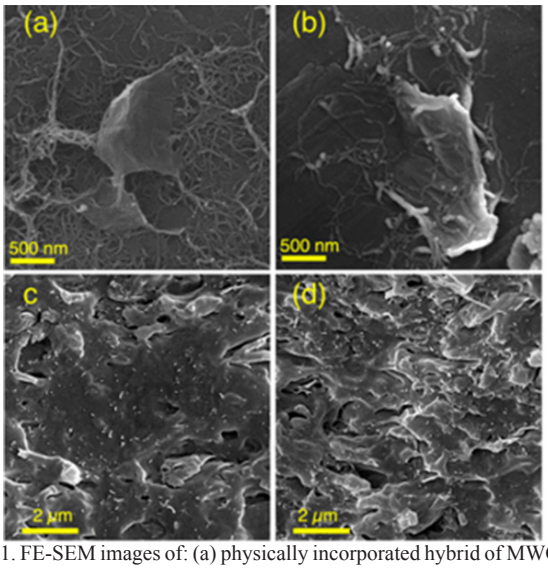

Fig. 1. FE-SEM images of: (a) physically incorporated hybrid of MWCNT and graphene, (b) chemically stitched hybrid of MWCNT and graphene, (c) HC-5, and (d) CHC-5.

chemically stitched hybrid causes an excellent dispersion in their nanocomposite, so in all parts of the image, MWCNTs and graphenes are present simultaneously, while in the nanocomposite of physically mixed nanoparticles, MWCNTs are accumulated in the central part of the image.

In continuation, the electrical and rheological percolation is investigated. Fig. 2a and 2b demonstrate the values of the real part of electrical conductivity and shear modulus at the lowest frequency of experiment versus weight fraction of the graphitic content of nanoparticles. The values of percolation threshold and critical exponent also are presented in Figs. 2c and 2d, respectively. First of all, the trend for percolation threshold is identical in σ' and G'; however, the values of the rheological percolation threshold are greater than the electrical percolation threshold, which is related to the fact that construction of a conductive path needs particles with about one-nanometer distance for electron tunneling while rheologically load carrier path needs about 50 nm particles' distance, scaled with the gyration radius of polymer chains. Also, as is

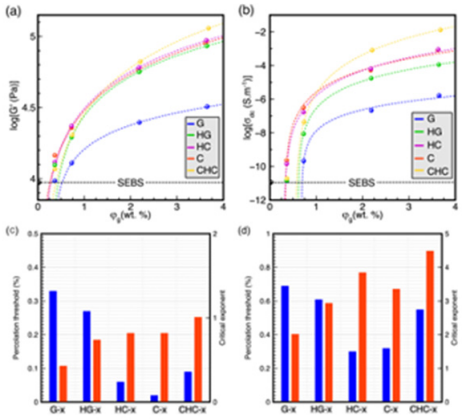

Fig. 2. Rheological (a) and electrical (b) percolation behavior of diverse nanocomposites and their corresponding fitting parameters in rheological (c) and electrical (d) percolation theory.

evident for both σ' and G', the percolation threshold of the C-x is lower than the G-x, indicating a higher capability of MWCNTs for making conductive pathways. Adding a minor part of an inhomogeneous nanoparticle and fabrication of hybrid samples can significantly decline the percolation threshold, attributed to the improvement in dispersion state. Contrary to HC-x, the percolation threshold of CHC-x is greater than C-x, which originates from the fact that MWCNTs are attached to the graphene sheets, and they act as selective clusters, which hindered their random distribution [3]. According to Figs. 2c and 2d, the trend for the critical exponent in electrical and rheological percolation is entirely identical. Similar to the percolation threshold, values of critical exponent for rheological percolation are less than electrical percolation. This unusual outcome is related to the polystyrene microdomains of SEBS, which act as reinforcing material, contributing nanoparticles in establishing the load carrier network. So, the role of nanoparticles in creating the load carrier network weakens, and critical exponent decreases. Another point that must be pointed here is the non-universal values (greater than 2.0) of electrical critical exponents. One of the reasons for this non-universality is the mechanism of charge transport on the molecular scale, which is quantum tunneling for nanocomposites of graphitic materials instead of the direct contact mechanism considered in the calculation of universal values based on percolation theory. Another reason for the values of critical exponent higher than universal values is the structured network of materials [4]. Hybrid samples are prone to create more structured networks than the composite of single-kind nanoparticles. The more structured network in hybrid samples is owing to the reduction in the inactive particles in the network. MWCNTs bridge among isolated graphene sheets and make them participate in the charge carrier network, and concurrently graphene sheets gather inactive and isolated MWCNTs in the conductive network. For the case of CHC-x, the conductive network is extremely structured, reflected from the huge decline in the inactive particles after stitching particles together.

Conclusion

Hybridization of inhomogeneous nanoparticles yields network structures with a high degree of dispersion and complexity, which makes them more efficient for reinforcement and charge conduction than the composite of single-kind nanoparticles.

References

[1] Sahini M. and Sahimi M., Applications of percolation theory, **242**, 3–4, 1st Edition, CRC, 1994.
[2] Du F., Scogna R.C., Zhou W., Brand S., Fischer J.E., and Winey K.I., Nanotube networks in polymer nanocomposites: rheology and electrical conductivity, *Macromolecules*, **37**, 24, 9048–9055, 2004.
[3] Yue L., Pircheraghi G., Monemian S.A., and Manas-Zloczower I., Epoxy composites with carbon nanotubes and graphene nanoplatelets-dispersion and synergy effects, *Carbon N.Y.*, **78**, 268–278, 2014.
[4] Yoonessi M. and Gaier J.R., Highly conductive multifunctional graphene polycarbonate nanocomposites, *ACS Nano*, **4**, 12, 7211–7220, 2010.

14-15 December 2021, Tehran, Iran
2nd International Conference on Rheology
ICOR 2021
article A-10-333-1

Peristaltic Transport of Solid Particles Suspended in a Viscoelastic Fluid: A Numerical Study

Mohammad Pourjafar[1*], B. Taghiloo[2], M. Ahmadi[2], A.R. Heidary[2], and Kayvan Sadeghy[2*]
1. Department of Mechanical Engineering, University of Tehran, P.O. Box 43841-119, Rezvanshahr, Iran
2. School of Mechanical Engineering, College of Engineering, University of Tehran, P.O. Box 14155-6619, Tehran, Iran
*sadeghy@ut.ac.ir

Abstract
Peristaltic transport of a circular rigid particle suspended in a viscoelastic fluid obeying Oldroyd-B model is numerically investigated in a planar two-dimensional channel using COMSOL software. For a rigid particle initially placed on the centerline of the channel, numerical results obtained on the basis of periodic boundary conditions suggest that, elastic stresses developed in a viscoelastic liquid has a retarding effect on the peristaltic transport of such solid particles. It is also concluded that smaller particle are more suitable than large particles for peristaltic transport when suspended in viscoelastic liquids. The results can be explained in terms of elastic stress developed in the liquid or on the surface of the particle.

Keywords: peristaltic, viscoelastic fluid, Oldroyd-B model, deborah number

Introduction

Peristaltic pumping is the nature's choice for fluid/particle transport in human body. One can mention, for example, transport of urine to the bladder through ureter (a 30-cm flexible tube) which is sometimes accompanied by kidney stones. The mechanism is also the basis of peristaltic pumps widely used in industry for the transport of slurries [1]. Recently, this mechanism have been used as micropump in microfluidic systems for the transport of physiological fluids and bio-particles [2,3]. Due to its unique features such as the fact that the fluid is not in direct contact with the rotary mechanism of the pump, this particular flow has been the subject of many studies in the past. As stands, we know almost everything about this flow, at least, for Newtonian fluids. For non-Newtonian fluids, there are still left much to be studied. For example, the effect of liquid's elasticity has not fully been addressed in the past. The present work tries to fill this gap in knowledge [4].

Mathematical Development

Fig. 1 shows a schematic of the flow geometry. It comprises two infinitely-extensible membranes which contains a rigid particle. We are assuming that there are a train of waves, and so only a single wave is considered for the analysis: The following waveforms are prescribed on the membranes at t = 0:

$$h_u = a + b\sin\left[(2\pi/\lambda)(x - ct)\right] \tag{1}$$

$$h_l = -a - b\sin\left[(2\pi/\lambda)(x - ct)\right] \tag{2}$$

Where, b is the wave's amplitude and c is wave speed. The liquid surrounding the particle is assumed to be viscoelastic and incompressible. Thus, the equations governing the flow are Cauchy equations together with continuity equation. Using appropriate scales for the length, time, velocity, pressure, and stress, in dimensionless form, the governing equations become:

$$\nabla \cdot \mathbf{u} = 0 \tag{3}$$

$$\mathrm{Re}\left(\mathrm{D}\mathbf{u}/\mathrm{D}t\right) = -\nabla p + \nabla \cdot \mathbf{T} + (1-\beta)\mathbf{d} \tag{4}$$

Where, u is the velocity vector, Re is the Reynolds number, T is the stress tensor, d is the rate-of-deformation tensor, and $\beta=\mu_s/\mu_p$ is the viscosity ratio, where subscript "s" refers to the solvent and subscript "p" refers to the polymer. For Oldroyd-B model, T is the total stress and we have: $T=T_s+T_p$ where the solvent is Newtonian and the polymeric stress obeys Maxwell model. In dimensionless form, the total stress satisfies the following equation:

$$\mathbf{T} + \mathrm{De}\overset{\nabla}{\mathbf{T}} = 2\beta\mathbf{d}. \tag{5}$$

Where, De is the Deborah number defined as: $De=\tau(c/a)$ where τ is the relaxation time. For the motion of the solid particle, we use rigid-body equations for its center of mass:

$$\vec{F}_s = \int_S d\vec{F}_s = M\left(d^2\vec{r}_{cm}/dt^2\right) \tag{6}$$

Where, F_s is the net surface force experienced by the particle, M is the mass of the particle, and r_{cm} is the location of the

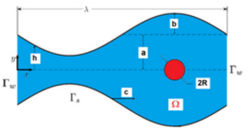

Fig. 1. Schematic showing the flow geometry on initial time.

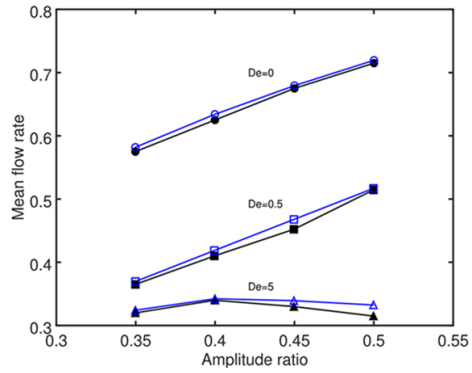

Fig. 2. Effect of Deborah number on the flow rate of Oldroyd-B liquid when subjected to peristaltic drive without particle when suspended in the liquid (α= 0.25, γ= 0.3, α= 0.5).

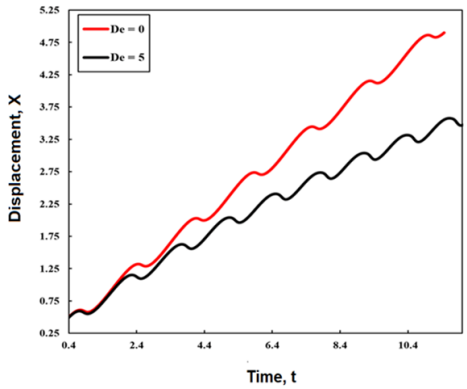

Fig. 3. Effect of Deborah number of the axial transport of a rigid particle in the course of time (α= 0.25, ϕ= 0.3, γ= 0.3, β= 0.5).

center-of-mass. To close the mathematical formulations, we need initial and boundary conditions. The boundary conditions needed to solve these equations are no-slip/no-penetration imposed on the walls and also the particle. We have also relied on periodic boundary conditions for all variables at inlet/outlet of the channel. As the initial condition, the fluid and particle are initially at rest. The flow is assumed to be occurring under creeping condition. We assume that the membranes are infinitely stretchable so that material points on the membranes move in the vertical direction only. We present our numerical results in terms of dimensionless numbers, which are:

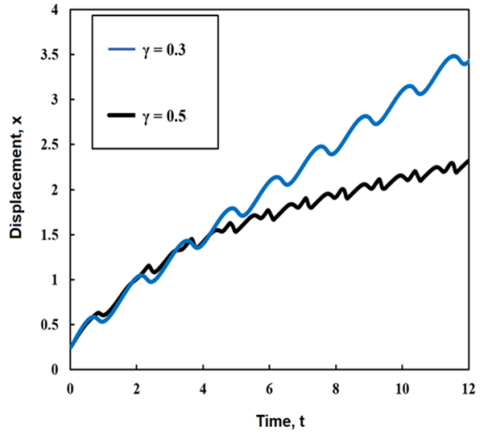

Fig. 4. Effect of particle size on its peristaltic transport when suspended in an Oldroyd-B liquid (α = 0.25, ϕ = 0.3, β = 0.5).

$$\alpha = a/\lambda,\ \varphi = b/a,\ \gamma = R/a \qquad (7)$$

Note that Re=ρca/(μ_s+μ_p) is assumed to be in creeping range. To solve these equations we employ the finite-element software COMSOL in moving-mesh mode. The code was verified using Newtonian results [3]. We fix the wavenumber and amplitude ratio and investigate the effect of De and γ. The flow of fluid and the motion of particle are both time-dependent, but they become periodic after a couple of periods.

Results and Discussion

Fig. 2 shows the effect of Deborah number on the time-averaged flow rate of the liquid with no particle present in the domain. This figure also includes numerical results reported by Chrispell *et al.* [4] (solid symbols) which were used for code-verification purposes. This figure clearly shows that elastic stresses developed in the liquid during its peristaltic motion have a retarding effect on its time-averaged flow rate. In fact, as can be seen in Fig. 3, these stresses also have a retarding effect on the axial transport of the particle. Fig. 4 shows that effect of particle size on its peristaltic transport. As can be seen in this figure, smaller particle move faster.

Conclusion

Based on the results obtained in this work, it can be concluded that elastic stresses developed in the bulk liquid and also on the surface of the particle has an impeding effect on the particle transport when propelled by peristaltic waves. The results also show that smaller particle are more suitable than large particle when immersed in a viscoelastic fluid and driven by peristaltic waves. The conclusion is that peristaltic mechanism is still a viable option for the transport of weakly elastic liquids with or without rigid particles suspended in the domain.

References

[1] Jaffrin M.Y. and Shapiro A.H., Peristaltic pumping, *Annu. Rev. Fluid Mech.*, **3**, 1971, 13–37.
[2] Taghiloo B., Pourjafar M., and Sadeghy K., On the use of peristaltic waves for the transport of soft particles: a numerical study, *Phys. Fluid*, **32**, 062108-20, 2020.
[3] Fauci L., A computational model of the fluid dynamics of undulatory and flagellar swimming, *Comp. Fluids*, **21**, 4, 583-598, 1992.
[4] Chrispell J. and Fauci L., Peristaltic pumping of solid particles immersed in a viscoelastic fluid, *Math. Model. Nat. Phenom*, **6**, 5, 67-83, 2011.

14-15 December 2021, Tehran, Iran
2nd International Conference on Rheology
ICOR 2021
article A-10-335-1

Rheology Provides Insight into Distinguishing between Unimodal and Bimodal Molecular Weight Distribution HDPE

Amir Malmir, Hossein Nazockdast*, and Fatemeh Goharpey
Department of Polymer Engineering and Color Technology, Amirkabir University of Technology,
P.O. Box 15875-4413, Tehran, Iran

*nazdast@aut.ac.ir

Abstract
In this work, the behavior of three HDPEs with different molecular weight distribution in the oscillation fields was investigated. In the low-frequency region, the difference between HDPEs can be observed. In addition, the relaxation time spectrum of them was calculated, and it shows difference between HDPEs in the long relaxation time region. besides, the molecular weight distribution of the HDPEs was estimated by generalized mixing rule. Consequently, it was observed that rheology could be used for distinguishing between Unimodal and Bimodal HDPEs.

Keywords: polyethylene, molecular weight distribution, relaxation time spectrum, shear flow

Introduction

Due to excellent processability, high chemical resistance, and good physical and mechanical properties, polyethylene holds the world's largest share in thermoplastic consumption. In addition, molecular structure and molecular weight distribution (MWD) of polyethylene determine processability in melt state and properties in solid-state. Nowadays, rheology and its results, because of high sensitivity to molecular structure, can be a powerful tool for investigating molecular structure and MWD. Static and dynamic shear flow use to characterize the viscoelastic properties of polymers. Concisely, transient shear and dynamic fields are more sensitive to molecular structure, and stress growth upon inception of steady shear and oscillation tests are typical for determining characteristics of polymers and nanocomposites.

In bimodal polyethylene, the chains with normal molecular weight (MW) determine processability, and the chains with very high molecular weight are used to improve properties. According to the previous research, bimodal PE can be similar to blends that include two types of polyethylene with unimodal MW. This blend was mixed in a unique way, and the compatibility of this blend can be investigated by rheology. The objective of this work is estimation the molecular structure and molecular weight distribution of three grades of polyethylene with different MWD.

Experimental

Materials

Three types of polyethylene as titled HMCRPE100, EX3 and 7000F that, respectively, produce in JAM, Amirkabir and Ilam petrochemical, are provided. Their characteristics is showed in Table 1.

Characterization

Rheological experiments were carried out by using a stress-controlled rheometer (MCR302, Anton Paar Physica) with a parallel-plate (25 mm diameter, 0.9 mm gap) system at temperature of 210 and 230 °C.

Table 1. Characteristic of the samples.

Commercial name	HMCPR100	EX3	7000F
Sample code	HDPE1	HDPE2	HDPE3
Density (g/cm^3)	0.957	0.945	0.97
MFI (g/10 min)	0.22	0.45	0.18

Results and Discussion

Fig. 1 illustrates the results of frequency sweep tests at small amplitude oscillatory (0.1%) and 210 °C. Generally, a decrease in frequency results in the enhancement of applied time. In neat polymers, chains in which the relaxation time is shorter than applied time can relax and not show any elastic response. Therefore, the low-frequency region is attributed to the chains or entanglements with a long relaxation time. According to Fig. 1a, HDPE3 shows independent behavior in the low-frequency region, which is a different response from other samples. Moreover, in Fig. 1b, HDPE3 demonstrates a broad deviation in high frequency in comparison to HDPE2. However, no deviation observes for HDPE1, and according to Time-Temperature Superposition, another test was carried out at

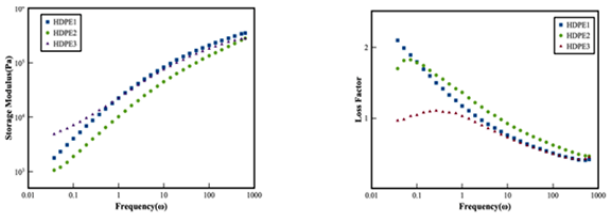

Fig. 1. (a) storage modulus versus frequency for the samples at 210 °C and (b) Loss factor versus frequency for the samples at 210 °C.

Table 2. Cross over details of the samples.

Samples	HDPE1	HDPE2	HDPE3
ω_c(rad/s)	2.3405	6.4387	1.2885
τ_d(s)	2.6845	0.9758	4.4864

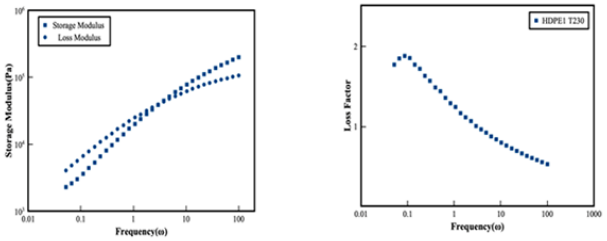

Fig. 2. (a) Storage modulus versus frequency for HDPE1 at 230 °C and (b) loss factor versus frequency for HDPE1 at 210 °C.

230 °C. In Fig. 2, similar behavior was observed in the low frequency at 230 °C, and this behavior will occur in the lower frequency at 210 °C. Hence, broad deviation in loss factor indicates that HDPE3 has uniform chains and other samples consist of two types of chains. In addition, HDPE1 contains chains with higher molecular weight compared to HDPE2 in the low-frequency region [1].

The cross over point indicates the reptation time of chains in the normal MW region, shown in Table 1. Based on the results, HDPE3 presents higher reptation time, demonstrating higher MW in the normal MW region. Relaxation time spectrum can be determined by viscoelastic properties obtained from oscillation test. The relation between frequency sweep test and relaxation time spectrum is shown in Eqs. (1) and (2). The calculated relaxation time in Fig. 2 shows that HDPE1 and HDPE3 have the highest and the lowest number of chains in the long relaxation time region, respectively.

The estimation of molecular weight distribution is presented in Eq. (3). G(t) is relaxation modulus, F is an integral kernel, m is the normalized molecular weight, and B is the donated generalized mixing parameter. The value of B in the linear mixing rule is 1 and in the quadratic mixing rule is 2 [2]. According to Eq. (4), G_0^N is plateau modulus that g_0 is a numerical factor, ρ is density, R is the gas constant, and T is the absolute temperature.

It seems that the plateau modulus is an intrinsic property and independent of the total number of entanglements per chain. Eqs. (5) and (6) make a relationship between relaxation modulus and storage and loss modulus [3].

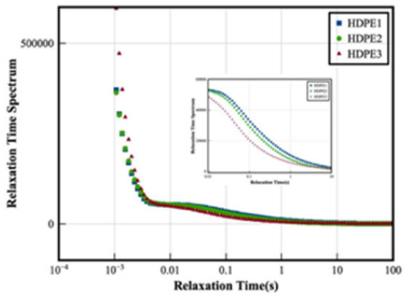

Fig. 3. Calculated relaxation time spectrum versus relaxation time for the samples.

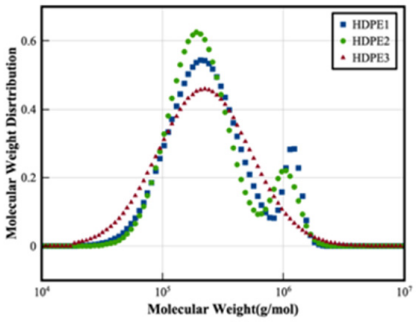

Fig. 4. Calculated molecular weight distribution versus molecular weight for the samples.

The Calculated molecular weight distribution in Fig. 4 indicates that the MWD of HDPE1 and HDPE2 is bimodal, whereas HDPE3 has broad unimodal MWD. In addition, in the very high MW region, HDPE1 has a higher molecular weight as a comparison to HDPE2.

Conclusion

The rheological behavior of three polyethylene with different MWD in the shear flow shows that HDPE3 has uniform chains, and others consist of two types of chains. In other words, HDPE3 has broad unimodal MWD whereas HDPE1 and HDPE2 have bimodal MWD, and in the high molecular weight region, HDPE1 has higher MW compared to HDPE2.

Equations

$$G'(\omega) = \int_0^\infty h(\tau) \frac{\omega^2\tau^2}{1+\omega^2\tau^2} \frac{d\tau}{\tau} \quad (1)$$

$$G''(\omega) = \int_0^\infty h(\tau) \frac{\omega\tau}{1+\omega^2\tau^2} \frac{d\tau}{\tau} \quad (2)$$

$$\frac{G(t)}{G_0^N} = \left(\int_{M_e}^\infty F^{\frac{1}{B}}(t, m) \frac{W(m)}{m} dm \right)^B \quad (3)$$

$$G_0^N = \frac{g_0 \rho RT}{M_e} \quad (4)$$

$$G'(\omega) = \omega \int_0^\infty G(t) \sin(\omega t)\, dt \quad (5)$$

$$G''(\omega) = \omega \int_0^\infty G(t) \cos(\omega t)\, dt \quad (6)$$

References

[1] Chaudhuri K. and Lele A.K., Rheological quantification of the extent of dissolution of ultrahigh molecular weight polyethylene in melt-compounded blends with high density polyethylene, *J. Rheol. (N. Y. N. Y)*, **64**, 1, 1–12, 2020.

[2] Thimm W., Friedrich C., Marth M., and Honerkamp J., An analytical relation between relaxation time spectrum and molecular weight distribution, *J. Rheol. (N. Y. N. Y)*, **43**, 6, 1663–1672, 1999.

[3] Talebi S., Duchateau R., Rastogi S., Kaschta J., Peters G.W.M., and Lemstra P.J., Molar mass and molecular weight distribution determination of UHMWPE synthesized using a living homogeneous catalyst, *Macromolecules*, **43**, 6, 2780–2788, 2010.

14-15 December 2021, Tehran, Iran
2nd International Conference on Rheology
ICOR 2021
article A-10-336-1

Rheology and Morphology of Dynamically Vulcanized Poly(lactic acid)/ Polyurethane (PLA/PU) Blend in Presence of Nanoparticles

Salar Haghjoo[1], Jafar Khademzadeh Yeganeh[1*], and Ismaeil Ghasemi[1,2]
1. Department of Polymer Engineering, Qom University of Technology, Postal Code 3716146611, Qom, Iran
2. Iran Polymer and Petrochemical Institute, Postal Code 13115-14977, Tehran, Iran

*jkh.yeganeh@gmail.com

Abstract
The presented research reports preparation of tough PLA/PU blend using simultaneous peroxide (BIPB)-induced dynamic vulcanization and addition of hydrophobic spherical silica nanoparticles (NPs). NPs were localized mainly in the PU droplets and at the interface where a layer of particles was formed with a small amount dispersed in the PLA matrix. The incorporation of NPs or BIPB induced compatibilization, causing a drastic decline in the size of PU droplets in addition to improving the interfacial adhesion. The effect of BIPB and NPs on the microstructural properties of the sample was investigated through rheological evaluations.

Keywords: poly(lactic acid), polyurethane, dynamical vulcanizate, nanocomposites

Introduction
As a biodegradable polymer, poly(lactic acid) (PLA) has been benefited from various advantages such as excellent biocompatibility, ease of processability, high modulus and mechanical strength compared to the conventional polymers, bio-based nature, and excellent transparency which have introduced it as a promising alternative to petroleum-based polymers. However, PLA suffers from inherent brittleness, which has limited its widespread commercial applications. Blending with a rubbery polymer is the most convenient, economic, and efficient method to toughen the PLA. The object of this study is to prepare toughened PLA/PU blend by simultaneous dynamic vulcanization and NPs addition.

Experimental
PLA (2003D, D-isomer content of about 4%) was supplied from NatureWorks®, USA. PU (Desmopan 385S) was supplied from Bayer. Aerosil R805, with a hydrophobic surface supplied by Degussa Corp. Bis(t-butylperoxy isopropyl)benzene (BIPB) was supplied by Rhein Chemie. The melt blending approach was adopted to obtain the specimens using a lab internal mixer (Brabender Plasticator, Germany) at 200 °C and a rotor speed of 80 rpm for 12 min.

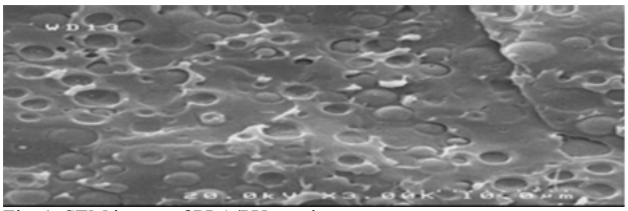
Fig. 1. SEM image of PLA/PU specimen.

Results and Discussion
SEM
Scanning electron microscopy (SEM) was performed to investigate the morphology of the samples (Figs. 1, 2, and 3). As anticipated, PLA/PU (75/25) sample showed a droplet-matrix morphology in which, PLA was the matrix. The blend exhibited a well-distinguished interface and large PU droplets and the cavities caused by interfacial debonding were visible (Fig. 1). This indicates an incompatible polymer blend leading to weak interfacial adhesion between the phases. After incorporating NPs or BIPB the size of PU droplets was greatly decreased and the interfacial adhesion improved (Figs. 2 and 3).

TEM
To explore the exact location of nanoparticles, TEM analysis was employed. NPs are mainly localized in the PU droplets and at the interface (Fig. 4).

Rheological Behavior
Fig. 5 shows storage modulus G'as a function of frequency for PLA/PU blend with and without nanoparticles. The neat PLA/PU blend exhibited terminal behavior with the scaling properties of approximately $G' \propto \omega^2$ which

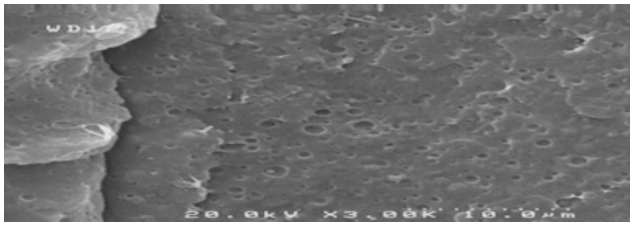
Fig. 2. SEM image of PLA/PU/BIPB specimen.

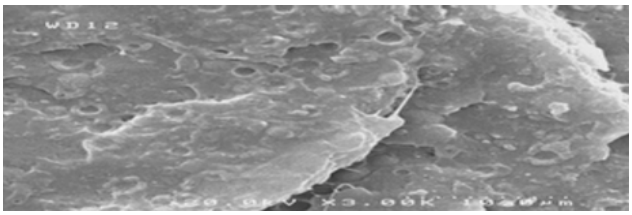

Fig. 3. SEM image of PLA/PU/R2 specimen.

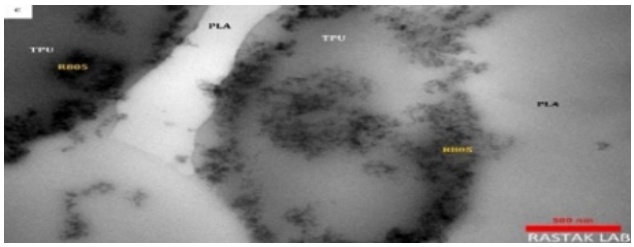

Fig. 4. TEM image of PLA/PU/R5 specimen.

exhibited a shoulder at the storage modulus which can be attributed to the contribution of the interface to the blend elasticity and the shape relaxation of the PU droplets in the PLA matrix [1]. It can be seen that the addition of 2 wt% nanoparticles sharply enhanced the low-frequency modulus and the slope of the G' curve considerably decreased (nonterminal behavior). At low NP contents and low frequencies, the sample behavior is controlled by the particle-induced changes in polymer chain dynamics. Thus, the large-scale polymer relaxations in the nanocomposites will be efficiently restrained at the presence of the NPs which prevented the viscous flow of molecular chains and also enhanced the elastic response. This indicates a favorable interaction between nanoparticles and PLA matrix. Furthermore, in polymer blends, the elasticity of the interface contributed to the overall elasticity at low frequencies. According to SEM images, the decrease of droplet size and improved interface upon NPs introduction enhanced the modulus. However, at nanosilica loadings of 5 wt% and higher, the low-frequency storage modulus was considerably enhanced and became almost independent of frequency (a plateau is observed). This is indicative of solid-like viscoelastic behavior implying that the nanosilica has formed a percolated network which spanned the sample and restrained the long-range motion of

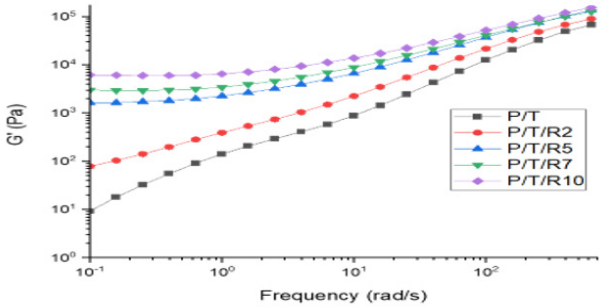

Fig. 5. Storage modulus as a function of frequency for PLA/PU blends with and without nanoparticles.

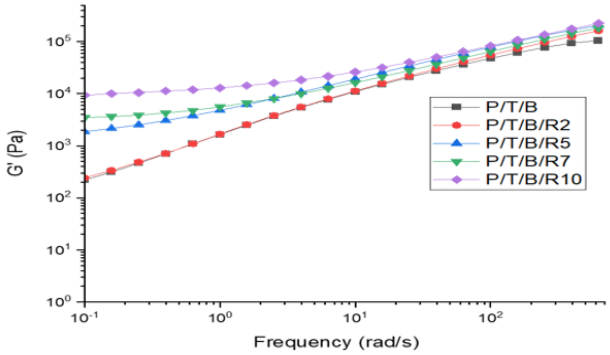

Fig. 6. Storage modulus as a function of frequency for dynamically vulcanized PLA/PU blends with and without nanoparticles.

polymer chains. Besides, the compatibilization effect of nanoparticles induced high interfacial area which increased dynamic moduli at low frequencies. At high frequencies, storage modulus was also enhanced suggesting short-range dynamics of polymer chains is restricted especially in the entanglement length scales [2]. Figure shows the dynamic moduli of the nanocomposite in presence of BIPB. Through comparison of Figs. 5 and 6, it can be seen that adding BIPB enhanced the dynamic moduli. This indirectly confirms dynamic vulcanization in the samples.

Conclusion

In this study, we prepared toughened PLA/PU blend by simultaneous dynamic vulcanization and the addition of nanoparticles. The incorporation of NPs and BIPB both induced compatibilization, subsequently the size of PU droplets was greatly decreased and the interfacial adhesion improved. On the other hand, simultaneous dynamic vulcanization and NPs addition exhibited a synergistic effect on the compatibilization of PU and PLA phases. The effect of BIPB and NPs on the microstructural properties of the samples was investigated through rheological evaluations.

References

[1] Khademzadeh Yeganeh J., Goharpey F., and Foudazi R., Rheology and morphology of dynamically asymmetric LCST blends: polystyrene/poly(vinyl methyl ether), *Macromolecules*, **43**, 20, 8670-8685, 2010.

[2] Moradi S. and Yeganeh J.K., Highly toughened poly(lactic acid)(PLA) prepared through melt blending with ethylene-*co*-vinyl acetate (EVA) copolymer and simultaneous addition of hydrophilic silica nanoparticles and block copolymer compatibilizer, *Polym. Test.*, **91**, 106735, 2020.

14-15 December 2021, Tehran, Iran
2nd International Conference on Rheology
ICOR 2021
article A-10-337-1

Evaluation of Printability of Carbon-Based Nanocomposite Samples Using Rheological Study

Amirreza Eftekhari[1*], Fatemeh Goharpey[1], and Milad Mehranpour[2]
1. Department of Polymer Engineering, Amirkabir University of Technology, P.O. Box 15875-4413, Tehran, Iran
2. Islamic Azad University, Science and Research Branch, Postal Code 1477893855, Tehran, Iran

*a.eftekhari@aut.ac.ir

Abstract
The purpose of this project is to investigate of the rheological properties for 3D printing of ABS-based systems and carbon nanoparticles including Nano carbon black and carbon nanotubes. The current evaluated hybrid system is more competitive compared to its CNT-based counterparts in terms of Economical aspects. FESEM images also present an acceptable dispersion of nanoparticles with desired rheological properties. The results extracted from the frequency sweep test indicate the development of a three-dimensional physical network of nanoparticles in the printed nanocomposites due to the extended frequency-independent (non-terminal) behavior for the storage modulus. It should be noted that these hybrid samples affect the complex viscosity trend less than that of CNT-based systems, which leads to better printability and prevent nozzle blockage. Also, considering the importance of elongation viscosity in the 3D printing process, the rheological behavior under the extensional field was investigated.

Keywords: conductive nanocomposites, carbon nanotubes (CNT), carbon black (CB), ABS, 3D printing, fused deposition modeling, rheology

Introduction

ABS, with easy processability, toughness, good dimensional stability, and also optimal chemical resistance, has been considered. Due to its good flexibility; ABS has a wide range of applications, including automotive, home appliances, and electronic parts [1]. FDM technology in 3D printing makes it possible to create electronic kits and sensors by adding small amounts of carbon nanoparticles. Since this material is a complex random copolymer made up of SAN copolymer and PB rubber phase (island-sea structure), it is important to study the rheology of this system. melt flow study is a key index in preparation of samples containing nanoparticles, so that flow obstruction in the nozzle causes poor printing and surface roughness [2]. That is why studying rheology is of increasingly importance. Rheological evaluation provides the ability to optimize nanoparticles dispersion and viscosity behavior. In this study, the optimal print was evaluated using shear and extensional mode tests.

Experimental

Materials

Acrylonitrile-butadiene-styrene (ABS) was supplied by Tabriz Petrochemical Co, Iran (SD150), the carbon nanotubes used in This Study were commercially available as multiwall carbon nanotubes (MWCNTs), NC7000, from Nanocyl Inc., Belgium. The multiwall had a carbon purity of 90%, average outer diameter of 9.5 nm, length up to 1.5 µm, and surface area of 250-300 $m^2.g^{-1}$. Commercially available super conductive carbon blacks, Ketjen Black EC 300 J were supplied by Lion Specialty Chemicals Co., Japan. Carbon black had a DBP absorption 360 $cm^3/100$ g and BET surface area 800 $m^2.g^{-1}$. Dichloromethane (DCM) and chloroform were purchased from dr. Mojallali Inc., Iran.

Preparation of Nanocomposites

Solution method was applied to prepare the masterbatch of nanocomposites. Then the masterbatch was added to neat ABS in Twin Screw Extruder Brabender DSE20 (L/D=40) at 230° and screw speed of 150 rpm and the

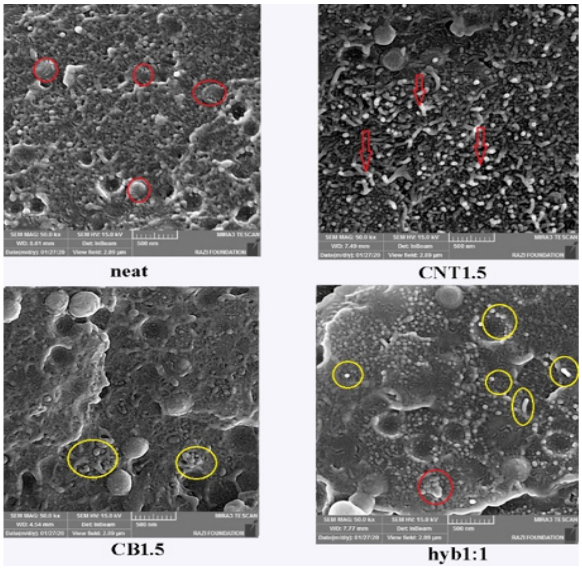

Fig. 1. FESEM images with 500 nm magnification: (a) neat sample, (b) sample containing 1.5% CNT, (c) sample 1.5% CB, and (d) sample contacting 0.75% CB and 0.75% CNT.

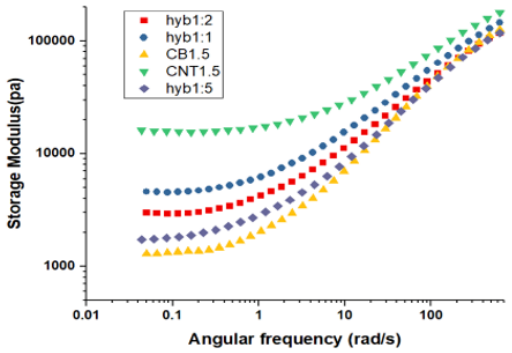

Fig. 2. Variation of a storage modulus of nanocomposites with 1.5% nanoparticles versus frequency.

nanocomposites achieves the desired percentages. The Production of filaments with 1.75±0.05 mm dimeter was done by single screw extruder (Noztek).

Results and Discussion

Fig. 1 shows the FESEM images of fracture surfaces of samples. The droplet-matrix morphology is clearly visible in neat sample. In Fig. 1b, CNT nanoparticles like worms and in Fig. 1c, CB nanoparticles are visible as aggregate, which is inevitable due to the small size of CB nanoparticles. Finally, CB aggregate and individual CNT nanoparticles can be seen in figure 1.d. In the frequency sweep test (Fig. 2) according to the FESEM image, a pure sample showed non-terminal behavior. In a sample containing 1.5% CB, a slight change in the storage modulus is observed compared to the 1.5% CNT sample, which is attributed to the unfavorable dispersion of nanoparticles. In the 1.5% CNT sample, the storage modulus distanced itself from the loss modulus, indicating solid like behavior. It should be noted that the unfavorable dispersion in the CB1.5 sample caused a rough surface in the printed sample, and also the printing of the CNT1.5 sample was not successful due to the nozzle blockage. The reason is the highly elastic behavior and high viscosity of the sample. Hybrid samples were prepared by replacing the amount of CB nanoparticles with CNT. By increasing the percentage of CNT nanoparticles in these samples, the storage modulus is significantly affected. However, this increase in the storage modulus of the hyb1: 1 sample is about one-third of the CNT1.5 sample, which is an advantage for 3D printing applications. Then, due to the existence of the extensional flow field in the convergent part of the nozzle and a more detailed study of the printing process, the elongation viscosity behavior was investigated [3]. The results of this test show the strain hardening behavior for all samples, which indicates the resistance of the elastic behavior of the material to extension. The maximum limit of strain hardening behavior is observed in the CNT1.5 sample, which is one of the main reasons for the interruption of printing process in this sample. On the other hand, with increasing printing speed, this behavior occurs quicker and with more slope, which leads to undesirable printing and rough surface (Fig. 3).

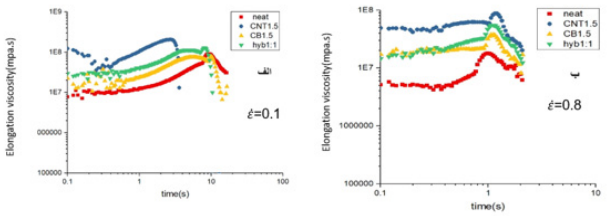

Fig. 3. Elongation viscosity versus time at two different extension rate.

Conclusion

Rheology provides a powerful tool to evaluate the nanoparticle dispersion state through a polymeric matrix. In this study, in order to evaluate the three-dimensional network of nanoparticles, a frequency sweep test was performed. No significant amount of storage modulus and time-independent behavior was observed. Also, the results of elongation viscosity test in this regard showed the strain hardening behavior; which was the maximum value in CNT1.5 sample and proves the non-printability of this sample. The hyb1:1 sample has a lower print modulus and also a lower viscosity than the CNT1.5 sample. This hybrid sample has desirable properties and is cost effective.

References

[1] Wyzgoski M.G., Acrylonitrile-Butadiene-Styrene, **1**, 241–243, 1974.

[2] Gnanasekaran K. et al., 3D printing of CNT- and graphene-based conductive polymer nanocomposites by fused deposition modeling, *Appl. Mater. Today*, **9**, 21–28, 2017.

[3] Mackay M.E., The importance of rheological behavior in the additive manufacturing technique material extrusion, *J. Rheol. (N. Y. N. Y).*, **62**, 6, 1549–1561, 2018.

14-15 December 2021, Tehran, Iran
2nd International Conference on Rheology
ICOR 2021
article A-10-338-1

Dynamic Mechanical and Rheological Properties of Liquid Crystal Elastomers Prepared via Thiol Acrylate Michael Addition Reaction

Parmida Harirchi, Mahshid Fallah-Darrehchi, and Payam Zahedi*
Nano-Biopolymers Research Laboratory, School of Chemical Engineering, College of Engineering, University of Tehran, Postal Code 1417935840, Tehran, Iran

*phdzahedi@ut.ac.ir

Abstract
Liquid crystal elastomers (LCE) as newly developed stimuli-responsive materials with combined properties of orienntational order of liquid crystals and elasticity of amorphous elastomers leading to reversible shape change (RSC) property which motivating factor simulate efficient system for artificial muscles. Moreover, fiber spinning of LCEs is problematic issue due to their low Mw and necessity of crosslinking reaction. The main reason for appearance of RSC property along with actuation-active properties, two stages of crosslinking is required. In this line, we provided LCE thin films by thiol-acrylate Michael addition (TAMA) reaction to evaluate fiber production feasibility. Therefore viscoelastic response of LCE samples after first stage of crosslinking and dynamic-mechanical behavior after second stage of crosslinking was evaluated. The results showed in LCE1 (PETMP:EDDET=50:50) specific structure has formed during 60 min and strain failure and fixity reached highest amount indicating that this sample could be suitable candidate for production of LCE-based fibers.

Keywords: liquid crystal elastomer, mesogen, rheology, TAMA, cross-linker

Introduction

Liquid crystal elastomers (LCEs) are the new class of responsive polymeric materials, possessing entropic elasticity combined with liquid crystal (LC) order. LCEs are responsive to various actuators including: mechanical stress, temperature variation, magnetic or electrical fields. One of the main reason of conspicuous physical properties appearance related to presence of mesogenic units into the polymeric chains as functional group or through the polymer backbone in the exposure of external stimuli. In fact, mesogens are the solid segments enabling polymeric chain parallel to a direction in which majority of LC units tend to reorient called director vector leading macroscopic shape changes at transition temperature (nematic↔isotropic, Tni) [1]. LCEs possess reversible shape change (RSC) feature without mechanical bias or specific environment. due to two-step crosslinking process. in the first step lightly cross-linked network during the polymerization and in the second, photo-initiated crosslinking process along with induced molecular patterning by utilization of mechanical loading or magnetic fields orientation of LCEs' chains. As the suitable balance of crosslink density in both steps lead to appear RSC property of LCEs which is the base of mimicking the muscular tissue. fibrillary topology of muscle structure motivated the researchers to fabricate micro-scale fibrous LCE via melt-spinning, electrospinning, microfluidic devices and direct ink writing) [2,3]. In all the above methods, lightly cross-linked LCE is injected through the patterned nozzle followed by photo-initiated crosslinking reaction. Therefore, the rheological properties of LCE should be determined to avoid morphological and rheological instabilities. The aim of this project is to synthesis of LCE by thiol acrylate Michael addition reaction accepted to click chemistry and possess high yields stereoselectivity, high rate, and room temperature cure system to evaluate their properties to evaluate rheological properties as contractile shape memory fibrils to mimic muscular tissues [4].

Experimental

In order to prepare LCE samples RM257 as mesogenic monomer was purchased from Wilshire Technologies, USA. 2,2'-(Ethylenedioxy) diethanethiol (EDDET) and Pentaerythritoltetra (3-mercaptopropionate) (PETMP) as crosslinking agent was provided from Sigma-Aldrich Co., (pilsburg, The Netherland). Dipropylamine (DPA was supplied from Merck Co., Germany. All the other chemicals were analytical reagent grades and were used without further purification.

To synthesize the three LCE samples which were different in terms of EDDET: PETMP molar ratio, firstly weighted monomer into the toluene was heated at 80 °C for 5 min. Afterwards, the stoichiometry amount of

Table 1. The amounts of mesogenic monomer and PETMP: EDDET for preparation of LCE samples.

Sample	RM 257	PETMP: EDDET
LCE_1	0.5	50:50
LCE_2	0.5	75:25
LCE_3	0.5	100:0

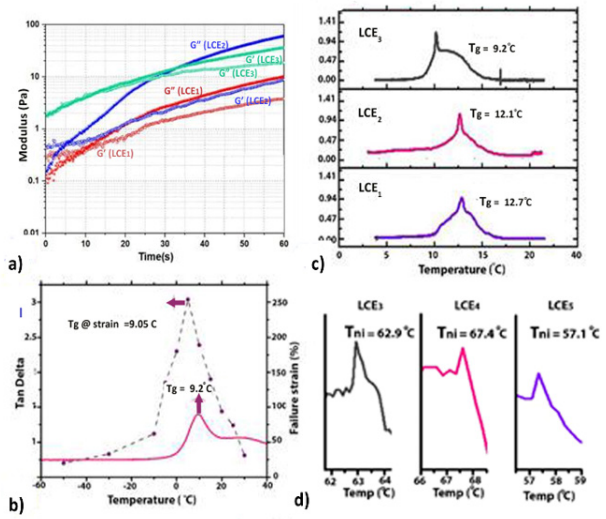

Fig. 1. (a) Storage and loss moduli of LCE samples, (b) strain failure vs temperature for LCE_1, (c) indication of Tg, and (d) Tni for LCE samples by DMTA test.

EDDET and PETMP was added to the monomer mixture according to the Table 1. Then diluted DPA in toluene was added to the container to accelerate TAMApolymerization procedure mounting 0.1% mole of RM257.

Results and Discussion

A rheometer (Anton Paar, Physica MCR 300) was used for all rheology data cone and plate geometry. After adding the PETMP storage and loss moduli as a function of time were obtained under oscillation with a strain of 3% and the frequency or 2 Hz for 1 h. As expected (Fig. 1a) the G' curves for all three specimens is lower than the G" curves, indicating that no cross-links are formed in 60 min. By setting the aliphatic spacer next to the cross-linker, intensification (increase of slope) of the curves was observed, which indicates the special structure. Also, all samples had a structure and this structure disappears under shear and time.

To evaluate RSP property of samples six samples (two samples from each one) subjected to 100 and 200% strain at the speed of 0.2 mm/s were used. The samples were irradiated with 265 wavelengths of UV light during the extension for 7 min. Then the fixity parameter illustrating the RSC feature, was calculated by Eq. (1) given tin Table 2:

$$\text{Fixity}(\%) = \frac{\varepsilon_{\text{fixed}}}{\varepsilon_{\text{applied}}} \times 100 \qquad (1)$$

Table 2. Fixity amounts for LCE samples at Ɛ=100% and Ɛ=200%.

Sample	fixity @ ε=100%	fixity @ ε=100%
LCE_1	91.3	96.5
LCE_2	79.3	88.5
LCE_3	74.0	83.70

Fixity amounts showed that all samples have RSC property and increase in strain led to increase in fixity amount which induced that higher extension reoriented mesogenic segments more efficiently. But the fixity amount for LCE1 revealed that this sample could completely retain shape memory. For more precision the strain failure amounts were plotted vs PETMP extent. Fig. 1b showed that LCE1 possessed the highest amount of strain failure and also the tan δ graph for LCE1 confirmed that this failure has taken place at Tg. The samples at the Ɛ=100% were selected for DMA test (DMA-Triton, Model, Tritec 2000 DMA, England) with heating ramp of 3 °C /min ranging from -60 °C to 120 °C. It can be concluded from Figs. 1c and 1d that tan δ graph had two extremums points belonging to Tg and Tni. Also by increasing the PETMP extent, the crosslinking density was increased leading to obtain higher Tg and Tni.

Conclusion

Dynamic-mechanical data and rheological studies of LCE samples prepared by TAMA reaction polymerization after first and second crosslinking processes respectively, showed that the by employing the PETMP:EDDET ratio of 50:50 gel formation in practical time interval and RSC property of LCE reached highest values fulfilling most significant features of an ideal artificial muscle.

References

[1] Barnes M. and Verduzco R., Direct shape programming of liquid crystal elastomers, *Soft Matter*, **15**, 5, 870-879, 2019.

[2] Barnes M., Sajadi S.M., Parekh S., Rahman M.M., Ajayan P.M., and Verduzco R., Reactive 3D printing of shape-programmable liquid crystal elastomer actuators, *ACS Appl. Mater. Interf.*, **12**, 25, 28692-28699, 2020.

[3] Wang Z., Wang Z., Zheng Y., He Q., Wang Y., and Cai S., Three-dimensional printing of functionally graded liquid crystal elastomer, *Sci. Adv.*, **6**, 39, eabc0034, 2020.

[4] Nair D.P. et al., The thiol-Michael addition click reaction: a powerful and widely used tool in materials chemistry, *Chem. Mater.*, **26**, 1, 724-744, 2014.

14-15 December 2021, Tehran, Iran
2nd International Conference on Rheology
ICOR 2021
article A-10-339-1

A New Thermo-responsive Nano Hydrogel Based on Cellulose Nano Crystal

Farhad Jamali[1], Fatemeh Goharpey[1], and Seyed Mohammad Mahdi Mortazavi[2*]
1. Department of Polymer and Color Engineering, Amirkabir University of Technology, P.O. Box 15875-4413, Tehran, Iran
2. Engineering Department, Catalyst Group, Iran Polymer and Petrochemical Institute, Postal Code 13115-14977, Tehran, Iran

*mohamadreza.rezaie@gmail.com

Abstract
This study investigates a new combination of PCL-PEG-PCL micelles in presence of cellulose nano crystal (CNC). A specific molecular weight with no thermogelling behavior was synthesized with ring-opening polymerization (ROP) catalyzed by $Sn(Oct)_2$. 30 wt% triblock solutions prepared to investigate sol-gel behaviors in water media. Different concentrations of CNC that hydrolyzed from cotton were used. In low concentrations of CNC there was no gelling state, but with increasing CNC concentration presence of a gel was detected by RMS measurements. G' and G'' crossover in the low and high frequencies indicates a new network. A new gelling state emerged by increasing CNC concentration up to 3% in which system gels in body temperature range. The thermogelling state was proved by the inverted-tube test in 30 s.

Keywords: PCL-PEG-PCL, hydrogel, thermogelling, cellulose nano crystal, thermoresponsive

Introduction

Block copolymers are a class of copolymers that monomers are organized in repeated units. Each discrete portion in the chain is referred as "blocks". The arrangement of an A-B or A-B-A type of hydrophobic and hydrophilic blocks makes copolymers amphiphilic [2]. Amphiphilic block copolymers have been widely employed for different technological applications.

Some of these copolymers indicate a thermogelling behavior, undergoing a sol-gel transition by changing temperature. This feature is an important fact to design thermogelling systems. They have gained huge attention since they can be used for biomedical and pharmaceutical applications.

Dehydration of the polymeric chain at the micellar state triggers the thermogelling as a result of increasing the temperature.

CNCs are a class of nanomaterials with rod-like shape owing to their physical/mechanical properties and high aspect ratio, which are generally obtained through acid hydrolysis of cellulose. They can form gels only at high concentrations or with additives such as salt [4], acids, polymers or through surface functionalization with cross-linkable groups. The combination of nanomaterials such as CNC with triblock hydrogels will result in improving rheological properties and adverting new features.

Experimental/Theoretical

ε-caprolactone, stannous octoate ($Sn(Oct)_2$), poly(ethylene glycol) (PEG) 2000 g/mol, dichloromethane were purchased from Aldrich. Anhydrous toluene and diethyl ether were purchased from Dr. Mojallali Industrial Chemical Complex Co. The PCL-PEG-PCL triblock copolymers prepared by ring-opening polymerization (ROP) of caprolactone in the presence of PEG. $Sn(Oct)_2$ was used as a catalyst. For example, to synthesize the PCL-PEG-PCL (800-2000-800) triblock copolymer, the procedure was choose as reported by Bae *et al.* [1].

Cotton was used as a cellulose source for obtaining CNC by hydrolyzing with sulphuric acid. 5 g cotton hydrolyzed in 64 wt% sulphuric acid in 45 °C for 45 min. The hydrolyzed cotton was quenched in cold water and diluted with excess deionized water to stop the reaction. Then centrifuged many times until the solution became stable. The solution was poured into a dialysis bag and the water constantly changed until it reached a neutral pH. In the next step, the resulting solution is freeze-dried to obtain solid CNCs. The nanocomposites were prepared in two steps: In the first step different concentrations of CNCs dispersed in deionized water with the help of an ultrasonic homogenizer (400 w, 20 kHz), In the second step copolymers were dissolved in the CNC colloids to form nanocomposites [5].

Results and Discussion

The structures of the PCL-PEG-PCL block copolymers were confirmed using ^{1}H-NMR analysis. According to Fig. 1, the two characteristic peaks at 4.07 and 4.23 ppm which related to PCL block formation are resolved in the NMR spectrum. The average molecular weight of PCL block segments can be calculated by dividing the area of corresponding peak at 4.23 to the area of the peak located at 4.07 [2].

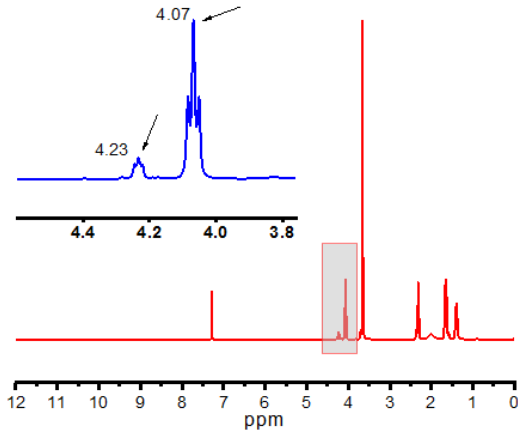

Fig. 1. ^{1}H-NMR graph of PCL-PEG-PCL triblock.

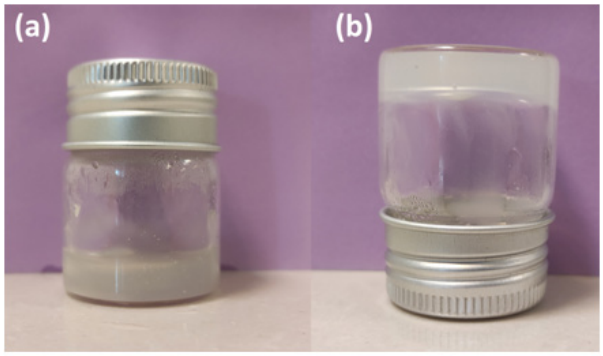

Fig. 2. (a) Sol state of TC3 at 25 °C and (b) gel state at 37 °C.

By preparing a sample of 30% by weight of polymer and two different 1 and 3% by weight of CNC, it was observed that at 25 °C, 1% by weight sample of CNC, called TC1, flows during the tube-inverted test time (30 s) and does not show drastic behavior change with temperature and does not gel in the body temperature range. 3% by weight sample of CNC, called TC3, according to Fig. 2 flows at 25 °C during the test period, but unlike TC1, it does not flow in the body temperature range during the test period and shows a gel state.

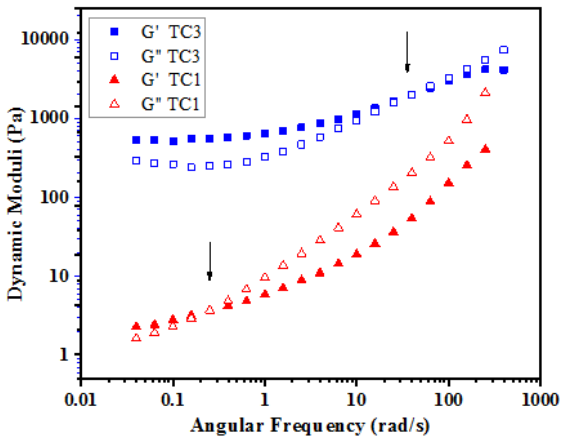

Fig. 3. Frequency sweep of TC3 and TC1 sample at a constant strain 1% and 25 °C.

Rheological tests were conducted using an Anton Paar MCR-302 rheometer with cone and plate geometry with a 25 mm diameter, a cone angle of about 1°. The dynamic moduli versus angular frequency is illustrated in Fig. 3 to observe 3D structures and their change by changing the CNC percentage. For TC1 presence of a three-dimensional structure at low frequencies with the passage of G' from G'' as well as the deviation from terminal behavior of G' at low frequencies can be detected [3]. But for TC3 a G' & G'' cross-over in the high frequencies was observed. In the low frequencies both G' and G'' show non-terminal behaviors that indicates the 3D network formation in the high percentage of CNC.

Conclusion

A novel combination of triblock micelles based on PCL-PEG-PCL and cellulose nano crystal was studied as a candidate for thermo-responsive hydrogels. Inverted-tube test shows that TC1 is sol in the temperature range of 25-37 °C. TC3 is sol at 25 °C but its behavior changes to be gel in 37 °C (body temperature). Rheological studies of the two samples showed that by increasing the CNC percentage, the presence of a 3D network will be favorable. The network of CNCs helped triblock micelles to find their new gel state and show thermo-responsive behavior.

Acknowledgment

Special thanks to the supports of Dr. Ahmadjo, and Dr. Heydarnezhad for their devoted guidance.

References

[1] Bae S.J., Suh J.M., Sohn Y.S., Bae Y.H., Kim S.W., and Jeong B., Thermogelling poly(caprolactone-*b*-ethylene glycol-*b*-caprolactone) aqueous solutions, *Macromolecules*, **12**, 5260-5265, 2005.

[2] Shuquan C., Yu L., and Ding J., Thermogelling of amphiphilic block copolymers in water: ABA type versus AB or BAB type, *Macromolecules*, **52**, 10, 3697-3715, 2019.

[3] Vidyasagar A., Ku S.H., Kim M., Kim M., Lee, H.S., and Pearce T.R. et al., Design and characterization of a PVLA-PEG-PVLA thermosensitive and biodegradable hydrogel, *ACS Macro Lett.*, **6**, 10, 1134-1139, 2017.

[4] Bertsch P., Schneider L., Bovone G., Tibbitt M.W., Fischer P., and Gstöhl S., Injectable biocompatible hydrogels from cellulose nanocrystals for locally targeted sustained drug release, *ACS Appl. Mater. Interfaces*, **11**, 42, 38578-38585, 2019.

[5] Moud A.A., Kamkar M., Sanati-Nezhad A., Hejazi S.H., and Sundararaj U., Viscoelastic properties of poly(vinyl alcohol) hydrogels with cellulose nanocrystals fabricated through sodium chloride addition: rheological evidence of double network formation, *Colloid. Surfaces A: Physicochem. Eng. Aspects*, **609**, 125577, 2021.

14-15 December 2021, Tehran, Iran
2nd International Conference on Rheology
ICOR 2021
article A-10-341-1

Rheological Properties of Gel Polymer Electrolyte Based on a Functionalized Graphene Nanocomposite

Pedram Manafi[1,2*], Hossein Nazockdast[1], and Mohammad Reza Manafi[3]
1. Department of Polymer Engineering and Color Technology, Amirkabir University of Technology, P.O. Box 15875-4413, Tehran, Iran
2. Research and Development Center, Jam Petrochemical Company, South Pars Special Economic Zone (Asalouyeh), P.O. Box 11368-75118, Iran
3. Department of Applied Chemistry, Islamic Azad University, South Tehran Branch, P.O. Box 17776-13651, Tehran, Iran

*pedram_manafi@aut.ac.ir

Abstract
The long-term device instability of liquid-electrolyte-based dye-sensitized solar cells declines their ionic conductivity and performance. These issues can be resolved using quasi-solid-state electrolytes. Despite the enhanced ionic conductivity of graphene nanoplatelets (GNP), their aggregation tendency has limited their application in quasi-solid-state electrolytes. The current study chemically modifies the GNP using polyethylene glycol (PEG) by an amidation reaction to obtain a dispersible nanostructure in a PVDF-HFP/PEO polymer-blended gel electrolyte. Maximum ionic conductivity (4.11×10–3 S.cm^{-1}) was recorded in the optimal nanocomposite gel polymer electrolyte (GPE) encompassing 0.75 wt% functionalized graphene-nanoplatelets (FGNP). The power conversion efficiency of the DSSC based on 0.75 wt% of GPE was 6.46%. By incorporation of optimum FGNP content, a homogenous particle network was fabricated capable of effective mobilization of the redox-active species by its amorphous matrix.

Keywords: electrolytes, microstructure, rheological properties, DSSC and graphene nano particle

Introduction

Dye sensitized solar cells (DSSCs) an electrochemical photovoltaic cell which converting solar energy to electricity with no environmental pollution and ecological destruction, have been attracted a lot of attention due to the easy fabrication, low cost cell assembly process, relatively high efficiency, scalable components, and no environmental issues [1–3]. Still leakage of liquid electrolyte is one of the remaining restrictions for its large-scale commercialization [4,5]. Various efforts have been aiming to substitute the liquid electrolyte by a gel polymer electrolyte (PGE) and solid polymer electrolyte (SPE) in order to overcome the weaknesses of liquid electrolytes [6]. Recently Gomari *et al*. [7] pioneerly grafted PEG onto graphene and used it in PEO electrolyte to increase the ionic conductivity by reducing the crystallinity of the nanocomposite. This study is motivated by aforementioned main concerns of DSSCs and let us to increase the efficiency of the instrument by developing a PGE. PVDF-HFP/PEO blend has been chosen to used, due to its exceptional ion conductivity and lower crystallinity compare to the pair components. In the light of above, two types of electrolyte were prepared and compared as (i) Gel (PVDF-HFP/PEO/IL), and (ii) Gel (PVDF-HFP/PEO/IL/GNP or FGNP). Then, the influence of FG nanomaterial reinforcement on structural, rheological, and electrochemical properties of PVDF-HFP/PEO electrolyte membranes was explored.

Experimental

The performance was further enhanced by synthesizing the ion–electron-conducting polymer composites with various contents of GNP and FGNP in PVDF-HFP/PEO: BMIMBF4: LiBF4 polymeric film. Different levels of functionalized or pristine graphene nanoplatelets (i.e., 0.1, 0.25, 0.5, 0.75, 1, or 1.5 wt% graphene relative to blend) were incorporated into the mixture containing a 10:1 w/w ratio of the BMIMBF4:LiBF4 redox complex couple and solvent. The black suspension was treated by 20 min of ultra-sonication while stirring to make sure on the formation of the homogenous dispersion of graphene, it was then incorporated into the PVDF-HFP and PEO mixture (60:40 w/w). The obtained mixture was further stirred at 80 °C until the complete dissolution of the polymer content followed by cooling down to the ambient temperature, which trigged the gelation process. The sample codes, as well as their composition, are listed in Table 1.

Results and Discussion

For differentiating the linear viscoelastic region from the nonlinear, investigating the dispersive stability of NPs and the influence of IL, the strain amplitude sweep tests were carried out under the controlled frequency (1 rad.s^{-1}) and the range of 0.05–100%. The storage modulus was

Table 1. Sample codes along with their respective composition.

Sample name	Polymer electrolyte	Constituents in weight percent
PVDF-HFP/PEO	Neat blend	60/40
Gel	PVDF-HFP/PEO: $BMIMBF_4$: $LiBF_4$	36/24: 36: 4
Gel-GNP(1)	PVDF-HFP/PEO: $BMIMBF_4$: $LiBF_4$: GNP	36/24: 36: 4: 1
Gel-FGNP(0.75)	PVDF-HFP/PEO: $BMIMBF_4$: $LiBF_4$: FGNP	36/24: 36: 4: 0.75

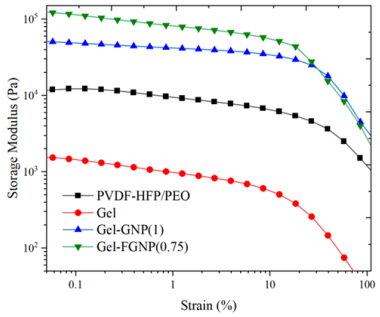

Fig. 1. Storage modulus versus strain amplitude.

plotted as a function of the strain amplitude for PVDF-HFP/PEO blend, Gel and its nanocomposites including GNP and FGNP as shown in Fig. 1. The linear-nonlinear transition of the viscoelastic behavior occurred at lower strain values in the Gel, Gel-GNP(1), and Gel-FGNP(0.75) as compared with the neat blend.

As can be seen, modulus reduction happens because of plasticizing effect of IL in the Gel sample. As can be seen, modulus reduction in Gel sample happens as a result of: (a) plasticizing effect of IL and (b) decreasing of physical crosslinking density. It should be noted that reduction of modulus, which happens by these two phenomena, are in competition with modulus improvement causes by gelation interactions. Thus, the linearity of the viscoelastic behavior was reduced and the storage modulus of the Gel sample was rapidly decreased after the critical strain. Also, this transition in the FGNP containing nanocomposites occurred at lower strains in comparison with pristine nanoplatelets. Such an observation could be assigned to the microstructural variations due to the presence of the functionalized graphene nanoplatelets and the breaking of several essential elastic linkages in the 3D framework of the nanoplatelets whose contents are more dominant in the functionalized nanoplatelets. Additionally, storage modulus exhibited a rapid decline in the Gel-FGNP(0.75) implying more robust 3D network structures when FGNPs are used instead of GNPs. Therefore, more linear rheological assessments were conducted within the linear viscoelastic region (at 0.5% amplitude). J–V plots of the as-prepared DSSCs are presented in Fig. 2. The efficiency of the PVDF-HFP/PEO electrolyte was calculated at 0.61%. The photovoltaic performance, as well as other parameters, exhibited a drastic enhancement upon the incorporation of IL, GNP, and FGNP in comparison with the blend electrolyte. The highest photo-conversion efficiency

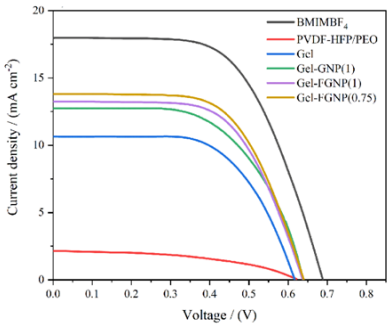

Fig. 2. J–V curves of DSSCs.

(5.30%) with an open-circuit voltage of 0.636 V was recorded in Gel-FGNP(0.75). The further incorporation of FGNP declined the DSSC performance due to the lowered ionic transport and enhanced crystallinity.

As the designed DSSCs were fabricated and tested at consistent temperatures and device components, the enhancement in JSC could not be assigned to the thermal acceleration of ions in the GPE or the different photoanode properties. Improvement in the dye regeneration kinetics is under the influence of the ion diffusion and charge transport efficiencies inside the electrolyte layer. Thus, it can increase the JSC values. Consequently, the elevated JSC could be ascribed to the ionic diffusion of the redox-active species through the bridged nanoparticle network. Such a phenomenon is a consequence of PEG functionalization, through a Grotthus-type electron hopping ion-exchange mechanism.

Conclusion

According to the results, the ion conductivity and DSSC performance are highly dependent on the accessibility of the free ions and incorporation of optimal ratios of additives within the polymer electrolyte. The mobility of the ions could be also affected by the free volume of PVDF-HFP/PEO which can be enhanced through incrementing the amorphous domains of the samples. The PEG-functionalized graphene nanoplatelets (FGNP) were employed as the filler and incorporated into PVDF-HFP/PEO and ionic liquid systems.

References

[1] Ren Y., Sun D., Cao Y., Tsao H.N., Yuan Y., Zakeeruddin S.M., Wang P., and Grätzel M., A stable blue photosensitizer for color palette of dye-sensitized solar cells reaching 12.6% efficiency, *J. Am. Chem. Soc.*, **140**, 2405–2408, 2018.

[2] Zhang W., Wu Y., Bahng H.W., Cao Y., Yi C., Saygili Y., Luo J., Liu Y., Kavan L., Mose r J.-E., Comprehensive control of voltage loss enables 11.7% efficient solid-state dye-sensitized solar cells, *Energy Environ. Sci.*, **11**, 1779–1787, 2018.

[3] Ferdowsi P., Saygili Y., Zakeeruddin S.M., Mokhtari J., Grätzel M., Hagfeldt A., and Kavan L., Alternative bases to 4-tert-butylpyridine for dye-sensitized solar cells employing copper redox mediator, *Electrochim. Acta.*, **265**, 194–201, 2018.

[4] Wu J.H., Hao S.C., Lan Z., Lin J.M., Huang M.L., Huang Y.F., Fang L.Q., Yin S., and Sato T., *Adv. Funct. Mater.*, **17**, 2645–2652, 2007.

[5] Wu J.H., Lan Z., Lin J.M., Huang M.L., Hao S.C., Sato T., and Yin S., A novel thermosetting gel electrolyte for stable quasi-solid-state dye-sensitized solar cells, *Adv. Mater.*, **19**, 4006–4011, 2007.

[6] Zebardastan N., Khanmirzaei M.H., Ramesh S., and Ramesh K., Presence of NaI in PEO/PVdF-HFP blend based gel polymer electrolytes for fabrication of dye-sensitized solar cells, *Mater. Sci. Semicond. Process.*, **66**, 144–148, 2017.

[7] Gomari S., Esfandeh M., and Ghasemi I., All-solid-state flexible nanocomposite polymer electrolytes based on poly(ethylene oxide): lithium perchlorate using functionalized graphene, *Solid State Ionics.*, **303**, 37–46, 2017.

14-15 December 2021, Tehran, Iran
2nd International Conference on Rheology
ICOR 2021
article A-10-344-1

Investigating the Effect of Giesekus' Mobility Parameter on the Secondary Flows in Microfluidic Devices

Ali Kazemzadeh[1], Mahdi Salami Hosseini[1*], and Mehdi Mostafaiyan[2]

1. Polymer Engineering Faculty, Sahand University of Technology, P.O. Box 51335-1996, Sahand New Town, Tabriz, Iran
2. Leibniz Institute of Polymer Research Dresden, Dresden, Germany

*salami@sut.ac.ir

Abstract

In microfluidic systems, the presence of biofluids is inevitable and these fluids are found in biopharmaceutical, medical and industrial applications. An important feature of biofluids is viscoelastic behaviors that result in rheological phenomena such as shear thinning, secondary flows, and elastic behavior. Researchers are always trying to numerically study these viscoelastic behaviors with different mathematical models such as Oldroyd-B model, Giesekus model, and so on. In this study, secondary flows in a semicircular channel were investigated using the Giesekus differential model. For several values of the Giesekus model parameters (α), we examined the secondary flows. We saw that with increasing the value of the α parameter, the secondary flow vortices changed and from two symmetric vortices reached four symmetric vortices. The maximum value of the secondary flow velocity to the primary flow was about 0.01 and by changing the secondary flow patterns to four vertices, the maximum value of the secondary flow velocity decreased.

Keywords: viscoelastic, microfluidic, giesekus, finite element method, simulation

Introduction

The application of the microfluidic devices grows constantly and these devices are going to become the future platform for many applications. Among the various applications of the microfluid devices sorting of synthetic and biological microparticles has become one of the ongoing research fields. Many research works have been devoted to study the mechanisms of particle sorting and improve the designs of the microfluidic devices [1,2].

Hydrodynamic interaction acts though different origins e.g., inertia and elastic effects [3]. Viscoelastic induced hydrodynamic interactions are one of the most interesting subjects which recently is used in sorting devices. The elasticity of the carrying media or continuous phase can alter the equilibrium position of the particles in the channel. The aim of the present study is to investigate the effect of Giesekus' mobility factor on formation and alteration of the microparticle in microfluidic channel. For this purpose, the flow field in the channel of an inclined channel with rectangular cross section was obtained considering Giesekus model and the induced secondary flow was studied.

Numerical Procedure

The flow was considered as a 3-D isothermal and steady state flow and the continuity and motion equation are considered, respectively, as:

$$\nabla.v = 0 \tag{1}$$

$$\rho(v.\nabla)v = -\nabla P + \nabla(\tau_s + \tau_p) \tag{2}$$

Where, v, ρ, τ_s, τ_p and P are velocity, density, solvent part and polymer part of the stress and pressure, respectively. In Eqs. (1) and (2), solvent and polymer part of the stress are taken as, where the polymeric parts was taken into accounts as Giesekus model:

$$\tau_s = -\mu_s\dot{\gamma} \tag{3}$$

$$\tau_p + \lambda_1\tau_{p(1)} - \alpha\frac{\lambda_1}{\lambda_p}\{\tau_p.\tau_p\} = -\eta_p\dot{\gamma} \tag{4}$$

Where, μ_s, τ_s, τ_p, λ_1, η_p, α, and $\dot{\gamma}$ are Newtonian viscosity, solvent stress, polymer part stress, relaxation time, polymer viscosity, mobility parameter and shear rate. To obtain the flow field, we used the DEVSS method [5] to solve the governing equations sets. The geometry of the microchannel and the considered boundary conditions were

Table 1. Characteristics of the fluid.

Parameter	Value
ρ	1000 (kg/m^3)
μ_s	0.001 (Pa.s)
η_p	1 (Pa.s)
λ_1	0.001 (s)
α	0.1, 0.3, 0.5

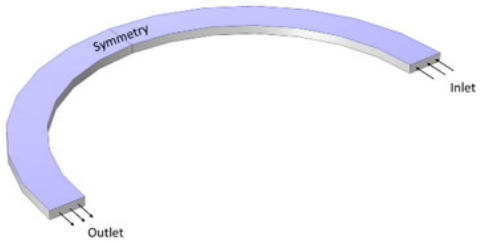

Fig. 1. The geometry of the microchannel with boundary conditions.

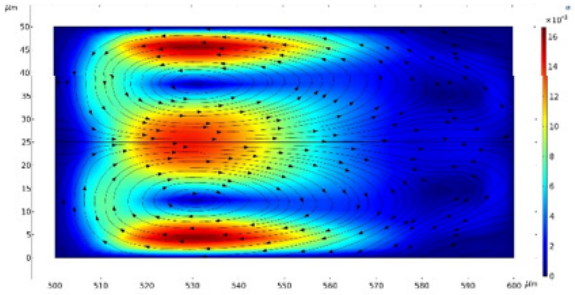

Fig. 2. Secondary flow in the cross section of the microchannel with α=0.1.

shown in Fig. 1. The height and width of the channel were 50 and 100 µm and the inner and outer radius of the channel were 950 and 1050 µm, respectively. The inlet flow rate was 20 µL/s and the fluid characteristics are shown in Table 1.

Results and Discussions

Fig. 2 shows the secondary flow of the case with α=0.1 in the cross section of the channel in the middle part of the channel. It can be seen that there are two vortices taking place adjacent to the inner wall.

Increasing the mobility parameter up to 0.3, induces more pronounced and extra two vertices which makes the total vertices become four (Fig. 2). Again, by increasing α up to 0.5, the intensity of the vertices near the outer wall become higher compare to lower values of the mobility parameters.

This observation can be interpreted by referring to the Giesekus model. As the mobility parameter increases, the elasticity of the fluid increases. The pronounced elasticity produces higher second normal stress, N_2, leading to induce

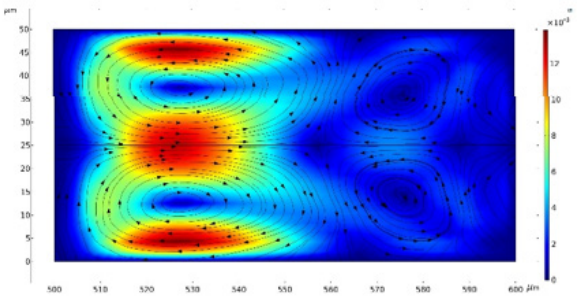

Fig. 3. Secondary flow in the cross section of the microchannel with α=0.3.

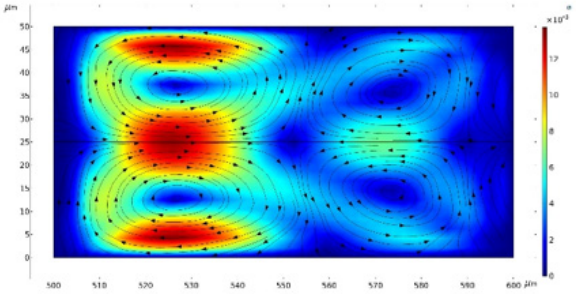

Fig. 4. Secondary flow in the cross section of the microchannel with α=0.5.

the secondary flow. At α=0.3, the later vertices become stronger than the case where α=0.1which makes the former vortices become weaker and increases the intensity of the newly formed vertices.

Conclusion

The flow field of a viscoelastic fluid was obtained in an inclined microchannel. The fluid was considered as Giesekus fluid. The effect of the mobility parameter in the Giesekus model was studied. Three different values for mobility parameter, α, were taken into accounts. The flow field was obtained by DEVSS method using finite element method. Results showed that increasing the mobility parameter, increased the elasticity followed by increasing second normal stress in the fluid leading to increase the intensity of the secondary flow. It was shown that at low mobility parameters, there were two vertices in the vicinity of the inner wall. Increasing the mobility parameter would decrease the intensity of these two vertices, creating and adding up two extra vertices in the vicinity of the outer wall. These finding can be used in designing new sorting microfluidics device which can be sed in many applications.

References

[1] Zhao Q., Yuan D., Zhang J., and Li W., A review of secondary flow in inertial microfluidics, *Micromachines*, **11**, 5, 461, 2020.

[2] Bazaz S.R., Mashhadian A., Ehsani A., Saha S.C., Krüger T., and Warkiani M.E., Computational inertial microfluidics: a review, *Lab Chip*, **20**, 6, 1023-1048, 2020.

[3] Chung A.J., A minireview on inertial microfluidics fundamentals: Inertial particle focusing and secondary flow, *BioChip J.*, **13**, 1, 53-63, 2019.

[4] Raoufi M.A., Joushani H.A.N., Razavi Bazaz S., Ding L., Asadnia M., and Ebrahimi Warkiani M., Effects of sample rheology on the equilibrium position of particles and cells within a spiral microfluidic channel, *Microfluid. Nanofluid.*, **25**, 9, 1-13, 2021.

[5] Rajagopalan D., Armstrong R.C., and Brown R.A. Finite element methods for calculation of steady, viscoelastic flow using constitutive equations with a Newtonian viscosity, *J. Non-Newton. Fluid Mech.*, **36**, 159-192, 1990.

14-15 December 2021, Tehran, Iran
2nd International Conference on Rheology
ICOR 2021
article A-10-346-1

CFD Analysis of Conical Bearing Hydrodynamic Lubrication Using Magnetorheological Fluids

Seyyed Amirreza Vaziri*, Mahmood Norouzi, and Pooria Akbarzadeh
Department of Mechanical Engineering, Shahrood University of Technology, Shahrood, Iran

*vaziri92amirreza@gmail.com

Abstract
Many engineering applications require to support radial and axial load simultaneously, the designers use the one conical bearing instead of two separate thrust and journal bearings, accordingly. Magnetorheological fluid (MRF) is a controllable fluid that exhibits drastic changes in rheological properties adjustable and interchangeable to the applied magnetic field strength. This article represents a numerical solution for hydrodynamic lubrication of conical bearing using magnetorheological lubricant. It can be useful for the bearing that the fluid flow, pressure generation, and dynamic behavior are to be controlled semi-actively. The smart fluids behave like visco-plastic fluids, so the Bingham plastic model is suitable for describing the behavior of these fluids. The performance characteristic of hydrodynamic conical bearing is investigated by means of three-dimensional computational fluid dynamics analysis using COMSOL-Multiphysics software. The conical bearing performance characteristics with MR lubricant are also presented and discussed in detail.

Keywords: magnetorheological fluid, bearing, hydrodynamic lubrication, bingham plastic, yield stress

Introduction

Due to conical bearing's various application, the researchers are interested in analyzing these type of bearing analytically, numerically, and experimentally [1-3]. Prabhu and Ganesan [4] studied the multi-recess conical hydrostatic thrust bearings considering the effect of rotational lubricant inertia. Khalil *et al*. [5] studied the effect of turbulent lubrication on the performance of externally pressurized circular and conical thrust bearings. Wada *et al*. [6,7] deduced the equivalent Reynolds equation of Bingham solid and also established the general theory on the core formation.

In this paper the core formation of Bingham solid in hydrodynamic lubrication of a conical bearing is investigated numerically. The shear stress distribution and pressure distribution according to the eccentricity ratio, L/D ratio and attitude angle are discussed in detail.

Governing Equations

The governing equations for isothermal, laminar, and incompressible MR fluid that are discretized in Comsol-Multiphysics are consisting of continuity and momentum equation as follows:

$$\frac{\partial \rho}{\partial t} + \nabla.(\rho \vec{V}) = 0 \tag{1}$$

$$\frac{\partial}{\partial t}\left(\rho \vec{V}\right) + \nabla.(\rho \vec{V}\vec{V})) = -\nabla p + \nabla.\overline{\overline{\tau}} + \vec{F} \tag{2}$$

MR fluids also act like Newtonian fluids in the absence of a magnetic field and show a constant viscosity, but with the presence of a magnetic field, the particles in the fluid orient in a certain direction and require a yield stress to flow. This refraction in non-Newtonian fluids can be simulated using the Bingham fluid model. In which the fluid is a function of the magnetic field and the yield stress, which is formulated as follow:

$$\begin{cases} \tau = \left(\dfrac{\tau_0(H)}{\dot{\gamma}_{gen}} + \eta\right)\dot{\gamma} & \sqrt{\dfrac{1}{2}\Pi_\tau} > \tau_0 \\ \dot{\gamma} = 0 & \sqrt{\dfrac{1}{2}\Pi_\tau} < \tau_0 \end{cases} \tag{3}$$

That the Π_τ is the second invariant of stress tensor, τ_0 is yield stress, η is the plastic viscosity and $\dot{\gamma}$ is the shear rate tensor that state as below.

$$\dot{\gamma} = \nabla V + \nabla V^T \tag{4}$$

In Eq. (3) the γ_{gen} is the generalized shear rate that state as below.

$$\dot{\gamma}_{gen} = \sqrt{\frac{1}{2}\Pi \dot{\gamma}} \tag{5}$$

Boundary Condition and Method of Solution

In the present numerical solution, the boundary conditions are such that the condition of non-slip is established in the walls, and also the bearing wall is considered fixed, and the journal wall is rotating at a certain rotational velocity. To prevent non-physical boundary conditions (i.e. negative pressure in fluid film) the half-Sommerfeld boundary condition is used, in which the negative pressures are ignored.

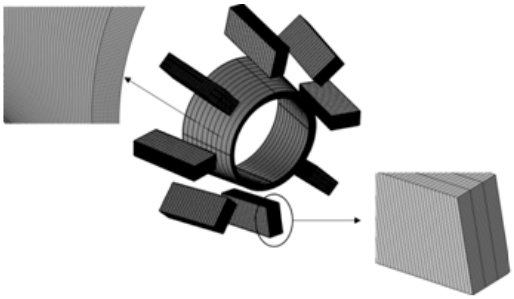

Fig. 1. Conical bearing griding and the selenoids positions.

$$v_r(at\ r=R_j)=v_r(at\ r=R_b)=v_\varphi(at\ r=R_b)= \\ v_z(at\ r=R_j)=v_z(at\ r=R_b)=0 \quad (6)$$

$$p-p_a\geq 0,\ \ at\ \pi\leq\varphi\leq 2\pi,\ z=0, z=L \quad (7)$$

The Navier Stocks and Maxwell equations are solved using the Finite element method, and the sets of equations solved using the Parallel Sparse direct solver (PARDISO). The PARDISO solver works on general systems of the form Ax=b. In order to improve sequential and parallel sparse numerical factorization performance, the solver algorithms are based on a Level-3 BLAS update, and they exploit Pipelining parallelism with a combination of left-looking and right-looking super node techniques. PARDISO is multithreaded on platforms that support multithreading. The package PARDISO is a thread-safe, high-performance, robust, memory efficient and easy to use software for solving large sparse symmetric and unsymmetrical linear systems of equations on shared-memory and distributed-memory multiprocessor

Results and Discussion

In this study, after reviewing the results related to bearing capacity for different meshes, the normal mesh is considered as a reference mesh that is shown in Fig. 1. Fig. 2 shows the pressure distribution for different eccentricity and cone angle. Fig. 3 compare the present study results with

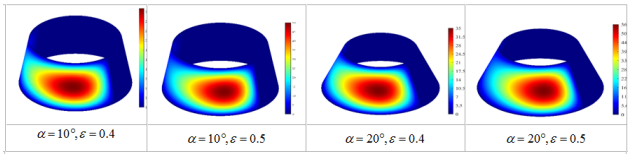

Fig. 2. Pressure distribution at with different cases of eccentric ratio and cone angle.

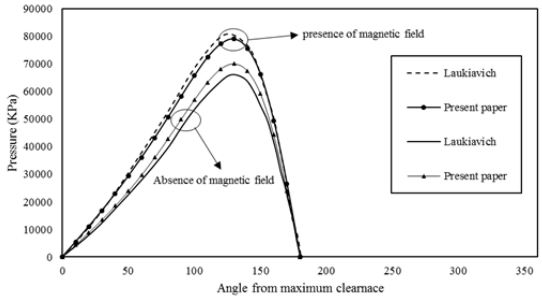

Fig. 3. Validation of present study.

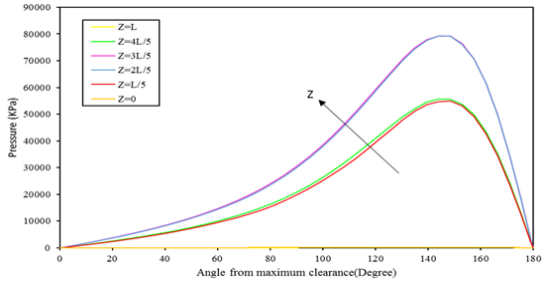

Fig. 4. Distribution of pressure versus angle of maximum clearance (φ) at various distances from the coordinate system center.

Laukiavich study [8]. Fig. 4 shows the pressure distribution versus angle of maximum clearance.

Conclusion

The following results can be expected from the presented study:

1. Core can easily form as film thickness increase.
2. The range of core increases as the relative velocity of the surface decrease.
3. The range of adherent core increases as the eccentricity ratio increases.
4. When the yield stress is larger a core is formed at smaller eccentricity.

References

[1] Srinivasan K. and Prabhu B.S., Steady state characteristics of conical hybrid bearings, *Wear*, **89**, 1, 57-67, 1983.

[2] Sinha P., Chandra P., and Bhartiya S., Analysis of a non-constant gap externally pressurized conical bearing with temperature and pressure dependent viscosity. *Proc. Inst. Mech. Eng., Part C: J. Mech. Eng. Sci.*, **214**, 5, 699-710, 2000

[3] Sharma S.C., Phalle V.M., and Jain S.C., Performance analysis of a multirecess capillary compensated conical hydrostatic journal bearing, *Tribology Int.*, **44**, 5, 617-626, 2011.

[4] Prabhu T.J. and Ganesan N., Analysis of multirecess conical hydrostatic thrust bearings under rotation, *Wear*, **89**, 1, 29-40, 1983.

[5] Khalil M.F., Kassab S.Z., and Ismail A.S., Performance of externally pressurized conical thrust bearing under laminar and turbulent flow conditions, *Wear*, **166**, 2, 147-154, 1993.

[6] Wada S., Hayashi H., and Haga K., Behavior of a Bingham solid in hydrodynamic lubrication: part 1, general theory, *Bull. JSME*, **16**, 92, 422-431, 1973.

[7] Wada S., Hayashi H., and Haga K., Behavior of a Bingham solid in hydrodynamic lubrication: part 3, application to journal bearing, *Bull. JSME*, **17**, 111, 1182-1191, 1974.

[8] Laukiavich C.A., Braun M.J., and Chandy A.J., A comparison between the performance of ferro-and magnetorheological fluids in a hydrodynamic bearing, *Proc. Inst. Mech. Eng., Part J: J. Eng. Tribology*, **228**, 6, 649-666, 2014.

14-15 December 2021, Tehran, Iran
2nd International Conference on Rheology
ICOR 2021
article A-10-348-1

Investigation on the Shear-Induced Gelation Behavior of PVA/Sodium Alginate/GO Nanocomposite Hydrogel

Abdolali Mehrjou[1] and Ismaeil Ghasemi[2*]
1. Department of Polymer Engineering and Color Technology, Amirkabir University of Technology, P.O. Box 15875-4413, Tehran, Iran
2. Faculty of Processing, Iran Polymer and Petrochemical Institute, Postal Code 13115-14977, Tehran, Iran

* i.ghasemi@ippi.ac.ir

Abstract
This study aims to prepare nanocomposite hydrogel based on poly(vinyl alcohol)/sodium alginate, reinforced by incorporating graphene oxide (GO) for use in strain sensors. Small Amplitude Oscillatory Shear (SAOS) flow was used to monitor hydrogel property. Additionally, GO surface was modified using polyethylene glycol (PEG) through the formation of covalent bonds between functional groups on the GO's surface and PEG chains. In the FTIR spectrum of GO-*g*-PEG, the characteristic peaks of different bonds were shifted, which proves the presence of new functional groups, and can be related to the reaction of GO and PEG. The variation of storage modulus showed the formation of hydrogel, and structural strength was find. In addition, self-healing of the samples due to the presence of sodium alginate was tracked using typical self-healing experiment.

Keywords: hydrogel, induced gelation, graphene oxide, surface modification, IPN

Introduction

There is fast growing interest in using nanoparticles such as graphene oxide (GO) in hydrogels. This could be because GO is a "super gelator" in aqueous solution, with a critical gelation concentration of less than 0.5 weight percent [1]. Smart materials have attracted the attentions of academics over the last few decades due to their unique applications in a wide range of industries. One of the most promising fields of smart materials, self-healing materials, has recently become a heated topic. Self-healing hydrogels based on noncovalent reactions and dynamic covalent interactions have received a lot of attention [2].

If stress relaxation is significantly faster than the time required for structural change, SAOS measurements can be used to track microstructure evolution in dispersions. The storage modulus indicates the number of network points in the gels and grows as the gelation process progresses. As a result, several studies have used SAOS measurements to track the degree of gelation.

We used rheological analysis to investigate the gelation of aqueous dispersions containing GO and polyvinyl alcohol (PVA). Surprisingly, our research found that SAOS can cause graphene dispersions to gel. Shake gels have also been observed in polymer dispersions, including other nanoparticles. The "shake gels" revert to the solution once the flow stops. The SAOS-induced hydrogels, on the other hand, were stable in this investigation.

Furthermore, sodium alginate plays an iconic role in having a self-healable hydrogel. To be more specific, having dynamic bonds is crucial for obtaining self-healing property: both PVA physical entanglements and sodium alginate ionic crosslinks can be broken up and repaired.

Experimental

Poly(vinyl alcohol) (PVA) was purchased from Sigma Aldrich (99 mol% hydrolyzed, ($\overline{M}_w$=13000 g). Graphene oxide nanoplatelets (3.4-7 nm thickness) was supplied from US Research Nanomaterials Inc, with a purity of 99.5% and 6-10 layers. PEG with a molecular weight of 400 g/mol was obtained from Merck. Sodium alginate (guluronic acid:mannuronic acid equal to 1.2:1) was purchased from Sigma Aldrich. Grafting of PEG on GO was done following the procedures reported in our previous work [3].

PVA powder was added into deionized water to prepare a solution under stirring at 80 °C for 1 h. After the PVA solution was cooled down to room temperature, 5 mL GO dispersion (5 mg/mL) was added into 5 mL PVA solution. Aqueous dispersions with two different PVA weight ratios to GO was prepared: GO concentration kept as 0.4 wt% in the dispersions prepared with PVA:GO=2:1 and 1:5, corresponding to 0.80 and 0.08 wt% PVA in the dispersions, respectively. Both dispersions kept under magnetic stirring for another 1 h. It is worth mentioning that hydrogel is not formed when PVA contents is less than or equal to 0.05 wt% in the dispersions. Next, 2 wt% solution of sodium alginate is added to each of the dispersions to obtain a PVA/GO/sodium alginate mixture under magnetic stirring. At last, each dispersion is added to 4 wt% aqueous solution of calcium chloride to prepare samples.

We measured G' and G'' with respect to frequency at constant shear (γ=10%) to corroborate the SAOS-induced gelation. Fig. 1 shows a typical storage modulus (G') and

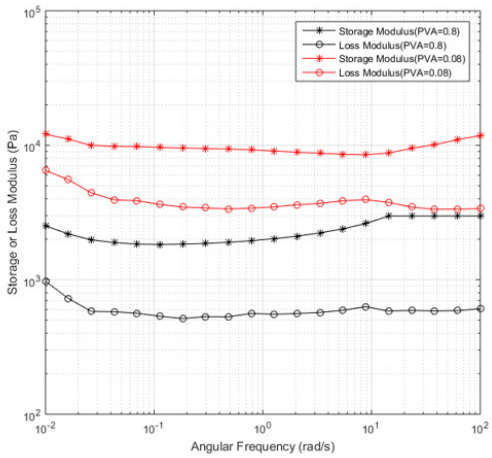

Fig. 1. The storage modulus (G') and the loss modulus (G'') of hydrogels with 0.8 wt% PVA (black) and 0.08 wt% PVA (red) by frequency sweep measurements.

loss modulus (G'') of hydrogels with 0.8 and 0.08 wt% PVA. These measurements have been done by a conventional frequency sweep from 0.01 rad/s to 100 rad/s in the rotational rheometer with parallel plate geometry with a gap size of 1.0 mm and a plate diameter of 50 mm.

Results and Discussion

According to the FTIR spectra of GO and GO-*g*-PEG presented in Fig. 2, the characteristic peak of C=O bond was moved to 1731 cm^{-1} which indicates the presence of ester groups. This peak proves the successful grafting of PEG on GO surface.

Regarding the formation of the double network hydrogel, it is clear that PVA chains are concentrated around GO nanoparticles, which are grafted to PEG long chains. As this aqueous solution is put under SAOS flow, the PVA chains create physical entanglements, and finally, they form a stable structure. Besides, sodium alginate and calcium chloride have already produced ionic bonds. The creation of physical entanglements coupled with ionic bonds leads to the formation of hydrogel nanocomposite. As shown in Fig. 1, G' and G'' at first had some fluctuations

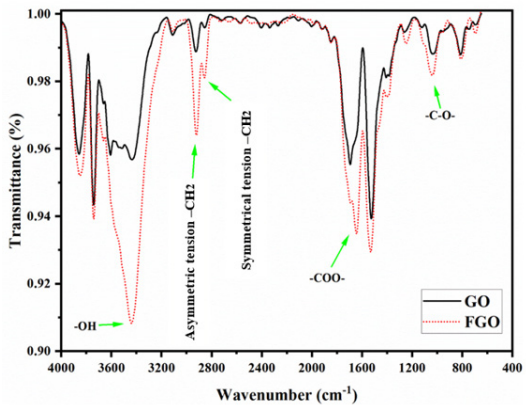

Fig. 2. FTIR spectra of graphene oxide (GO) and PEG-*g*-GO (FGO).

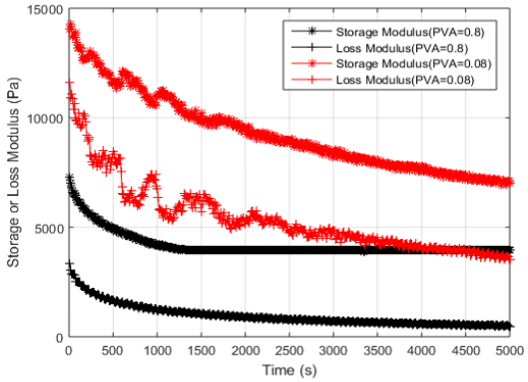

Fig. 3. Time evolution of storage modulus (G') and loss modulus (G'') of hydrogels with 0.8 wt% PVA (black) and 0.08 wt% PVA (red) at ω=1 rad/s.

until they reach a plateau. Moreover, G' is always higher than G'' at all frequencies mentioned in this study. These findings suggest that SAOS may impact the gel structure. If this is the case, traditional frequency sweep dynamic moduli cannot be used to measure the structural properties of hydrogels.

We measured G' and G'' with respect to time at constant frequency (ω=1 rad/s) to validate the SAOS-induced gelation. For hydrogel (0.8 wt. percent PVA), the time evolution of G' and G'' at ω=1 rad/s is presented in Fig. 3. G' decreases over time until it reaches a plateau. Also, G' plot is always above the G'' plot in Fig. 3. The behaviors of G' and G'' at other frequencies are likewise indicating SAOS stress causes the GO hydrogels to restructure. The struggle between the development and breakdown of gel-networks in SAOS flow increases the number of network sites until a stable state is obtained.

Conclusion

In summary, a facile approach is presented to prepare dynamic hydrogels using poly(vinyl alcohol) (PVA), sodium alginate, graphene oxide, and water as the main components. Small amplitude oscillatory shear (SAOS) stress thickens the GO hydrogels. When the hydrogels are agitated at lower frequencies, the thickening is more noticeable. The SAOS-induced gelation described in this study differs from regular polymer gelation. These findings support the development of a new rheological theory to explain such a phenomenon.

References

[1] Hu Y.-L. et al., *Appl. Phys. Lett.*, **100**, 16, 161101, 2012.
[2] Jing X et al., Sensors and actuators b: chemical, **295**, 159-167, 2019.
[3] Karimi S., Ghasemi I., and Abbassi-Sourki F., A study on the crystallization kinetics of PLLA in the presence of graphene oxide and PEG-grafted-graphene oxide: effects on the nucleation and chain mobility, *Compos. Part B: Eng.*, **158**, 2019.

14-15 December 2021, Tehran, Iran
2nd International Conference on Rheology
ICOR 2021
article A-10-355-1

A Numerical Study on the Impact of a Viscoelastic Drop onto the Same Quiescent Fluid Film

Mohammadreza Rezaie[1*], Mahmood Norouzi[1], Mohammadhassan Kayhani[1], and Seyed Mohammad Taghavi[2]
1. Department of Mechanical Engineering, Shahrood University of Technology, P.O. Box 316, Shahrood, Iran
2. Department of Chemical Engineering, Laval University, Quebec, GIV 0A6, Canada
*mohamadreza.rezaie@gmail.com

Abstract
In the present study, we study, numerically, the effect of fluid viscoelasticity on drop impacts onto same quiescent fluid films. The axisymmetric incompressible flow momentum equations combined with the viscoelastic constitutive equation are solved, using the finite volume method (FVM). The volume of fluid (VOF) technique is used to track the free-surface of the liquid. Here, the Oldroyd-B model is used as the constitutive equation for the viscoelastic phase. The dynamics of the crown parameters are quantified by considering the flow parameters, including the fluid's elasticity. The results indicate that the numerical solutions show good agreement with the previous studies. Generally, the fluid's elasticity can enlarge the crown dimension at different thicknesses of the fluid film. Moreover, at the intermediate value of the Weissenberg number, the extensional force in the crown wall can control the crown propagation. Furthermore, the results reveal that the effects of the Weber number on this problem are more significant at higher values of the Weissenberg number.

Keywords: drop impact, crown formation, numerical analysis, viscoelastic fluid, Oldroyd-B model

Introduction

The dynamics of the crown formation due to the impact of a drop onto a thin liquid film is of interest in fluid mechanics and engineering applications. Many studies [1,2] have investigated the crown formation problem in Newtonian fluids. However, the effects of the fluid's rheological properties, especially the elasticity and the nonlinear viscosity, have received less attention in the literature. Lampe *et al*. [3] have experimentally investigated the water drop impact on viscoelastic wormlike micelle polymer solutions. Tome *et al*. [4] have numerically investigated the viscoelastic drop impact on the same liquid pool. Recently, Rezaie *et al*. [5] have numerically studied the impact of a plane two-dimensional drop onto a pre-existing liquid film in a viscoelastic fluid.

In this study, by using the finite volume method (FVM) and the VOF technique, the governing equations are solved. The Oldroyd-B model is used as the constitutive equation for the viscoelastic phase. The effects of the main flow parameters on the evolution of the crown are investigated in detail.

Mathematical Formulation

The schematic illustration of present problem is shown in Fig. 1. The governing equations for the incompressible viscoelastic fluid flow as follows:

$$\nabla \cdot v = 0, \tag{1}$$

$$\frac{\partial(\rho v)}{\partial t} + \nabla \cdot (\rho v v) = -\nabla p + \nabla \cdot \tau + \rho g + F_s. \tag{2}$$

In this study, the Oldroyd-B model is used as follows:

$$\tau + \lambda \overset{\nabla}{\tau} = 2\eta \left(\varepsilon + \frac{\lambda \eta_s}{\eta} \overset{\nabla}{\varepsilon} \right) \tag{3}$$

Results and Discussion

The results of the present work are verified based on the numerical results of previous studies [6,7], for the width of the drop, as shown in Fig. 2. The dimensionless forms of the radius (R) and the height (Z) are:

$$R^* = \frac{R}{D}, \quad Z^* = \frac{Z}{D}. \tag{4}$$

Fig. 3 shows that the effect of the elasticity on the crown height is greater than that on the crown radius. It is clear that, by increasing the fluid's elasticity, the fluid's elasticity can enlarge the crown parameters. Fig. 4 portraits the crowns shape for different fluids.

In Fig. 5, the effect of the fluid film thickness on the maximum height of the crown is presented at different Weissenberg numbers. With an increase in the fluid film thickness, the maximum height of the crown (Z^*_{max}) increases. Fig. 6 compares the crown dimensions (Z^* and R^*) at different Weber and Weissenberg numbers.

Fig. 7 depicts the effects of the viscosity ratio (β) on the crown dynamics at different Weissenberg numbers. As shown in Fig. 7, the effect of the viscosity ratio on the crown height is more considerable than that on the crown radius. Moreover, at larger Wi, the crown height increases by increasing the viscosity ratio.

Conclusion

The results of the numerical investigation show that the fluid's elasticity can increase the crown dimensions for large values of the Weissenberg number (Wi>1). Whereas, at lower values of the Weissenberg number (Wi≤1), the crown dynamics can be complex. By increasing the Weber number, the time variation of the crown parameters

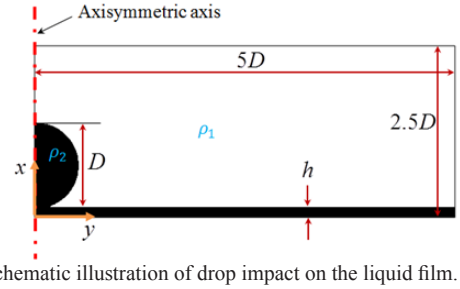

Fig. 1. Schematic illustration of drop impact on the liquid film.

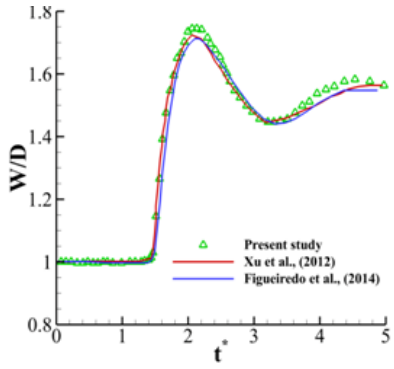

Fig. 2. Comparison between the drop width predicted in our work and that in the previous studies [6,7].

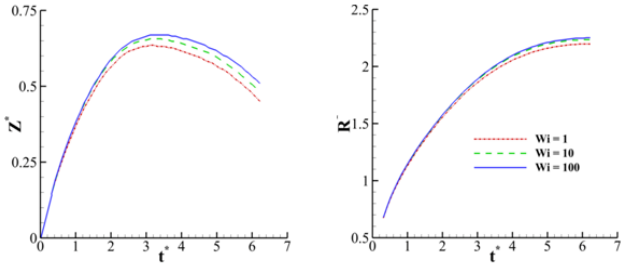

Fig. 3. The effect of the fluid's elasticity on the crown parameters.

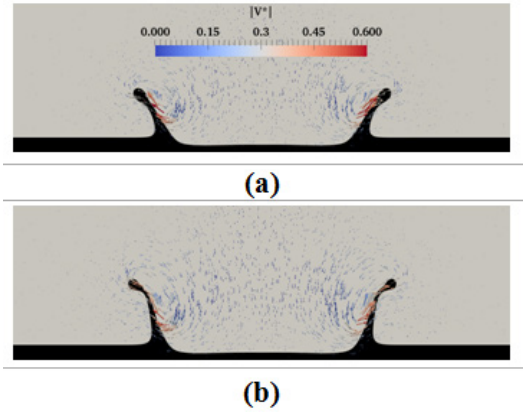

Fig. 4. Crown shape at different Weissenberg numbers at t*= 2.8 for 0.2, 0.1, and 400 (a) 1, (b) 100.

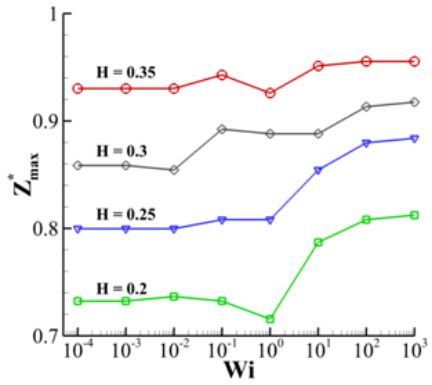

Fig. 5. Variation of the maximum crown height with the Weissenberg number for Re=175, β=0.1, and We=400.

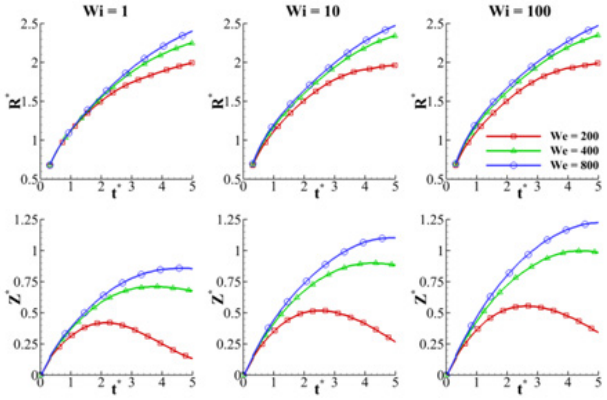

Fig. 6. Time variation of the crown radius and height with the Weber number for Re=175, H=0.2, and β=0.3.

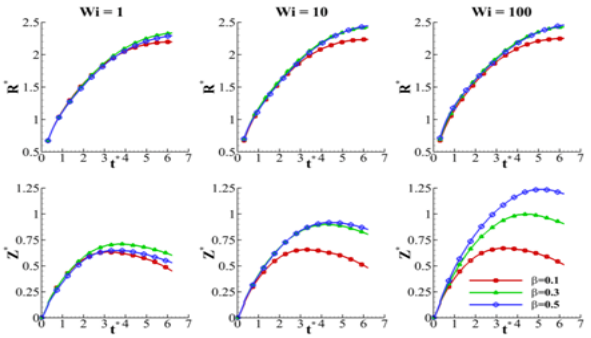

Fig. 7. Time variation of crown radius and height with viscosity ratio for 175, 0.2, and 400.

increases. Also, at larger values of the Weissenberg number, the effect of the viscosity ratio on the is significant.

References

[1] Rieber M. and Frohn A., A numerical study on the mechanism of splashing, *Int. J. Heat Fluid Flow*, **20**, 5, 455-461, 1999.

[2] Nikolopoulos N., Theodorakakos A., and Bergeles G., Normal impingement of a droplet onto a wall film: a numerical investigation, *Int. J. Heat Fluid Flow*, **26**, 1, 119-132, 2005.

[3] Lampe J., DiLalla R., Grimaldi J., and Rothstein J.P., Impact dynamics of drops on thin films of viscoelastic wormlike micelle solutions, *J. Non-Newton. Fluid Mech.*, **125**, 1, 11-23, 2005.

[4] Tomé M.F., Grossi L., Castelo A., Cuminato J.A., McKee S., and Walters K., Die-swell, splashing drop and a numerical technique for solving the Oldroyd B model for axisymmetric free surface flows, *J. Non-Newton. Fluid Mech.*, **141**, 2, 148-166, 2007.

[5] Rezaie M.R., Norouzi M., Kayhani M.H., and Taghavi S.M., Numerical analysis of the drop impact onto a liquid film of non-linear viscoelastic fluids, *Meccanica*, **56**, 8, 2021-2038, 2021.

[6] Xu X., Ouyang J., Jiang T., and Li Q., Numerical simulation of 3D-unsteady viscoelastic free surface flows by improved smoothed particle hydrodynamics method, *J. Non-Newton. Fluid Mech.*, **177-178**, 109-120, 2012.

[7] Figueiredo R.A., Oishi C.M., Afonso A.M., Tasso I.V.M., and Cuminato J.A., A two-phase solver for complex fluids: studies of the Weissenberg effect, *Int. J. Multiphas Flow*, **84**, 98-115, 2016.

14-15 December 2021, Tehran, Iran
2nd International Conference on Rheology
ICOR 2021
article A-10-389-1

Rheology of Self-Assembled Polystyrene Block Polyacrylic Acid

Farnaz Farbod and Fatemeh Goharpey*
Amirkabir University of Technology, P.O. Box 15875-4413, Tehran, Iran

*goharpey@aut.ac.ir

Abstract
A series of polystyrene block polymethyl acrylate (PS-PMA) with varying molecular mass and narrow molecular weight distributions were prepared by atom transfer radical polymerization. Polystyrene block poly acrylic acid block copolymers (PS-PAA) were produced by hydrolysis with trifluoracetic acid and all of the BCP's properties were characterized by GPC, H-NMR, and FT-IR. Self-assemblies of PS-PAA with remarkable property of high chi parameter were observed by AFM micrographs after solvent annealing with THF atmosphere at room temperature. Rheological techniques have been used to study phase transition of block copolymers. Order to disorder transition temperatures were identified as a sharp drop in storage modulus while order to order transition temperatures were indicated by maximum in tan δ. Transition temperatures attributed to endothermic and exothermic peaks in DSC curves were in accordance with rheology measurements.

Keywords: self-assembly, pattern, rheology, polystyrene block polyacrylic acid, rheology, DSC

Introduction

Self-assembly of block copolymers has been widely studied for nanopatterning application including alternative way of lithography for semiconductor industry. In an attempt to reach sub 10 nm pattern periodicity, we demonstrate synthesis, characterization and self-assemblies of PS-PAA as one of the best candidate of BCPs for self-assembly thanks to its high chi parameter. ATRP method was used for PS-b-PMA synthesis, followed by hydrolysis with TFA. Temperature sweep and DSC analysis were used for determination of transition temperatures of BCPs.

Experimental

ATRP synthesis of BCPs were done as described elsewhere [1,2]. PS-PAA were obtained after hydrolysis by TFA as a mild condition procedure. Successful synthesis and hydrolysis reaction process were checked and characterized by GPC, H-NMR, and FTIR tests. Thin films on the pre-cleaned wafer silicones were obtained by spin coating and solvent annealing procedure were performed at room temperature under toluene THF atmosphere. Self-assembled BCPs were observed by AFM images.

Results and discussion

Temperature sweep of PS74-PAA28, PDI=1.16, was performed at 2 °C/min of heating rate with fixed strain and angular frequency of 0.2% and 1 rad/s, respectively. Samples were prepared in our laboratory made silicon mold circular pill shape by solution casting of block copolymers in toluene solvent followed by 2 days solvent evaporation at room temperature followed by 1 day heating at 50 °C in vacuum oven. Linear regime determination was carried out first, and then temperature sweep and frequency sweep tests were performed in the linear regime. In every test fresh sample was used. Two sharp decreases of storage modulus, about two orders of magnitude, at 80 and 153 °C followed by two overlaps of G' and G" at 84 and 157 °C were observed. First sharp storage modulus reduction indicates an order-order transition while the second of this phenomena implies order disorder transition. Another two order to order transition temperatures occurred at 91 and 112 °C/min according to Fig. 1, at maximum value of tan delta and overlapping point of G' and G", respectively. Rheology experiment of temperature sweep also shows two distinct glasses transition temperature attributed to two blocks of block copolymer at 84 and 157 °C where both moduli overlap each other. In summary, as it shows in rheology test figure, important phase transition temperatures include: order to order transition temperatures (T_{OOT}) are 80, 112, 91, 153, Tg: 84; order to disorder transition temperature is

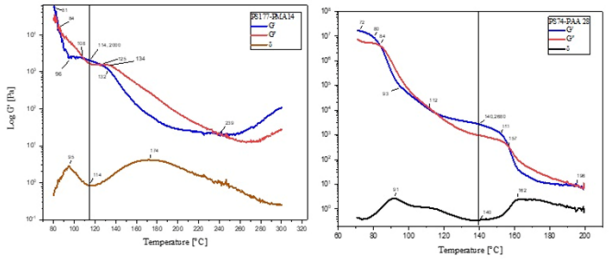

Fig. 1. Temperature sweep test.

Table 1. Mw and PDI are represented from GPC, N, and f as volume fractions were computed by H NMR analysis. DSC and rheometer results were used to deduced Tg values.

Sample	Mw(g/mol)	PDI	f%	Tg
PS42-PAA16	13392	1.17	22	NA
PS51-PAA26	16022	1.20	27	NA
PS74-PMA28	18528	1.16	25	23-75
PS74-PAA28	16103	1.33	22	96-157
PS124	23601	1.08	0	NA
PS74	10057	1.10	0	NA

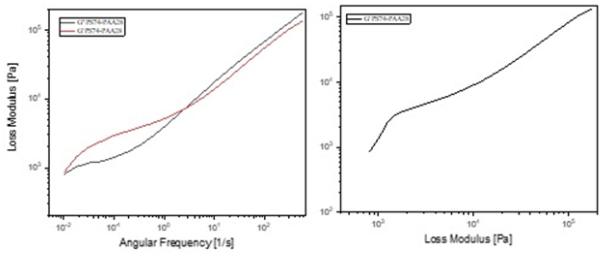

Fig. 2. Frequency sweep test.

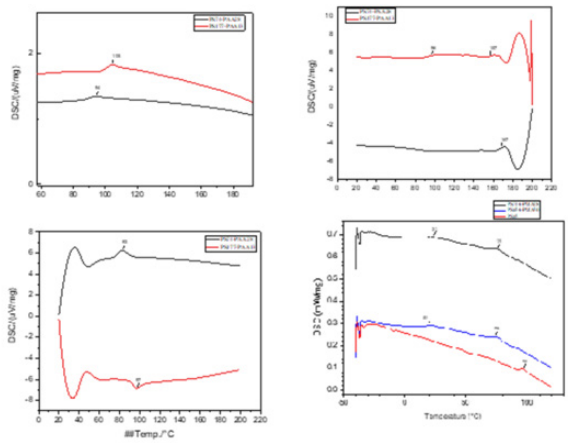

Fig. 3. DSC curves of PS-b-PAA.

(TODT): 157 °C. T_{OOT}'s attribute to main order to order phase transitions from HPL (hexagonal perforated lamellar to double gyroid (DG) to C (cylinder). Little divergence in Tg, measured by DSC and rheometer is expected (Figs. 1 and 3) [3-9]. Fig. 2 shows frequency sweep experiment of PS74-PAA28 at 90 °C and fixed strain of 0.2%. In the plot of log G' versus log w with slope 0.9 (G~w0.9, G"~w0.4) at terminal zone indicates ordered structure of block copolymer and order to order transition during test were observed by slope changes of storage modulus [9]. Glass transition temperature (Tg) of PS and PS-b-PMA is observed as inflection points of heat capacity jump in Fig. 3. It implies that methyl acrylate rotation of side groups

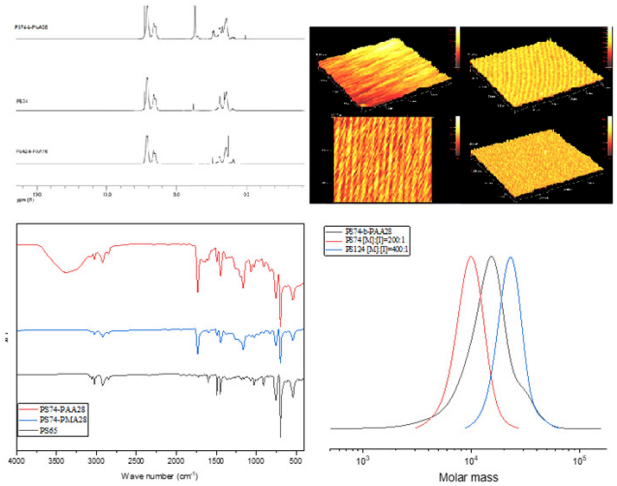

Fig. 4. H-NMR, FTIR, GPC, and AFM images of BCPs.

caused Tg reduction as it is obvious in Fig. 2 after block copolymerization of PS-Be, glass transition temperature of polystyrene reduced from 96 to 73, and methyl acrylate contribution growth in block copolymer was influenced on T_g reduction.

Conclusion

PS-PAA BCPs were successfully synthesized and characterized. Lamellae and HPL structure were observed with sub 10 nm feature size. Temperature sweep was conducted to determine order to disorder and order to order transition temperature which were in accordance with DSC results.

References

[1] Abraham S., Ha C.-S., and Kim I., Synthesis of poly(styrene-block-tert-butyl acrylate) star polymers by atom transfer radical polymerization and micellization of their hydrolyzed polymers, *J. Polym. Sci. Part A: Polym. Chem.*, **43**, 24, 6367-6378, 2005

[2] Ma Q. and Wooley K.L., The preparation of t-butyl acrylate, methyl acrylate, and styrene block copolymers by atom transfer radical polymerization: Precursors to amphiphilic and hydrophilic block copolymers and conversion to complex nanostructured materials, *J. Polym. Sci. Part A: Polym. Chem.*, **38**, S1, 4805-4820, 2000.

[3] Moon Jeong Park K.C., Interplay between cubic and hexagonal phases in block copolymer solutions, *Langmuir*, **21**, 1403-1411, 2005.

[4] Che-Yi Chu W.-F.L., Tsai J.-C., Lai C.-S., Lo S.-C., Chen H.-L., and Hashimoto T., Order−order transition between equilibrium ordered bicontinuous nanostructures of double diamond and double gyroid in stereoregular block copolymer, *Macromolecules*, **45**, 2471−2477, 2012.

[5] Chang Dae Han D.M.B., Effect of volume fraction on the order-disorder transition in low molecular weight polystyrene-bzock-polyisoprene copolymers. Order-disorder transition temperature determined by rheological measurements, *Macromolecule*, **28**, 5043-5062, 1995.

[6] Guillaume Delaittre B.C., Kinetics of in-Situ formation of poly(acrylic acid)-b-polystyrene amphiphilic block copolymers via nitroxide-mediated controlled free-radical emulsion polymerization. Discussion on the effect of compartmentalization on the polymerization rate, *Macromolecules*, **41**, 2361-2367, 2008.

[7] Kim J.K. et al., Determination of order−order and order−disorder transition temperatures of sis block copolymers by differential scanning calorimetry and rheology, *Macromolecules*, **31**, 12, 4045-4048, 1998

[8] Wang C.-Y. and Lodge T.P., Kinetics and mechanisms for the cylinder-to-gyroid transition in a block copolymer solution, *Macromolecules*, **35**, 18, 6997-7006, 2002.

[9] Minghai Li Y.L., Nie H., Bansil R., and Steinhart M., Kinetics of HEX-BCC transition in a triblock copolymer in a selective solvent: time resolved small angle X-ray scattering measurements and model calculations, *Macromolecules*, **40**, 9491-9502, 2007.

Iranian Society of Rheology

Office: Department of Polymer Engineering,
Amirkabir University of Technology, Tehran, Iran
Tel: 0930 230 7582, Telfax: +9821 6454 2437
E-mail: info@ir-sor.com, Website: ir-sor.com